



PB94-104502

**Seismic Resistance of Reinforced Concrete
Frame Structures Designed Only
for Gravity Loads:**

**Part I - Design and Properties of a
One-Third Scale Model Structure**

by

J.M. Bracci¹, A.M. Reinhorn² and J.B. Mander³

December 1, 1992

Technical Report NCEER-92-0027

NCEER Project Numbers 89-1001A, 90-1001A and 91-3111B

NSF Master Contract Number BCS 90-25010

and

NYSSSTF Grant Number NEC-91029

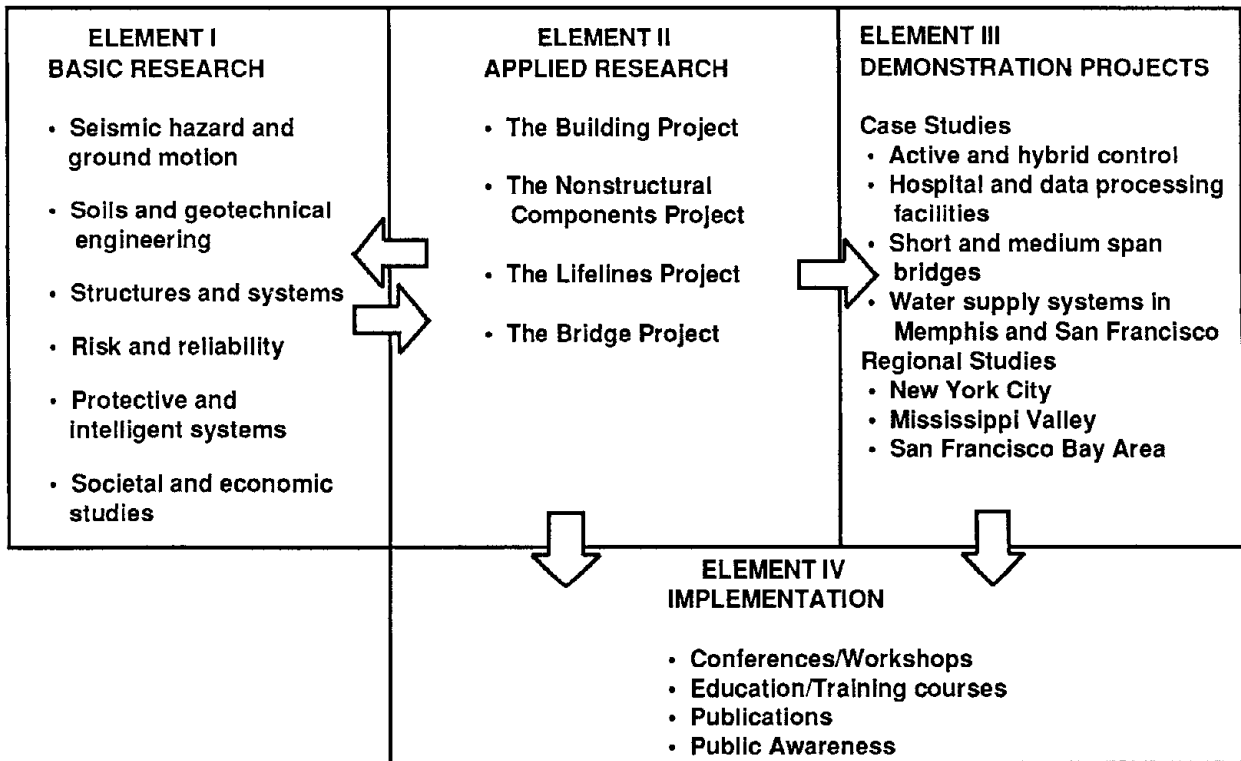
- 1 Research Associate, Department of Civil Engineering, State University of New York at Buffalo
- 2 Professor, Department of Civil Engineering, State University of New York at Buffalo
- 3 Assistant Professor, Department of Civil Engineering, State University of New York at Buffalo

NATIONAL CENTER FOR EARTHQUAKE ENGINEERING RESEARCH
State University of New York at Buffalo
Red Jacket Quadrangle, Buffalo, NY 14261

PREFACE

The National Center for Earthquake Engineering Research (NCEER) was established to expand and disseminate knowledge about earthquakes, improve earthquake-resistant design, and implement seismic hazard mitigation procedures to minimize loss of lives and property. The emphasis is on structures in the eastern and central United States and lifelines throughout the country that are found in zones of low, moderate, and high seismicity.

NCEER's research and implementation plan in years six through ten (1991-1996) comprises four interlocked elements, as shown in the figure below. Element I, Basic Research, is carried out to support projects in the Applied Research area. Element II, Applied Research, is the major focus of work for years six through ten. Element III, Demonstration Projects, have been planned to support Applied Research projects, and will be either case studies or regional studies. Element IV, Implementation, will result from activity in the four Applied Research projects, and from Demonstration Projects.



Research in the **Building Project** focuses on the evaluation and retrofit of buildings in regions of moderate seismicity. Emphasis is on lightly reinforced concrete buildings, steel semi-rigid frames, and masonry walls or infills. The research involves small- and medium-scale shake table tests and full-scale component tests at several institutions. In a parallel effort, analytical models and computer programs are being developed to aid in the prediction of the response of these buildings to various types of ground motion.

Two of the short-term products of the **Building Project** will be a monograph on the evaluation of lightly reinforced concrete buildings and a state-of-the-art report on unreinforced masonry.

The **structures and systems program** constitutes one of the important areas of research in the **Building Project**. Current tasks include the following:

1. Continued testing of lightly reinforced concrete external joints.
2. Continued development of analytical tools, such as system identification, idealization, and computer programs.
3. Perform parametric studies of building response.
4. Retrofit of lightly reinforced concrete frames, flat plates and unreinforced masonry.
5. Enhancement of the IDARC (inelastic damage analysis of reinforced concrete) computer program.
6. Research infilled frames, including the development of an experimental program, development of analytical models and response simulation.
7. Investigate the torsional response of symmetrical buildings.

One of the key accomplishments in the development of evaluation methods for existing buildings was the design and shake-table testing of three-story gravity-load designed buildings at the University at Buffalo and at Cornell University. These tests followed extensive preparatory full and reduced-scale component tests and the development of computer models.

This is the first in a series of three reports summarizing the test program at the University at Buffalo. It presents the design of a prototype three-story concrete building for gravity loads and the design of the reduced-scale model. The initial dynamic characteristics of the model are also described.

ABSTRACT

This report is Part I of a three-part series prepared for a comprehensive **Evaluation** of typical gravity load designed low-rise reinforced concrete frame buildings (lightly reinforced concrete structures) for seismic adequacy. The study was done at State University of New York at Buffalo - Earthquake Simulation Laboratory on a 1:3 scale building model designed for gravity loads only. No considerations were made for seismic resistance and the general non-seismic detailing provisions of ACI-318-89 were used for the design. The one-third scale three story model, one-bay by three-bay, of a typical office building was constructed to represent the critical interior bay of a prototype structure.

Components of structure, i.e., structural subassemblages of columns, column-to-beam joints and column-beam-slabs models were constructed from the same materials as the structural model and at same scale. These components were tested with cyclic loading to failure to determine their structural parameters and ultimate limits. The results of components study are the subject of Part II of the Evaluation Series.

A series of varying intensity simulated ground motion tests were performed on the one-third scale building model using scaled accelerograms on the shaking table to represent minor, moderate, and severe earthquakes. The dynamic characteristics of the model after each seismic event were identified from white noise shaking table tests. Analytical models were developed to predict and interpret the seismic response of the building model based on identified member properties from engineering approximations, component tests, and an experimental response fit. It is shown in Part III of the Evaluation report series that the response predictions based on integrating the behavior from component tests (presented in Part II of the Evaluation report series) provide adequate correlation of the seismic structural response behavior, emphasizing the importance of such component testing. A damage evaluation of the building model is presented to assess the structural integrity after the induced ground motions in terms of damage states. A newly modified damage model is proposed to incorporate the additional damage from P-delta effects in columns.

It is shown in this report series that gravity load designed structures have some inherent strength for resisting seismic forces. However a weak column - strong beam behavior was evident in the experimental response and large story drifts, beyond 2% of the story height (exceeding current code recommended limits), may develop during strong earthquakes (see Part III of this Evaluation Series).

Part I of the Evaluation Series (this report) presents the design objectives, geometric dimensions, material strengths and initial dynamic properties of the model building, along with the simulated base motions, so that analytical models can be developed and used to predict the inelastic response of the model building during more severe earthquakes. The initial vibration tests and the response from a minor earthquake are presented to enable analytical structural modeling and verification of elastic response.

ACKNOWLEDGEMENTS

Funding for this work was provided through the National Center for Earthquake Engineering Research (NCEER) Contract No. 891001A, 901001A, and 913111B under the National Science Foundation Master Contract No. ECE-86-07591 and the State of New York. The support is gratefully acknowledged.

The authors are grateful for the collaboration and assistance of Profs. Richard N. White and Peter Gergely of Cornell University throughout the duration of this study.

The authors also acknowledge the assistance and contributions of Paul Reifler, Inc. (Mr. Tom Tallman and Mr. Bill Haas) and Master Builders, Inc. (Mr. Jim Shea) for materials toward the construction of the model building. Their devoted assistance was key to the success of the project.

A special thanks is expressed to the laboratory technicians, Dan Walch, Mark Pitman, Dick Cizdziel, Xiaoqing Gao, and Paul Pattarroyo for their help and expertise during the construction and testing of the model. Thanks are also extended to all the undergraduate students who took an active part in the construction of the model. Their dedication to this project is gratefully acknowledged.

TABLE OF CONTENTS

SECTION	TITLE	PAGE
1	INTRODUCTION	
1.1	Background.....	1-1
1.2	Previous Studies Related to Lightly Reinforced Concrete Frame Buildings	1-4
1.2.1	Column Strength and Ductility	1-4
1.2.2	Beam Strength and Ductility	1-6
1.2.3	Beam-Column Joints	1-7
1.2.4	Frame Model Structures	1-8
1.3	Concluding Remarks on Previous Studies on R/C Buildings	1-9
1.4	Overall Objectives of Research Program	1-10
1.5	Collabrative Studies of LRC Frame Structures	1-11
1.6	Scope of this Report	1-13
2	PROTOTYPE R/C FRAME STRUCTURE	
2.1	Introduction	2-1
2.2	Structural Layout	2-1
2.3	Design Loads	2-3
2.4	Slab Design.....	2-4
2.5	Beam Analysis and Design.....	2-6
2.6	Column Design.....	2-9
2.7	Joint Design	2-12
2.8	Summary Discussions	2-15
3	ONE-THIRD SCALE R/C FRAME MODEL	
3.1	Introduction	3-1
3.2	Model Geometry.....	3-2
3.3	Model Materials.....	3-8
3.3.1	Concrete Properties	3-8
3.3.2	Reinforcing Steel Properties	3-15
3.3.2.1	Heat Treatment of Steel Reinforcement.....	3-16
3.4	Reinforcement Details	3-17
3.5	Mass Similitude	3-23

TABLE OF CONTENTS (cont.)

SECTION	TITLE	PAGE
3.6	Instrumentation.....	3-26
3.6.1	Load Cells	3-30
3.6.2	Displacement Transducers	3-30
3.6.3	Accelerometers.....	3-31
3.6.4	Linear Potentiometers	3-31
3.6.5	Data Acquisition System.....	3-31
3.7	Testing Program	3-33
3.7.1	Identification of Structural Dynamic Properties	3-33
3.7.2	Selection of Ground (Shaking Table) Excitation.....	3-34
3.7.3	Selection of Peak Ground Accelerations.....	3-37
3.7.4	Shaking Table Testing Program.....	3-39
4	IDENTIFICATION OF DYNAMIC CHARACTERISTICS - ELASTIC RESPONSE	
4.1	Introduction	4-1
4.2	Identification Procedures.....	4-2
4.2.1	Frequency Domain Identifications.....	4-2
4.2.1.1	Modal Shapes	4-2
4.2.1.2	Damping Characteristics	4-7
4.2.2	Identification of Structural Stiffness and Damping	4-8
4.2.3	Internal Energy Quantification.....	4-10
4.3	Experimental Results.....	4-12
4.3.1	Impact Hammer Test.....	4-12
4.3.2	Pull-Back Tests	4-14
4.3.3	Snap-Back Tests.....	4-15
4.3.4	White Noise Test.....	4-17
4.4	Dynamic Characteristics of Model.....	4-19
4.4.1	Properties of Unloaded Model - Impact Hammer Test.....	4-19
4.4.2	Properties of Loaded Model - Pull-Back Tests	4-21
4.4.3	Properties of Loaded Model - Quick Release (Snap-Back) Free Vibration Tests.....	4-22

TABLE OF CONTENTS (cont.)

SECTION	TITLE	PAGE
4.4.4	Properties of Loaded Model - Initial White Noise Excitation on Shaking Table.....	4-26
4.5	Analytical Identification of Dynamic Characteristics	4-33
4.5.1	Comparison of Analytical and Experimental Dynamic Characteristics	4-35
4.6	Response to Minor Earthquake	4-38
4.6.1	Global Response.....	4-38
4.6.2	Local Response	4-39
4.6.3	Dynamic Properties after Minor Shaking	4-41
4.7	Summary Discussions	4-71
5	CONCLUSIONS.....	5-1
6	REFERENCES	6-1
	APPENDIX A SCALING FACTORS FOR MODELING OF DYNAMIC BEHAVIOR.....	A-1
	APPENDIX B GEOMETRIC LAYOUT, STRAIN GAGING, AND CALIBRATION CHARTS OF LOAD CELLS.....	B-1

LIST OF FIGURES

FIGURE	TITLE	PAGE
1-1	Current Research Program	1-2
2-1	General Layout of the Idealized Prototype Building.....	2-2
2-2	Slab Reinforcement Details	2-5
2-3	Frame Subassemblage and Loading	2-6
2-4	Bending Moment Design Envelop and Strengths	2-10
2-5	Beam Details	2-11
2-6	Interaction Diagrams for the Columns	2-13
2-7	Column Reinforcement Details	2-14
3-1	General Layout of the Prototype Building	3-3
3-2	General Layout of the Model Structure	3-4
3-3	Model Structure on the Shaking Table	3-7
3-4	Gradation Analysis of the Concrete Mix.....	3-10
3-5	Sequence of Concrete Pouring of the Model.....	3-10
3-6	Stages in the Construction of the Model	3-11
3-7	Average Concrete Specimen Strength Versus Time	3-13
3-8	Concrete Stress-Strain Relations from 4 in. x 8 in. Representative Test Cylinders.....	3-14
3-9	Measured Representative Stress-Strain Relationships of the Reinforcing Steel	3-16
3-10	Layout of Slab Steel Reinforcement.....	3-18
3-11	Details of Beam Steel Reinforcement	3-19
3-12	Typical Beam and Slab Reinforcements	3-21
3-13	Detail of the Column Steel Reinforcement	3-22
3-14	Concrete Blocks on the Model	3-27
3-15	Lead Bricks on the Model	3-29
3-16	Instrumentation Identification and Locations.....	3-32
3-17	Ground Motions for the Taft N21E Accelerogram Component.....	3-35
3-18	Elastic Response Amplifications for the Scaled Taft N21E Component	3-36
4-1	Typical Frequency Response for Determining Damping Characteristics	4-7
4-2	Story Transfer Functions from an Impact Hammer Test.....	4-13
4-3	Pull-Back Loading and Displacement Measurement Loacations.....	4-14

LIST OF FIGURES (cont.)

FIGURE	TITLE	PAGE
4-4	Third Story Displacement Response from a Third Floor Snap	4-15
4-5	Acceleration Story Response from that Story Snap	4-16
4-6	Base Acceleration Motion of the White Noise Excitation, WHN_B	4-17
4-7	Story Level Acceleration Response from WHN_B.....	4-18
4-8	Fourier Transform of the Story Level Accelerations from the Snap-Back Tests.....	4-24
4-9	Inverse Fourier Transform of Filtered Frequencies.....	4-25
4-10	Fourier Transform of the Base Acceleration Motion for WHN_B	4-29
4-11	Transfer Functions of the Story Level Accelerations from WHN_B.....	4-30
4-12	Smoothed Transfer Functions of the Story Level Accelerations from WHN_B.....	4-31
4-13	Story Shear versus Inter-Story Drift Histories for WHN_B	4-32
4-14	Shaking Table Motion for the Taft N21E Base Motion, PGA 0.05 g.....	4-47
4-15	Story Displacement Time Histories for TFT_05.....	4-48
4-16	Story Shear Force Time Histories for TFT_05.....	4-49
4-17	Overlaid Global Response Time History Segments for TFT_05	4-50
4-18	Story Displacements and Shears at Maximum First Story Drift for TFT_05	4-51
4-19	Story Shear versus Inter-Story Drift Histories for TFT_05.....	4-52
4-20	Energy Time History for TFT_05	4-53
4-21	Member Designation	4-54
4-22	Base Column Shear Forces for TFT_05	4-55
4-23a	Interaction Histories for the South-East Columns from TFT_05.....	4-56
4-23b	Interaction Histories for the North-East Columns from TFT_05.....	4-57
4-24a	First Story Beam Bending Moment Time Histories for TFT_05 - South Side	4-58
4-24b	First Story Beam Bending Moment Time Histories for TFT_05 - North Side	4-59
4-25a	Moment versus Curvature for TFT_05 - Exterior Joint	4-60
4-25b	Moment versus Curvature for TFT_05 - Interior Joint	4-61
4-26	Moment Diagram at Maximum First Story Drift from TFT_05	4-62
4-27	Observed Structural Damage after TFT_05	4-63
4-28	Measured Damage State of the Model after TFT_05.....	4-64

LIST OF FIGURES (cont.)

FIGURE	TITLE	PAGE
4-29	Transfer Functions of the Story Level Accelerations from WHN_C.....	4-65
4-30	Smoothed Transfer Functions of the Story Level Accelerations from WHN_C.....	4-66
4-31	Story Shear versus Inter-Story Drift Histories for WHN_C	4-67
4-32	Transfer Functions of the Story Level Accelerations from WHN_D.....	4-68
4-33	Smoothed Transfer Functions of the Story Level Accelerations from WHN_D.....	4-69
4-34	Story Shear versus Inter-Story Drift Histories for WHN_D	4-70
B-1	Load Cell Geometric Layout	B-3
B-2	Strain Gage Positioning and Wiring.....	B-4
B-3	Load Cell Calibration Setup	B-5
B-4	Calibration Curves for a Typical Load Cell	B-6

LIST OF TABLES

TABLE	TITLE	PAGE
1-1	NCEER Publications Summarizing Current Study.....	1-12
2-1	Design Loads for the Building	2-3
2-2	Slab Design	2-4
2-3	Yield Line Theory Analysis	2-7
2-4	Design Beam Bending Moments	2-8
2-5	Design Actions of the Columns	2-9
3-1	Mix Design Formula for the Model Concrete.....	3-8
3-2	Concrete Properties of the Model Structure.....	3-13
3-3	Reinforcing Steel Properties of the Model Structure	3-15
3-4	Shaking Table Testing Sequence for the Model	3-40
4-1	Identification Testing Program of Model.....	4-1
4-2	Dynamic Characteristics of the Unloaded Model	4-37
4-3	Dynamic Characteristics of the Loaded Model.....	4-37
4-4	Maximum Response for Minor Earthquake TFT_05.....	4-39
4-5	Dynamic Properties and Stiffness Matrix before and after TFT_05.....	4-43
4-6	Low Amplitude Initial Stiffnesses from the Shear versus Inter-Story Drift Histories	4-44
4-7	Analytical and Experimental Comparison of the Dynamic Properties	4-44
4-8	Dynamic Properties and Stiffness Matrix after TFT_05 from WHN_C and WHN_D	4-46
4-9	Low Amplitude Initial Stiffnesses from the Shear versus Inter-Story Drift Histories	4-46

SECTION 1

INTRODUCTION

1.1 Background

The study presented herein is part of a comprehensive research program sponsored by the National Center for Earthquake Engineering Research (NCEER) on the seismic damage assessment and performance evaluation of buildings in zones of low seismicity, such as in the Eastern and Central United States. Buildings in such zones are typically designed only for gravity loads ($U = 1.4D + 1.7L$, herein referred to as GLD) according to the non-seismic detailing provisions of the code. These buildings are also termed lightly reinforced concrete (LRC) structures throughout this study. Although such structures are designed without consideration of lateral loads, they still possess an inherent lateral strength which may be capable of resisting some minor and moderate earthquakes. However the deficient detailing of members can lead to inadequate structural performance during seismic activity.

Two main parts from the current study (i) a seismic performance **Evaluation** of gravity load designed R/C Frame Buildings and (ii) an evaluation of seismic **Retrofit** of R/C frame structures. The first part will be mentioned as **Evaluation** and the second as **Retrofit**.

A research program on the **Evaluation of the seismic performance of gravity load designed R/C frame buildings** was developed and carried out according to the plan outlined in Fig. 1-1.

Based on a survey of typical building construction practices in the Eastern and Central United States (Lao, 1990 and El-Attar et al., 1991a and 1991b), a one-third scale model was constructed and tested on the shaking table in the State University of New York (SUNY) at Buffalo Earthquake Simulation Laboratory. The prototype design, model construction and similitude, initial dynamic characteristics, shaking table testing program along with the simulated ground motions, and the elastic response of the model from minor base motions are presented in Part I of the Evaluation Report Series (this report). Based on this report, analytical models can be developed and used to predict the inelastic response of the model building during more severe earthquakes.

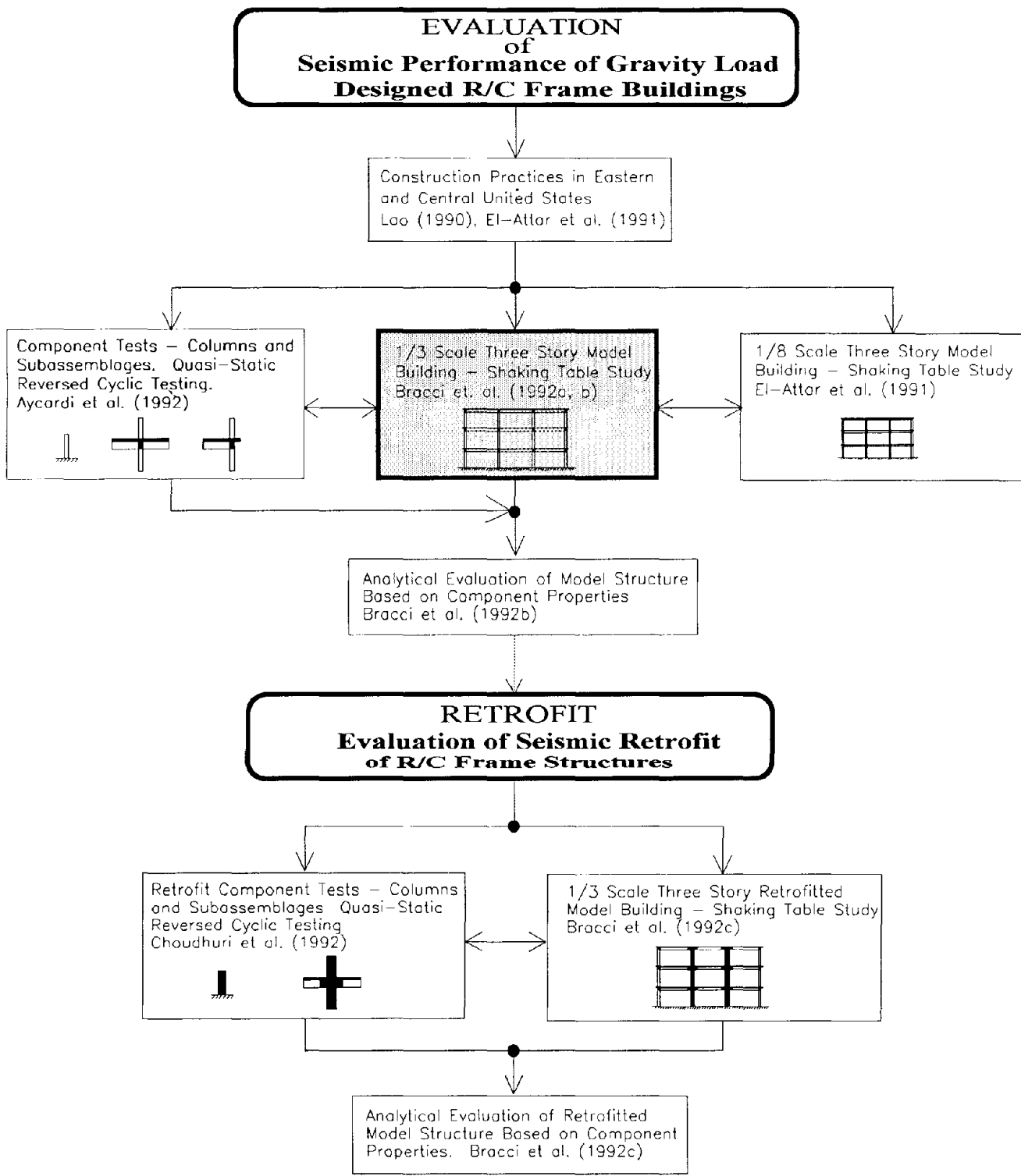


FIG. 1-1 Research Context - Seismic Performance of Gravity Load Designed Reinforced Concrete Frame Buildings

Companion reduced scale slat-beam-column subassemblages were also constructed with the same materials in conjunction with the construction of the one-third scale model building are presented in Part II of the Evaluation Report Series (Aycardi et al., 1992). The components were tested under quasi-static reversed cyclic loading and conducted prior to the testing of the model building. The results of the component tests were used to identify the behavior of localized members and subassemblages of the structure and the member properties for predicting the overall response of the model building with analytical tools.

The experimental and analytical performance of the model building during moderate and severe shaking is presented in Part III of the Evaluation Report Series (Bracci et al., 1992a). The analytical predictions of the model building during these earthquakes are presented based on member behavior developed from engineering approximations and component tests. Some of the conclusions of the evaluation study are that the response of the model is governed by weak column - strong beam behavior and large story drifts develop under moderate and severe earthquakes. A one-eighth scale model of the same prototype building was also constructed and tested at Cornell University by El-Attar et al. (1991b) as part of a collaborative study with SUNY/Buffalo. A comparison of the response behavior between the two scale models is also presented.

A second part of this research program was conducted to evaluate various **seismic retrofit techniques for R/C frame structures** typically constructed in low seismicity zones (see Fig. 1-1). Based on the seismic behavior of the one-third scale model from the previous study, a series of retrofit schemes were proposed for improved seismic resistance and presented Part II of the Retrofit Report Series (Bracci et al, 1992b).

In Part I of the Retrofit Report Series (Choudhuri et al., 1992) of this research program, a capacity analysis and redesign method for seismic retrofitting of R/C structures is developed and tested. Retrofit using an improved concrete jacketing technique was selected and first performed on companion components. The retrofitted components were then tested under quasi-static reversed cyclic loading and used to identify the behavior of the individual members. Retrofit of the components was also performed to verify the constructability of the retrofit technique for the model building.

The work done in Part I of the Retrofit Report Series is used as base to evaluate and model the member properties of the beam column components with the concrete jacketing technique and is used further for predicting the response of the overall retrofitted model building with analyses

presented in Part II of the Retrofit Report Series (Bracci et al, 1992b). Based on analytical estimates, a global seismic retrofit for the one-third scale model building was proposed and constructed. An experimental and analytical shaking table study of the retrofitted model building was then conducted and the response behavior is presented. The main conclusions from this study are that seismic retrofit of gravity load designed R/C frame buildings: (i) can be designed to successfully enforce a strong column - weak beam behavior; and (ii) is a viable economic and structural alternative as compared to demolition and reconstruction of another.

1.2 Previous Studies Related to Lightly Reinforced Concrete Frame Buildings

In an attempt to determine the behavior of gravity load designed buildings during seismic events, the following outlines some of the previous work conducted on non-seismically and seismically detailed reinforced concrete (R/C) components and frame models under the influence of large lateral loads. However, most of the recent research has been focused on appropriate detailing for the most adverse seismic design scenario. Little work has been done on poorly detailed R/C elements.

1.2.1 Column Strength and Ductility

Reversed cyclic response of R/C columns have been studied by several investigators to determine the influence of important variables such as: varying axial loads, confinement, location of lap splices and construction joints, LRC columns, etc.

Paulay et al. (1981) tested a number of well detailed R/C columns of octagonal and square cross sections with lap splices in the plastic hinge regions. For the square columns, the longitudinal bars were cranked inward at the lap. They showed that the columns performed satisfactorily for displacement ductilities up to 4. There was no evidence of bond slip at the laps and the lateral pressures from the confining steel in the plastic hinge region improved anchorage. However, yielding of the longitudinal reinforcement was restricted to a very small length adjacent to the critical section, which resulted in extremely high longitudinal steel strains. The spirally confined octagonal column was tested with side-by-side laps of the longitudinal reinforcement. It was found that spalling of the cover concrete occurred and created poor local bond conditions for the lap region. Their conclusions were that lapped splices in potential plastic hinge regions should only be used when the design level of structural displacement ductility is less than 3.0 and lapping should be done by cranking the bars into the core concrete rather than by side-by-side lapping.

Abrams (1987) studied the effect of varying the axial load in LRC columns. It was shown that additional axial load on columns increase the stiffness, flexural strength, and shear capacity. However, Saatciogle and Ozcebe (1989) report that added axial loads also increase stiffness degradation and energy dissipation of the section.

Priestley and Park (1987) summarized an extensive study on the performance of various well detailed concrete bridge columns subjected to combined axial load and bending. Their results indicate that current methods (ACI-318) for predicting flexural strength underpredicts the true flexural capacity due to the enhanced concrete strength from confinement and strain hardening of the longitudinal reinforcement. A new design method was proposed for predicting the flexural strength and ductility of confined bridge columns.

Mander et al. (1988a) conducted tests on well detailed R/C short columns with circular, square, and rectangular cross sections. Various arrangements of longitudinal and transverse reinforcement were investigated to study the effect of confinement on the stress-strain curve in terms of strength and ductility. The quantity of the confining steel was shown to have been a significant parameter in member response and strength. In a companion paper, Mander et al. (1988b) also developed an analytical stress-strain model for confined concrete.

Panahshahi et al. (1992) performed full-scale experimental tests to study the behavior of compression lap splices in reinforced concrete members subject to high-level repeated cyclic loads. They concluded that compression lap splices can be designed to sustain a minimum of 12 inelastic cycles, with a maximum bar strain of at least three times the yield strain. A design splice length of $35 d_b$ was recommended for grade 60 reinforcement with a clear cover of at least $1.5 d_b$ and a minimum concrete strength of 4 ksi. Closely spaced, uniformly distributed stirrup-ties were also recommended along the entire splice length and extending an effective depth d beyond the splice.

Azizinamini et al. (1992) performed full-scale testing of columns with different transverse reinforcement details. They showed that the flexural capacity of columns increased with axial load but ductility reduced considerably. With additional transverse reinforcement, the ductility capacity of the column increased with the limiting strain being well above 0.003.

1.2.2 Beam Strength and Ductility

Since the design philosophy of strong column - weak beam is desired under seismic excitations, the following researchers have studied some of the effects of hinge occurrence in beams.

Paulay and Bull (1979) and Park and Milburn (1983) studied the effect of relocating the potential beam plastic hinges from the face of the columns. It was suggested from their studies to move the potential beam hinge the smaller distance of either the beam height or 500 mm. from the column face. Buchanan (1979) also constructed spandrel beams by moving the potential beam hinge toward the center of the span. Paulay and Priestley (1992) also summarized some of this and other related work.

Nmai and Darwin (1984) quasi-statically tested several lightly reinforced concrete cantilevered beams of varying reinforcement ratios, nominal stirrup capacities, stirrup spacing, and ratios of positive to negative reinforcement. They concluded from the cyclic tests that: (i) the low reinforcement ratio reduces the maximum shear and compressive stresses in beams; (ii) a reduced stirrup spacing and an increased positive to negative steel ratio increases the total energy dissipation capacity. However the increase positive to negative steel ratio also increases the induced shear and the energy demand; (iii) a decrease in maximum shear stress, an increase in concrete strength, and an increase in nominal stirrup capacity will improve the performance of R/C beams.

Al-Haddad and Wight (1986) performed an analytical study on the feasibility and consequences of moving the potential beam plastic hinge zones a certain distance from the column face. Their design guidelines suggest to locate the potential beam hinges one beam depth from the column face.

Al-Nahlawi and Wight (1989) studied the shear behavior of LRC beams with and without web reinforcement and with 1% longitudinal reinforcement. The stirrup spacing in the beams were varied from 0 to $d/3$ (d = beam depth). An equation was developed for providing minimum transverse reinforcement in beams. It was shown that the minimum transverse reinforcement ratio increased with concrete strength, which is in contrast of the ACI-318.

Soroushian and Choi (1989) studied the cyclic bond deterioration of varying diameter beam reinforcement in confined concrete beam members due to repeated inelastic cycling. They showed that the bond strength decreases as the bar diameter increases and a slight increase occurred in the prepeak local bond tangent stiffness as the bar diameter decreases.

Slab Width Effects

Wallace and Krawinkler (1984) quasi-statically tested small scale beam-column joints and compared their results to similar full scale tests. They concluded that the slab width from ACI-318 grossly underestimates the slab contribution to beam moment capacity. However with full slab width contribution of slab steel, the moment capacity is overestimated.

Durrani and Wight (1987) quasi-statically tested seismically detailed beam-column joints with transverse beams and a floor slab. They showed that the slab had a significant contribution in the moment capacity of the beams. The flexural strength of the columns were 1.9 times greater than the beams without the slab and were only 1.3 times greater with the slab. They concluded that ignoring the slab effects in the beam moment capacity might lead to erroneous evaluation of the collapse mechanism which may in turn lead to a weak-column-strong-beam failure instead of a desired strong-column-weak-beam mechanism.

Wolfgram-French and Boroojerdi (1989) quasi-statically tested well-detailed one-half scale R/C beam-column-slab joints to determine the influence of the torsional stiffness of the transverse beams on the effective slab width participation. They concluded that the effective width of slab was greater for models with increased torsional stiffness. At an inter-story drift of 2%, the measured flexural strengths were within 10% of the strength which considers the slab flange width from ACI-318. However the maximum measured flexural strengths exceeded the strength using the ACI-318 slab flange width by about 37% and was about 20% less than the strength using the full slab flange width. It was found that the moment strength with a slab flange width of about one-third the span length on each side of the beam was similar to the maximum measured moments.

The established text by Park and Paulay (1975) provides an overview of beam strength and ductility capacities in well-detailed R/C structures. A more current text by Paulay and Priestley (1992) expands on the more recent developments.

1.2.3 Beam-Column Joints

Paulay (1989) showed, through equilibrium, the internal force distributions of seismically loaded beam-column joints for determining maximum joint shear stresses. He found that the interior forces rearrange themselves after the tensile strength of the core concrete is lost due to diagonal cracking. He also showed that beams dilate rather than confine joint cores. Therefore the width

of the beam relative to the width of the column is irrelevant in terms of joint performance. However, beams that run transverse to the direction of motion provide some beneficial confinement of the joint cores. The performance of interior joints loaded in two orthogonal directions was consistently found to be deficient as compared to the performance of identically reinforced joints in one-way loading.

Zerbe and Durrani (1990) indicated that the slab has a significant effect on the joint stiffness and strength. For joint shear design, it was recommended that the effective slab of twice the beam depth on each side be used. Furthermore the slab participation was found to reduce stiffness degradation and be dependent on the story drift.

Pessiki, Conley, Gergely, and White (1990) tested several LRC beam-column joints with typical reinforcement details found in the Central and Eastern United States which include: (i) lightly confined lap splices in columns just above story level; (ii) discontinuous beam reinforcement in the beam-column joints; (iii) little or no joint confining steel; (iv) construction joints located above and below beam-column joints. However, the specimens did not include transverse beams or slabs, the importance of which were previously discussed. It was observed that pull-out of the discontinuous beam reinforcement was the mode of failure in this joint and the column lap splice (and construction joint) location was not critically damaged. The recorded joint shears with discontinuous beam reinforcement were about 20% smaller than the shears with continuous beam reinforcement.

1.2.4 Frame Model Structures

Although component testing can be used to identify various parameters, behaviors, and deficiencies of individualized members and components of structures, full model testing is required to capture the overall response characterizations of structures. The following studies include some scale model R/C building tests conducted on shaking tables.

Wilby et al. (1973) tested a seismically designed 1/5 scale, one-bay by one-bay six story R/C model on the shaking table. They observed that a significant reduction (80%) in the model stiffness occurred from shaking, which was attributed to poor bond of the model reinforcement (plain wires). The transverse (with respect to the input motion) beams increased the model stiffness by about 18%. However, these beams suffered severe torsional cracks at the conclusion of testing. They reported that an accurate prediction of the model stiffness and damping was essential for the analytical models.

Blondet et al. (1980) performed shaking table tests on a seismically designed 7/10 scale two story, one-bay by one-bay office building. However, due to small column loads, the flexural strength of the beams were 50% stronger than the column. They concluded that: (i) the model stiffness was much less than predicted using gross section properties and the ACI-318 formula for elastic modulus; (ii) the response was governed by the first mode; and (iii) most of the damage resulted in the columns of the first floor with an incipient soft-story collapse mechanism.

Bertero et al. (1984), in a US-Japan cooperative earthquake research program, performed shaking table tests on a seismically designed 1/5 scale seven story, two-bay by three-bay R/C frame-wall structure. They concluded the importance of the following: (i) the three dimensional interaction of the wall-frame system due to deformation variations between the walls and the frames; (ii) the significant effects of axial load variations on the lateral stiffness, column strength, and wall strength; (iii) the importance of controlling the amount of shear at the critical regions of the main members of the structure; and (iv) the tremendous contributions of the floor slab to the ultimate strength of the structure.

Shahrooz and Moehle (1987) performed shaking table tests on a seismically designed (ACI-318-83) 1/4 scale six-story, two-bay by two-bay R/C framed structure with 50% setback at its midheight. The test structure reached a base shear demand in excess of seven times the design base shear. Several factors were identified for the overstrength: (i) the contribution of the floor slab to beam flexural strength; (ii) column and beam overstrength resulting from detailing requirements; and (iii) actual material properties.

1.3 Concluding Remarks on Previous Studies on R/C Buildings

It should be noted that most of the preceding studies focused on examining the performance of buildings for the most adverse seismic events and systematically searching for the benefits of good detailing. It appears that little work has been done on the performance of poorly detailed structures during seismic events of varying intensity ground motions, which can be representative of minor, moderate, and severe earthquakes. The present study attempts to address the following for the varying intensity ground excitations: (i) identifying the strengths and deficiencies of such structures; (ii) identifying the behavior of individual members and components; and (iii) identifying the overall behavior of the structure and possible collapse mechanisms.

Another shortcoming of the previous studies is that there is no link between the behavior of individual members (and components) and the behavior of the overall structural system. A main objective of the current study is to explore the possibility of integrating the behavior and properties of individual members from component testing to develop analytical tools for predicting the seismic response of the overall structure.

1.4 Overall Objectives of Research Program

The objectives of the overall research program are summarized below along with the corresponding NCEER publications from Table 1-1:

1. Investigate the performance and principal deficiencies of typical LRC frame buildings during earthquakes through shaking table testing of a one-third scale model under minor, moderate, and severe earthquakes. (*Seismic Resistance of R/C Frame Structures Designed only for Gravity Loads: Parts I and III*, Evaluation report series, by J.M. Bracci, A.M. Reinhorn, and J.B. Mander)
2. Identify the potential collapse mechanisms for typical LRC frame buildings. (*Seismic Resistance of R/C Frame Structures Designed only for Gravity Loads: Part III*, Evaluation report series, by J.M. Bracci, A.M. Reinhorn, and J.B. Mander)
3. Determine the behavior and material properties of individual members and sub-assemblages of the structure. (*Seismic Resistance of R/C Frame Structures Designed only for Gravity Loads: Part II*, Evaluation report series, by L.E. Aycardi, J.B. Mander, and A.M. Reinhorn)
4. Determine the contribution of components in the overall response of the structure near collapse. (*Seismic Resistance of R/C Frame Structures Designed only for Gravity Loads: Parts II and III*, Evaluation report series, by J.M. Bracci, L.E. Aycardi, A.M. Reinhorn, and J.B. Mander)
5. Compare the measured response of the model building with that predicted by analytical models developed from engineering approximations or from component tests using a non-linear time history dynamic analysis. (*Seismic Resistance of R/C Frame Structures Designed only for Gravity Loads: Part III*, Evaluation report series, by J.M. Bracci, A.M. Reinhorn, and J.B. Mander)

6. Investigate appropriate local and global retrofit techniques for improving the seismic performance of LRC buildings. (*Evaluation of Seismic Retrofit of R/C Frame Structures: Part II*, Retrofit report series, by J.M. Bracci, A.M. Reinhorn, and J.B. Mander)
7. Investigate the seismic performance of the retrofitted model building and compare the measured response with the response of the original (unretrofitted) model from the same earthquakes. (*Evaluation of Seismic Retrofit of R/C Frame Structures: Part II*, Retrofit report series, by J.M. Bracci, A.M. Reinhorn, and J.B. Mander)
8. Determine the behavior and material properties of the retrofitted members and subassemblages of the structure. (*Evaluation of Seismic Retrofit of R/C Frame Structures: Part I*, Retrofit report series, by D. Choudhuri, J.B. Mander, and A.M. Reinhorn)
9. Determine the contribution of retrofitted and unretrofitted components in the overall response of the structure near collapse. (*Evaluation of Seismic Retrofit of R/C Frame Structures: Part I*, Retrofit report series, by D. Choudhuri, J.B. Mander, and A.M. Reinhorn)
10. Compare the measured response of the retrofitted model building with that predicted by analytical models developed from engineering approximations or from component tests using a non-linear time history dynamic analysis. (*Evaluation of Seismic Retrofit of R/C Frame Structures: Part II*, Retrofit report series, by J.M. Bracci, A.M. Reinhorn, and J.B. Mander)

1.5 Collaborative Studies of LRC Frame Structures

El-Attar et al. (1991a and 1991b) performed a study on the seismic behavior of LRC frame buildings using small scale model testing. Two models were constructed: (1) a one-sixth scale two story, one-bay by one-bay office building (El-Attar et al., 1991a); and (2) a one-eighth scale three story, one-bay by three-bays office building (El-Attar et al., 1991b). The latter model was a smaller scale replica of the model presented in this study and was part of a collaborative study by Cornell University and SUNY at Buffalo on LRC framed structures typically constructed in low seismicity zones. The reinforcement details were based on construction practices in the Eastern and Central United States since the early 1900's. Shaking table tests were performed

TABLE 1-1 NCEER Publications Summarizing Current Study

EVALUATION SERIES:
Seismic Resistance of R/C Frame Structures Designed only for Gravity Loads
<i>Part I: Design and Properties of a One-Third Scale Model Structure</i> (by J.M. Bracci, A.M. Reinhorn, and J.B. Mander), NCEER-92-0027
<ul style="list-style-type: none"> (i) Identification of deficiencies of current engineering practice. (ii) Scale modeling. (iii) Experimental identification of structural characteristics. (iv) Ground motions for structural evaluation and experimental program. <p>Note: This report serves as bare material for evaluation of analytical tools.</p>
<i>Part II: Experimental Performance of Subassemblages</i> (by L.E. Aycardi, J.B. Mander, and A.M. Reinhorn), NCEER-92-0028
<ul style="list-style-type: none"> (i) Identify behavior and deficiencies of various components in structures. (ii) Identify member characteristics for developing analytical models to predict the seismic response of the one-third scale model structure. <p>Note: This report serves as evaluation of structural characteristics to be incorporated in the evaluation of the entire structural system.</p>
<i>Part III: Experimental Performance and Analytical Study of Structural Model</i> (by J.M. Bracci, A.M. Reinhorn, and J.B. Mander), NCEER-92-0029
<ul style="list-style-type: none"> (i) Investigate the performance and principal deficiencies of typical gravity load designed frame buildings during earthquakes through shaking table testing of a one-third scale model under minor, moderate and severe earthquakes. (ii) Identify the potential collapse mechanisms for such typical frame buildings. (iii) Compare the measured response of the model building with that predicted by analytical models developed from (1) engineering approximations, (2) component tests, and (3) an experimental fit using a non-linear time history dynamic analysis. <p>Note: This report emphasizes the structural behavior, collapse margins via damage, and efficiency of predictions using component properties evaluated from tests.</p>

RETROFIT SERIES:
Evaluation of Seismic Retrofit of R/C Frame Structures
<i>Part I: Experimental Performance of Retrofitted Subassemblages</i> (by D. Choudhuri, J.B. Mander, and A.M. Reinhorn), NCEER-92-0030
<ul style="list-style-type: none"> (i) Presentation of retrofit techniques. (ii) Identify constructability and behavior of retrofitted components. (iii) Identify retrofitted member characteristics for developing analytical models to predict seismic response of the retrofitted model building.
<i>Part II: Experimental Performance and Analytical Study of Retrofitted Structural Model</i> (by J.M. Bracci, A.M. Reinhorn, and J.B. Mander), NCEER-92-0031
<ul style="list-style-type: none"> (i) An analytical seismic evaluation of retrofitted gravity load designed frame buildings using various local and global retrofit techniques. (ii) Shaking table testing of one of the proposed retrofit techniques on the 1/3 scale model under minor, moderate, and severe earthquakes. (iii) Verify a change in formation of the potential collapse mechanism under ultimate load from an undesirable column-sidesway/soft-story mechanism to a more desirable beam-sidesway mechanism. (iv) Compare the measured response of the retrofitted model building with that predicted by analytical models developed from engineering approximations and component tests using a non-linear time history dynamic analysis.

using the scaled Taft S69E accelerogram at various levels of peak ground acceleration. The behavior of the two story model was summarized as follows: (i) The response was dominated by the first mode of vibration; (ii) Very large deformations occurred with severe stiffness degradation; (iii) Plastic hinges and flexural cracks formed in the columns outside the joint panel above and below the slab. No hinging was observed in the beams; (iv) Column lap splices were not critical; (v) Damage was primarily concentrated to the first story; and (vi) Pull-out of the discontinuous rebars was observed at a severe PGA.

The behavior of the three story model was summarized as: (i) The response was dominated by the first mode of vibration; (ii) Similar mode shapes were identified throughout the seismic tests; (iii) Very large deformations occurred with severe stiffness degradation; (iv) Significant P-delta effects for the severe earthquakes; (v) The column shears were dependent on axial load and the shear in the interior columns were twice the exterior; (vi) Deformations, damage, and energy dissipation primarily occurred to the first story; (vii) Plastic hinges and flexural cracks formed in the columns outside the joint panel above and below the slab. No hinging was observed in the beams; (viii) Column lap splices were not critical; and (ix) Pull-out of the discontinuous rebars was not observed.

Various references to El-Attar et al (1991a and b) are made throughout this study as a direct comparison of seismic response for the different scale models.

1.6 Scope of this Report

This report presents the design objectives, geometric dimensions, material strengths, and initial dynamic properties of the model building, along with the simulated base motions, so that analytical models can be developed and used to predict the inelastic response of the model building during more severe earthquakes. The initial vibration tests and the response from a minor earthquake are presented to enable analytical structural modeling and verification of elastic response. The following outlines the contents in each section:

Section 2 details the gravity load design of a prototype three-story moment resisting R/C frame building. No considerations are made for seismic resistance and the general non-seismic detailing provisions of ACI-318 are used for this design. The LRC building is considered to be representative of low-rise building construction in the Eastern and Central United States. Finally some of the expected deficiencies and resulting member actions from seismic motions are summarized.

Section 3 firstly presents the design, construction, similitude, and instrumentation of a one-third scale model. Next, the relevant base motions and peak magnitudes of base motion for an experimental study using shaking table excitations are discussed and presented. Finally, the testing program for the model, which includes the structural dynamic identification and earthquake simulation tests, is outlined.

Section 4 outlines a procedure for identifying the dynamic characteristics of a structure from the experimental time history response and the frequency domain story transfer functions. The initial dynamic characteristics of the model and comparisons among identification tests are presented and summarized. Finally, the response of the model during a minor earthquake (elastic response) is presented, along with the subsequent dynamic characteristics.

Section 5 presents a summary and conclusions of the first phase of the research program.

SECTION 2

PROTOTYPE R/C FRAME STRUCTURE

2.1 Introduction

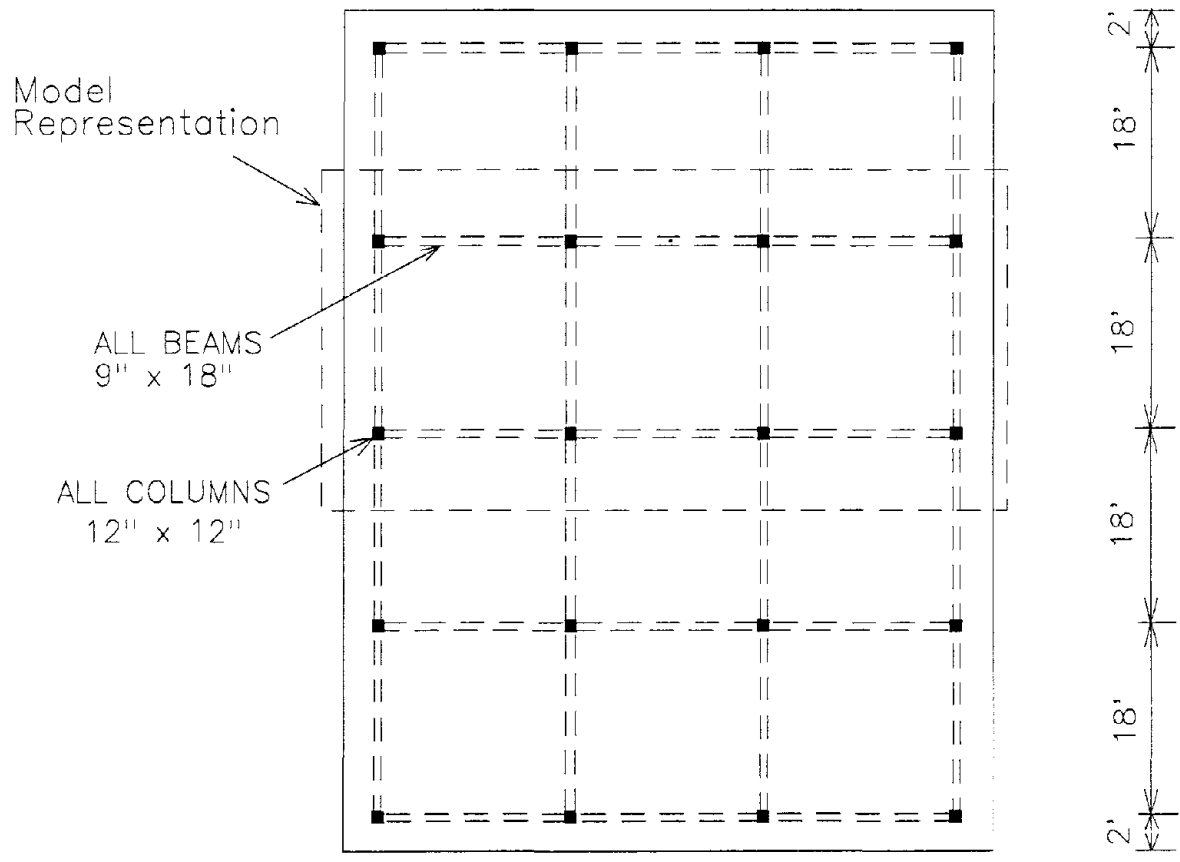
The design of a typical three-story moment resisting reinforced concrete framed structure typically used for offices is presented in this section. The structure is considered to be representative of low-rise buildings constructed in the Eastern and Central United States. Such structures are designed primarily to carry only gravity loads, since wind loads seldom govern for low-rise buildings. Thus no considerations are made for seismic resistance and the general non-seismic detailing provisions of the ACI 318-89 code are used for this design, herein after referred to as the Code.

The prototype structure is selected such that an experimental shaking table test could be performed on a scaled model structure in the State University of New York (SUNY) at Buffalo Earthquake Simulation Laboratory. The limitations of the model structure are based on geometric lengths, height, and weight capacity of the shaking table. Details of the model structure are presented in Section 3.

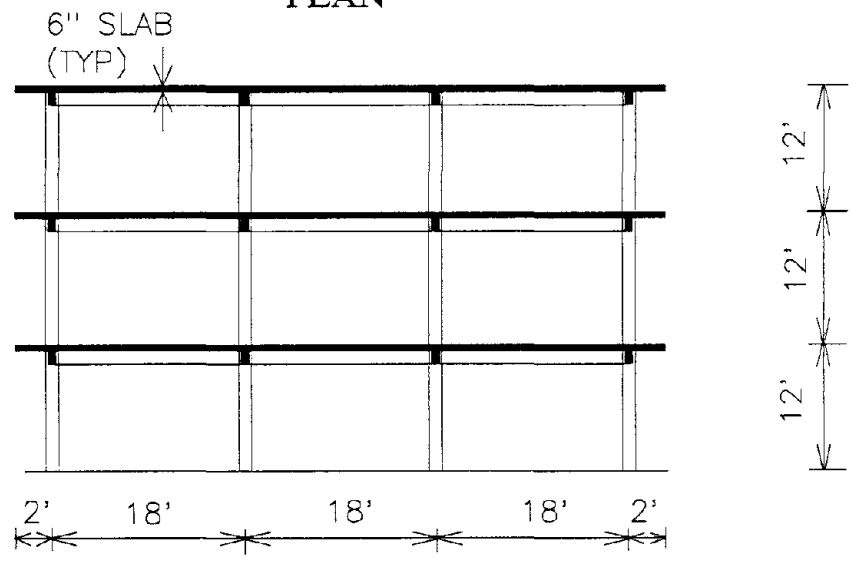
The relative dimensions adapted for the frame members of the idealized prototype structure were based on a survey of typical construction practices in the eastern United States conducted by El-Attar et al. (1991a and 1991b) at Cornell University and Lao (1990) at SUNY at Buffalo. The survey showed that the relative story heights are typically 12 ft. and the bay widths vary from 16 to 30 ft. The basic material strengths assumed for the design of the structure are ASTM 615 Grade 40 steel ($f_y = 40$ ksi) and ordinary Portland cement concrete with a specified 28 day strength (f'_c) of 3,500 psi. The structure is assumed to be built on stiff soil/rock conditions such that no soil-interaction or differential settlements needed to be considered.

2.2 Structural Layout

The general layout of the idealized three-story prototype office building is shown in Fig. 2-1. Due to the shaking table geometric constraints, three 12 ft. story heights with 18 ft. bay widths are adopted herein to enable a one-third scale model to be constructed and tested in the Earthquake Simulation Laboratory. The model structure is representative of the critical interior bay section of the prototype structure.



PLAN



FRONT ELEVATION

FIG. 2-1 General Layout of the Idealized Prototype Building

2.3 Design Loads

The design loads for the typical office building are shown in Table 2-1. The gravity load combination of $1.4 D + 1.7 L$ is the only design loading used to achieve the most adverse stresses in the members of the structure.

TABLE 2-1 Design Loads for the Building

<i>Dead Loads</i>	
Floors and Roof (6 in. slab)	75 psf
Ceilings	9 psf
Interior Partitions	20 psf
Electric and Water	5 psf
Total Slab Dead Load	109 psf
<i>Live Loads</i>	
1 st , 2 nd and Roof**	50 psf
1.4 D + 1.7 L	0.238 ksf
<i>Additional Dead Loads</i>	
Beam Self-Weight	0.113 plf
Column Self-Weight	0.15 plf
Exterior Walls (Curtain Walls)	0.562 plf

** The roof loading, based on snow loads, varies from geographic locations within the United States. For simplicity, the design roof loading is the same as the office loads of the floors below.

2.4 Slab Design

The direct design method from Section 13.6 of the Code is used to design the floor slab. Then the ultimate load capacity of the designed slab is verified using yield line theory, Park and Gambale (1980).

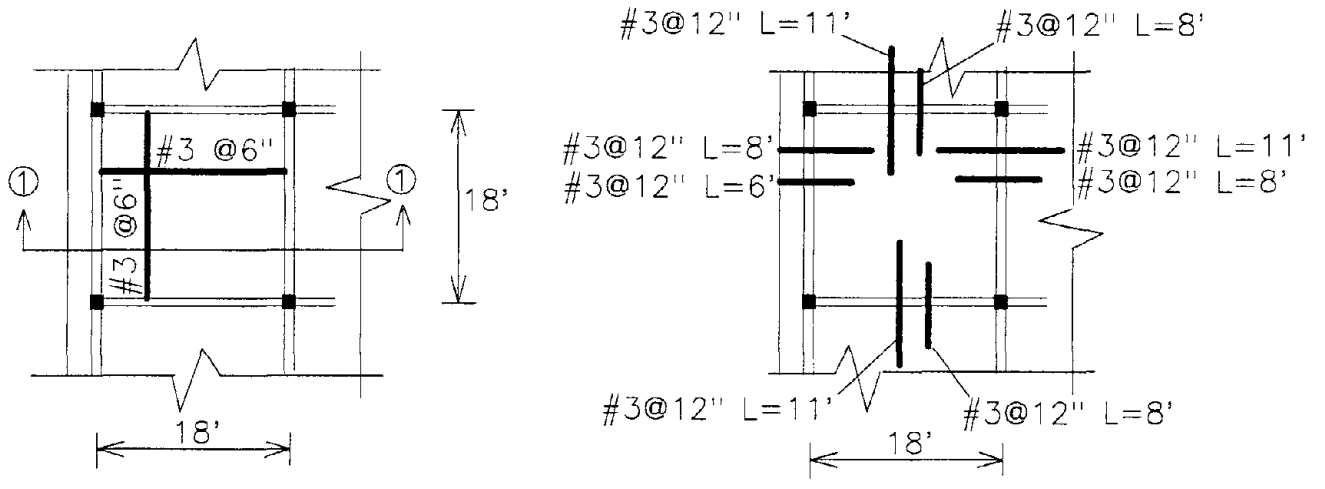
Table 2-2 lists the design and provided moments along with the respective provided reinforcement for an design slab loading of 0.238 ksf (1.4 D + 1.7 L) from Table 2-1 using the direct design method. According to Section 7.12 of the Code, the minimum temperature and shrinkage reinforcement ratio, ρ , for a slab is 0.002 (#3 @ 9"). Based on the design moments and for ease in construction, a doubly reinforced slab is adapted with #3 bars at 6 in. centers ($\rho = 0.003$) in both directions, top and bottom as shown in Fig. 2-2. Curtailment of the slab reinforcement is in accordance with the Code.

The slab reinforcement details are shown in Fig. 2-2.

TABLE 2-2 Slab Design

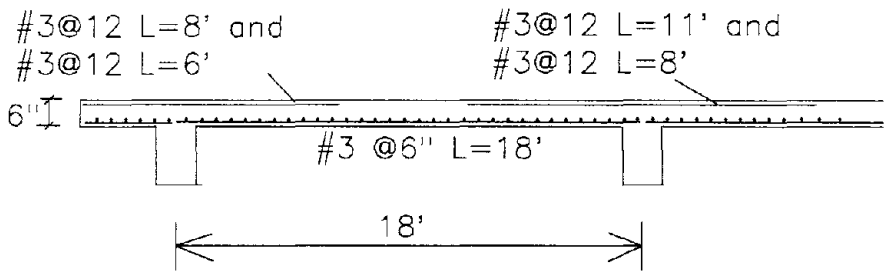
	Exterior Span			Interior Span	
	Exterior Support	Mid-Span	Interior Support	Support	Mid-span
<i>Column Strip (6"x75")</i>					
Design Moment (k-in/in)	-0.892	+1.767	-2.158	-2.017	+1.092
<i>Middle Strip (6"x108")</i>					
Design Moment (k-in/in)	-0.592	+2.733	-3.350**	-3.108	+1.683
Provided Bars	#3 @ 6"	#3 @ 6"	#3 @ 6"	#3 @ 6"	#3 @ 6"
Provided Moment (k-in/in)	-3.258	3.258	-3.258	-3.258	3.258

** Moments may be redistributed by up to 10% in accordance with Clause 13.6.7 of the Code.



a) Bottom Reinforcement

b) Top Reinforcement



C) Section 1-1

FIG. 2-2 Slab Reinforcement Details

It was considered of interest to determine the ultimate strength of the slab by yield line theory. Table 2-3 shows a series of possible collapse mechanisms for the designed slab that are used to determine the ultimate loading capacity. For the interior slab panels, it is assumed that all sides are fully fixed. For the exterior slab panels, it is assumed for the most adverse case that two sides are simply supported and the others are fixed (corner slab panel). For the final collapse mechanism, it is assumed that the negative yield lines start at the end of the top reinforcement with a simply supported end condition (no moment capacity) such that a 10 ft. square yielding panel mechanism would form. It can be observed that the governing ultimate load distribution capacity for the slab is 0.36 ksf for a corner slab, which is 51% above the required design strength of $1.4 D + 1.7 L$.

2.5 Beam Analysis and Design

The design moments of the beams are determined in accordance with the strength provisions of Section 8.9 of the Code under the factored load combinations of $1.4 D + 1.7 L$. The factored live load is placed on two adjacent spans to obtain the most adverse negative bending moments adjacent to the column faces and placed on alternate spans to obtain the maximum mid-span positive bending moments for the beam. Slab loads, placed in the respective beams locations, are composed of two 9 ft. x 18 ft. triangular load distributions from the tributary areas of the beams. Moment distribution is used for the elastic analysis of the frame subassembly under gravity loads as shown in Fig. 2-3.

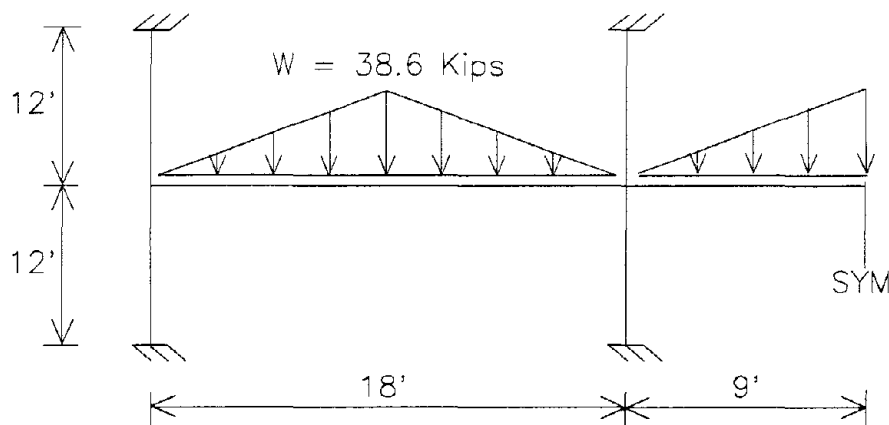
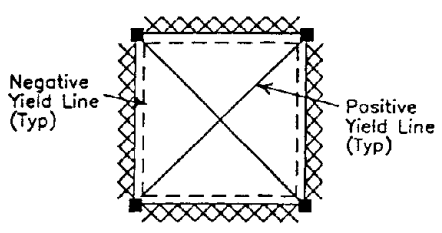
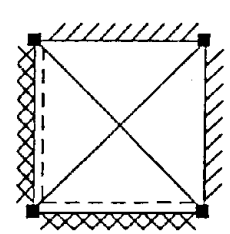
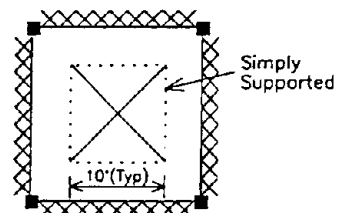


FIG. 2-3 Frame Subassembly and Loading

Table 2-3 Yield Line Theory Analysis

Location	Mechanism	Fixity	Panel Type	w_u (ksf)
Interior Slab		All Sides Fixed	Interior	0.48
Corner Slab		Two Sides Fixed and Simply Supported	Exterior	0.36
Any		All Sides Simply Supported	Any	0.78

Note: ————— = positive (sagging) yield line
 - - - - - = negative (bowing) yield line
 XXXXXX = fixed end condition
 // // // // = simply supported condition

It was also of interest to compare the design moments based on the moment coefficient methods given in Section 8.3 of the Code. This approach can essentially be regarded as an implicit lower bound plastic design solution provided the following conditions are met:

- a) There are two or more spans;
- b) Span lengths are approximately equal;
- c) Loads are uniformly distributed;
- d) Unit live load does not exceed three times the unit dead load;
- e) Members are prismatic.

For compatibility with condition "c" from above, it is assumed that the total beam load is uniformly distributed in contrast to the two triangular distributions.

Table 2-4 shows the design bending moments from the elastic analysis moment distribution method and ACI approximate method of continuous beam analysis. It can be observed that the methods of analysis result in distinctly different mid-span positive design moment in the beams. It is evident that the uniformly distributed load assumption could be unconservative under certain conditions. This can be corrected by noting that the mid-span moments for a simply supported beam increase by 33% for a triangular load distribution in contrast to a uniform load distribution, shown in parenthesis in Table 2-4. Therefore it is concluded that the moment coefficient method provides a satisfactory solution and compares well with the more rigorous elastic analysis.

TABLE 2-4 Design Beam Bending Moments

Direction	Exterior			Interior	
	Ext. Column Face (Kip-in)	Mid-span (Kip-in)	Int. Column Face (Kip-in)	Column Face (Kip-in)	Mid-span (Kip-in)
Frame Analysis	-390	+860	-920**	-880	+570
Moment Coefficient	-516 (wL/16)	+590 (787) (wL/14)	-826 (wL/10)	-750 (wL/11)	+516 (686) (wL/16)

** Section 8.4 of the Code allows for redistribution of negative moments of 13% in accordance with the steel reinforcement ratios.

The nominal bending moment capacities of the beams are shown in Fig. 2-4 along with the different design load cases for each floor from moment distribution and the design moments from the moment coefficient method. Since the positive reinforcement is discontinuous in the beam-column joints, the full moment capacity is achieved a full development length from the end of the rebars. However, for positive moment capacities near the ends, the effective rebar areas are assumed to be reduced by the ratio of the provided and required embedment lengths. Therefore a linear variation in moment capacity exists.

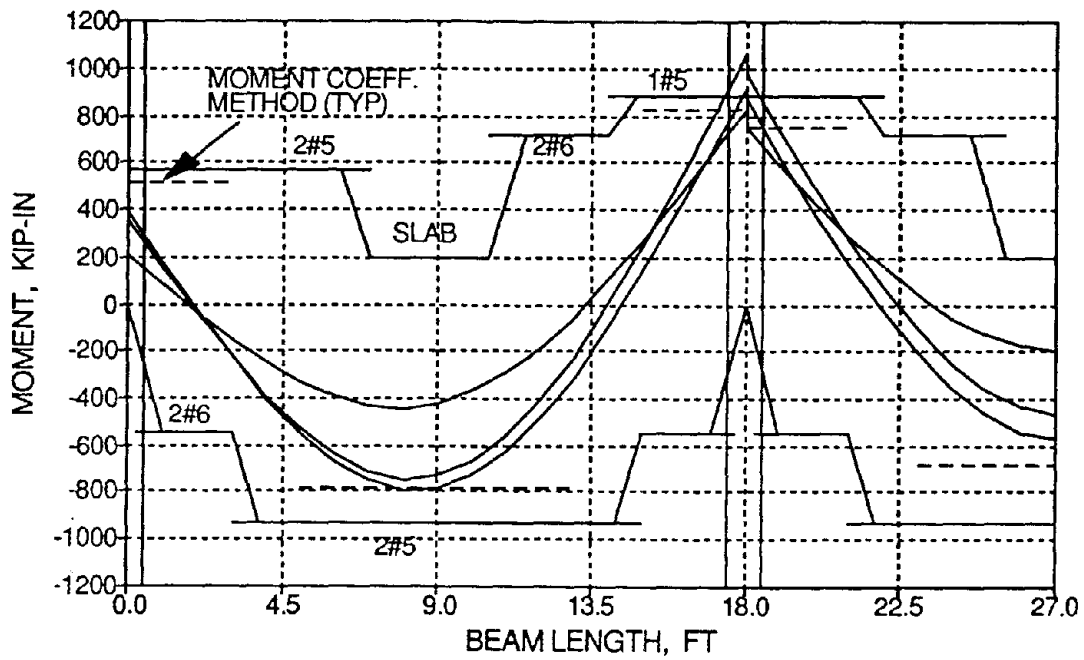
The beam shear force design envelop, shown in Fig. 2-5a, is determined from the triangular gravity loads distributions on the beams from Fig. 2-3. The beam shear strength is composed of contributions from the concrete and reinforcing steel according Section 11.1 of the Code and also shown in Fig. 2-5a. It will be noted that if the required shear force was less than 50% of the dependable concrete shear capacity, V_c , then no transverse steel would be required according to the Code. The steel layout for the beams is shown in Figs. 2-5b and 2-5c.

2.6 Column Design

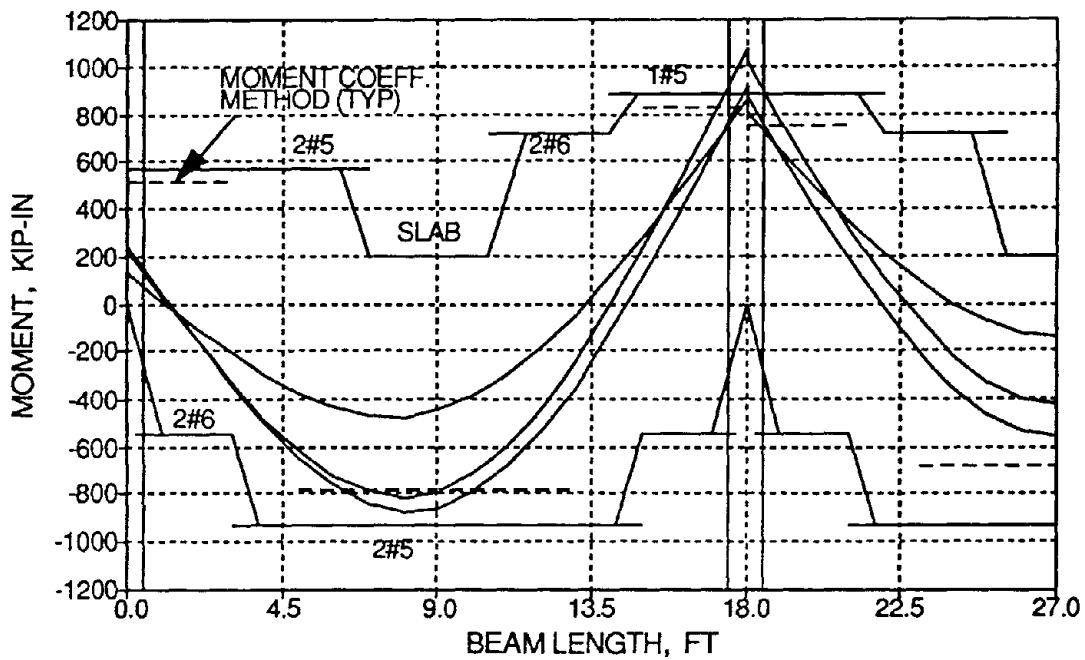
Table 2-5 summarizes the axial loads and design bending moments with moment magnification due to slenderness effects for the columns in accordance with Section 8.8 of the Code.

TABLE 2-5 Design Actions of the Columns

Location	Floor #	Label	M_u (kip-in)	P_u (kips)
Exterior	3	E3	300.7	54.4
	2	E2	257.2	119.4
	1	E1	315.3	185.1
Interior	3	I3	147.0	101.6
	2	I2	153.5	203.3
	1	I1	242.6	304.9

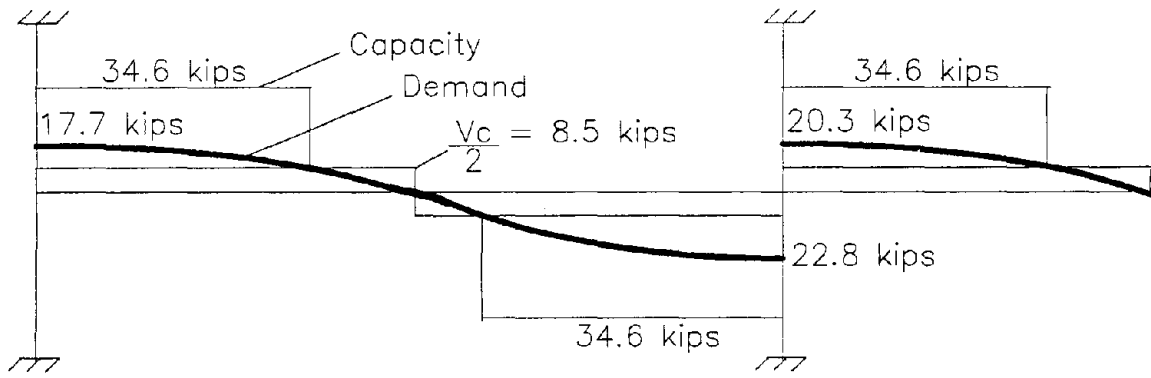


(a) First and Second Floors

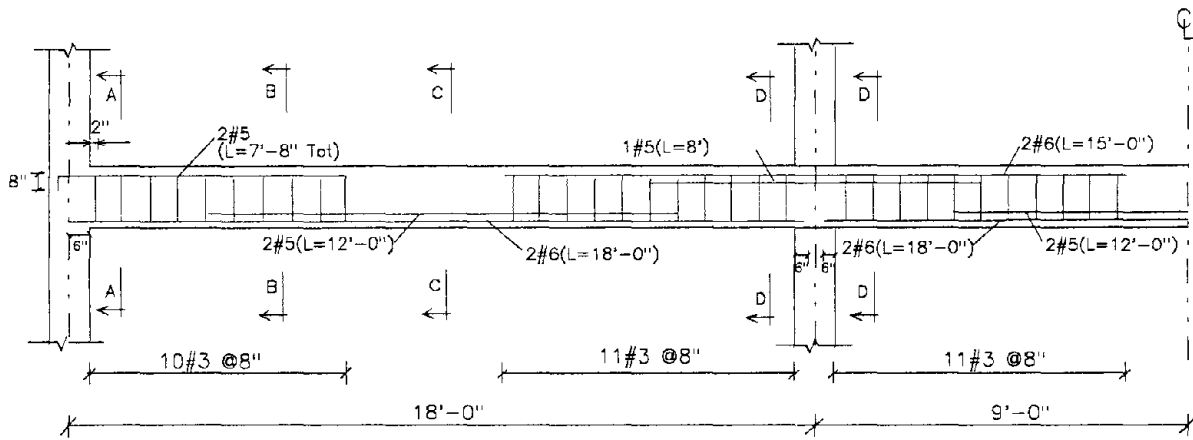


(b) Roof

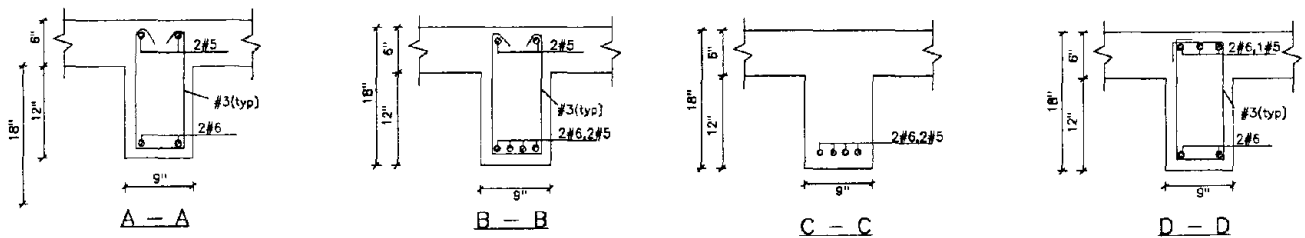
FIG. 2-4 Bending Moment Design Envelop and Strengths



a) Shear Force Diagram



b) Beam Steel Layout



c) Beam Sections

FIG. 2-5 Beam Details

The interaction diagrams for the interior and exterior columns with the design actions for each floor (labeled as E# and I#) are shown in Fig. 2-6 for a 12 in. square column. It will be noted from Fig. 2-6 that a lower bound curve is shown for the required minimum steel volume of 1%. An upper bound curve for a steel volume of 3% is also shown. This curve is considered to be a practical upper limit for construction purposes. If design loadings had fallen outside this curve, then the column size would have been increased rather than providing additional steel. But it is evident that the minimum longitudinal reinforcing steel would suffice. Thus, four #6 rebars are adapted to reinforce the column.

The maximum shear force developed from the factored gravity loads in the columns is 4.9 kips. From Section 11.3.1.2 of the Code, the concrete shear strength of the column, V_c , is 16.4 kips. Therefore the maximum tie spacing permitted by the code (ACI 318-89 Section 7.10.5) is used. Thus, #3 ties at 12 in. spacing are used throughout the column length except in the lap splice locations near the footing and slab levels where the tie spacing was 6 in. in accordance with the Code.

The required lap splice lengths of deformed bars in compression according to the Code is 12 in. But based on the survey of typical construction practices in the eastern United States, the splice length was observed to be 18 in. Also, the lap splices were typically located just above the foundation and slab levels.

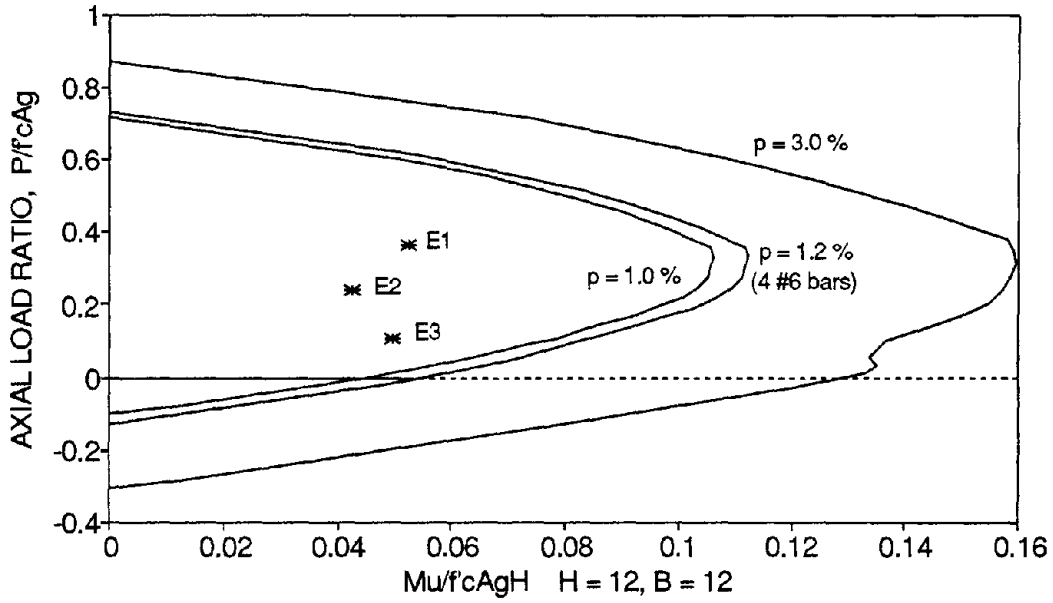
The column reinforcement details are shown in Fig. 2-7.

2.7 Joint Design

For the design of the exterior beam-column joints for non-seismic detailing provisions, ACI 318-89 Section 11.12.1.2 requires a minimum shear reinforcement ($A_v = 50 * b_w * s / f_y$) be provided in the joint area. Thus #3 ties at 6 in. spacing are needed in the exterior joint zones. No joint reinforcement is required by the code in the interior joints.

INTERACTION DIAGRAM - EXTERIOR COLUMNS

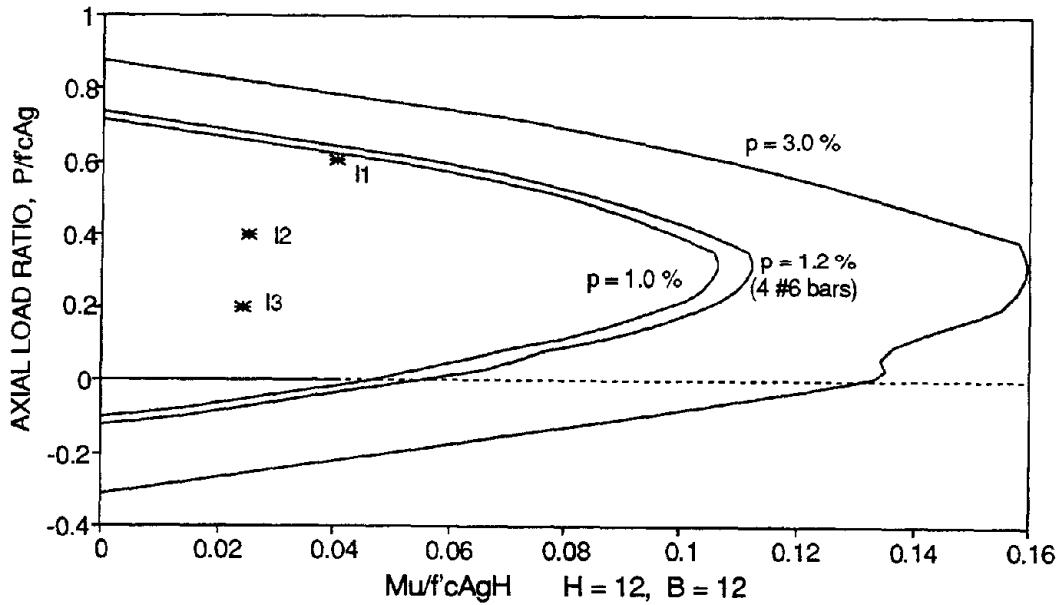
$f'_c = 3.5 \text{ ksi}; f_y = 40 \text{ ksi}; g = 0.85$



(a) Exterior

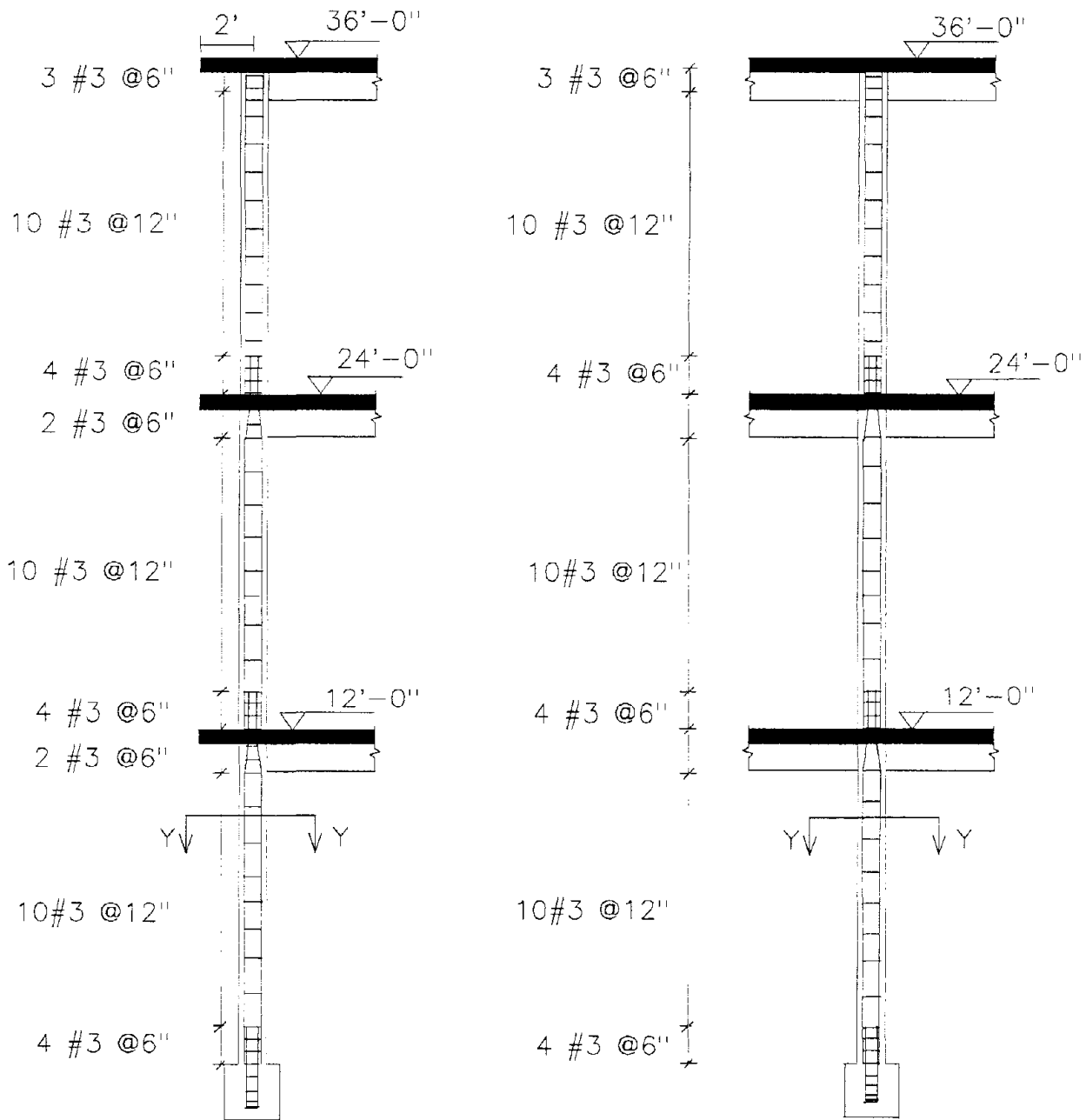
INTERACTION DIAGRAM - INTERIOR COLUMNS

$f'_c = 3.5 \text{ ksi}; f_y = 40 \text{ ksi}; g = 0.85$



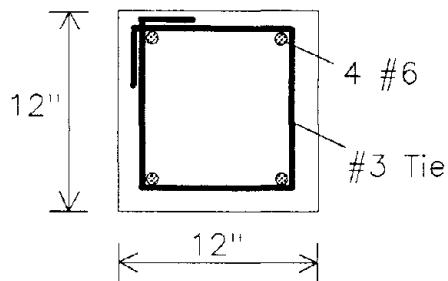
(b) Interior

FIG. 2-6 Interaction Diagrams for the Columns



Exterior Column

Interior Column



Section Y-Y

FIG. 2-7 Column Reinforcement Details

2.8 Summary Discussions

The design of a prototype three-story moment resisting reinforced concrete framed structure is presented in this section for the design loads of $1.4 D + 1.7 L$ (gravity load design). Since earthquake loads are neglected and the wind loads on a three story structure are relatively small after the design loading combinations, no lateral loads are considered for the design. The detailing for the structure was in accordance with the general non-seismic provisions of the ACI Code.

Under large seismic or lateral loads, some of the expected deficiencies and resulting member actions of a gravity load designed building with non-seismic detailing provisions are the following:

1. The moment capacity of the columns do not exceed the moment capacity of the beams. Therefore under large lateral loads, hinging would develop in the columns and result in an undesirable column-sidesway failure mechanism.
2. Lack of adequate transverse (shear reinforcement) and confining steel in members and joints. The large shear forces in the column members from seismic loads can lead to hoop fracture, which in turn can lead to buckling of the longitudinal reinforcement or shear failure. Therefore an undesirable column failure or hinging would develop and possibly result in an undesirable column-sidesway or soft-story collapse mechanism.
3. Discontinuity of the longitudinal beam reinforcement in the beam-column joints. Under seismic loads, large positive moments can develop in the beams; thus introducing the possibility of pull-out of the longitudinal positive beam reinforcement from the joint due to the lack of proper development length. However, this reduced beam moment capacity can be beneficial in the case of weak column - strong beam behavior.
4. Construction joints are located at the slab levels. During seismic activity, the upper and lower portions of the columns experience the most adverse stress actions. Therefore, the construction joints at the slab levels create the increased possibility of hinging to form in the columns and the development of a column sidesway or soft story failure mechanism.
5. Lap splices of column reinforcement at slab levels. The deficiencies are the same as #3 from above.

SECTION 3

ONE-THIRD SCALE R/C FRAME MODEL

3.1 Introduction

Recent earthquakes, starting with the San Fernando earthquake in 1971, caused an increase in earthquake awareness in the United States. This awareness is no longer concentrated only in zones of high seismicity, but also in zones of low to medium seismicity as well. Although the probability of a damaging earthquake occurring within low to medium seismic zones may be small, the potential risk for catastrophic structural collapses and large losses of life in heavily populated cities initiated the need to develop reliable methodologies for evaluating the seismic damage potential of existing and new structures.

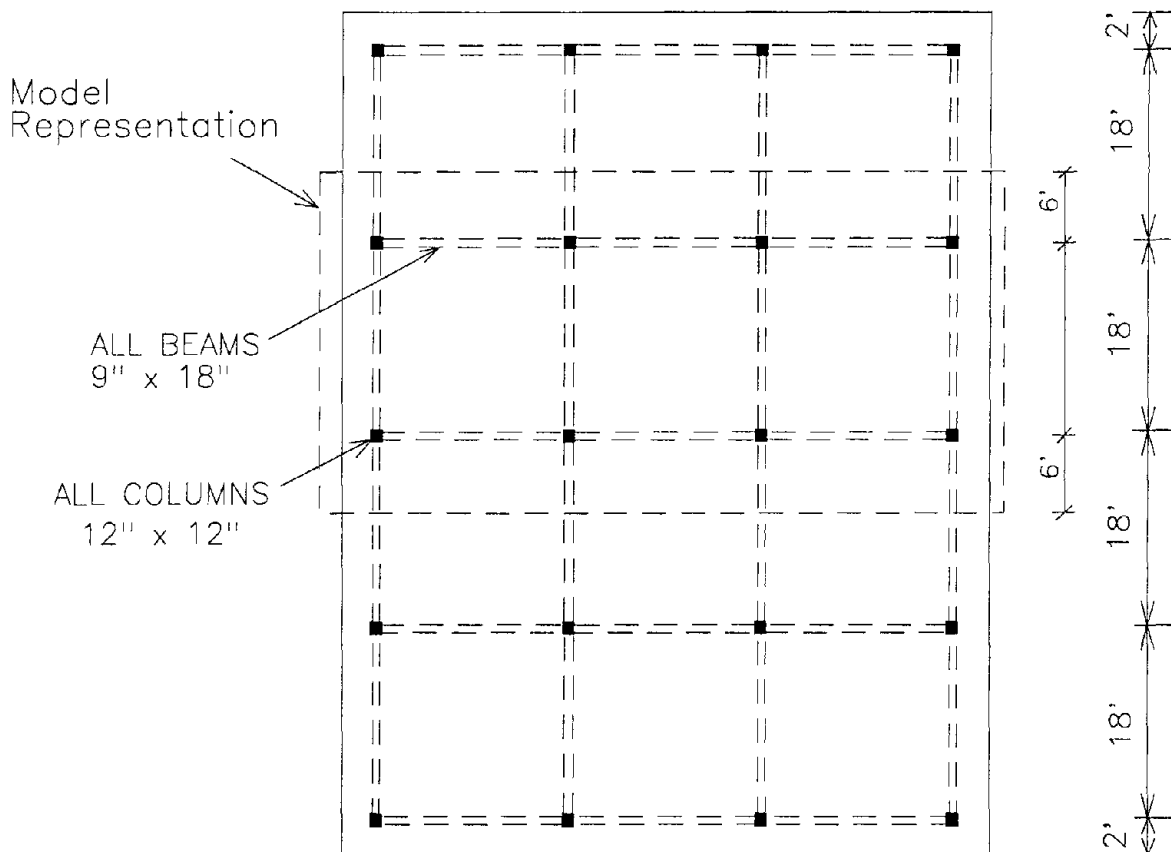
The study presented herein focuses on an experimental and analytical investigation of the seismic response of a one-third scale model of a lightly R/C frame building. The model is representative of an interior bay section of the prototype structure presented in Section 2. This structure is considered to be representative of low-rise buildings typically constructed in the Eastern and Central United States, which are designed primarily to carry only gravity loads with no considerations for seismic resistance. A cooperative study was also conducted at Cornell University by El-Attar et al. (1991b) on a one-eighth scale model replica of the same prototype structure. Various references to the above work are made throughout this study as a direct comparison between the different scale models.

The design of the prototype three-story moment resisting reinforced concrete frame structure with typical office loads was presented in Section 2 for non-seismic detailing code requirements (ACI 318-89). In order for the model to fit within the geometric constraints and load capacity of the State University of New York at Buffalo shaking table, a one-third (1/3) scale model was designed and constructed. Appendix A shows a table of the scale factors for various parameters for modeling dynamic behavior of structures with constant accelerations, since gravitational accelerations can not be varied. Reference to Appendix A is made throughout this section in regard to parameter scaling factors.

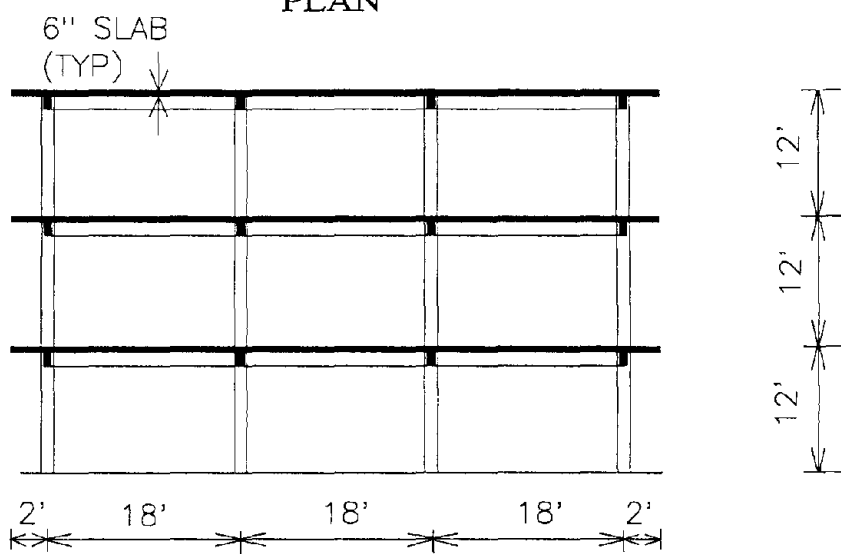
This section details: (i) the design, construction, and instrumentation of the one-third scale model; (ii) the selected base motion and peak magnitudes of base motion for the shaking table excitations; and (iii) the testing program for the model, which includes the structural dynamic identification and shaking table tests.

3.2 Model Geometry

The general layout of the 3-story prototype office building is again shown in Fig. 3-1. The geometric layout of the one-third scale model structure, shown in Fig. 3-2, is achieved using a geometric length scale factor of 3 (see Appendix A). The model represents the critical interior bay of the prototype building with two overhanging sides of one-third bay width. The one-third bay width is chosen due to the results of Wolfgram-French et al. (1989) in the testing of one-half scale models of interior beam-column-slab components under cyclic loading. Their results concluded that the flange width for the slab contribution of flexural strength in the beams was approximately one-third the bay width on each side of the beam. Fig. 3-3 shows the model on the shaking table in the SUNY at Buffalo Earthquake Simulation Laboratory.



PLAN



FRONT ELEVATION

FIG. 3-1 General Layout of the Prototype Structure

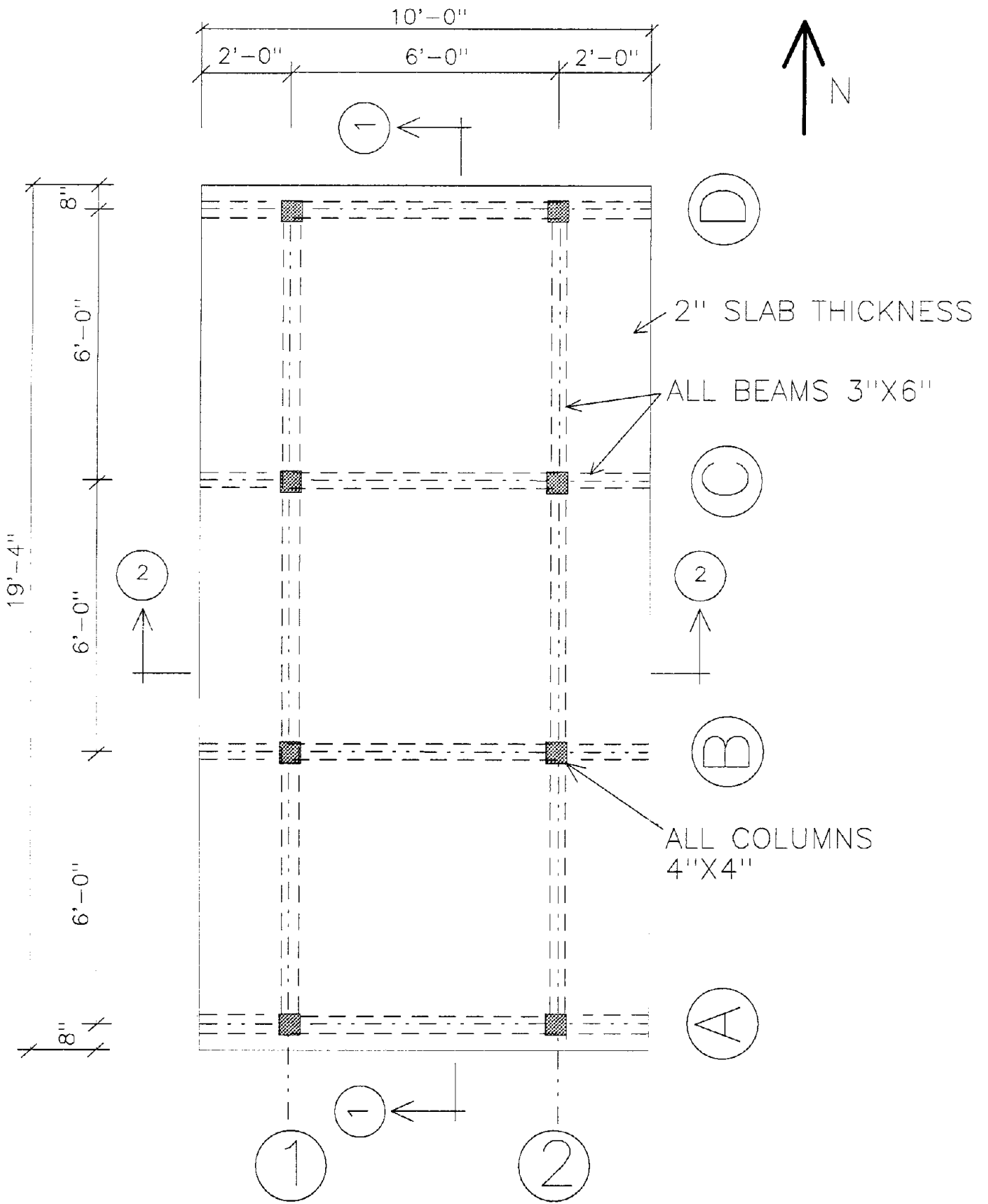
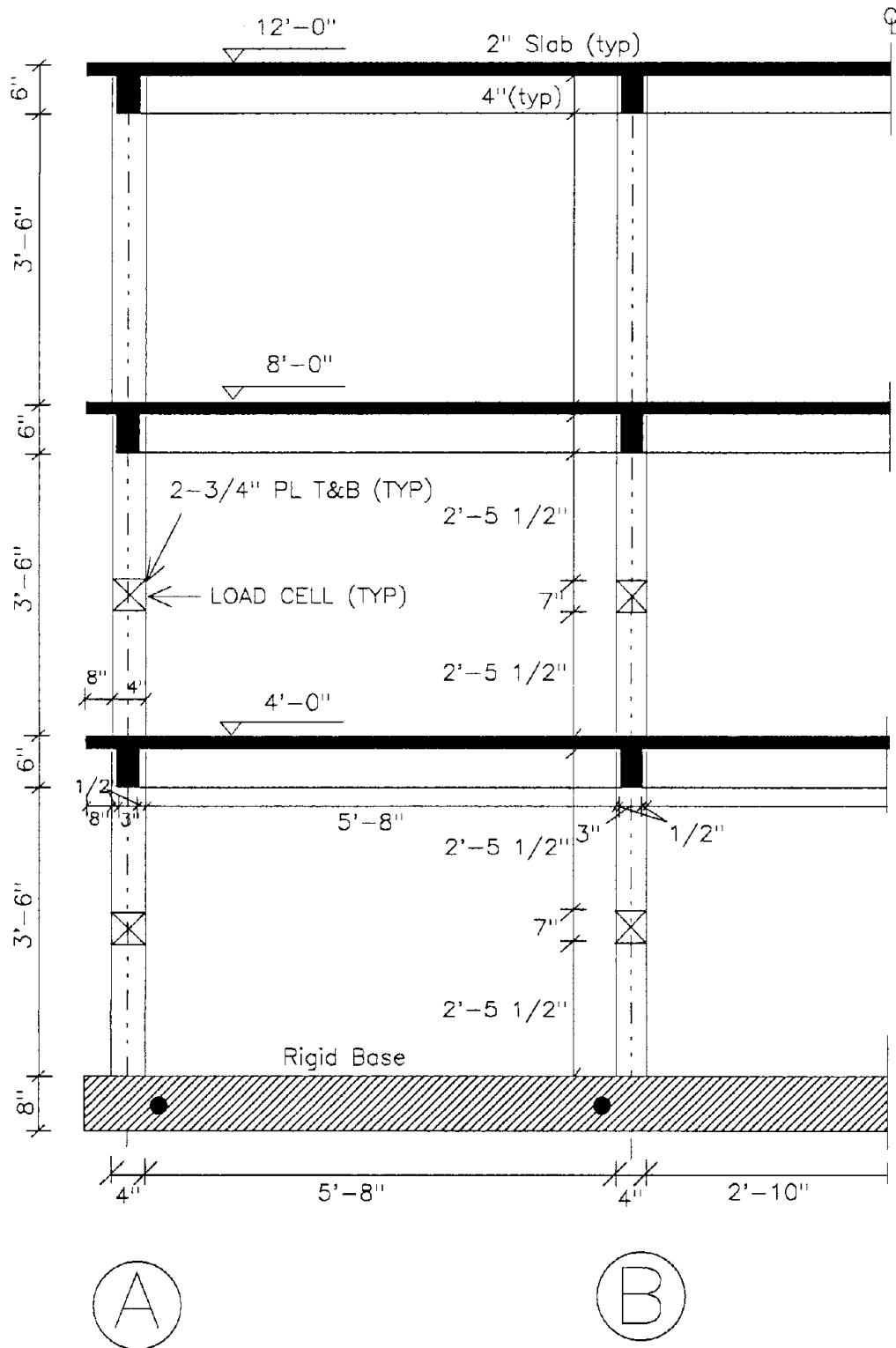
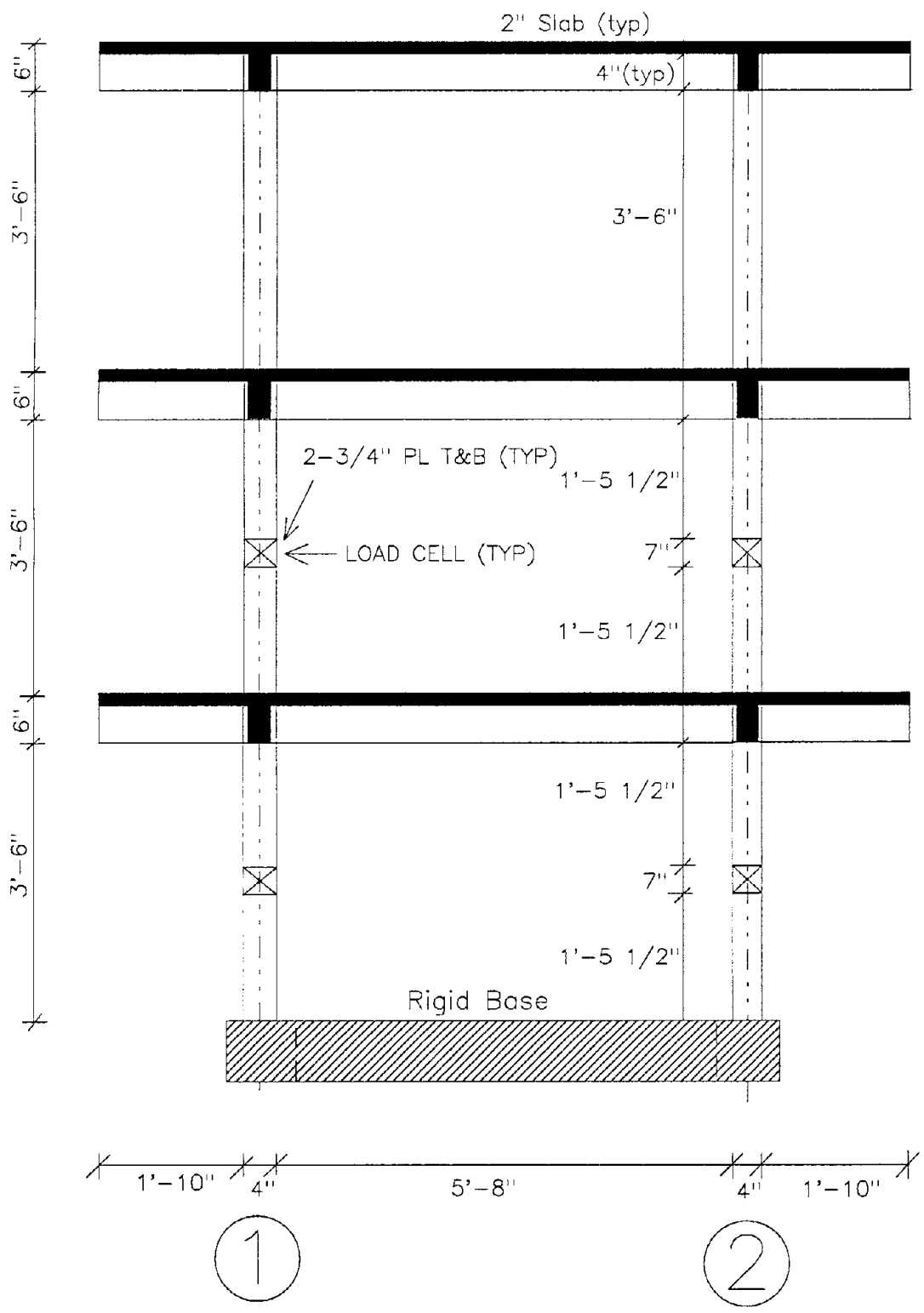


FIG. 3-2a Geometric Layout of the Model Structure



Section 1-1

FIG. 3-2b Continued



Section 2-2

FIG. 3-2c Continued

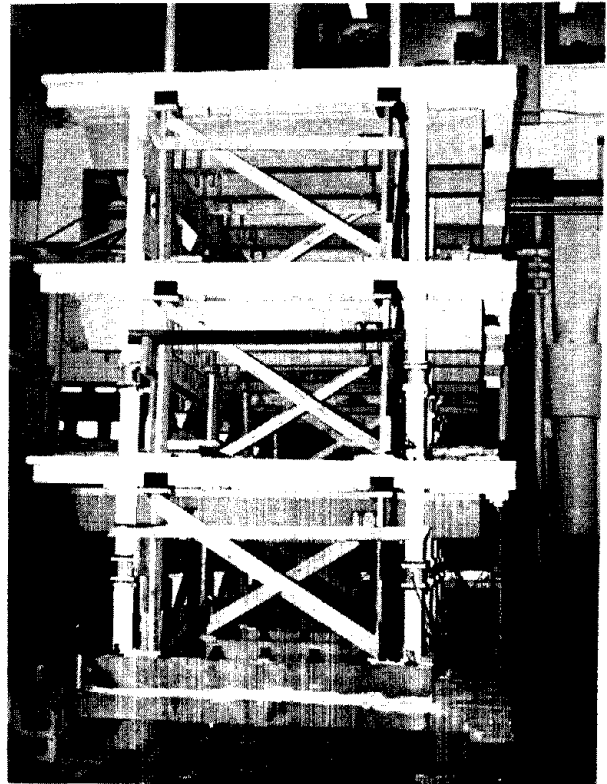
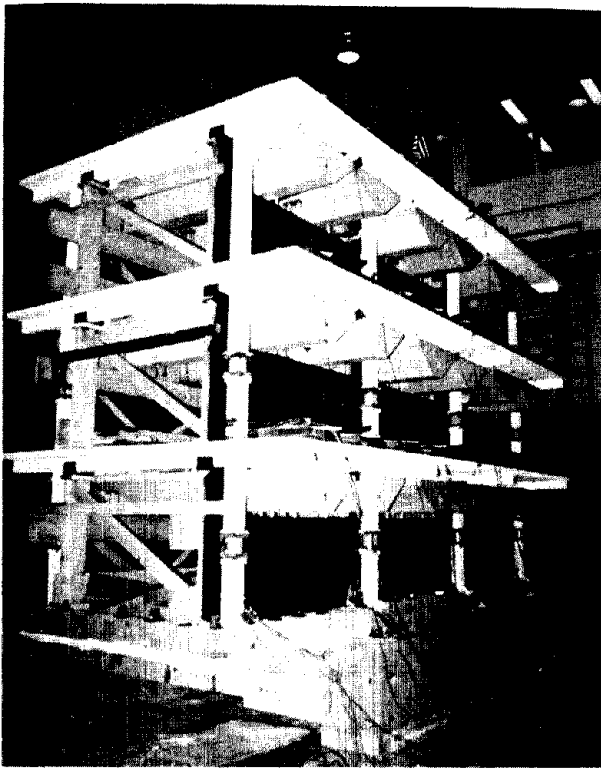
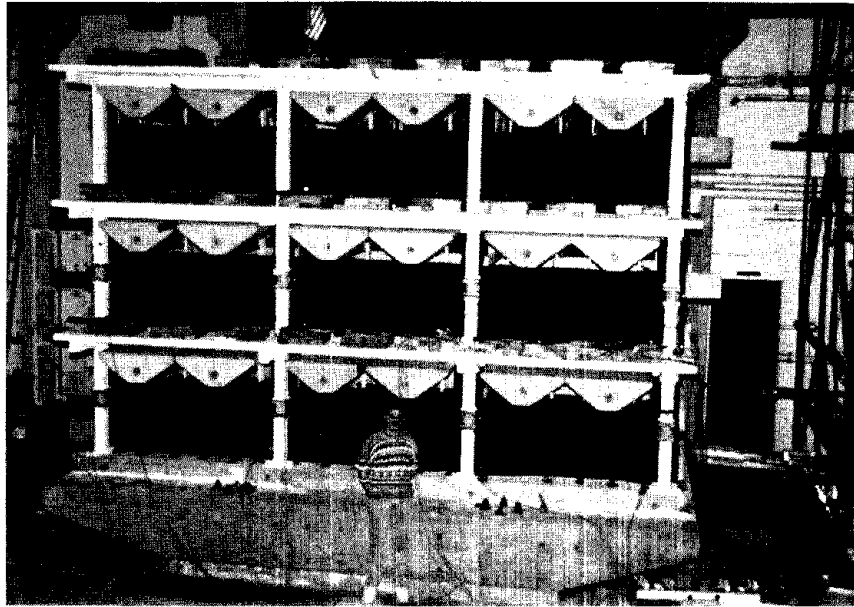


FIG. 3-3 Model Structure on the Shaking Table

3.3 Model Materials

Materials used in the construction of the model are identical to the materials in the prototype structure. Therefore, the scale factors are appropriately developed based on the principles of modeling the same acceleration and material and are shown in Appendix A.

3.3.1 Concrete Properties

The concrete mix analysis and design was formulated on a computer program supplied by a local concrete batching plant. Based on trial mixes from various recipes, a design mix was established for a 28 day target strength of 3500 psi, slump of 4 in., and maximum aggregate size of 1/2 in (#1 crushed stone). Table 3-1 shows the mix formula for a one cubic yard batch of concrete.

TABLE 3-1 Mix Design Formula for the Model Concrete

Ingredient	Weight
Type I Cement	490 lb
Concrete Sand	1487 lb
#1 Crushed Stone	1785 lb
Water	242 lb
Superplasticizer	39.2 oz
Micro-Air	2.9 oz

The mix formulation is based on a saturated, surface dry concrete sand. The water : cement (: sand : stone) ratio is 0.5 : 1.0 (: 3.0 : 3.6). The full gradation analysis of the aggregates in the concrete mix is shown in Fig. 3-4.

Fig. 3-5 shows the sequence of concrete pouring for the model. The small volume batches used in the columns (pours #1, #2, #4, #5, and #7) were mixed in the SUNY at Buffalo Laboratory with the materials from a local concrete batching plant in proportions with Table 3-1. The large

volumes required for the beams and slabs (pours #3, #6, and #8) were mixed at the local concrete batching plant with the same materials and trucked to the laboratory. Fig. 3-6 shows several stages in construction of the model which include the story level formwork layout.

Cylinder specimens, 4 in. diameter by 8 in. height, were moist cured in the laboratory near the model to associate the achieved cylinder strengths with the actual concrete strengths of the model. Fig. 3-7 shows the specimen strength gain with age of each pour along with an empirical equation for concrete strength as a function of age, Nilson (1987), as shown in Eq. (3.1).

$$\frac{f'_{ct}}{f'_{c28}} = \frac{t}{4 + 0.85t} \quad (3.1)$$

which t = cylinder age in days
 f'_{c28} = 28 day strength of the 4 in. x 8 in. cylinders
 f'_{ct} = cylinder strength at age t .

Concrete stress-strain relationships are presented in Fig. 3-8 for the column and beam-slab components in the structure according to the pour numbers from Fig. 3-5. These curves were taken from a representative test cylinder specimen for each pour. The strain value at maximum stress is found to be 0.002, which is typical for prototype concrete in actual construction. A substantial variation can be observed in the mix strengths for the different components, even though all mixes had the same target strength. The final strengths were very sensitive to moisture variations in the materials and the widely varying ambient temperatures at the time of construction. The results of the concrete specimen tests are presented in Table 3-2.

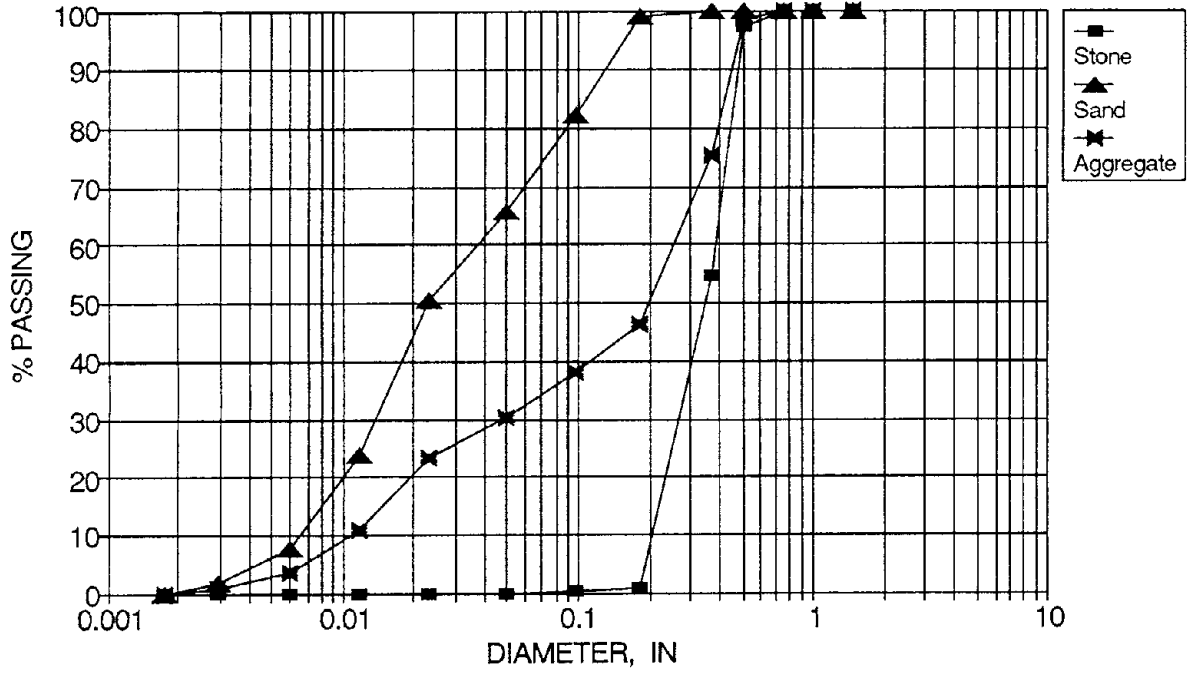


FIG. 3-4 Gradation Analysis of the Concrete Mix

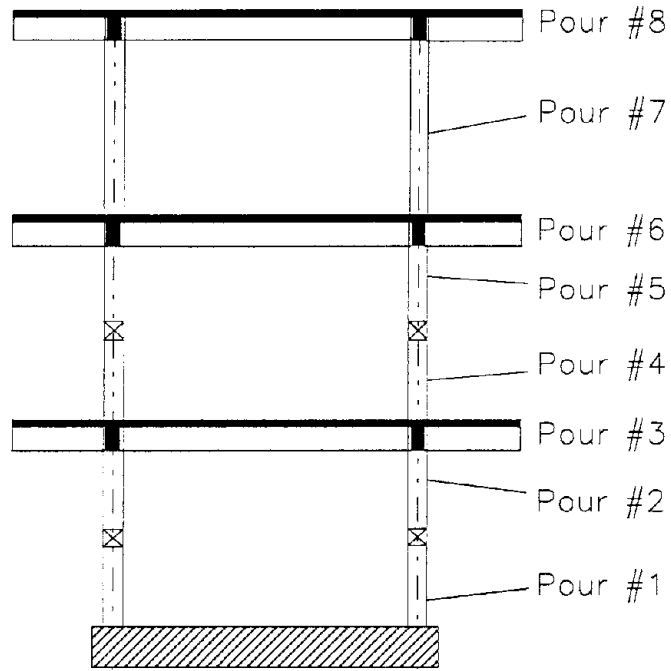


FIG. 3-5 Sequence of Concrete Pouring of the Model

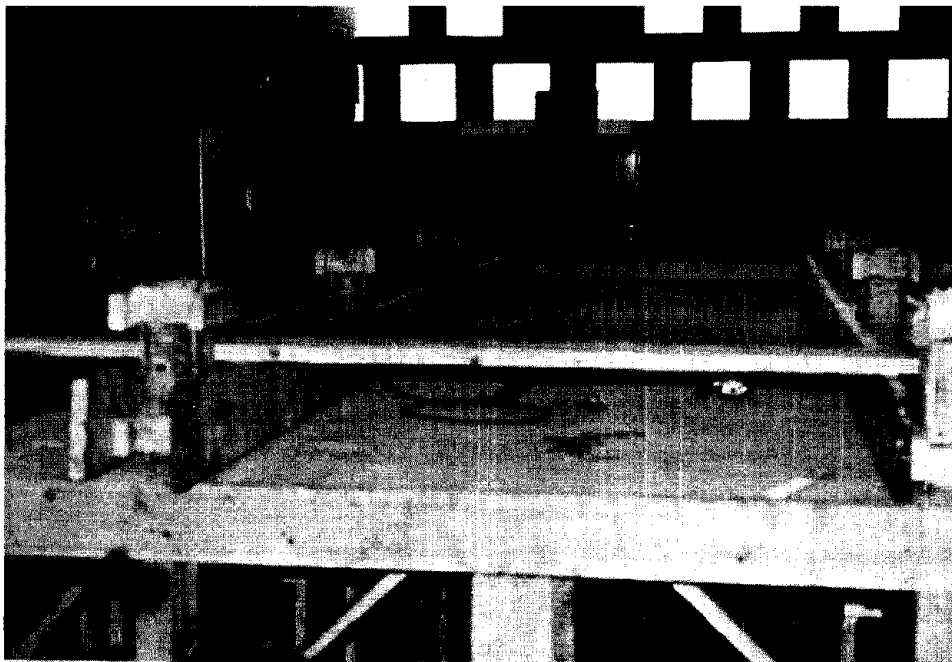
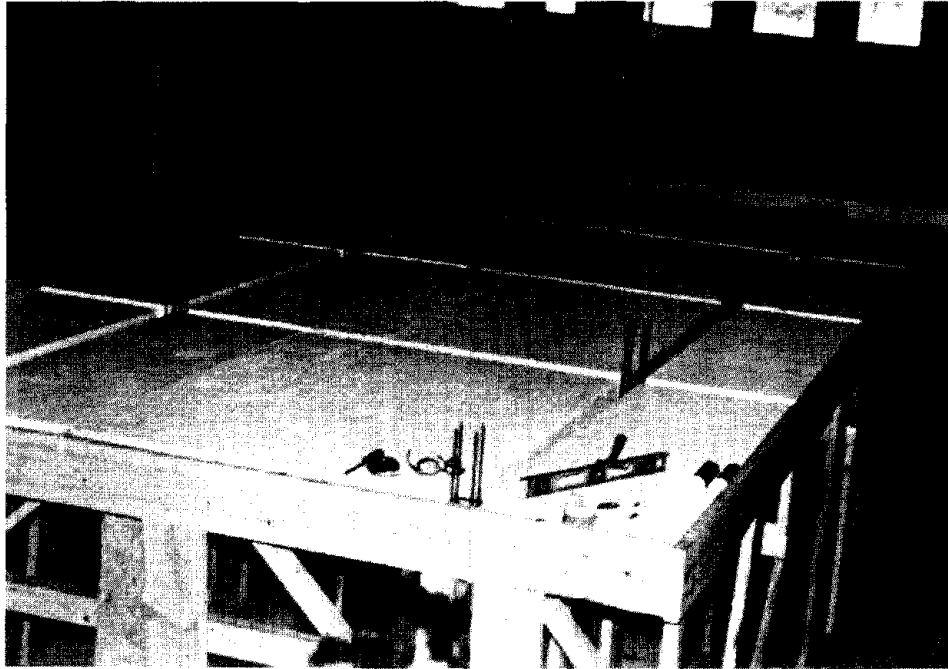


FIG. 3-6a Stages in the Construction of the Model

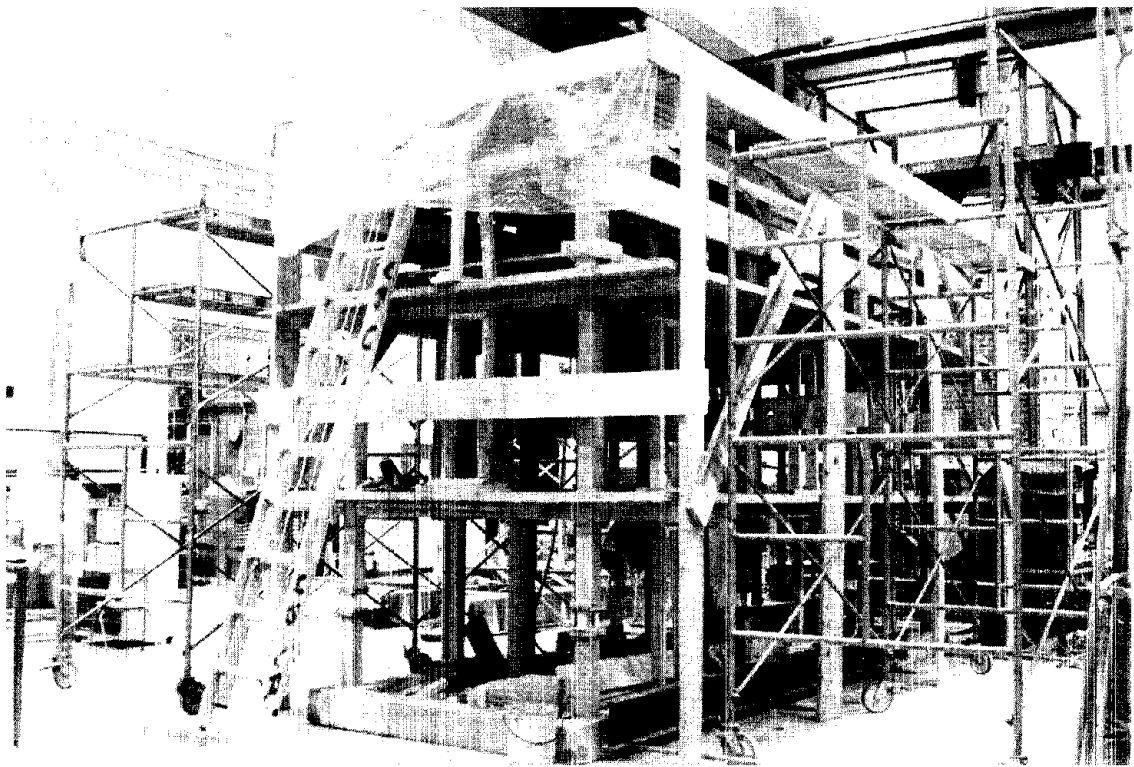
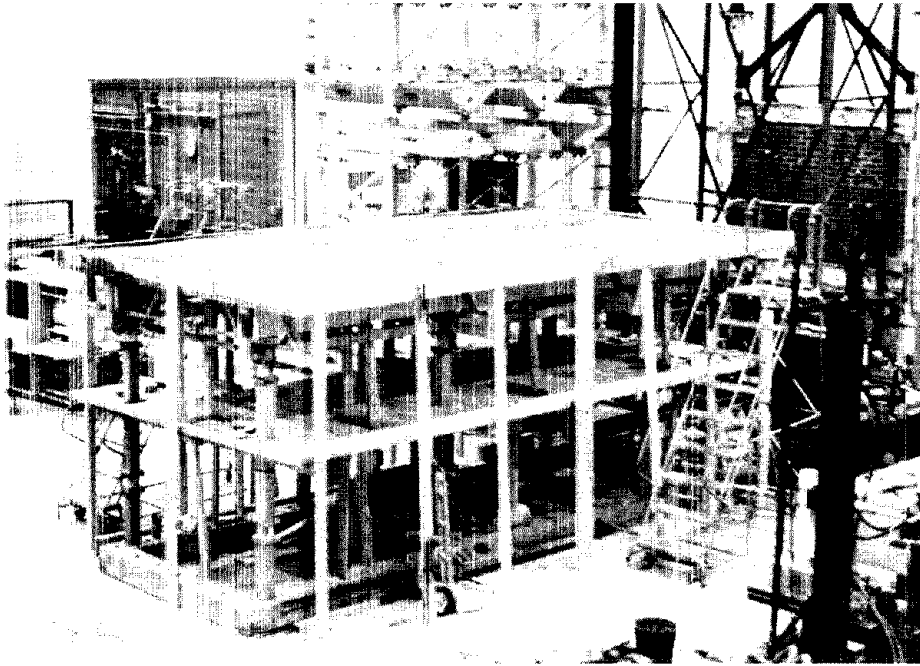


FIG. 3-6b Cont'd

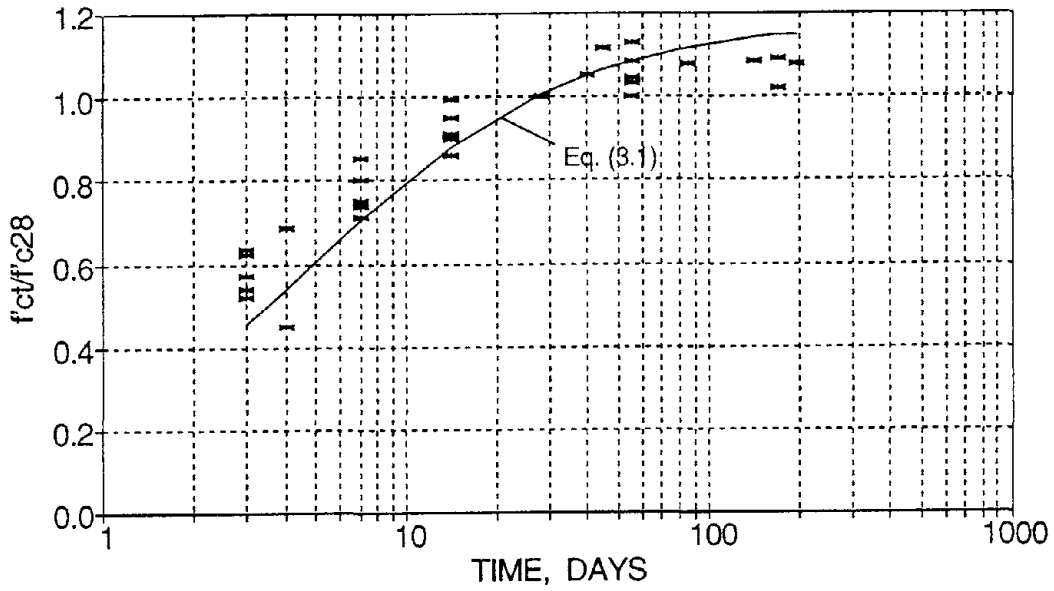
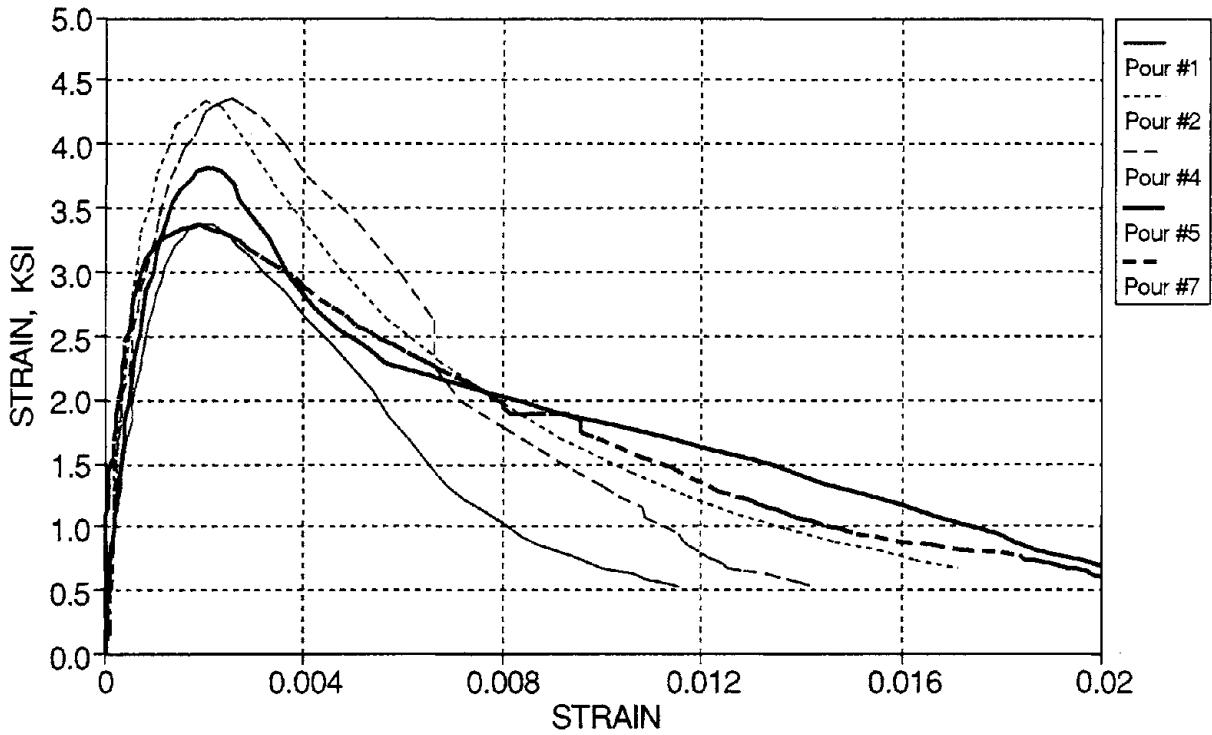


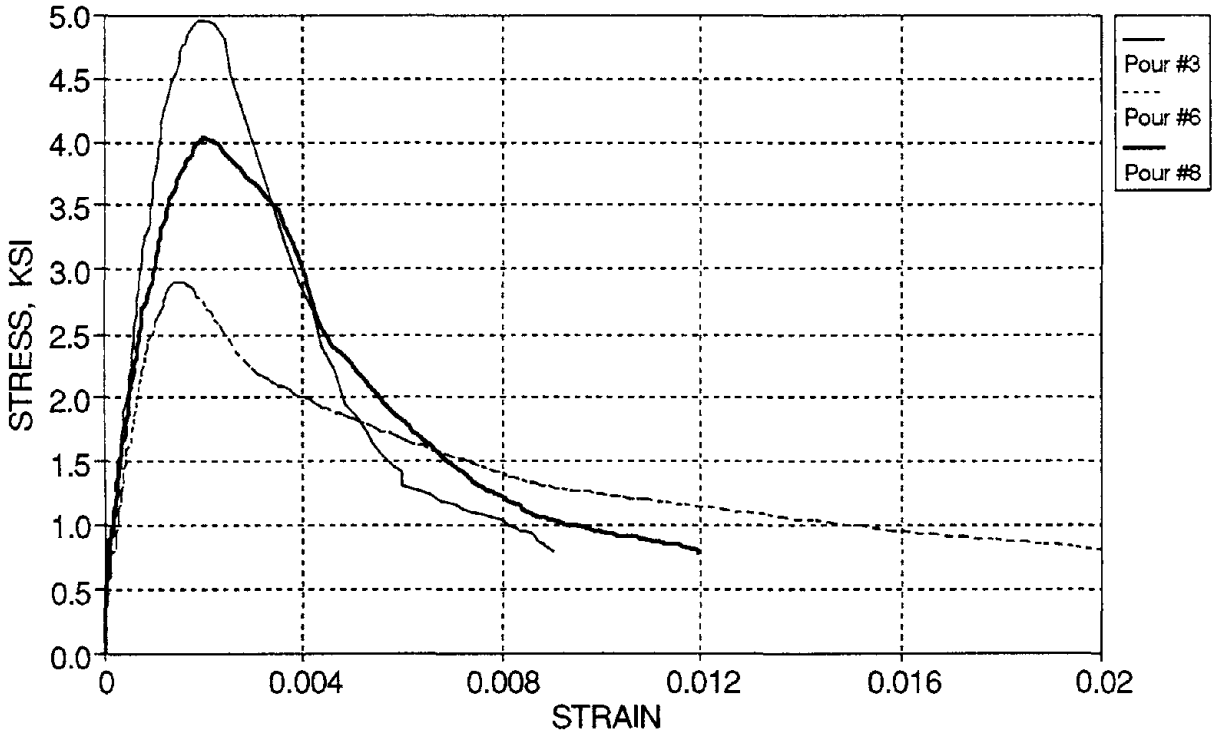
FIG. 3-7 Average Concrete Specimen Strength Versus Time

TABLE 3-2 Concrete Properties of the Model Structure

Pour Number and Location	f'_c (ksi)	E_c (ksi)	ϵ_{co}	ϵ_{spall}
1. Lower 1st Story Columns	3.38	2920	0.0020	0.011
2. Upper 2nd Story Columns	4.34	3900	0.0020	0.017
3. 1st Story Slab	4.96	3900	0.0021	0.009
4. Lower 2nd Story Column	4.36	3900	0.0026	0.014
5. Upper 2nd Story Column	3.82	3360	0.0022	0.020
6. 2nd Story Slab	2.92	2930	0.0015	0.020
7. 3rd Story Columns	3.37	3800	0.0019	0.020
8. 3rd Story Slab	4.03	3370	0.0021	0.012



(a) Columns



(b) Beam-Slabs

FIG. 3-8 Concrete Stress-Strain Relations from 4 in. x 8 in. Representative Test Cylinders

3.3.2 Reinforcing Steel Properties

The reinforcing steel used in the design of the prototype building are #3, #5, and #6 deformed rebars with yield strength (f_y) of 40 ksi and cross-sectional rebar areas (A_b) of 0.11, 0.31, and 0.44 in², respectively. Yield force ($A_b * f_y$) similitude of the model reinforcement is accomplished with a scale factor of 9 (see Appendix A). Therefore based on the tensile testing of selected reinforcement and yield force similitude, the reinforcing slab steel used in the 3-story model is a gauge 12 ($A_b = 0.0093$ in² and $d_b = 0.109$ in.) galvanized, 2 in. square wire mesh with an average measured yield strength of 58 ksi. The transverse reinforcing steel (hoop steel) is a gauge 11 black wire with a cross-sectional area of 0.0113 in², diameter of 0.12 in., and an average measured yield strength of 56 ksi. The longitudinal reinforcing steel consists of annealed D4 and D5 rebars of cross-sectional areas of 0.04 and 0.05 in. and diameters of 0.225 and 0.252 in., respectively (annealing of the rebars is described in the next sub-section). Representative stress-strain relationships of the reinforcing steel used in the model are shown in Fig. 3-9.

Table 3-3 summarizes the average measured properties of the reinforcing steel used in the model structure.

TABLE 3-3 Reinforcing Steel Properties of the Model Structure

Bar	d_b (in.)	A_b (in ²)	f_y (ksi)	E_s (ksi)	f_{max} (ksi)	ϵ_u
#12 ga.	0.109	0.0093	58	29900	64	0.13
#11 ga.	0.120	0.0113	56	29800	70	-
D4	0.225	0.0400	68	31050	73	0.15
D5	0.252	0.0500	38	31050	54	-

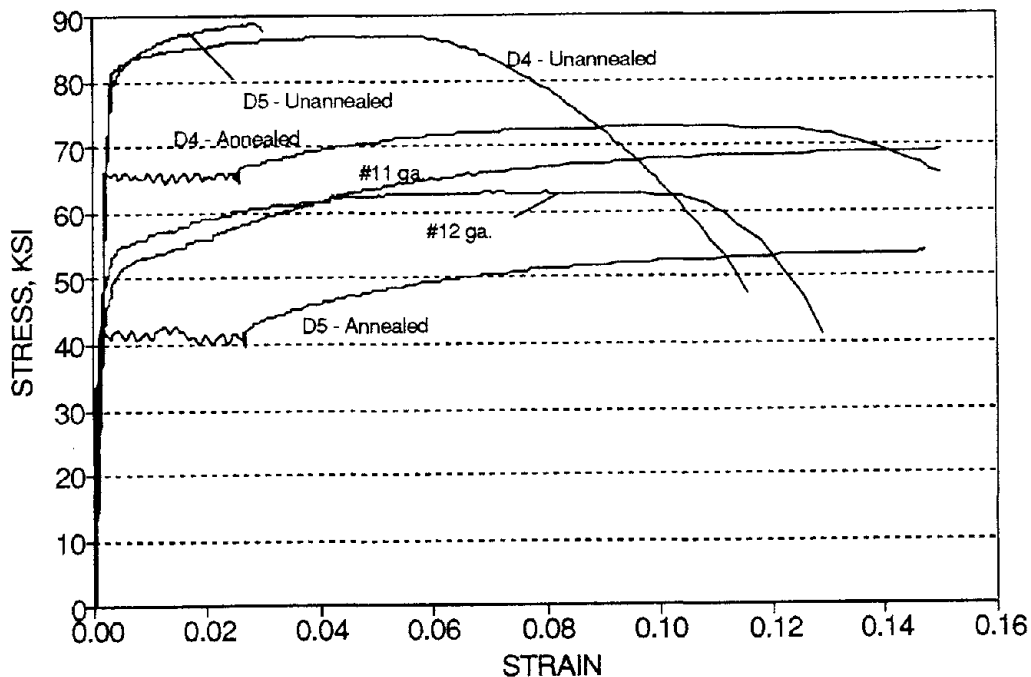


FIG. 3-9 Measured Representative Stress-Strain Relationships of the Reinforcing Steel

3.3.2.1 Heat Treatment of Steel Reinforcement

D4 and D5 rebars are used to satisfy the yield force ($A_b \cdot f_y$) similitude of #5 and #6 rebars. From Appendix A, the scale factors for stress and area similitude are 1.00 and 9.00, respectively. Therefore yield force similitude can be satisfied by scaling the area of reinforcement with the same yield stress as the prototype. The D5 rebar satisfies cross-sectional area (A_b) similitude with a #6 rebar. However the D5 rebar originally has a high yield strength, no yield plateau, and low ductility. Therefore, heat treatment (annealing) was used to lower the original yield strength (f_y) of 82 ksi to between 40 and 60 ksi for yield force similitude and also to improve the properties of the rebar by relieving some of the internal stresses. The rebars were annealed in a large electric oven at different temperatures ranging between 900°F and 1140°F for a total of 3 hours (1 hour to heat the oven, 1 hour of annealing, and 1 hour to cool). The resulting yield strength of the D5 rebar after annealing drastically varied between 35 and 70 ksi with a very slight change in oven temperature. Therefore it is concluded that annealing the D5 rebar to produce a yield strength between 40 and 60 ksi could not confidently be reached and similitude with a #6 rebar is not satisfied. But at high temperatures (1140°F), the average yield strength of the D5 rebar is about 38 ksi, which satisfies yield force similitude with a #5 rebar.

The D4 rebar was also annealed at different temperatures between 900°F and 1140°F to produce a yield strength between 49 and 73 ksi for yield force similitude with a #6 rebar. At a temperature of 1140°F, the average yield strength consistently reached was 68 ksi. Based on yield force similitude, the D4 rebar represented a #6 rebar with a yield strength of 55.6 ksi. Since a grade 40 steel has yield strengths between 40 and 60 ksi, the D4 rebar satisfied similitude with a #6 rebar.

Both the original and annealed stress-strain relationships for the D4 and D5 rebars are shown in Fig. 3-9.

3.4 Reinforcement Details

The following provides details of the reinforcing steel used in the model based on scale factor of 3 for geometric length similitude (see Appendix A).

The slab steel in the prototype structure was designed in Section 2.4 by the direct design method of the ACI 318-83. The design required #3 rebars at 6 in. spacing in different sections of the slab. To avoid excess labor in the construction of the 3-story model, a 2 in. square mesh composed of gauge 12 galvanized wires was chosen for acceptable similitudes of strength and geometric spacing length. Since the slab strength was not the main emphasis for this study, the slight disparities of slab steel placement due to the mesh was considered satisfactory for the experiment. Fig. 3-10 shows the layout details for the top and bottom reinforcing steel mesh in the slab.

The longitudinal (direction of motion) and transverse (perpendicular to the direction of motion) beam reinforcement details for the model are shown in Fig. 3-11 based on the prototype design from Section 2.5. The beam cage reinforcement along with the slab steel reinforcement in the formwork of a typical story slab is shown in Fig. 3-12.

Fig. 3-13 shows the reinforcement details for the columns in the model based on the prototype design from Section 2.6.

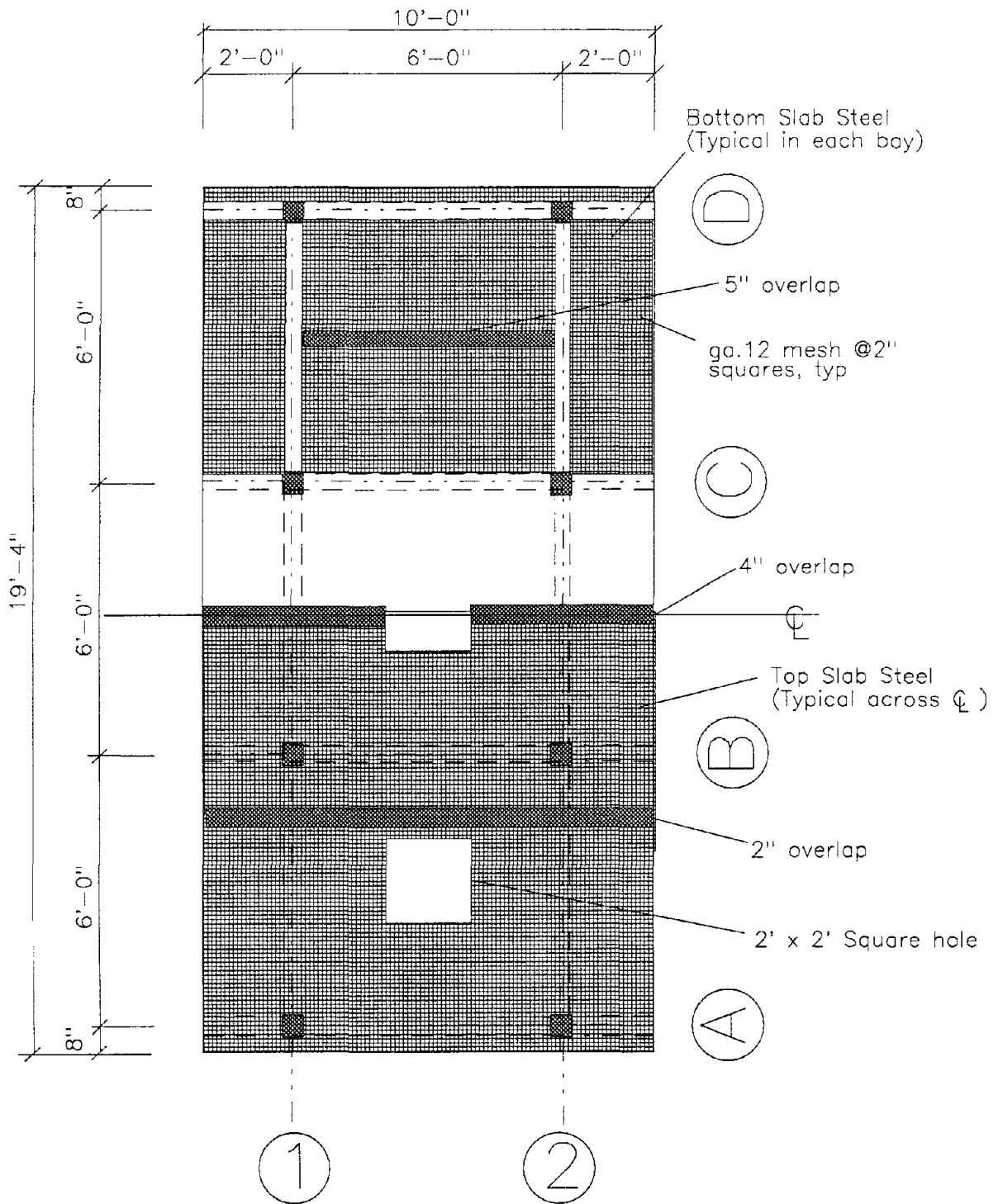
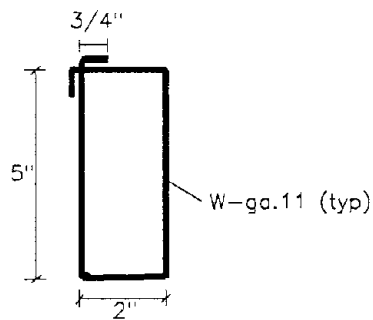
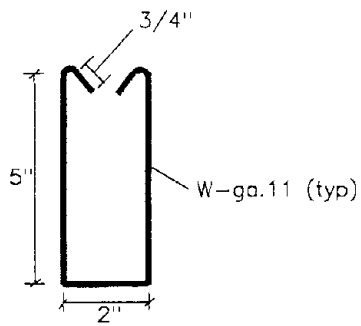
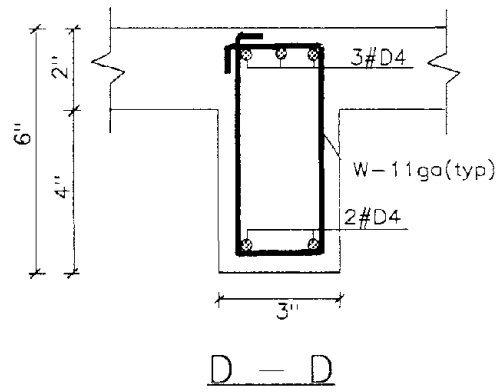
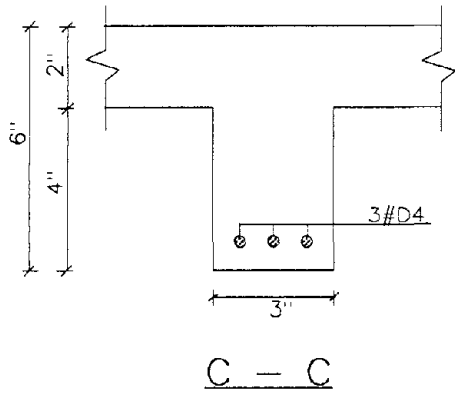
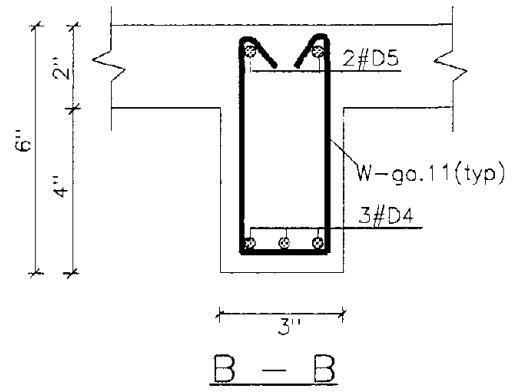
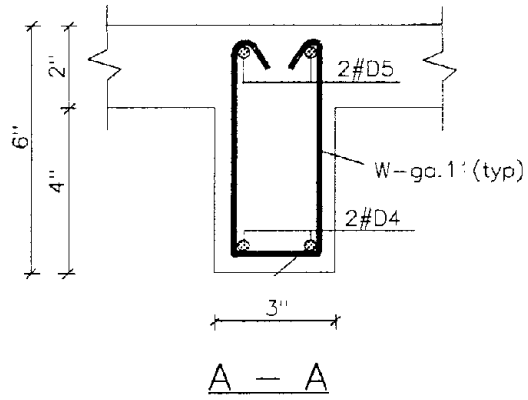


FIG. 3-10 Layout of Slab Steel Reinforcement



Beam Sections

FIG. 3-11b Continued

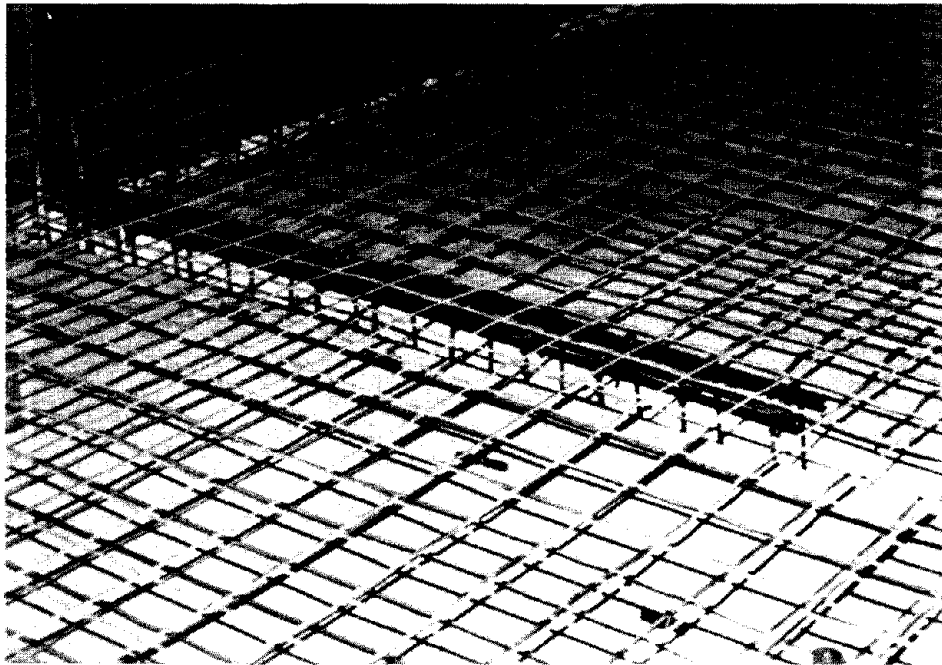
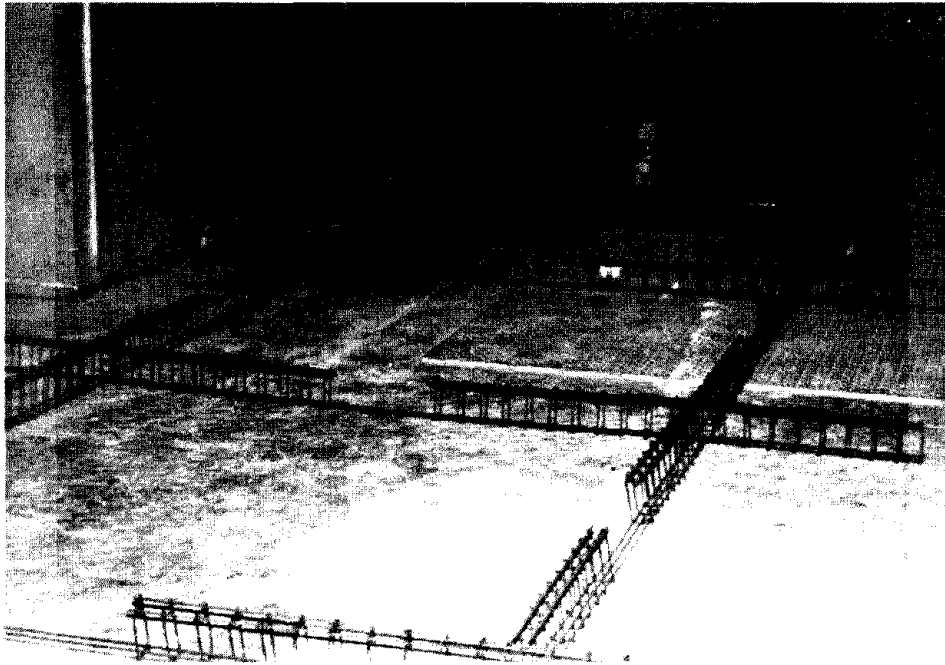
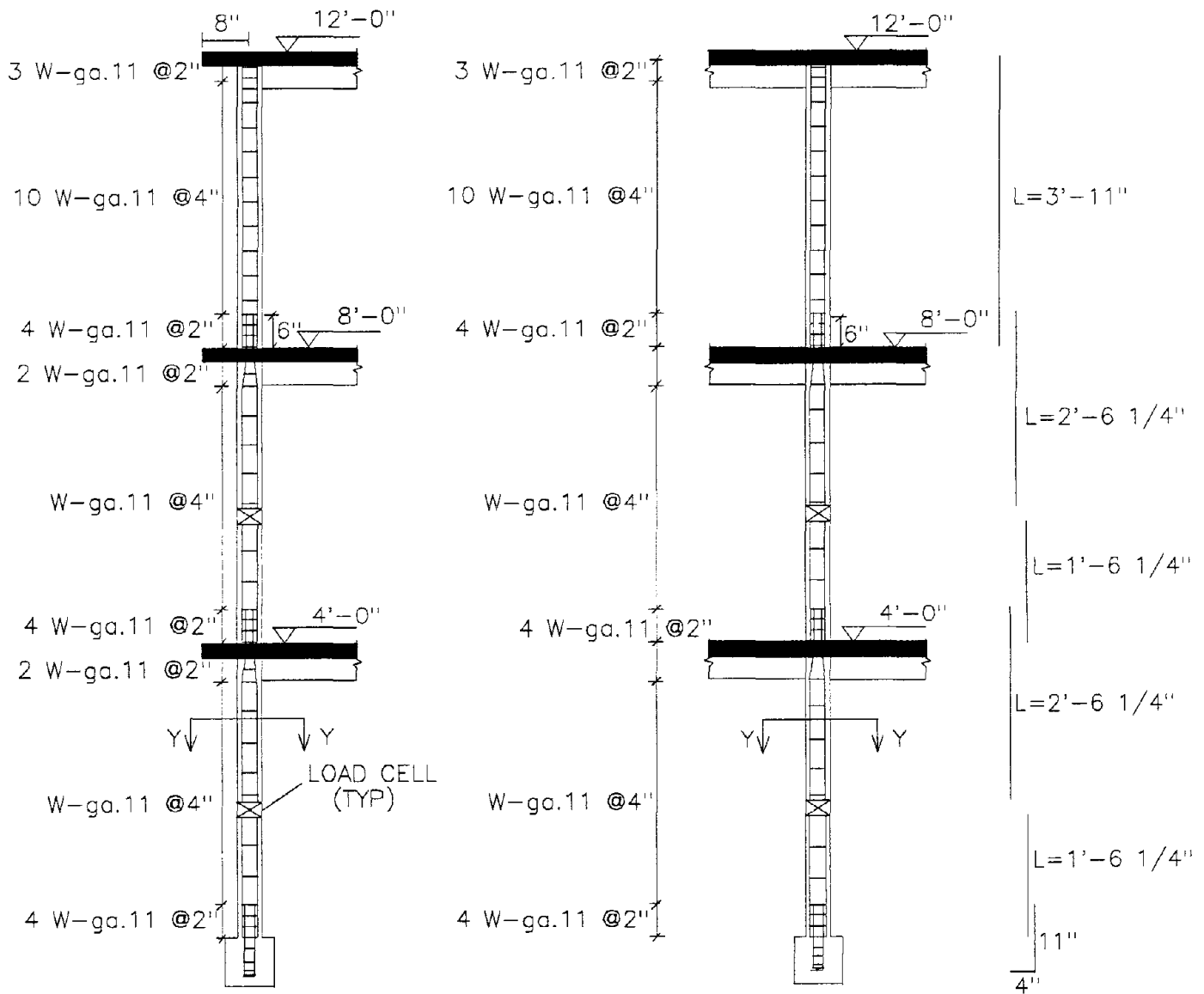
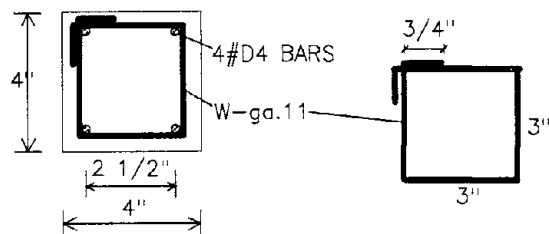


FIG. 3-12 Typical Beam and Slab Reinforcements



(a) Exterior Section

(b) Interior Section



(c) Section Y-Y

FIG. 3-13 Detail of the Column Steel Reinforcement

3.5 Mass Similitude

For proper modeling of dynamic behavior, mass similitude of the model must be satisfied. Using the constant acceleration scaling and same material for the model, an additional mass must be applied to the model to compensate for the difference in the required and provided material densities. From Appendix A for constant acceleration, constant material stiffness, and appropriate geometric length scaling, the required scaling factor for material density, λ_p^{req} , is:

$$\lambda_p^{req} = 1 / \lambda_l \quad (3.2)$$

where λ_l = scale factor for geometric length

But the material in the model consists of the same material as in the prototype. Therefore the provided material density is the same as in the prototype such that:

$$\lambda_p^{prov} = 1 \quad (3.3)$$

If no correction is applied in the model structure, then the mass, gravitational force, frequency, and impulse would not be scaled in the proper fashion, since the required and provided material densities are different (see Appendix A). Therefore an adjustment of the material density is provided by adding masses to the model structure.

The mass, m , is defined as the product of the material density, ρ , and material volume, V , as follows:

$$m = \rho V \quad (3.4)$$

Since the scaling factor for material volume is λ_l^3 (see Appendix A), the required and provided masses of the model are defined below:

$$m_m^{req} = m_p \cdot 1/\lambda_l^2 \quad (3.5a)$$

$$m_m^{prov} = m_p \cdot 1/\lambda_l^3 \quad (3.5b)$$

where m_m^{req} = required mass of the model
 m_m^{prov} = provided mass of the model
 m_p = mass of the prototype

Therefore from the difference in material density properties, the provided mass is less than required for similitude. To correct this difference, an additional mass, Δm , is provided in the model as follows:

$$\Delta m = m_p \cdot (1/\lambda_l^2 - 1/\lambda_l^3) \quad (= 2/27 m_p) \quad (3.6a)$$

Since the scaling factor for required gravitation acceleration is 1.00 from Appendix A, the additional weight required in the model is:

$$\Delta W_m = 2/27 W_p = 2/27 \lambda_l^3 W_m^{prov} = 2 W_m^{prov} \quad (3.6b)$$

Therefore the additional required mass is twice the weight of the model.

A more convenient determination of the required mass of the model to satisfy similitude is through the gravitational force (dead plus live loads). The required gravitational force (weight) of the model, W_m^{req} , is defined in terms of the gravitational force of the prototype and the appropriate scale factor from Appendix A as follows:

$$W_m^{req} = W_p \cdot 1/\lambda_l^2 = 1/9 W_p \quad (3.7)$$

where W_p = gravitational force of the prototype structure
 λ_l = geometric length scale factor

In some codes, 25% of the live load can be considered as inertial mass for design earthquake loading. But based on weight limitations in the actuators of the shaking table, the live load is not considered for mass similitude. The mass similitude for the model is determined only from the dead loads of the prototype building which act within the floor area of the model. The prototype structural dead weight per floor within the floor area of the model is shown as follows:

Beams:	= 25.6 k/floor	(0.11 k/ft)	(3.8)
Columns:	= 12.6 k/floor	(0.15 k/ft)	
Slab:	= 130.5 k/floor	(75 psf)	
Ceiling:	= 15.6 k/floor	(9 psf)	
Electric:	= 8.7 k/floor	(5 psf)	
Partitions:	= 34.8 k/floor	(20 psf)	
Total: W_p	= 228.0 k/floor		

Therefore the required weight of the model per floor (W_m) is determined from Eq. (3-7) as 25.3 k/floor ($W_p/9$).

The self weight of the model per floor is shown below:

Beams:	= 0.95 k/floor	(0.0125 k/ft)	(3.9)
Columns:	= 0.47 k/floor	(0.0167 k/ft)	
Slab:	= 4.83 k/floor	(0.025 psf)	
Total: W_m	= 6.25 k/floor		

Therefore the additional weight required per floor is $\Delta W_m = 19.05 \text{ k/floor}$. To make up for the weight deficiency for mass similitude, additional weights in the form of concrete blocks and lead bricks were used. Six 2 kip concrete blocks attached to the slab of the interior bays for each floor in four locations as shown in Fig. 3-14. Below the slab is a half-moon steel plate in which two 1-1/2 in. diameter threaded rods connect to the reinforced concrete block. The 3/4 in. plywood and 2 in. x 4 in. wood beneath the slab provide enough filler so that the concrete blocks have about 3/4 in. clearance from the longitudinal beams to prevent stiffening. A 1/2 in. diameter high strength threaded rod was used to connect the half-moon to the top of the slab. The nut was tightened on top of another half-moon steel plate above the slab, which rests on a 3/4 in. x 4 in. x 8 in. piece of plywood. The piece of plywood distributes the load of the concrete block on the slab and provides a cushion to prevent the stiffening of the slab.

In addition to the concrete blocks, 2 in. x 4 in. x 8 in. lead bricks, each weighing 26.5 lbs., were positioned in two layers in groups of 16 bricks near cut holes in each overhanging slab. Fig.

3-15a shows 9 groups of such bricks along each overhanging side of the structure. The steel rod, tightened with a nut on top of the unistrut, attach the lead bricks to the slab as shown in Fig. 3-15b. Rubber strips were placed beneath the lead bricks to provide a gap between the slab and the lead bricks to prevent the stiffening of the slab.

The weight of the connectors for the attachment of the additional weights to the slab was approximated to be 0.6 kips per floor.

Wood safety frames, shown in Fig. 3-3, were installed at the base, first, and second floors to guard against possible collapse of the model during the shaking table tests. To prevent disturbance in the response of the structure, the wood frames were constructed to act independently of the structural system except at very large story drifts. The approximate weight of the frames was 0.5 kips per floor.

Therefore including the self weight of the model (6.25 kips/floor), concrete blocks (12.0 kips/floor), lead bricks (7.63 kips/floor), connectors (0.6 kips/floor), and wood bracing (0.5 kips/floor), the total provided model weight, W_m , is 27.0 kips per floor with a margin of error of ± 0.3 kips per floor. The total weight of the model is 6.7% heavier based on proper scaling of the dead mass similitude of the prototype structure. But the excess weight may be regarded as a partial live load contribution.

Note that the required mass in the model is determined based on the total mass of the prototype structure [Eq. (3.5a) or Eq. (3.7)], which includes the mass of the columns, beams, slabs, and superimposed dead and live loads. However, the additional weights required are only attached at the story level slabs for convenience and not distributed to all the members of the model. But since the mass of the story slabs, beams, and superimposed loads are substantially greater than the mass of the columns, the errors introduced are insignificant for mass similitude.

3.6 Instrumentation

The following sub-sections detail the instrumentation used in recording the structural response of the one-third scale model for dynamic excitations along the longitudinal axis of the model (North-South direction).

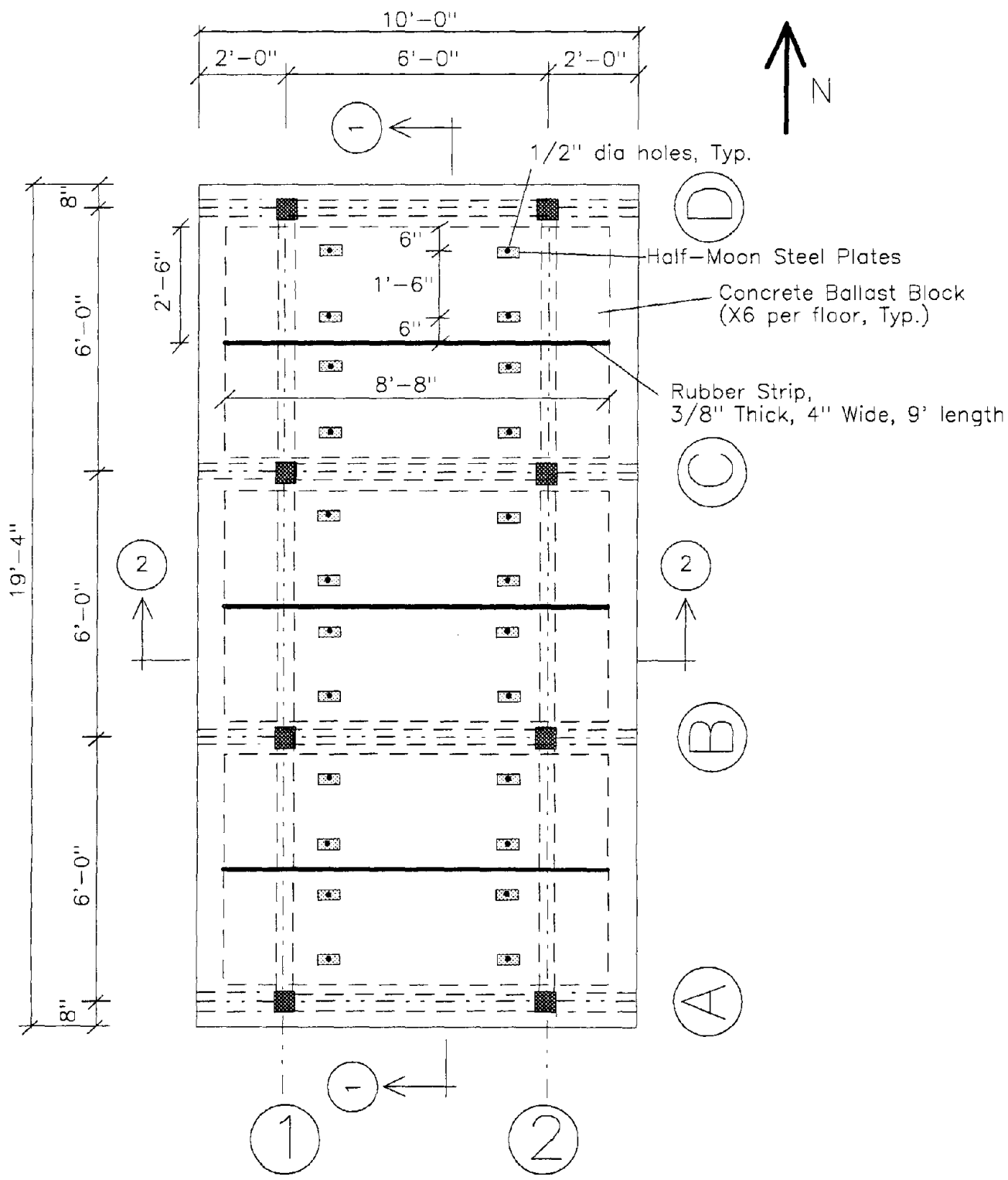
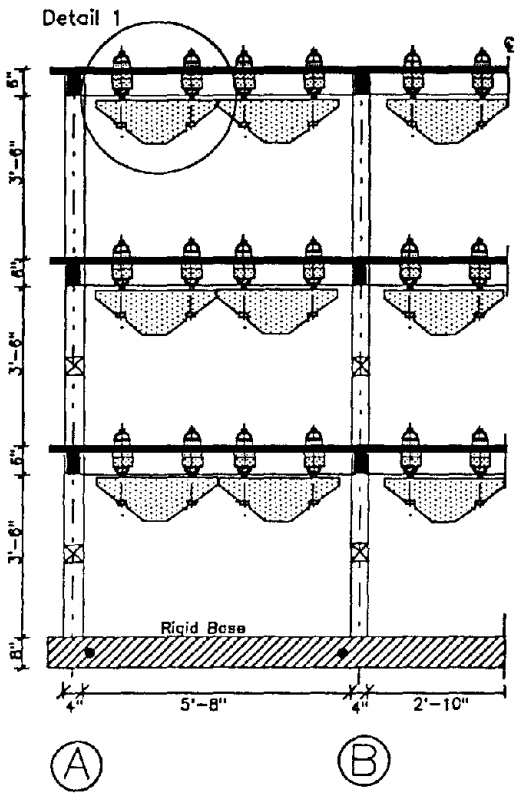
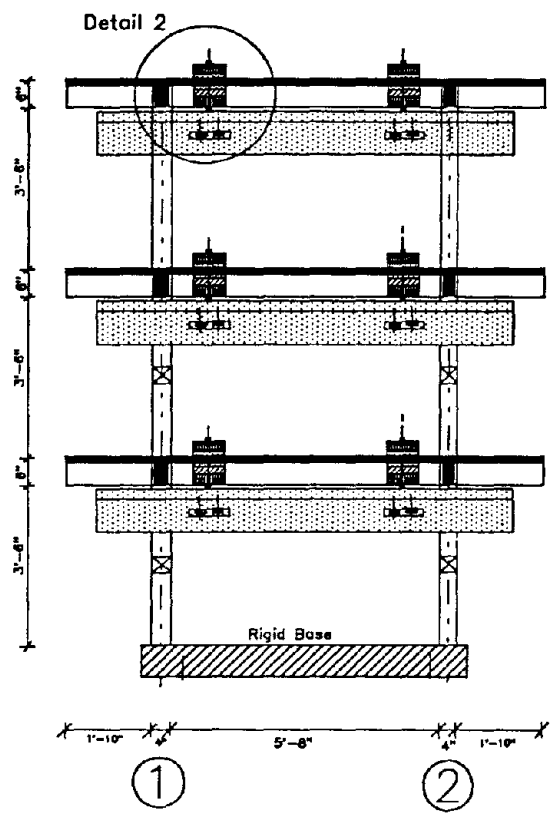


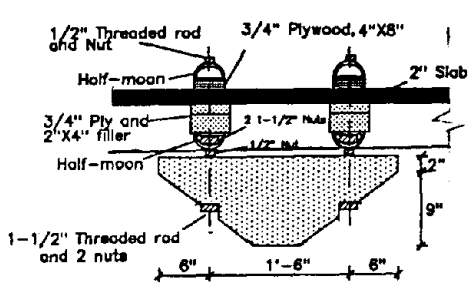
FIG. 3-14a Concrete Blocks on the Model



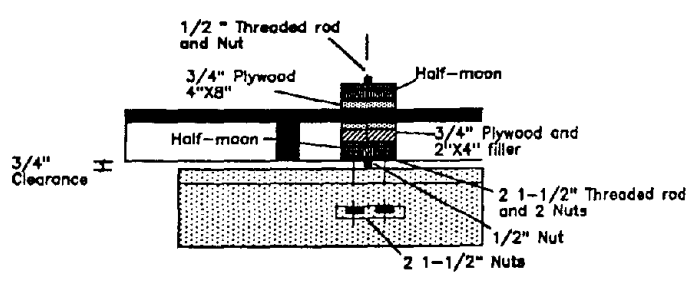
Section 1-1



Section 2-2

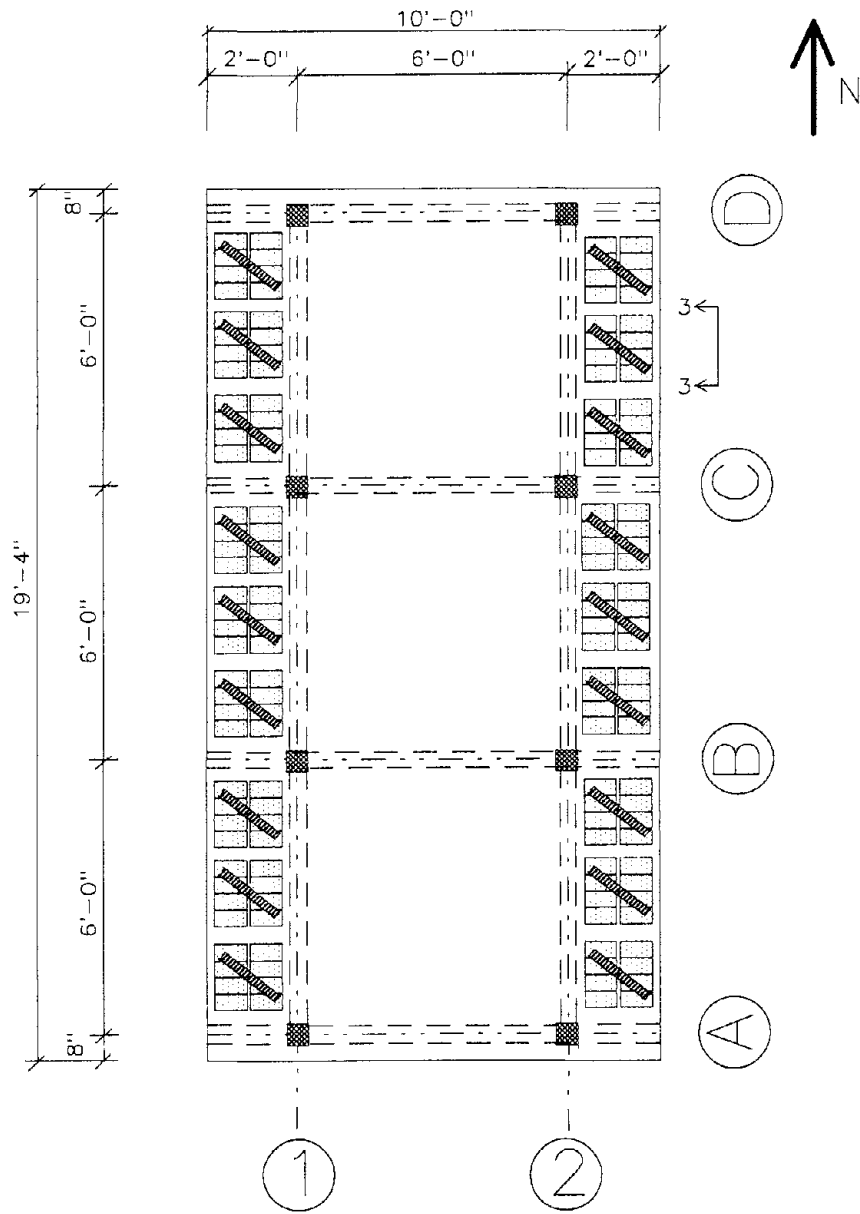


Detail 1

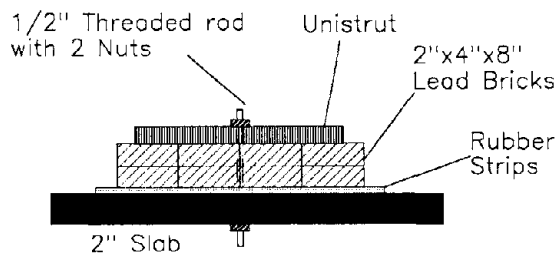


Detail 2

FIG. 3-14b Continued



(a) Plan



(b) Elevation 3-3

FIG. 3-15 Lead Bricks on the Model

3.6.1 Load Cells

Special force transducers (load cells) to measure the internal force response of the model, which included axial loads, shear forces, and bending moments, have been fabricated of mild steel and installed in the mid-story heights of the first and second story columns, shown in Figs. 3-1 and 3-16. The shear forces and bending moments were recorded in both the direction of motion and transverse to the direction of motion. The load cells were designed such that the stiffness was similar to the concrete column. Appendix B outlines the geometric layout, strain gaging, signal conditioning, and calibration of the load cells.

Four actively wired load cells were installed on the east side of the first and second story columns of the model. While four inactive ("dummy") load cells were installed on the west side to maintain symmetrical column stiffness in the model. Load cells were located in the first and second stories to complete the bending moment diagram for the critical first story beams. Due to the large cost of manufacturing and wiring, load cells were not installed in the third story columns and wired only along the east side of the model.

The mid-story height of the column was chosen because: it is normally close to the point of contraflexure resulting in small bending moments for lateral loads and hence the development of minimal steel stresses; and the disruption of regular column stiffness would not greatly affect the column deflection patterns.

Based on the yield strength of the steel, the axial, shear, and bending moment capacity ratings of the load cells are ± 40 kips, ± 5 kips, and ± 40 kip-in, respectively.

3.6.2 Displacement Transducers

Linear displacement sonic transducers (TemposonicsTM) were used to measure the absolute response displacements in the longitudinal (horizontal) direction of the base and each story level of the model during the shaking table tests. Fig. 3-16 shows the location of the displacement transducers (designated by tag name D#) mounted on the east and west base and column-slab intersections on the north side of the model. The displacement transducers: have global displacement ranges of ± 6 in., ± 8 in., and ± 10 in.; accuracies of $\pm 0.05\%$ of the full scale displacements, 0.003, 0.004 and 0.005 in., respectively; were conditioned by a generic power supply and manufacturer amplifier-decoders; and were calibrated for the respective full scale displacement per 10 volts.

3.6.3 Accelerometers

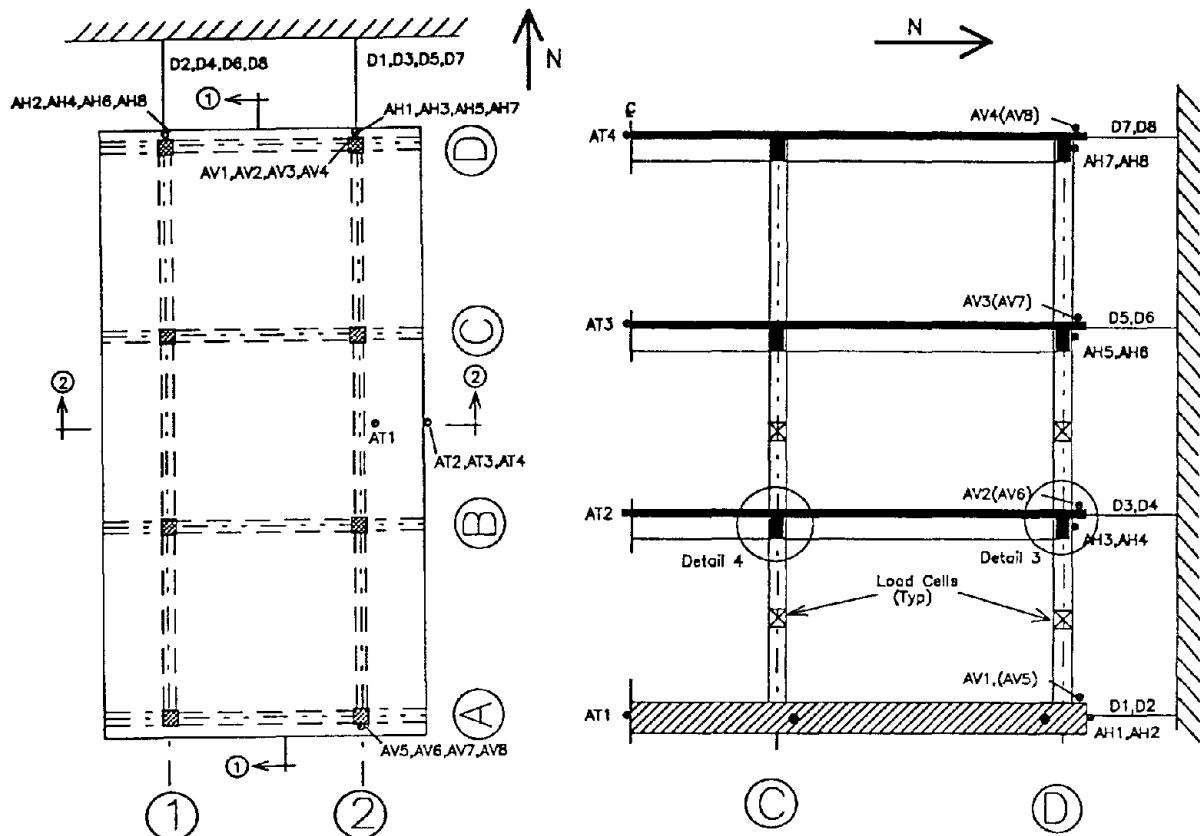
Resistive accelerometers (EndevcoTM, 25g) were used to measure the absolute story level accelerations of the model. Fig. 3-16 shows the position of each accelerometer with the respective tag name at the base, first, second, and third stories of the model in the direction of motion (designated by tag name AH#), transverse to motion (designated by tag name AT#), and for vertical motion (designated by tag name AV#). In the direction of motion, accelerometers were mounted on the east and west sides of the structure to detect any torsional response or out-of-phase motions. The accelerometers were conditioned with 2310 Vishay Signal Conditioning Amplifiers, which filtered frequencies above 25 Hz., calibrated for an acceleration range of ± 2 g per 10 volts, and have nonlinearities of $\pm 1.0\%$ of the recorded acceleration.

3.6.4 Linear Potentiometers

Linear potentiometers were installed at the north-east interior (designated by tag name PI#) and exterior (designated by tag name PE#) beam-column joints to measure displacements occurring on each side of the members of the joint. The readings of the potentiometers were used to find the average curvatures in each member of the instrumented interior and exterior joint. Fig. 3-16 shows the positioning of the potentiometers on the beams, columns, and slab. High strength epoxy was used to secure the aluminum square tube to the concrete members. The potentiometers used in the model have global displacement ranges of ± 0.25 and ± 0.50 in., linear accuracies of $\pm 1.0\%$ of the full scale displacement, 0.0025 and 0.0050 in., respectively, and conditioned with 2310 Vishay Signal Conditioning Amplifiers with calibration factors for the full scale displacement per 10 volts and again filtering frequencies above 25 Hz.

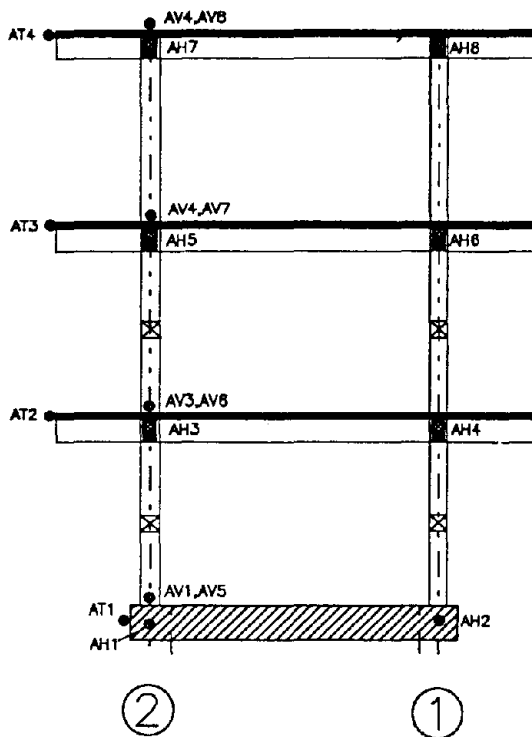
3.6.5 Data Acquisition System

The analog output readings from the instrumentation were recorded digitally using an Optim Megadac 5533A Data Acquisition System. The output recordings were stored on a laser disk and local personal computer at a frequency of 0.01 seconds.

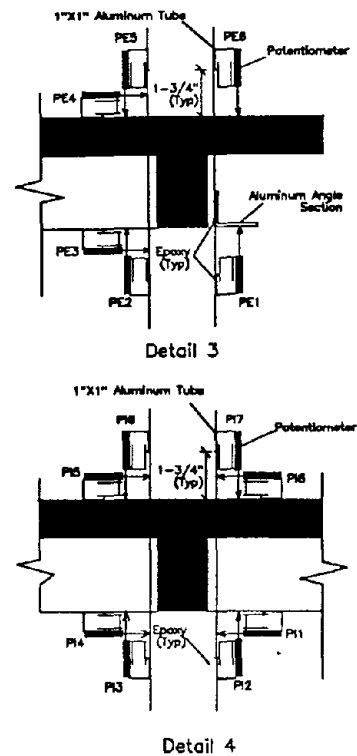


(a) Plan

(b) Section 1-1



(c) Section 2-2



(d) Details

FIG. 3-16 Instrumentation Identification and Locations

3.7 Testing Program

The testing program was divided in two parts: (i) identification of dynamic properties; and (ii) identification of inelastic behavior from strong base motion (simulated earthquakes).

3.7.1 Identification of Structural Dynamic Properties

The important structural dynamic properties are: (i) the natural frequencies (periods); (ii) the modal shapes; (iii) the equivalent viscous damping ratios; and (iv) the stiffness matrix of the model. Several tests were performed to determine these properties. Some of the tests were performed to determine the adequacy of testing technique for the identification process. These tests are:

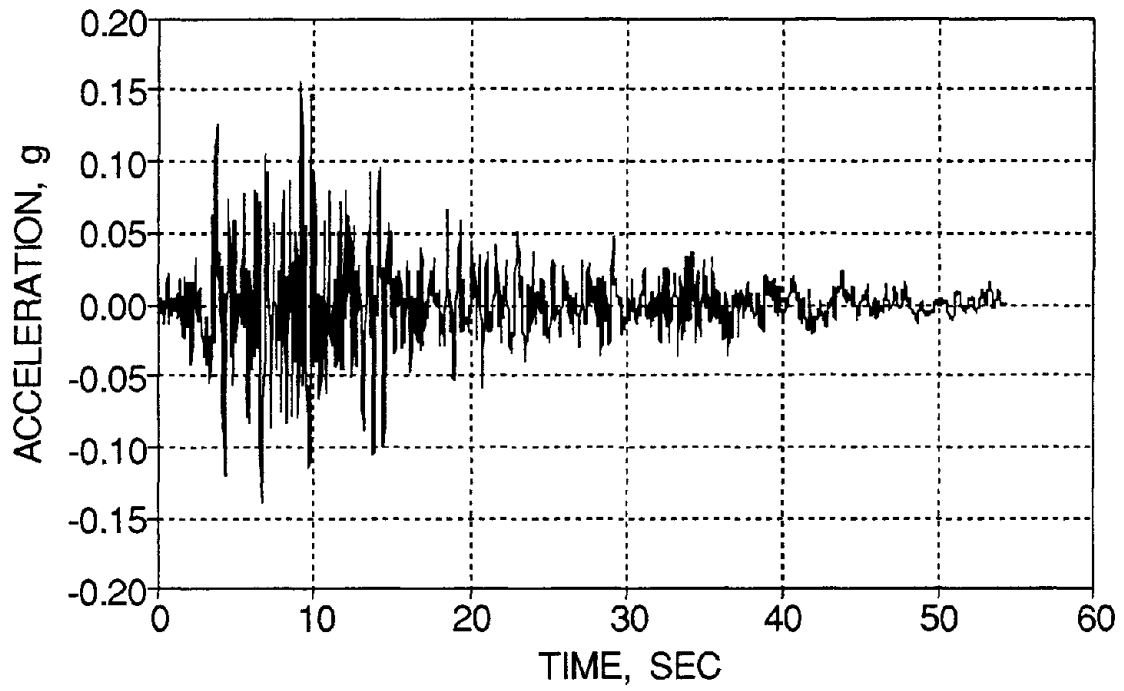
1. *Impact Hammer Test (HAMMER)* - An impact hammer was used to excite the unloaded (bare) model for identification of the initial dynamic characteristics from the transfer functions of the story level acceleration time histories. Since the magnitude of excitation from an impact hammer was small, excitation of the higher modes of the model was nominal. Therefore the results achieved from the HAMMER test were expected to be accurate only for the first mode.
2. *Pull-Back Test (PULL)* - Each floor of the model was statically loaded with a prescribed tensile force in the pre-cracked range for identification of the flexibility and stiffness matrix of the loaded model. Then were from an eigenvalue analysis, the initial natural frequencies and modal shapes were identified.
3. *Snap Test (SNAP)* - Each floor of the model was statically loaded and quickly released (snapped) to generate free vibrations for the loaded model. The initial dynamic characteristics were identified from the Fourier Transforms of the story level acceleration time histories.
4. *White Noise Test (WHN_B)* - A wide banded (0 to 50 Hz.) white noise base displacement applied by the shaking table was used to determine the initial dynamic characteristics of the model. The peak base acceleration was scaled to 0.024 g to provide enough excitation such that the modes of vibration could be identified.

Analysis of the test results for identification of the dynamic characteristics of the model are discussed in Section 4.

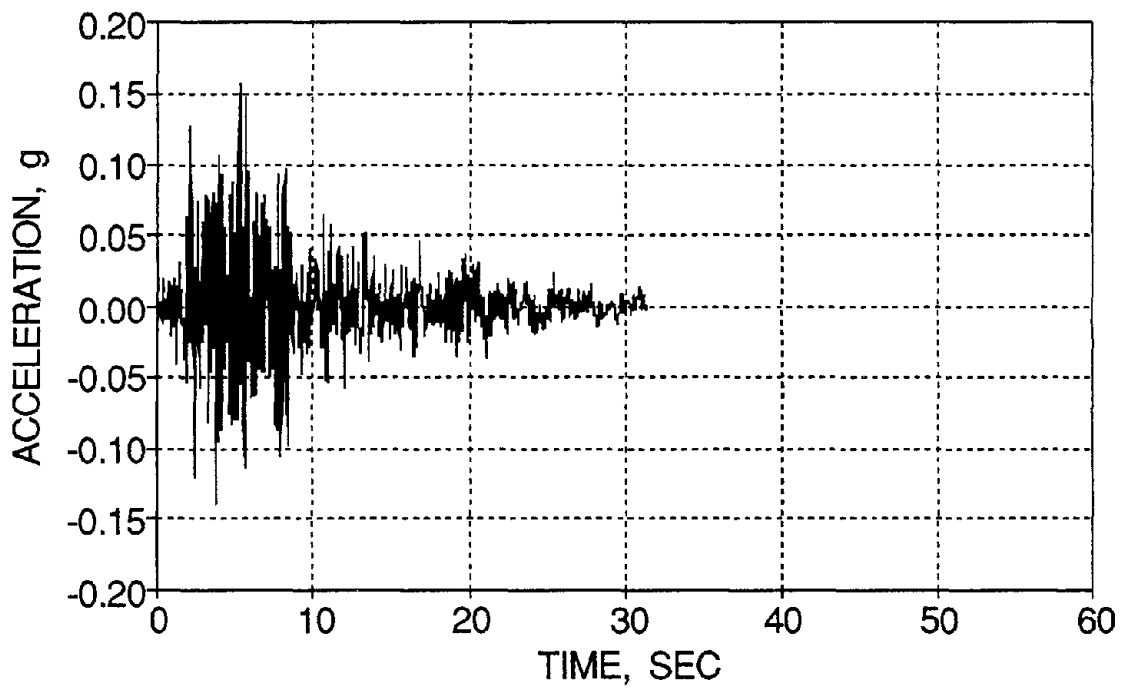
3.7.2 Selection of the Ground (Shaking Table) Excitation

Since the model structure is representative of low-rise R/C framed buildings typically constructed in the Eastern and Central United States, the base motion chosen for excitation was to reflect a probable type earthquake that would occur in these regions. An important point to note about ground motions is that they general vary in magnitude and frequency content. Also the local soil conditions and location of typical structures with respect to the epicenter of the earthquake are generally different for each structure. Therefore, this creates unrelated ground motion characteristics in the various structures. Furthermore, since predictions of magnitude and frequency content characteristics of earthquakes in these regions can not accurately be assessed primarily due to soil conditions, an earthquake to be chosen should be such that large magnitudes of base motion occur over a wide range of frequencies. This will dynamically excite a larger number of such typical buildings of varying natural frequencies and geographic locations.

In view of the previous discussion, the N21E ground acceleration component (accelerogram) of the July 21, 1952 Taft Earthquake at the Lincoln School Tunnel site in California was selected for the shaking table motion to excite the model structure. The original accelerogram, shown in Fig. 3-17a, has a total ground excitation time history of 54.4 seconds with a peak ground acceleration (PGA) of 0.156 g at 9.1 seconds. To satisfy time similitude requirements of the actual earthquake for the one-third scale model (see Appendix A), a scale factor of $1/\sqrt{3}$ is used to compress the time history of the accelerogram. Fig. 3-17b shows the scaled ground motion of the Taft N21E earthquake used in testing the one-third scale model.



(a) Full Scale Taft N21E



(b) One-Third Scale Taft N21E

FIG. 3-17 Ground Motions for the Taft N21E Accelerogram Component

Fig. 3-18 shows the elastic response spectra (acceleration amplifications) for a single degree of freedom system (SDOF) excited by the Taft N21E component ground motion for 2%, 5%, 10%, and 20% damping ratios. The period range for elastic amplification of a single degree of freedom system with a 2% damping ratio (typical in R/C structures) is found to be from 0.0 seconds to about 0.8 seconds. Since this amplification occurs over a wide range of periods, a large class of structures would theoretically undergo some amplifications. Therefore the Taft N21E component is considered acceptable for the experiment. Shown in Fig. 3-18, the model has an initial first mode natural period of about 0.57 seconds and a damping ratio of about 2%. This corresponded to a 33% amplification in story level acceleration according to the response spectra for an elastic SDOF with a 2% damping ratio. It should be noted that El-Attar et al. (1991b) used the Taft S69E component for their simulated base motions. However, the response spectra for the Taft N21E and S69E components are similar.

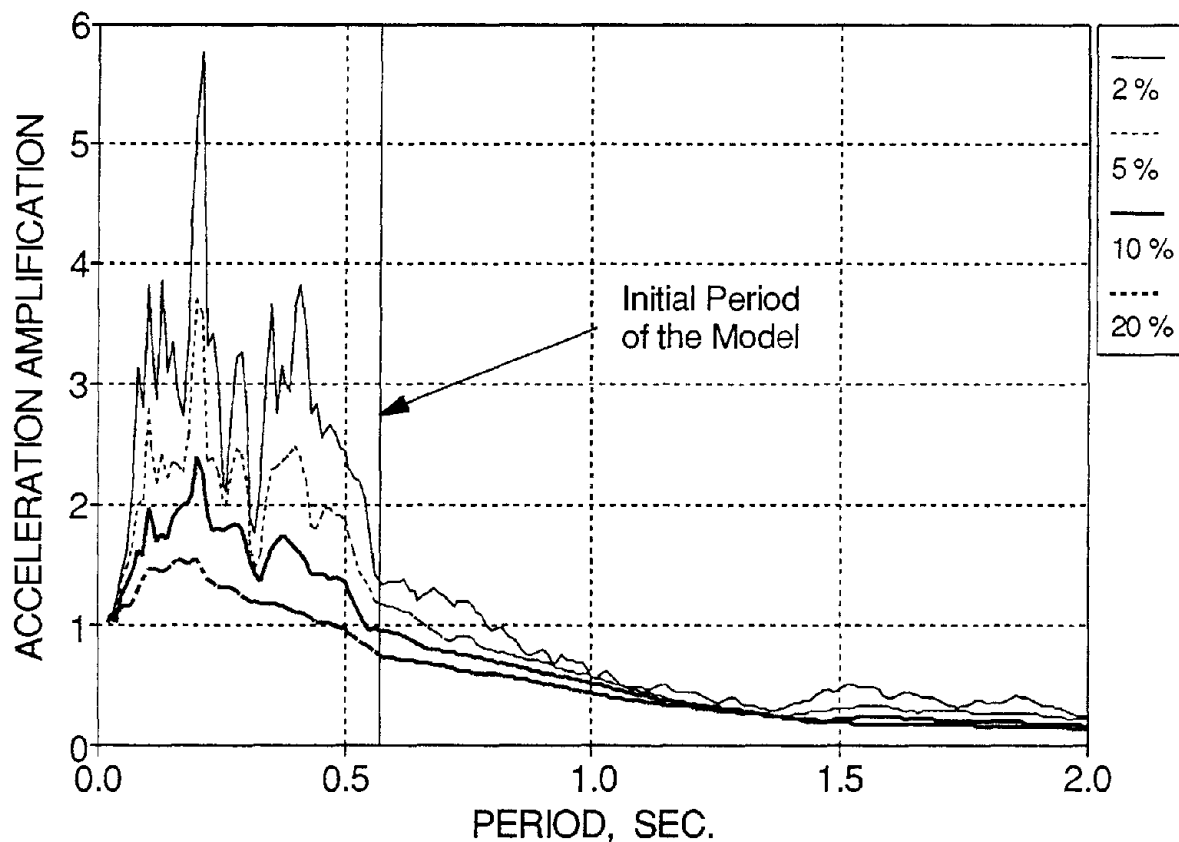


FIG. 3-18 Elastic Response Amplifications for the Scaled Taft N21E Component

3.7.3 Selection of Peak Ground Accelerations

One of the objectives for the shaking table experiments is to observe the structural response, including damage to the model from different intensity (damaging) ground motions. To accomplish these goals with the earthquake chosen, the amplitude of the ground motion, Taft N21E, was scaled such that the peak acceleration for the earthquakes are 0.05 g, 0.20 g, and 0.30 g. These three earthquakes are representative of minor-moderate, moderate-severe, and severe ground motions, respectively in terms of ensuing structural damage. The following outlines each damaging earthquake ground motion:

(a) Minor Base Motion

The minor base motion excitation (PGA 0.05 g) is used to investigate the pre-yield behavior of the model structure. Minor ground motions occur periodically in the Eastern and Central United States as well as around the world. In the Eastern and Central United States where the ground conditions tend to be more stiff and rigid, earth tremors can also be expected to travel great distances before being fully damped out. Therefore many areas would experience minor ground motions from a moderate or severe earthquake that may have occurred many miles away. Therefore structures must be capable of withstanding a minor ground motion with very little structural damage, if any at all.

Since the model response is expected to be primarily governed by elastic deformations for the minor ground motion excitation, this ground motion is also very important for comparing the experimental response with analytical response from any linear or non-linear dynamic analysis program. The comparisons between the experimental and analytical response are expected to be very similar under these levels of loading and would therefore validate further testing.

Another reason for a low level base motion is to verify the proper functioning of the instrumentation on the model. If malfunctions exist, the instrumentation could be fixed or replaced without a drastic change in the characteristics of the model, since elastic response has no permanent deformations or energy dissipation.

(b) Moderate Base Motion

The moderate earthquake (PGA 0.20 g) was used to investigate the inelastic behavior of the model structure. Jacobs (1990) mentions that the return period for such an earthquake in the Eastern and Central United States, magnitude 5.0 or less on the Richter Scale, is about 3 years. NEHRP (1991) locally quantifies the peak acceleration magnitude of earthquakes with return periods of 500 years and 2500 years throughout the United States. The 500 year return period earthquake for typical cities in the Eastern United States, such as New York City and Buffalo, have peak acceleration magnitudes of about 0.15 g and 0.10 g, respectively. If earthquake effects are to be factored by conventional load factors for design (1.4) and for torsional effect considerations for non-symmetric striking direction (1.1), the peak design accelerations for a 500 year return period earthquake are about 0.22 g and 0.15 g, respectively. Therefore this motion can be considered as representative of a design type earthquake with a 500 year return period for typical cities in the Eastern and Central United States.

In some codes for earthquake resistance in seismic zones, a structure should remain serviceable with only minor repairs being required in cracked members upon a thorough damage inspection of the structure. But since the model structure was not designed for lateral loads, the potential for heavy damage was probable. With analytical predictions from an inelastic dynamic analysis [using IDARC, Kunnath et al. (1990)], the Taft N21E component with a PGA of 0.20 g created moderate damage to the model structure in the form of some inelastic cracking and yielding in members.

(c) Severe Base Motion

The severe earthquake (PGA 0.30 g) was used to investigate the near collapse (plastic) mechanism for the model structure. The return period for an earthquake of Richter magnitude of 6.0 or greater in the Eastern and Central United States is about 22 years, [Jacobs (1990)]. NEHRP (1991) recommends peak ground accelerations for a 2500 year return period earthquake of about 0.3 g and 0.2 g, respectively for New York City and Buffalo. For factored load design including torsional effects, this corresponds to peak accelerations of about 0.45 g and 0.30 g, respectively. Therefore this motion can be considered as representative of a design type earthquake with a 2500 year return period for typical cities in the Eastern and Central United States.

Most seismic design codes recommend design in which a structure is expected to develop moderate damage from a severe ground motion, with collapse prohibited. The resulting damage would also be such that with repair or retrofit, the structure could regain its serviceability condition. However, since the model structure considered in this study is not designed for lateral loads, the potential for collapse is prominent. Cracking, yielding, plastification of the members and joints, and possible structural collapse are the expected damage in the model. The peak magnitude of ground acceleration to be selected for the experimental study has to be such that the probability for collapse of the model would be small, but the expected damage would be high. A replica one-eighth scale model structure was tested with a PGA of 0.35 g with damage, but not collapse, El-Attar et al. (1991b). However, the same model was then tested to collapse with a PGA of 0.80 g for identification of the resulting collapse mechanism. Aycardi et al. (1992) had tested quasi-statically the critical components of the one-third scale model in a cyclic behavior to ultimate capacity (presented in Part II of this evaluation report series). Based on close observations of these component tests and analytical predictions (from IDARC) for the model structure after the superposition of the 0.05 g and 0.20 g ground motions (Taft N21E), a normalized PGA of 0.30 g was selected for the severe base motion. A PGA of 0.35-0.40 g would be near complete collapse as shown in Part III of this evaluation report series.

3.7.4 Shaking Table Testing Program

Table 3-4 shows a summary of the shaking table testing program. For proper calibration of the shaking table, an uncompensated white noise excitation, WHN_A, was used for table motion to analyze the table efficiency. Following some adjustments in amplification of the table, a compensated white noise excitation, WHN_B, was derived and used to identify the initial dynamic properties of the model. Note that a compensated white noise shaking (test label - WHN-#) was used after every earthquake test for identification of the prevailing dynamic characteristics of the model.

The response during minor earthquake is presented in Section 4 of this study. The response during the moderate and severe earthquakes is presented in Part III of the evaluation report series (see Section I).

TABLE 3-4 Shaking Table Testing Sequence for the Model

Test #	Date	Test Label	Test Description	Purpose
1	2/21/91	WHN_A	Uncompensated White Noise, PGA 0.024 g	Table Calibration
2	2/21/91	WHN_B	Compensated White Noise, PGA 0.024 g	Identification
3	2/21/91	TFT_05	Taft N21E, PGA 0.05 g	Minor Earthquake, Elastic Response
4	2/21/91	WHN_C	Compensated White Noise, PGA 0.024 g	Identification
5	2/22/91	WHN_D	Compensated White Noise, PGA 0.024 g	Identification
6	2/22/91	TFT_20	Taft N21E, PGA 0.20 g	Moderate Earthquake, Inelastic Response
7	2/22/91	WHN_E	Compensated White Noise, PGA 0.024 g	Identification
8	2/22/91	TFT_30	Taft N21E, PGA 0.30 g	Severe Earthquake, Inelastic Response
9	2/22/91	WHN_F	Compensated White Noise, PGA 0.024 g	Identification

SECTION 4

IDENTIFICATION OF DYNAMIC CHARACTERISTICS - ELASTIC RESPONSE

4.1 Introduction

The identification of the initial dynamic characteristics of the undamaged model structure are presented first. The characteristics of importance include the following: natural frequencies; modal shapes; equivalent viscous damping ratios; stiffness matrix; and modal participation factors. These characteristics are found through a series of different tests described in Section 3.7.1 using the story displacement and acceleration time history response and frequency domain response of the story transfer functions. Table 4-1 show the testing program for identification of the dynamic characteristics of the undamaged model.

Table 4-1 Identification Testing Program of Model

Test #	Description	Test Label
1	Impact Hammer Test	HAMMER
2	Pull-Back Test	PULL
3	Snap-Back Test	SNAP
4	Compensated White Noise	WHN_B

The theoretical background for determining the dynamic characteristics of a structure from both the experimental time history response and frequency domain story transfer functions is presented. The experimental test results are compared to analytical predictions from STAAD™ (1989). The comparisons and discrepancies among the various tests and analytical predictions are also discussed.

Following the identification of the initial dynamic characteristics of the model, the minor earthquake motion is used to excite the model. This level of excitation is used to identify the elastic (pre-yield) concrete structural properties of the model. The global and local response of the model from this superimposed base motion are presented.

4.2 Identification Procedures

The following derivations show that the natural frequencies, modal shapes, and elastic equivalent viscous damping characteristics of a structure can be determined from the transfer functions of the story acceleration response of the structure and the base motion. Herein, a transfer function is defined as an output structural response normalized by a superimposed input base motion in the frequency domain, (i.e. the Fourier Transform of a story level acceleration time history normalized by the Fourier Transform of the base acceleration time history).

For sake of completeness, the logarithmic-decrement and half-power (bandwidth) methods are also presented for determining the equivalent viscous damping characteristics from the response in the time and frequency domains, respectively.

Next, the stiffness and damping matrices are derived in terms of the mass and orthogonal modal shape matrices.

4.2.1 Frequency Domain Identifications

Modal identifications can be developed from frequency domain analysis procedures. The following describes the identification technique.

4.2.1.1 Modal Shapes

Eq. (4.1) shows the general equation of motion for a multi-degree-of-freedom (MDOF) system excited by a horizontal base acceleration motion, $\ddot{x}_g(t)$.

$$\mathbf{M}\ddot{\mathbf{x}}(t) + \mathbf{C}\dot{\mathbf{x}}(t) + \mathbf{K}\mathbf{x}(t) = -\mathbf{m}\ddot{x}_g(t) \quad (4.1)$$

where \mathbf{M} = Mass matrix of the structure
 \mathbf{C} = Viscous damping matrix of the structure
 \mathbf{K} = Stiffness matrix of the structure
 $\ddot{x}_g(t)$ = Ground (base) acceleration time history
 $\mathbf{m} = \mathbf{M} \cdot \bar{\mathbf{I}}$ = Mass vector of the structure
 $\bar{\mathbf{I}}$ = Identity vector
 $\mathbf{x}(t)$ = Relative story displacement vector time history
 $\dot{\mathbf{x}}(t)$ = Relative story velocity vector time history
 $\ddot{\mathbf{x}}(t)$ = Relative story acceleration vector time history

The relative story displacement vector, $\mathbf{x}(t)$, can be expressed in modal form by the product of the modal shape matrix, Φ , and modal story displacement vector, $\eta(t)$, of the structure as follows:

$$\mathbf{x}(t) = \Phi \cdot \eta(t) \quad (4.2)$$

Therefore Eq. (4.1) can be expressed in modal form by inserting Eq. (4.2) and the displacement time derivatives as follows:

$$\mathbf{M}\Phi\ddot{\eta}(t) + \mathbf{C}\Phi\dot{\eta}(t) + \mathbf{K}\Phi\eta(t) = -\mathbf{m}\ddot{x}_g(t) \quad (4.3)$$

Multiplying Eq. (4.3) by the transpose of the k-th mode shape, ϕ_k^T , and using modal shape orthogonality properties (discussed in Section 4.2.2), the resulting uncoupled equation of motion for the k-th mode of vibration becomes:

$$M_k^* \ddot{\eta}_k(t) + C_k^* \dot{\eta}_k(t) + K_k^* \eta_k(t) = -\phi_k^T \mathbf{m} \ddot{x}_g(t) \quad (4.4)$$

where $M_k^* = \phi_k^T \mathbf{M} \phi_k$ = k-th modal mass
 $C_k^* = \phi_k^T \mathbf{C} \phi_k$ = k-th modal viscous damping
 $K_k^* = \phi_k^T \mathbf{K} \phi_k$ = k-th modal stiffness

For convenience, the mode shapes are normalized by the mass matrix such that $M_k^* = 1$ (in Section 4.2.2, it is discussed how this can be accomplished). The results imply that $\Phi_k^T \mathbf{M} = \Phi^{-1}$.

The modal story displacements and displacement time derivatives (velocities and accelerations) for the k-th mode can be transformed into the frequency domain by using the Fourier Transform. The base acceleration can also be converted to the frequency domain in a similar fashion. The resulting equation of motion for the k-th mode in the frequency domain becomes:

$$-\omega^2 \eta_k(\omega) + 2i\omega \xi_k \omega_k \eta_k(\omega) + \omega_k^2 \eta_k(\omega) = -\Gamma_k \ddot{x}_g(\omega) \quad (4.5)$$

where ω = frequency (rad/sec)
 ξ_k = damping ratio for the k-th mode
 ω_k = k-th natural frequency (rad/sec)
 $\Gamma_k = \Phi_k^T \mathbf{m}$ = k-th modal participation factor

Solving Eq. (4.5) for the k-th modal displacement in the frequency domain results in the following:

$$\eta_k(\omega) = \frac{\Gamma_k \cdot \ddot{x}_g(\omega)}{\omega_k^2 - \omega^2 + 2i\omega \xi_k \omega_k} \quad (4.6)$$

The absolute story accelerations, $\ddot{\mathbf{a}}(t)$, can be represented as follows:

$$\ddot{\mathbf{a}}(t) = \ddot{\mathbf{x}}(t) + \ddot{x}_g(t) \quad (4.7)$$

Using Eq. (4.2) and converting to the frequency domain, Eq. (4.7) results in the following:

$$\ddot{\mathbf{a}}(\omega) = -\omega^2 \Phi \eta(\omega) + \ddot{x}_g(\omega) \quad (4.8)$$

Premultiplying Eq. (4.8) by $\Phi_k^T \mathbf{M}$ results in:

$$\Phi_k^T \mathbf{M} \ddot{\mathbf{a}}(\omega) = -\omega^2 \eta_k(\omega) + \Phi_k^T \mathbf{M} \ddot{x}_g(\omega) \quad (4.9)$$

Define the absolute k-th modal acceleration, $\zeta_k(\omega)$, for each floor as:

$$\zeta_k(\omega) = \Phi_k^T \mathbf{M} \ddot{\mathbf{a}}(\omega) = -\omega^2 \eta_k(\omega) + \Gamma_k \ddot{x}_g(\omega) \quad (4.10)$$

Therefore Eq. (4.5) can be represented as:

$$\ddot{\zeta}_k(\omega) + 2i\omega\xi_k\omega_k\eta_k(\omega) + \omega_k^2\eta_k(\omega) = 0 \quad (4.11)$$

Solving for the absolute modal story accelerations for the k-th mode in terms of the modal story displacement in Eq. (4.11) results in the following:

$$\ddot{\zeta}_k(\omega) = -(2i\omega\xi_k\omega_k + \omega_k^2) \cdot \eta_k(\omega) \quad (4.12)$$

Substituting Eq. (4.6) into Eq. (4.12), the absolute modal story accelerations for the k-th mode can be obtained in terms of the base acceleration as follows:

$$\ddot{\zeta}_k(\omega) = \frac{-\Gamma_k \cdot (2i\omega\xi_k\omega_k + \omega_k^2)}{\omega_k^2 - \omega^2 + 2i\omega\xi_k\omega_k} \cdot \ddot{x}_g(\omega) \quad (4.13)$$

Since $\Phi_k^T \mathbf{M} = \Phi^{-1}$ in Eq. (4.10) and considering the superposition of the modes of vibration, the absolute j-th floor acceleration can be expressed as follows:

$$\ddot{a}_j(\omega) = \sum_{k=1}^n [\phi_{jk} \cdot \ddot{\zeta}_k(\omega)] \quad (4.14)$$

where $\ddot{a}_j(\omega)$ = j-th floor absolute acceleration
n = modes of vibration
 ϕ_{jk} = k-th mass normalized mode shape for the j-th floor (DOF)

Substituting Eq. (4.13) into (4.14), the absolute floor accelerations can be represented as follows:

$$\ddot{a}_j(\omega) = \sum_{k=1}^n \left[\frac{-\Gamma_k \cdot (2i\omega\xi_k\omega_k + \omega_k^2)}{\omega_k^2 - \omega^2 + 2i\omega\xi_k\omega_k} \cdot \phi_{jk} \right] \ddot{x}_g(\omega) \quad (4.15)$$

The transfer function is defined as the ratio of a output structural response to a superimposed input base motion in the frequency domain. Therefore, the transfer function for the j-th floor, $\mathbf{H}_j(\omega)$, can be represented by dividing Eq. (4.15) by the input base acceleration, $\ddot{x}_g(\omega)$. Eq. (4.16) shows the resulting transfer function.

$$\mathbf{H}_j(\omega) = \sum_{k=1}^n \frac{-\Gamma_k \cdot (2i\omega\xi_k\omega_k + \omega_k^2)}{\omega_k^2 - \omega^2 + 2i\omega\xi_k\omega_k} \cdot \phi_{jk} = \sum_{k=1}^n \mathbf{h}_k(\omega) \cdot \phi_{jk} \quad (4.16)$$

However when a structure is lightly damped, the k-th peak magnitude of the j-th floor transfer function occurs very close to the k-th mode natural frequency, thus $\omega = \omega_k$. Also for small damping and well separated modes (narrowbanded systems), the i-th transfer function peak at the k-th natural frequency, $\mathbf{h}_i(\omega_k)$, with resonance at a distant frequency from ω_k , approaches a small value, ϵ , and can be neglected. Only $\mathbf{h}_k(\omega_k)$, with resonance at ω_k , has a significant value. Therefore the sum in Eq. (4.16) simplifies to the product $\mathbf{h}_k(\omega_k) \cdot \phi_{jk}$. Hence the peak of the j-th transfer function at the k-th natural frequency can be represented as follows:

$$|\mathbf{H}_j(\omega_k)| = \frac{\Gamma_k \sqrt{1 + 4\xi_k^2}}{2\xi_k} \cdot \phi_{jk} \quad (4.17)$$

Therefore the peak of the j-th transfer function at the k-th natural frequency is proportional to the magnitude of the mass normalized mode shape for the k-th mode and the j-th degree of freedom. The constant of proportionality is a function of the damping ratio and modal participation factor for the k-th mode. Since the constant of proportionality is the same for all degrees of freedom for the k-th mode, the ratio of the peaks in the transfer functions for the different degrees of freedom at the k-th natural frequency are equal to the ratio of the mode shapes for the k-th mode.

The phase angles for the mode shapes are also determined experimentally from the Fourier Transform of the story accelerations as a function of the natural frequencies as follows:

$$\theta(\omega_i) = \tan^{-1} \left(\frac{I(\omega_i)}{R(\omega_i)} \right) \quad (4.18)$$

where $\theta(\omega_i)$ = phase angle for the j-th floor at ω_i

ω_i = i-th natural frequency

$I(\omega_i)$ = imaginary part of the Fourier Ampl. of the j-th story acceleration at ω_i

$R(\omega_i)$ = real part of the Fourier Ampl. of the j-th story acceleration at ω_i

Therefore by comparing the phase angles for each story at the natural frequencies, the mode shape phases can be determined.

4.2.1.2 Damping Characteristics

From Eq. (4.17), the elastic equivalent viscous damping factor for the k-th mode, ξ_k , can be estimated from the experimentally determined j-th story transfer function magnitude, k-th mass normalized mode shape at the j-th DOF, and the k-th modal participation factor as follows:

$$\xi_k = \sqrt{\left[\left(\frac{2 | \mathbf{H}_j(\omega_k) |}{\phi_{jk} \Gamma_k} \right)^2 - 4 \right]^{-1}} \quad (4.19)$$

The equivalent viscous damping characteristics of an elastic structure can also be determined from a frequency domain response analysis using the well known half-power (bandwidth) method, Clough and Penzien (1975). The k-th mode damping factor is determined from the frequencies at which the response at the k-th natural frequency, ρ_{f_k} , is reduced by $(1/\sqrt{2})$ or frequencies for which the power input is half the input at resonance as shown in Fig. 4-1. Hence the k-th mode viscous damping factor, ξ_k , can be determined by the following:

$$\xi_k = \frac{f_2 - f_1}{f_2 + f_1} = \frac{f_2 - f_1}{2f_k} \quad (4.20)$$

where $f_1, f_2 =$ frequencies when $\rho_{f_1}, \rho_{f_2} = (1/\sqrt{2})\rho_{f_k}$ (See Fig. 4-1)
 $f_k =$ k-th natural frequency

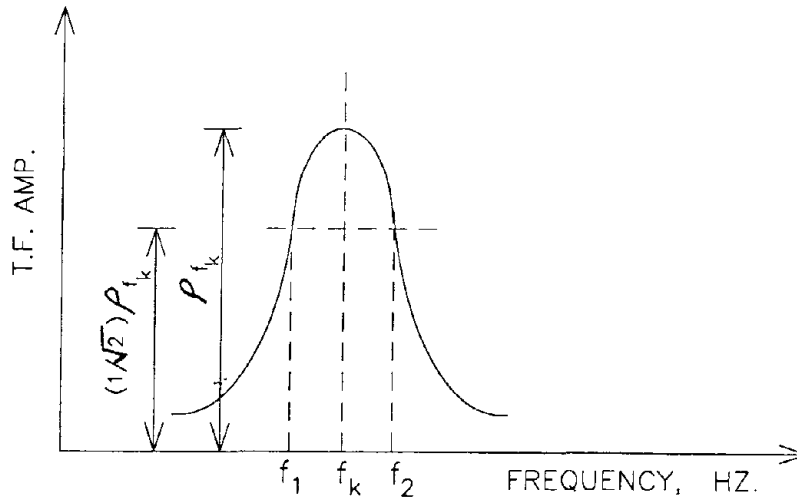


FIG. 4-1 Typical Frequency Response for Determining Damping Characteristics

The equivalent viscous damping characteristics of an elastic SDOF system can also be determined from the decay of a free vibration time history response of the system. From the well known logarithmic decrement method, Craig (1981) and many others, the damping factor, ξ , is estimated by considering peak response which are several cycles apart as follows:

$$\xi = \frac{\ln(v_n/v_{n+m})}{2\pi m} \quad (4.21)$$

where n = Starting cycle
 m = arbitrary number of cycles from starting cycle
 v_n = Response at cycle n
 v_{n+m} = Response at cycle $n+m$

The free vibration decay method can also be used on the response signals from MDOF systems which are primarily governed by a single mode of vibration, as in a SDOF.

4.2.2 Identification of Structural Stiffness and Damping

A diagonal generalized (modal) mass matrix, \mathbf{M}_n , is obtained from the mass and orthogonal modal shape matrices as follows:

$$\mathbf{M}_n = \Phi^T \mathbf{M} \Phi \quad (4.22)$$

where Φ = Modal shape matrix
 \mathbf{M} = Mass matrix

The mass normalized modal shape vectors are found by normalizing the i -th mode shape vector by the root of the i -th modal mass, $\phi_{ni} = \phi_i \cdot M_{ni}^{-1/2}$. The normalized modal shape matrix, Φ_n , can then be constructed from the superposition of the normalized modal shape vectors as follows:

$$\Phi_n = [\phi_{n1}, \phi_{n2}, \dots, \phi_{nm}] \quad (4.23)$$

The new generalized mass matrix, developed from the normalized modal shape matrix, has the orthonormal relationship of:

$$\Phi_n^T \mathbf{M} \Phi_n = \mathbf{I} \quad (4.24)$$

where \mathbf{I} = Identity matrix

Using these orthonormal properties, the stiffness matrix, \mathbf{K} , can be represented as follows:

$$\Phi_n^T \mathbf{K} \Phi_n = \Omega \quad (4.25)$$

where Φ_n = Normalized modal shape matrix

Ω = Diagonal natural frequency matrix $[\omega_1^2, \omega_2^2, \dots, \omega_n^2]$

ω_i = i-th natural frequency (rad/sec)

Therefore the stiffness matrix can be identified as:

$$\mathbf{K} = \Phi_n^{-T} \Omega \Phi_n^{-1} \quad (4.26)$$

From the orthonormal conditions from Eq. (4.24), the following can be derived:

$$\Phi_n^{-T} = \mathbf{M} \Phi_n \quad (4.27a)$$

$$\Phi_n^{-1} = \Phi_n^T \mathbf{M} \quad (4.27b)$$

Therefore substituting Eqs. (4.27a) and (4.27b) into Eq. (4.26) results in the following:

$$\mathbf{K} = \mathbf{M} \Phi_n \Omega \Phi_n^T \mathbf{M} \quad (4.28)$$

Therefore Eq. (4.28) is used to identify the stiffness matrix of a structure from the known mass matrix, experimentally determined natural frequencies, and orthonormal modal shape matrix.

For a typical shear-type building with lumped story level masses and rigid floors, the stiffness matrix can be described as follows:

$$\mathbf{K} = \begin{pmatrix} k_3 & -k_3 & 0 \\ -k_3 & k_2 + k_3 & -k_2 \\ 0 & -k_2 & k_1 + k_2 \end{pmatrix} \quad (4.29)$$

where $k_i = i$ -th story stiffness

A comparison of these story stiffnesses is observed throughout the testing of the model structure for deterioration.

The damping matrix can be developed by assuming proportional damping with the same theory as the stiffness matrix determination as follows:

$$\mathbf{C} = \mathbf{M}\Phi_n \zeta \Phi_n^T \mathbf{M} \quad (4.30)$$

where $\zeta =$ Diagonal matrix $[2\xi_1\omega_1, 2\xi_2\omega_2, \dots, 2\xi_n\omega_n]$

$\xi_i =$ i -th mode damping ratio

$\omega_i =$ i -th natural frequency (rad/sec)

4.2.3 Internal Energy Quantification

The energy equation for a N -story building subjected to a base motion was derived by Uang and Bertero (1990) as follows:

$$\frac{1}{2} \dot{\mathbf{v}}_t^T \mathbf{M} \dot{\mathbf{v}}_t + \int \mathbf{f}_d^T d\mathbf{v} + \int \mathbf{f}_s^T d\mathbf{v} = \int \left(\sum_{i=1}^N m_i \ddot{v}_i \right) dv_g \quad (4.31)$$

where $\mathbf{M} =$ diagonal mass matrix

$\dot{\mathbf{v}}_t =$ absolute velocity vector

$\mathbf{v} =$ relative displacement vector

$\mathbf{f}_d =$ damping force vector

$\mathbf{f}_s =$ restoring force vector

$m_i =$ lumped mass of the i -th floor

$\ddot{v}_i =$ absolute acceleration at the i -th floor

$v_g =$ ground displacement

The kinetic energy, E_K , of a N -story building is calculated from the summation of the kinetic energy at each floor level as follows:

$$E_K = \frac{1}{2} \dot{\mathbf{v}}_t^T \mathbf{M} \dot{\mathbf{v}}_t = \frac{1}{2} \sum_{i=1}^N m_i (\dot{v}_{ti})^2 \quad (4.32)$$

where \dot{v}_{ti} = absolute velocity at the i-th floor

The input energy, E_I , to the N-story building is calculated from the summation of the work done by the inertia forces ($m_i \ddot{v}_{ti}$) at each floor for the superimposed ground displacement as follows:

$$E_I = \int \left(\sum_{i=1}^N m_i \ddot{v}_{ti} \right) dv_g \quad (4.33)$$

Note that the summation of the inertia forces at each floor is the induced base shear force on the structure.

The energy absorbed by the restoring forces, E_A , can be resolved into the irrecoverable hysteretic (dissipated) energy, E_H , and recoverable elastic strain energy, E_S , as follows:

$$E_A = \int \mathbf{f}_s^T d\mathbf{v} = E_S + E_H \quad (4.34)$$

where

$$E_S = \sum_{i=1}^N \frac{V_i^2}{2K_i}$$

$$E_H = \sum_{i=1}^N \int V_i d\delta_i - \sum_{i=1}^N \frac{V_i^2}{2K_i}$$

V_i = undamped story shear force history

K_i = unloading stiffness of the story shear versus inter-story drift history

δ_i = inter-story drift history

Therefore the viscous damped energy, E_D , can be determined as follows:

$$E_D = \int \mathbf{f}_d^T d\mathbf{v} = E_I - E_K - E_H - E_S \quad (4.35)$$

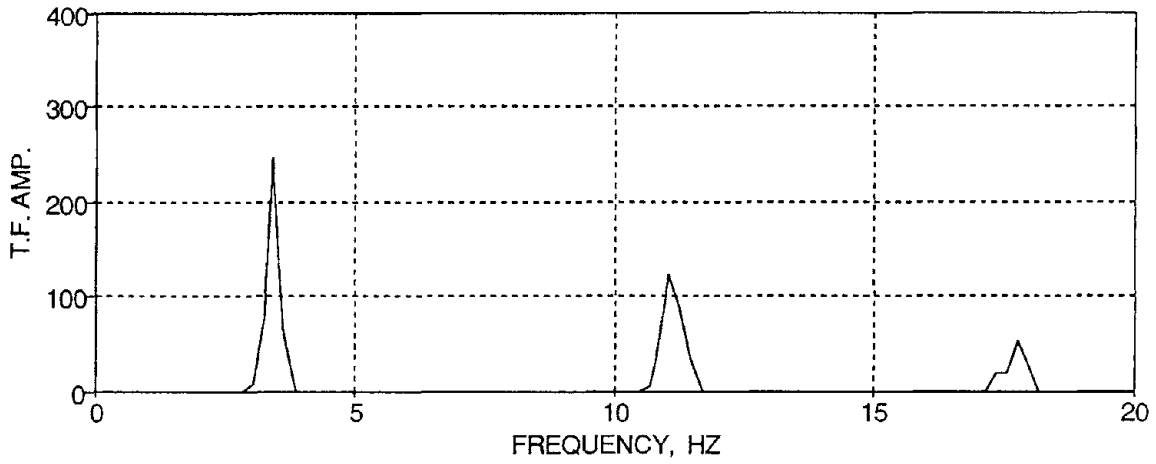
However note that the experimentally recorded story shear forces include the effects of the equivalent viscous damping present. Therefore the absorbed/dissipated hysteretic and viscous damped energies will be lumped together in the experimental study.

4.3 Experimental Results

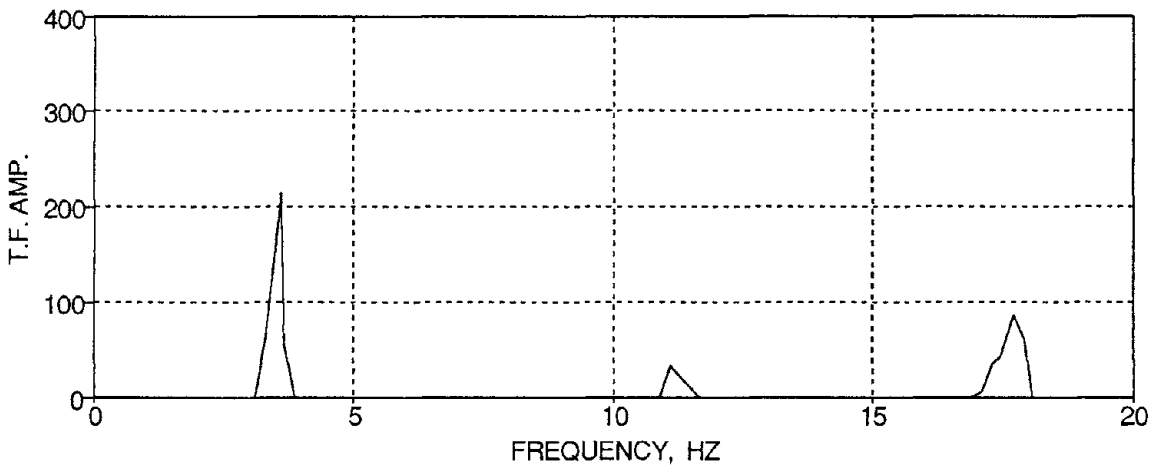
The order of the test response results for identification of the initial dynamic characteristics of the model are in accordance with Table 4-1.

4.3.1 Impact Hammer Test

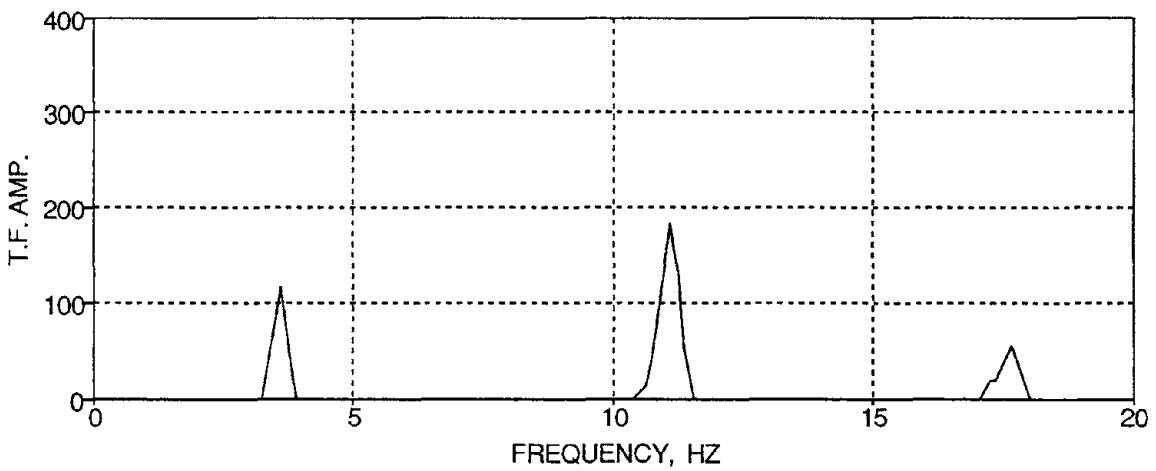
After the unloaded three story model was lifted and secured to the shaking table, an impact hammer (test label - HAMMER) was used to excite the model for identification of the dynamic characteristics of the unloaded (bare) model. Since an impact hammer can only provide a low magnitude of excitation with each strike, an average of five hammer strikes on the third story of the model was used for determination of the story transfer functions. Fig. 4-2 shows the average transfer functions from a spectrum analyzer for the first (4.2c), second (4.2b), and third (4.2a) stories in the frequency domain from hammer strikes to the third floor. The definition and application of transfer functions are discussed in the identification procedures (Section 4.2).



(a) First Floor



(b) Second Floor



(c) Third Floor

FIG. 4-2 Story Transfer Functions from an Impact Hammer Test

4.3.2 Pull-Back Tests

Once the additional balast weights were loaded on the model for mass similitude, a measured flexibility matrix (F_{ij}) of the loaded model, Eq. (4.36), was obtained by statically loading the center of the bay for each floor with horizontal tensile loads of about 0.5 and 1.0 kips (test label - PULL) and recording story displacements at the east and west floor-slab levels with the displacement transducers (D3 - D8). Fig. 4-3 shows a detail of the horizontal tensile loading and displacement measurement locations on the model. The coefficients of the flexibility matrix are then determined based on an average of four displacement readings for each story loading, two displacement readings for each horizontal story load.

$$F_{ij} = \begin{pmatrix} 7.18 & 4.77 & 2.33 \\ 4.64 & 4.36 & 2.18 \\ 2.20 & 2.13 & 1.95 \end{pmatrix} \times 10^{-2} \text{ in/kip} = \begin{pmatrix} f_{m,m} & f_{m,u} & f_{m,l} \\ f_{u,m} & f_{u,u} & f_{u,l} \\ f_{l,m} & f_{l,u} & f_{l,l} \end{pmatrix} \quad (4.36)$$

where i = floor displacement location
 j = floor pull location
 I,II,III = first, second, and third floors, respectively

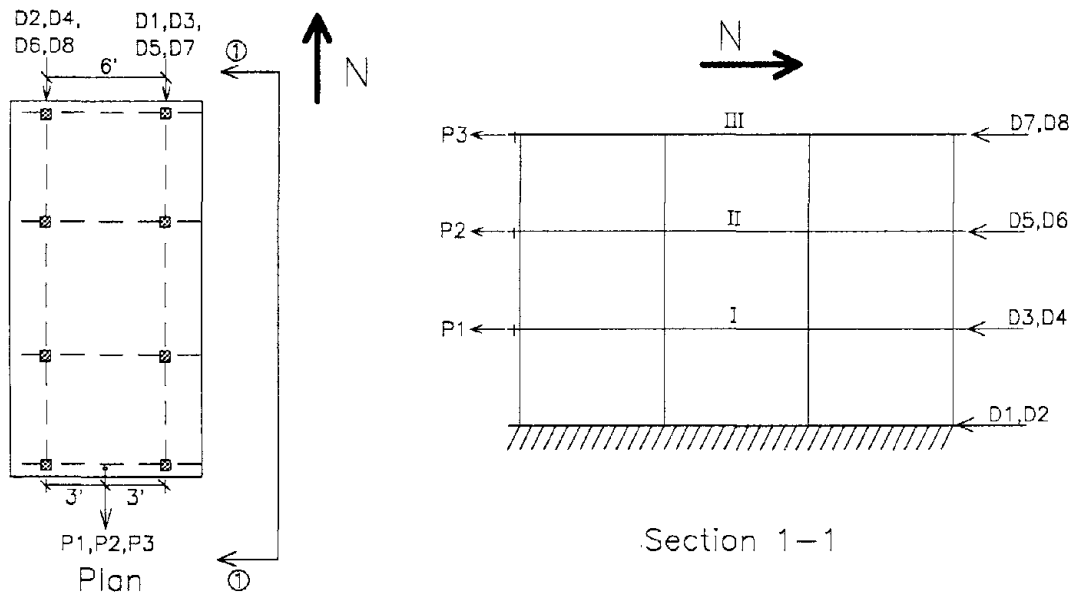


FIG. 4-3 Pull-Back Loading and Displacement Measurement Locations

4.3.3 Snap-Back Tests

Quick release (snap-back) tests were next performed on the loaded model (test label - SNAP). Each floor of the model is statically loaded with a horizontal tensile force of about 1.0 kip (same locations as test PULL, see Fig. 4-3) and quickly released (snapped) permitting the model to vibrate freely. Fig. 4-4 shows the third story displacement time history response (displacement transducer D7) from a third floor snap. It can be observed that a static displacement of 0.083 in. is produced from a horizontal tensile load of about 1.1 kips. The story level horizontal acceleration response are recorded through the accelerometers (AH3 - AH8). Fig. 4-5 shows the acceleration response time history for each floor of the model when that floor is snapped.

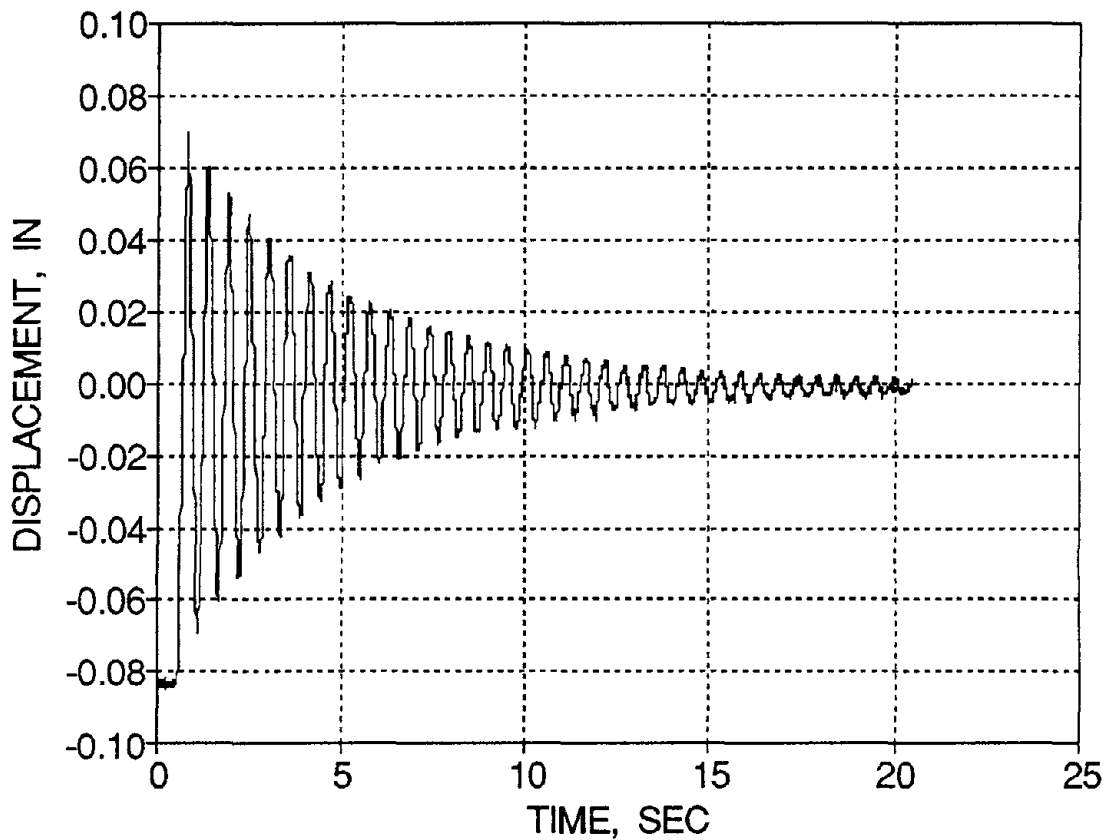
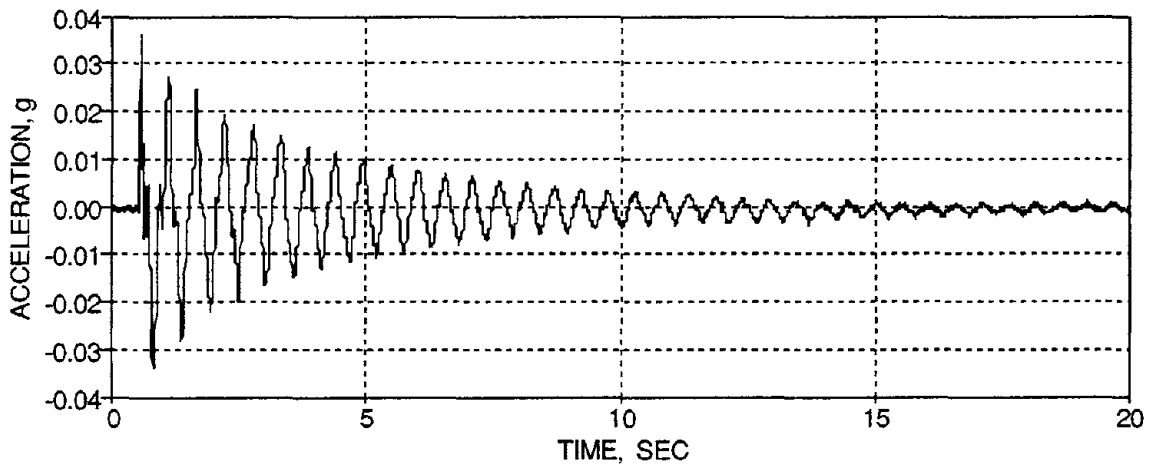
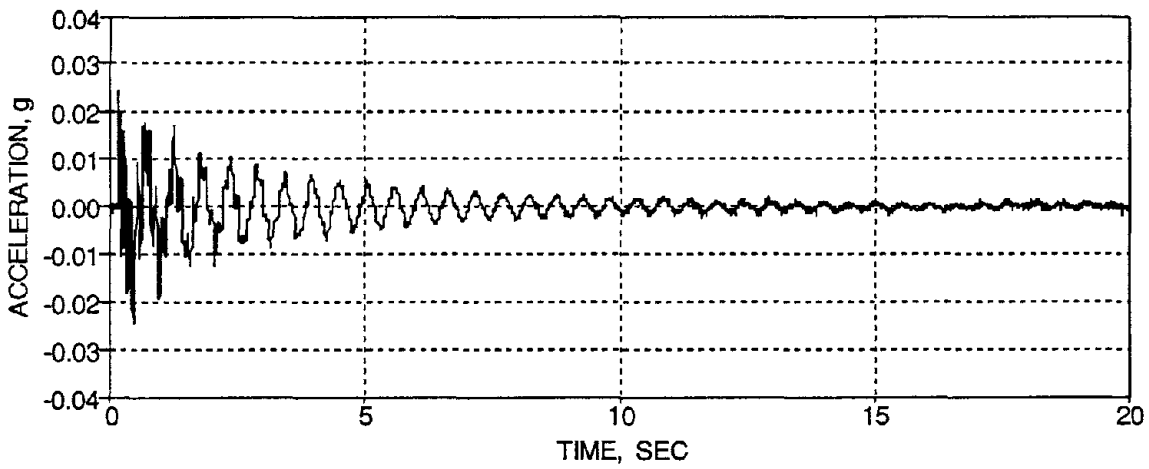


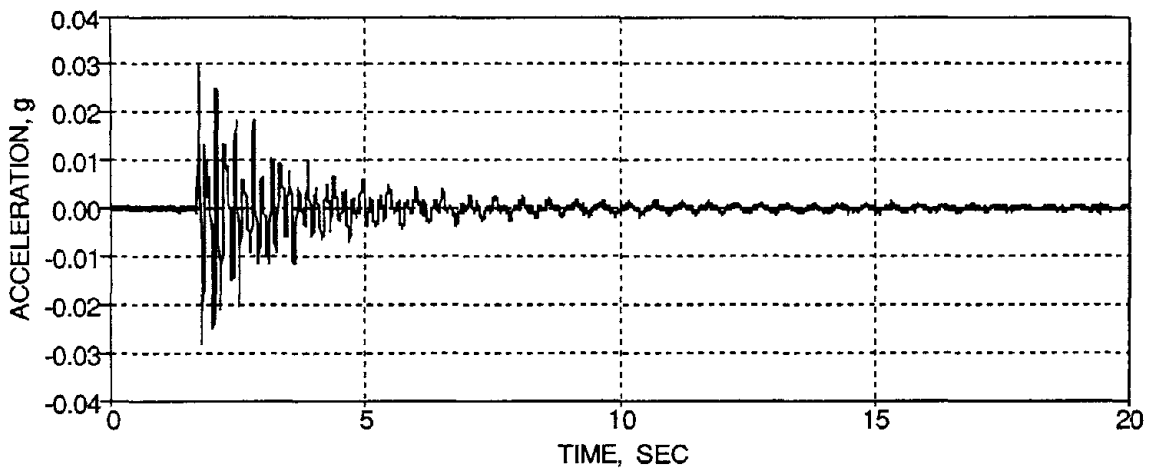
FIG. 4-4 Third Story Displacement Response from a Third Floor Snap



(a) Third Floor



(b) Second Floor



(c) First Floor

FIG. 4-5 Acceleration Story Response from that Story Snap

4.3.4 White Noise Test

The first motion of the shaking table that was used to excite the loaded model, including the wood safety frames, was a wide banded frequency response (0 - 50 Hz.) white noise excitation, test label WHN_A. This white noise test was used for proper calibration of the shaking table. After the shaking table was recalibrated, a compensated white noise excitation, WHN_B, was derived and used for the identification of the initial dynamic characteristics of the model. Fig. 4-6 shows the base acceleration motion of the shaking table for the white noise excitation WHN_B. The peak acceleration of the base can be observed as about 0.024 g. The story level acceleration response from WHN_B are shown in Fig. 4-7.

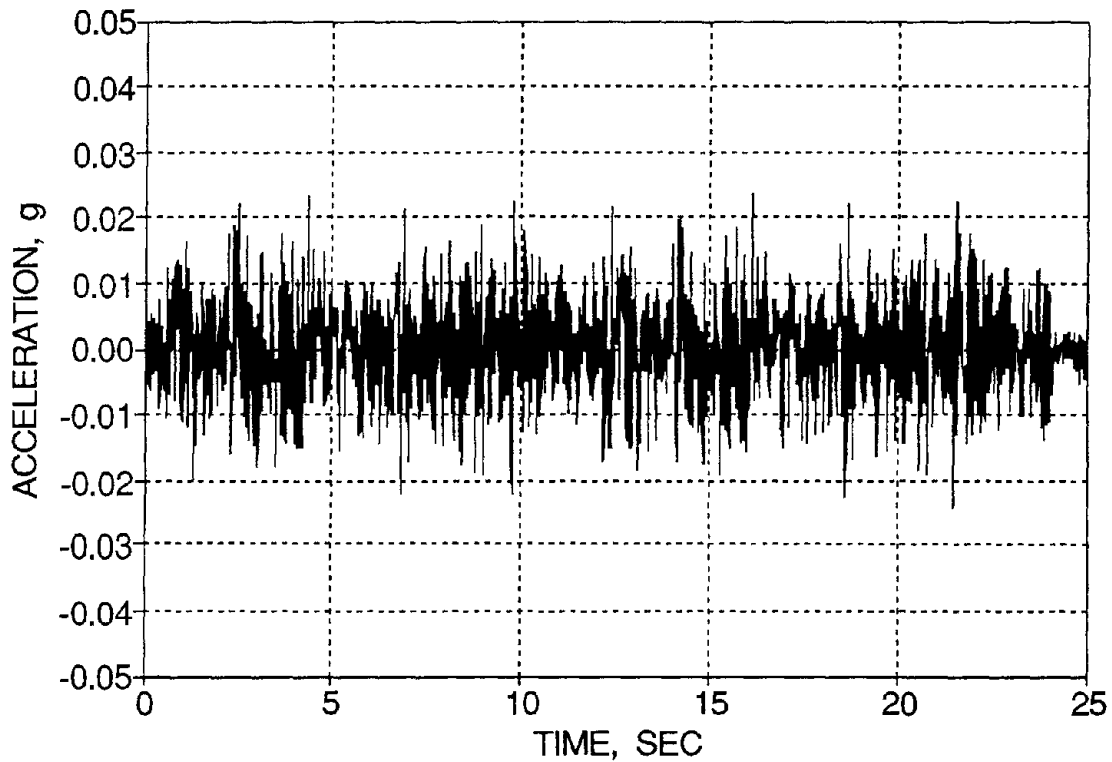
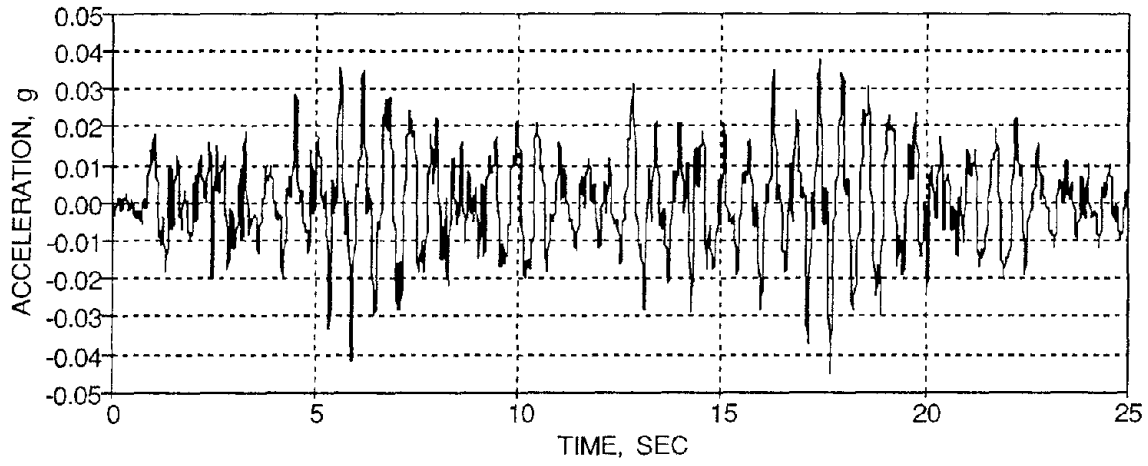
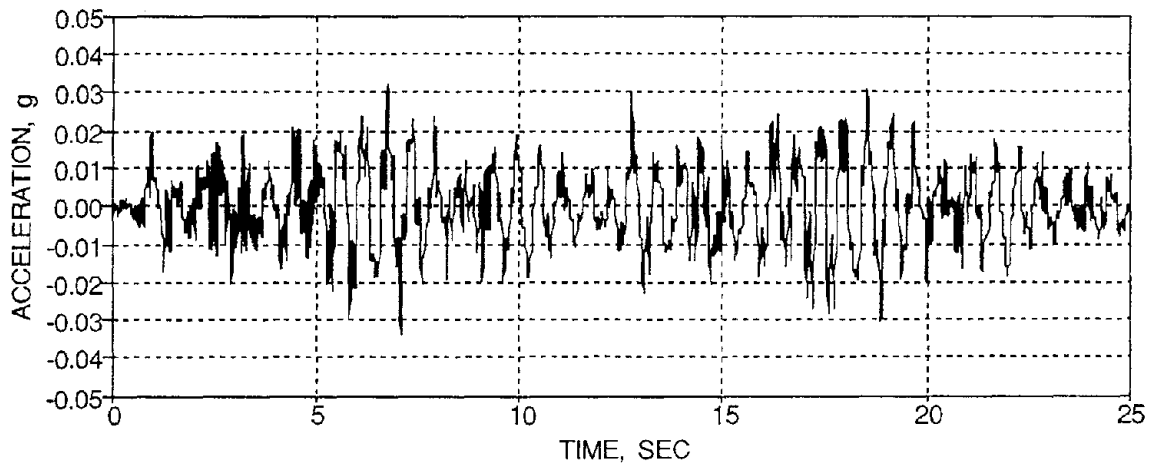


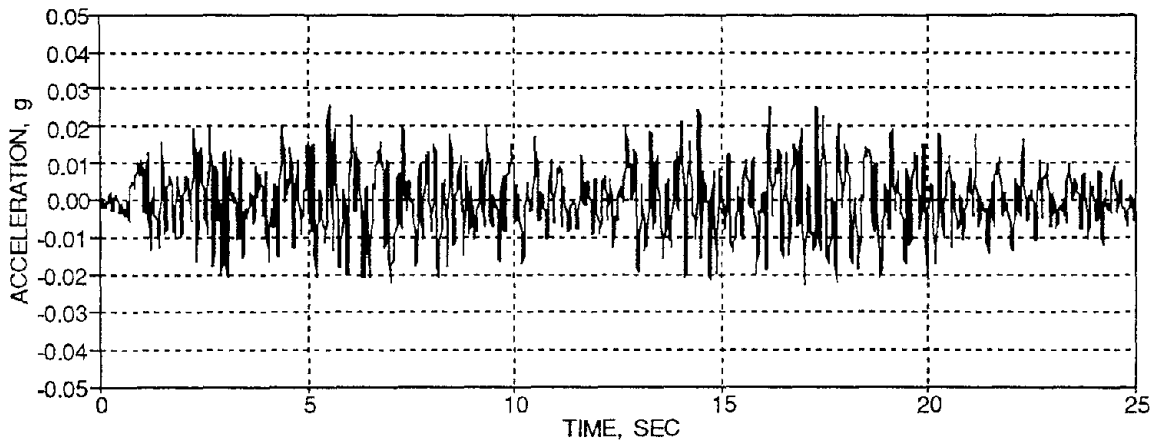
FIG. 4-6 Base Acceleration Motion of the White Noise Excitation, WHN_B



(a) Third Floor



(b) Second Floor



(c) First Floor

FIG. 4-7 Story Level Acceleration Response from WHN_B

4.4 Dynamic Characteristics of Model

A complete list of the identified natural frequencies and equivalent viscous damping characteristics of the unloaded and loaded model from the following tests are presented in Tables 4-2 and 4-3, respectively. The identified modal shapes, stiffness, and viscous damping matrices are presented in Tables 4-4 through 4-8, respectively.

4.4.1 Properties of Unloaded Model - Impact Hammer Test

Since the story transfer functions have small damping and well separated modes (see Fig. 4-2), the assumptions made in the development of the previous section are justified. Therefore, the peaks occur precisely at the natural frequencies of the unloaded model, \mathbf{f}_i^u , and are identified as follows:

$$\mathbf{f}_i^u = \begin{pmatrix} 3.40 \\ 11.00 \\ 17.60 \end{pmatrix} \text{ Hz.} \quad (4.37)$$

where $i = \text{mode of vibration}$

Since the story transfer functions have small damping and well separated modes, the ratio of the story transfer function magnitudes at the k-th natural frequency is equal to the ratio of the k-th mode shape. From the phase angles of the story transfer functions at each natural frequency, the modal shape matrix, Φ_{ij}^u , for the unloaded model is identified as shown below:

$$\Phi_{ij}^u = \begin{pmatrix} 1.00 & -0.67 & -0.62 \\ 0.82 & 0.18 & 1.00 \\ 0.47 & 1.00 & -0.63 \end{pmatrix} = \begin{pmatrix} \Phi_{III,1} & \Phi_{III,2} & \Phi_{III,3} \\ \Phi_{II,1} & \Phi_{II,2} & \Phi_{II,3} \\ \Phi_{I,1} & \Phi_{I,2} & \Phi_{I,3} \end{pmatrix} \quad (4.38)$$

where $i = \text{degree of freedom, where } i = \text{III being the third floor}$
 $j = \text{mode of vibration}$

The equivalent viscous damping factors of the unloaded model are estimated using the half-power (bandwidth) method, Eq. (4.20), from the story transfer functions as 2.7%, 1.5%, and 1.0%, respectively.

Based on an estimated quantities presented in Section 3.5, the mass matrix for the unloaded for mass similitude model, \mathbf{M}_{ij}^u , is shown below:

$$\mathbf{M}_{ij}^u = \begin{pmatrix} 0.0162 & 0.0000 & 0.0000 \\ 0.0000 & 0.0162 & 0.0000 \\ 0.0000 & 0.0000 & 0.0162 \end{pmatrix} \text{ kip/in/sec}^2 \quad (4.39)$$

The stiffness matrix of the unloaded model, \mathbf{K}_{ij}^u , is identified using Eq. (4.28) and shown below:

$$\mathbf{K}_{ij}^u = \begin{pmatrix} 70.1 & -72.1 & 10.3 \\ -72.1 & 115.5 & -59.2 \\ 10.3 & -59.2 & 97.3 \end{pmatrix} \text{ kip/in} \quad (4.40)$$

The story stiffnesses of the unloaded model, defined in Eq. (4.29), are identified using Eq. (4.40) and shown below:

$$\mathbf{k}_i^u = \begin{pmatrix} 72.1 \\ 59.2 \\ 38.1 \end{pmatrix} \text{ kip/in} \quad (4.41)$$

Similarly, the damping matrix of the unloaded model was identified using Eq. (4.30) and shown below:

$$\mathbf{C}_{ij}^u = \begin{pmatrix} 0.028 & -0.007 & -0.003 \\ -0.007 & 0.028 & -0.005 \\ -0.003 & -0.005 & 0.033 \end{pmatrix} \text{ kip-sec/in} \quad (4.42)$$

4.4.2 Properties of Loaded Model - Pull-Back Tests

Pull-back tests were performed on the loaded model to obtain the flexibility matrix and indirectly the stiffness matrix. The minor lack of symmetry in the off-diagonal terms of the measured flexibility matrix, Eq. (4.36), is primarily due to the averaging in determining the matrix and experimental errors in the instrumentation for small loadings and displacements. The modulus of elasticity of a R/C member is also nonlinearly a function of the magnitude of the displacement (strain). Therefore deviations in the flexibility matrix are also expected from the low amplitude story displacements for the pull-back tests. For analytical evaluations, a symmetric flexibility matrix, $\bar{\mathbf{F}}_{ij}$, and an "error" matrix, \mathbf{E}_{ij} , are determined by averaging the off-diagonal terms from Eq. (4.36) and are shown in Eq. (4.43a) and (4.43b).

$$\mathbf{F}_{ij} = \bar{\mathbf{F}}_{ij} + \mathbf{E}_{ij} \quad (4.43a)$$

$$\mathbf{F}_{ij} = \begin{pmatrix} 7.18 & 4.70 & 2.27 \\ 4.70 & 4.36 & 2.16 \\ 2.27 & 2.16 & 1.95 \end{pmatrix} + \begin{pmatrix} 0.00 & -0.07 & -0.07 \\ 0.07 & 0.00 & -0.03 \\ 0.07 & 0.03 & 0.00 \end{pmatrix} \times 10^{-2} \text{ in/kip} \quad (4.43b)$$

Inverting the symmetric flexibility matrix for the model, $\bar{\mathbf{F}}_{ij}$, from Eq. (4.43b) results in a measured stiffness matrix, \mathbf{K}_{ij} , as shown below:

$$\mathbf{K}_{ij} = \begin{pmatrix} 47.4 & -52.7 & 3.2 \\ -52.7 & 109.3 & -59.8 \\ 3.2 & -59.8 & 113.9 \end{pmatrix} \text{ kip/in} \quad (4.44)$$

The story stiffnesses of the loaded model, defined in Eq. (4.29), are identified from Eq. (4.44) and shown below:

$$\mathbf{k}_i = \begin{pmatrix} 52.7 \\ 59.8 \\ 54.1 \end{pmatrix} \text{ kip/in} \quad (4.45)$$

Based on an estimated quantities presented in Section 3.5, the mass matrix for the loaded model, \mathbf{M}_{ij} , is shown below:

$$\mathbf{M}_{ij} = \begin{pmatrix} 0.070 & 0.000 & 0.000 \\ 0.000 & 0.070 & 0.000 \\ 0.000 & 0.000 & 0.070 \end{pmatrix} \text{ kip/in/sec}^2 \quad (4.46)$$

From an eigenvalue (free vibration) analysis for a lightly damped system, the circular natural frequencies, ω_i , are determined by equating the determinant of $[\mathbf{K}_{ij} - \mathbf{M}_{ij}\omega_i^2]$ to zero. The natural frequencies, \mathbf{f}_i , are thus identified as:

$$\mathbf{f}_i = \begin{pmatrix} 1.76 \\ 5.34 \\ 8.15 \end{pmatrix} \text{ Hz.} \quad (4.47)$$

The mode shapes of the model are also determined from the eigenvalue analysis by equating $[\mathbf{K}_{ij} - \mathbf{M}_{ij}\omega_i^2]\phi_i$ to zero for each mode i , where ϕ_i is the i -th vector mode shape. By assembling these mode shapes, the modal shape matrix is identified as follows:

$$\Phi_{ij} = \begin{pmatrix} 1.00 & -0.82 & -0.41 \\ 0.76 & 0.55 & 1.00 \\ 0.40 & 1.00 & -0.88 \end{pmatrix} \quad (4.48)$$

4.4.3 Properties of Loaded Model - Quick Release (Snap-Back) Free Vibration Tests

Each floor of the model was statically loaded and then quickly released (snapped) to create free vibrations of the model. Based on the floor snapped, the Fourier Transform of the acceleration response of that story from Fig. 4-5 are shown in Fig. 4-8. Again for small damping and well separated modes (see Fig. 4-8), the peaks in the Fourier Transform occur precisely at the natural frequencies of the model, just as in a transfer function. Thus the natural frequencies of the model are identified as:

$$\mathbf{f}_i = \begin{pmatrix} 1.86 \\ 5.66 \\ 8.40 \end{pmatrix} \text{ Hz.} \quad (4.49)$$

Fig. 4-8a shows that the third floor acceleration frequency response from a third floor snap is primarily governed by the first mode of vibration (since the peak response amplitude at the first mode natural frequency is much greater than the peak response amplitudes at the second and third mode natural frequencies). Hence from the third floor free vibration acceleration response time history, shown in Fig. 4-5a, the first mode equivalent viscous damping factor is determined to be 2.5% using the logarithmic decrement method, Eq. (4.21).

The second and third mode damping factors are determined from the logarithmic decrement method for each mode after the time functions are filtered in the frequency domain. The filtered Fourier Transforms are determined by the product of the Fourier Amplitudes and the step functions, $u_i(f)$, shown in Eq. (4.50a) and (4.50b), respectively.

$$u_2(f) = \begin{cases} 1.0 & \text{when } 2.93\text{Hz.} \leq f \leq 7.23\text{Hz.} \\ 0.0 & \text{when } f < 2.93\text{Hz.} \text{ or } f > 7.23\text{Hz.} \end{cases} \quad (4.50a)$$

$$u_3(f) = \begin{cases} 1.0 & \text{when } 7.28\text{Hz.} \leq f \leq 11.04\text{Hz.} \\ 0.0 & \text{when } f < 7.28\text{Hz.} \text{ or } f > 11.04\text{Hz.} \end{cases} \quad (4.50b)$$

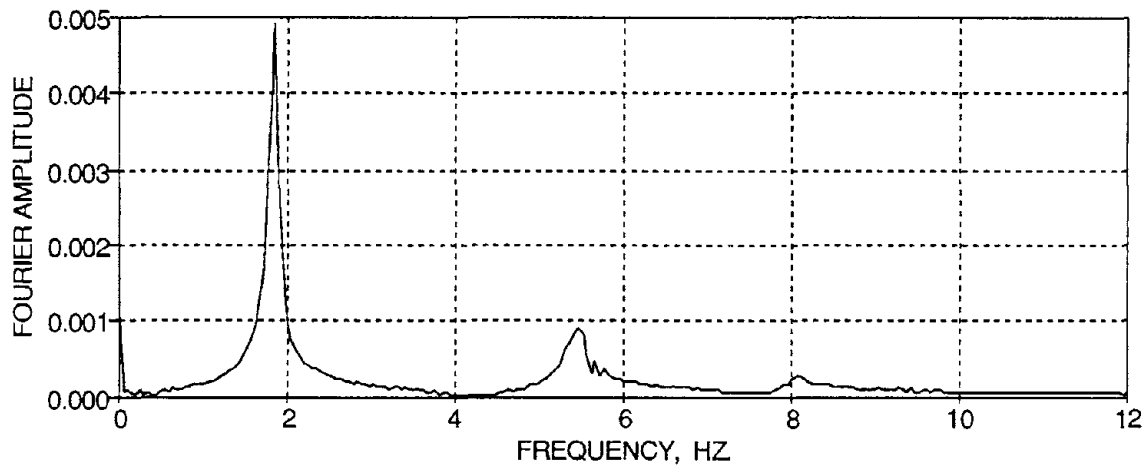
where f = frequency (Hz.)

Then these filtered Fourier Transforms for the second and third modes are multiplied by a normalized Gaussian window or function $g(f)$, shown in Eq. (4.51), to lessen the effect of the frequencies away from the natural frequency of that mode and thereby reduce the noise in the signal and leakage in the transform.

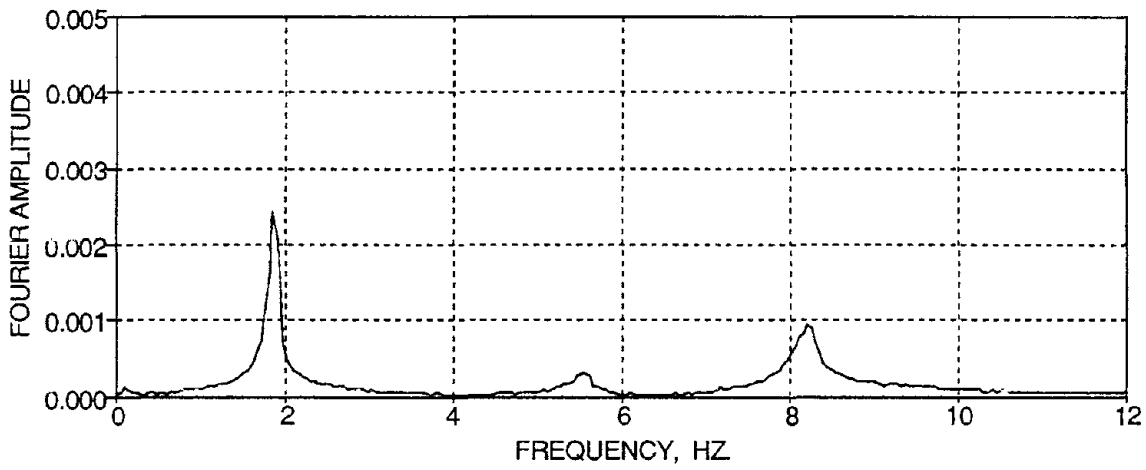
$$g(f) = \frac{1}{\sqrt{2\pi}\sigma} e^{-(f-\bar{f})^2/2\sigma^2}, \quad -\infty < f < \infty \quad (4.51)$$

where \bar{f} = resonant natural frequency, 5.56 Hz. and 8.30 Hz., respectively

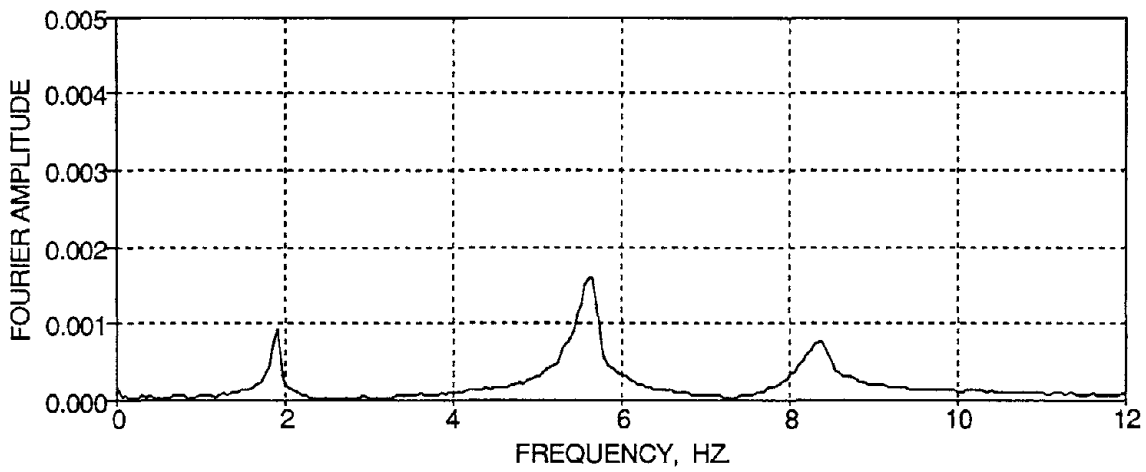
σ = variable standard deviations of 18.6% and 13.3% of the frequency range, respectively



(a) Third Floor

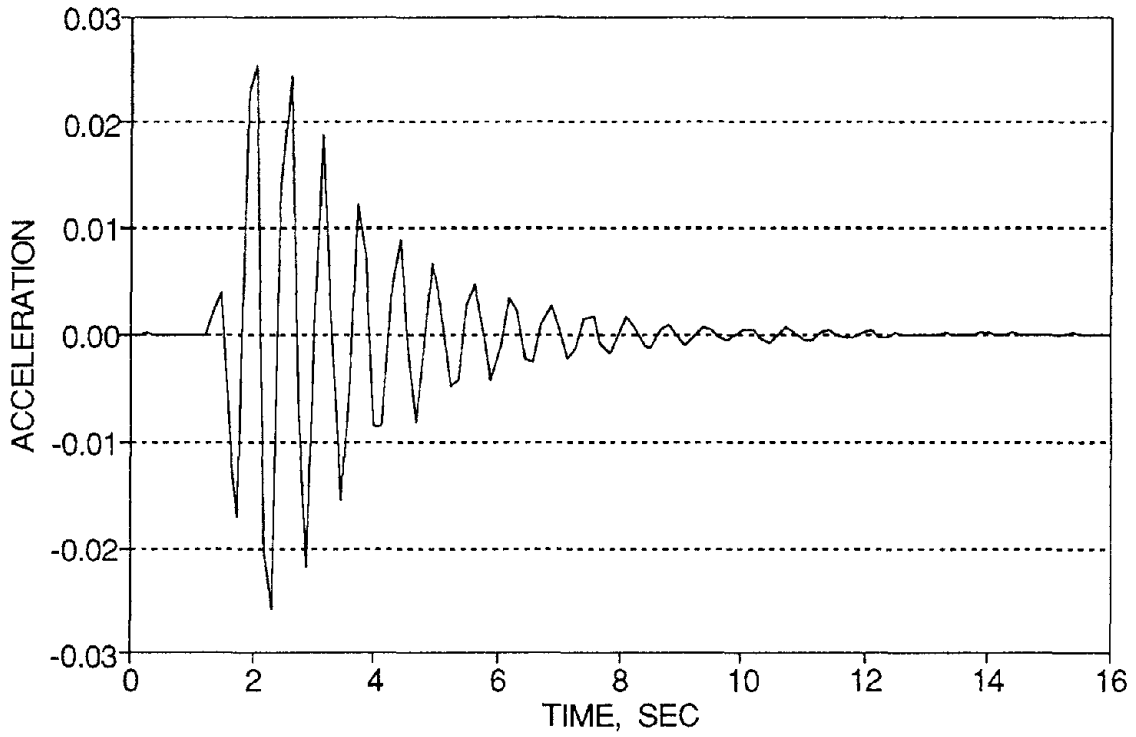


(b) Second Floor

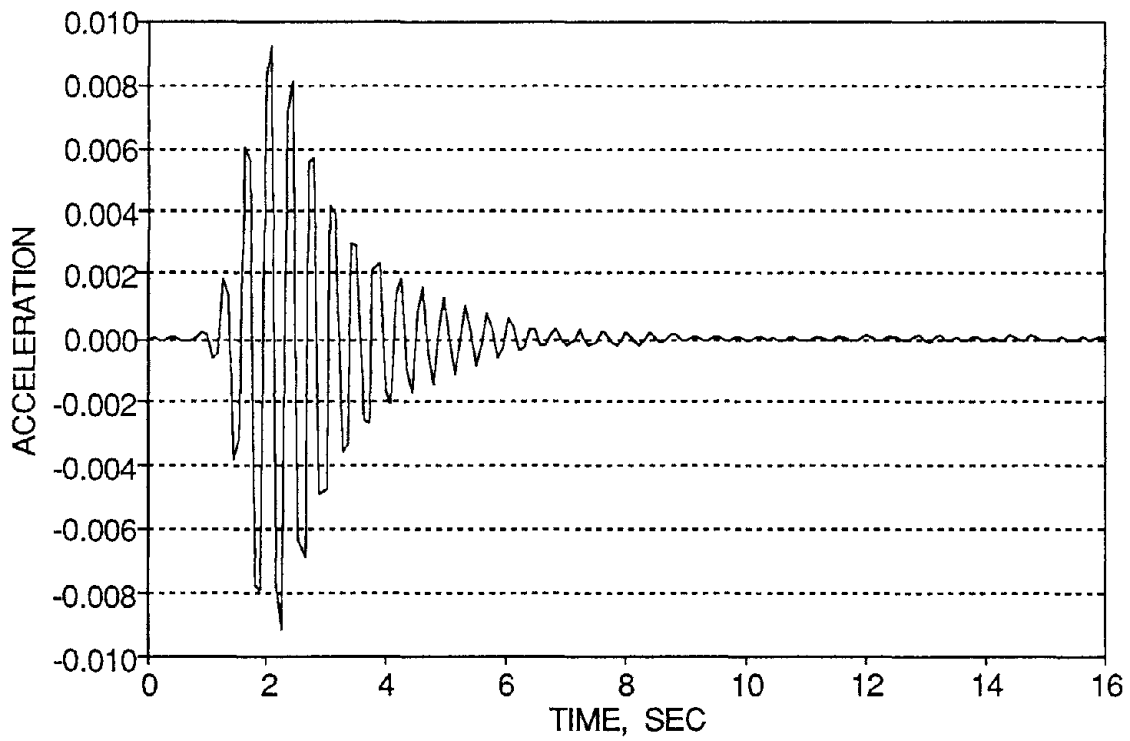


(c) First Floor

FIG. 4-8 Fourier Transform of the Story Level Accelerations from the Snap-Back Tests



(a) Second Mode



(b) Third Mode

FIG. 4-9 Inverse Fourier Transform of Filtered Frequencies
4-25

The inverse Fourier Transforms (time domain response) for the second and third modes of vibration are shown in Fig. 4-9a and 4.9b, respectively. The damping factors for these modes are then determined from Eq. (4.21) as 4.8% and 4.0%, respectively.

4.4.4 Properties of Loaded Model - Initial White Noise Excitation on Shaking Table

A white noise shaking table excitation was also used to determine the dynamic characteristics of the model. Fig. 4-10a shows the Fourier Transform of the input white noise base acceleration motion from Fig. 4-6 and Fig. 4-10b shows the smoothed signal using a moving average of 7 digital points to reduce the noise. A wide banded excitation in the frequency domain is observed.

The story transfer functions, comprised of the Fourier Amplitudes of the story level accelerations from Fig. 4-7 normalized by the Fourier Amplitudes of the input base motion in Fig. 4-10, are shown in Fig. 4-11. It can be observed that the transfer functions near the second and third mode natural frequencies have several sharp peaks or dominant frequencies. This phenomenon developed due to the non-linear behavior of the cracked reinforced concrete members from the white noise excitation. The cracking creates a stick-slip type condition causing excitation of several frequencies near the second and third natural frequencies. The transfer functions near the first natural frequency shows only one clear dominant frequency. Therefore, the influence of cracking does not appear to affect the structural response in this mode during this input excitation.

Since transfer functions for inelastic (non-linear) behavior in R/C members have many peaks near a mode of vibration as opposed to an elastic system with only one clear dominant frequency, the modal natural frequencies are identified through an average procedure for that mode. This is accomplished by smoothing the transfer function using a moving average of every 3 digital points in the signal. Fig. 4-12 shows the resulting smoothed transfer functions for WHN_B. Therefore the average modal natural frequencies are thus identified as:

$$\mathbf{f}_i = \begin{pmatrix} 1.78 \\ 5.32 \\ 7.89 \end{pmatrix} \text{ Hz.} \quad (4.52)$$

Since the transfer functions again have small damping and well separated modes (see Figs. 4-11 and 4-12), the modal shape matrix, Eq. (4.53), is thus determined from the ratio of the transfer function magnitudes for each floor at each natural frequency and the comparison of phase angles at each natural frequency for each degree-of-freedom.

$$\Phi_{ij} = \begin{pmatrix} 1.00 & -0.82 & -0.46 \\ 0.80 & 0.46 & 1.00 \\ 0.42 & 1.00 & -0.83 \end{pmatrix} \quad (4.53)$$

Some smoothing techniques result in considerable drops in the response amplitudes of the transfer functions. And since the half-power method considers the response amplitude at a certain frequency, equivalent viscous damping identifications could be distorted. But it can be observed in Fig. 4-12 that the smoothing technique presented results in minor drops in the peak magnitudes of the transfer functions. Therefore the equivalent viscous modal damping factors are determined through the half-power (bandwidth) method from the smoothed transfer functions for each story (Fig. 4-12) as 2.0%, 2.4%, and 2.0%, respectively and are shown in Table 4-3. By considering the wide range of dominant frequencies (near the second natural frequency), the second mode damping factor is observed to be slightly higher than for the other modes. Some contributions of hysteretic damping may have occurred for this mode due to the cracking in the members of the model, accompanied by slight shifts of frequencies (stiffness changes).

The estimated viscous damping factors are also found from the transfer functions using Eq. (4.19) as 1.7%, 1.6%, and 1.4% for the first, second, and third modes, respectively. Take note that the damping factors were calculated based on the smoothed story transfer functions to account for the high frequency noise in the signal.

From the orthogonal modal shape matrix in Eq. (4.53), the stiffness matrix is derived using Eq. (4.28) and is shown below:

$$\mathbf{K}_{ij} = \begin{pmatrix} 51.9 & -53.4 & 2.5 \\ -53.4 & 102.4 & -54.4 \\ 2.5 & -54.4 & 104.7 \end{pmatrix} \text{ kip/in} \quad (4.54)$$

The story stiffnesses of the loaded model, defined in Eq. (4.29), are identified from Eq. (4.54) and shown below:

$$\mathbf{k}_i = \begin{pmatrix} 53.4 \\ 54.4 \\ 50.3 \end{pmatrix} \text{ kip/in} \quad (4.55)$$

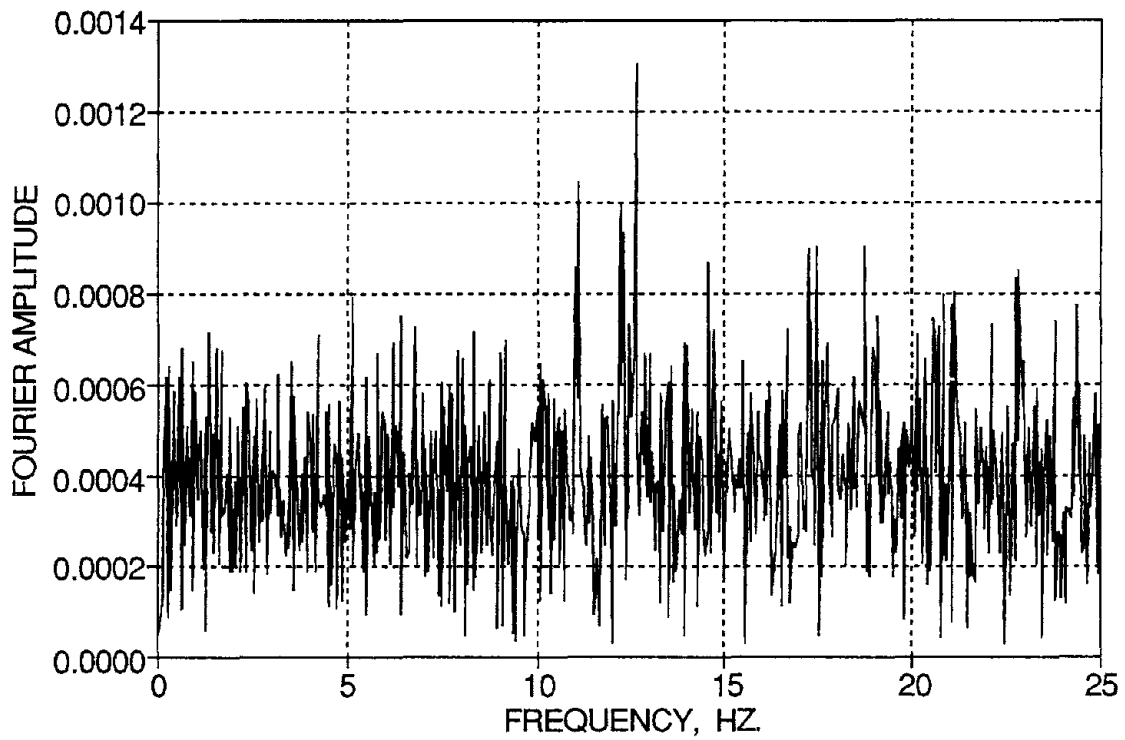
Similarly, the damping matrix is derived from Eq. (4.30) and is shown below:

$$\mathbf{C}_{ij} = \begin{pmatrix} 0.072 & -0.042 & -0.012 \\ -0.042 & 0.097 & -0.029 \\ -0.012 & -0.029 & 0.112 \end{pmatrix} \text{ kip-sec/in} \quad (4.56)$$

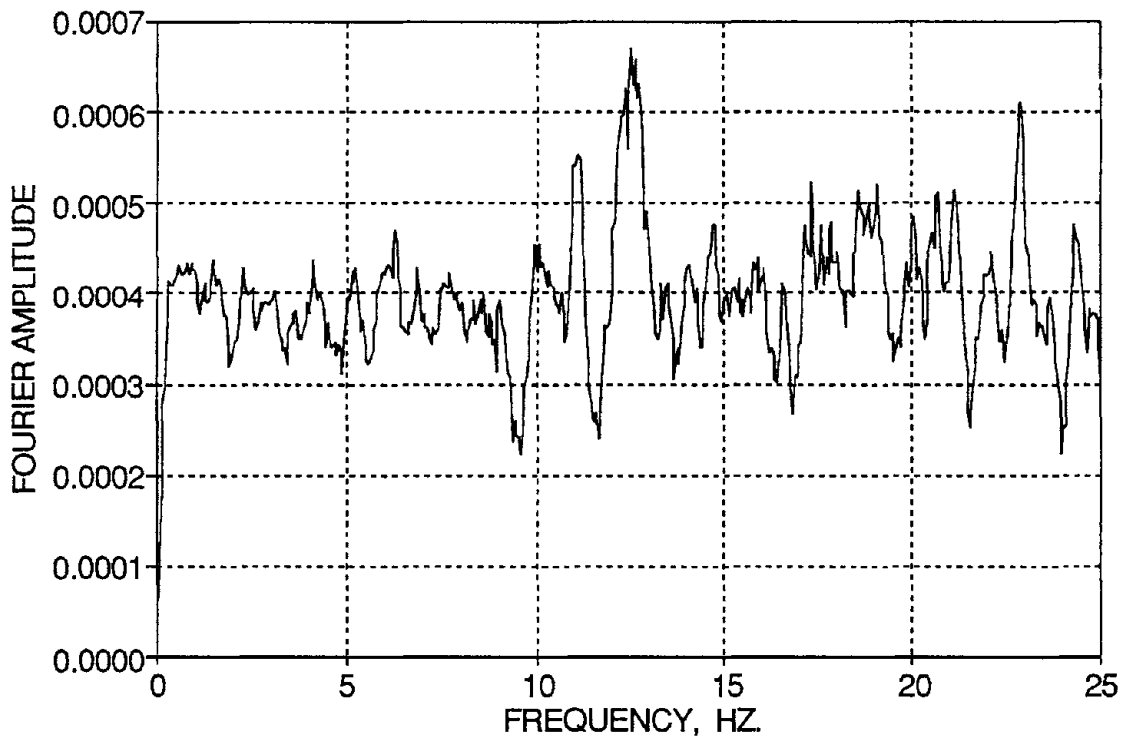
The initial modal participation factors, Γ_k , are determined from the results of the white noise test using the derivations in Section 4.2.1.1 as:

$$\Gamma_k = \begin{pmatrix} 0.44 \\ 0.12 \\ -0.06 \end{pmatrix} \quad (4.57)$$

Fig. 4-13 shows the story shear versus inter-story drift histories for WHN_B. The initial stiffnesses from these histories are identified as 51.2 kip/in, 42.2 kip/in, and 40.0 kip/in, respectively. It can also be observed that loops occurred in these histories. Although it is important to note that these loops are not a result of inelastic hysteresis but from the equivalent viscous damping from the cracked R/C members of the structure. Therefore the story shears and drifts recorded through the instrumentation includes the effects of viscous damping as stated previously. For the following experimental white noise excitations, a comparison of these initial stiffnesses are examined for correlating the stiffness degradation in the structure.

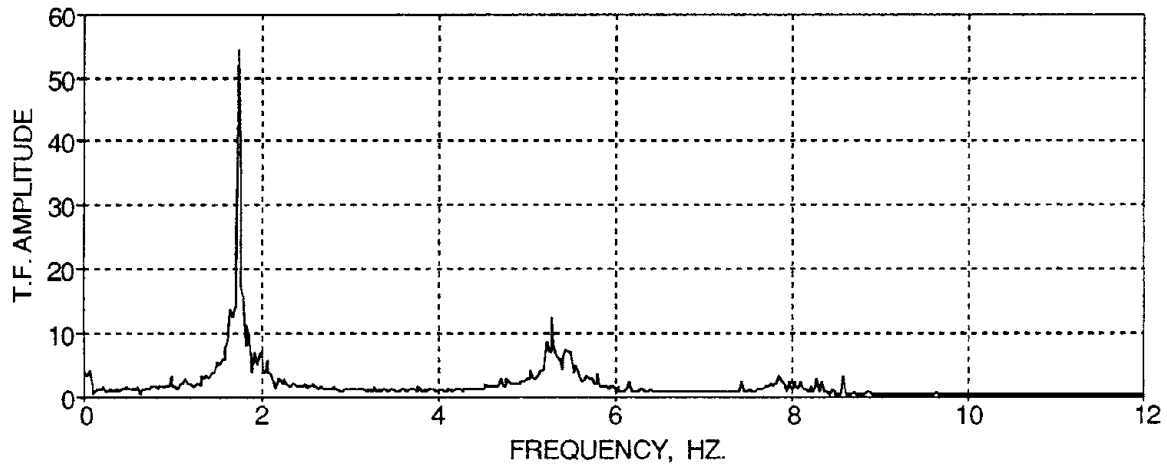


(a) Fourier Transform

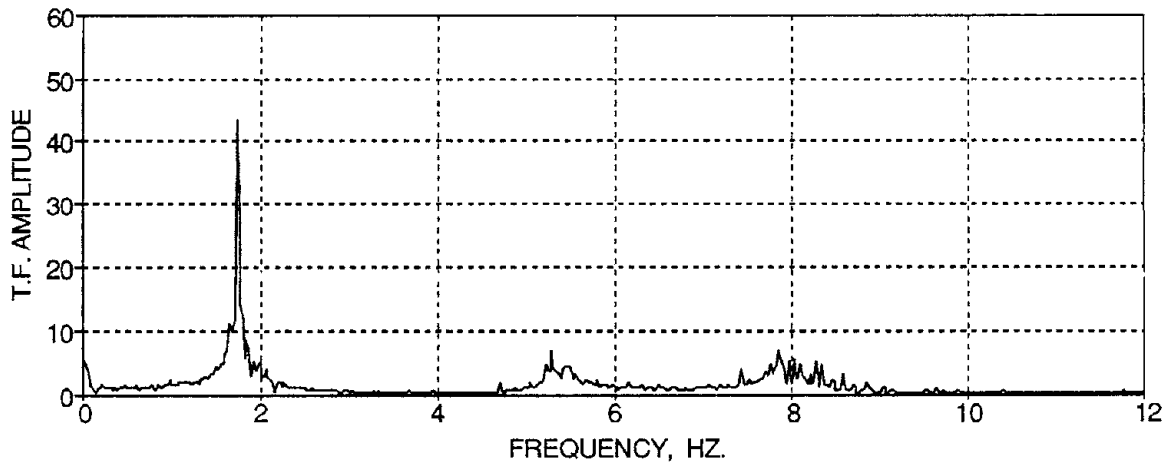


(b) Smoothed Fourier Transform

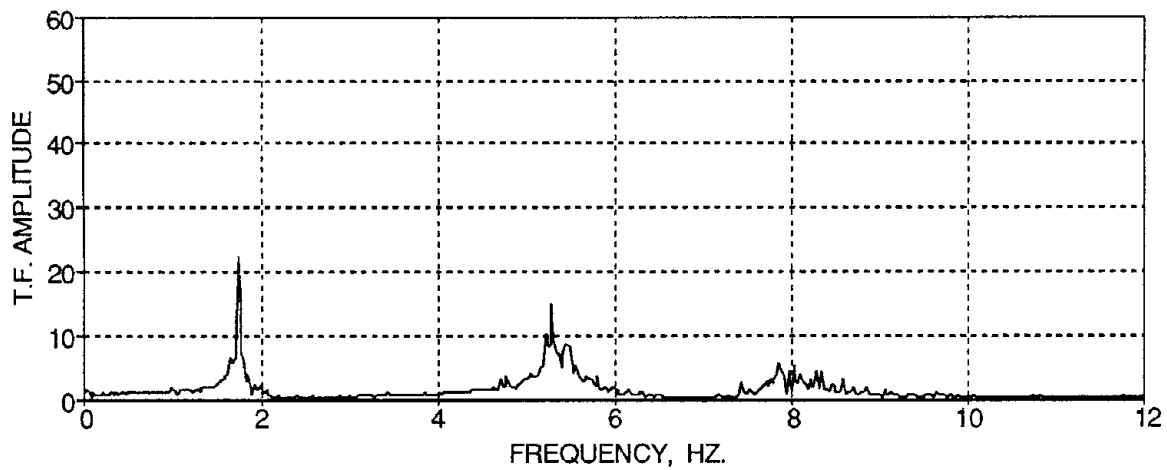
FIG. 4-10 Fourier Transform of the Base Acceleration Motion for WHN_B



(a) Third Floor

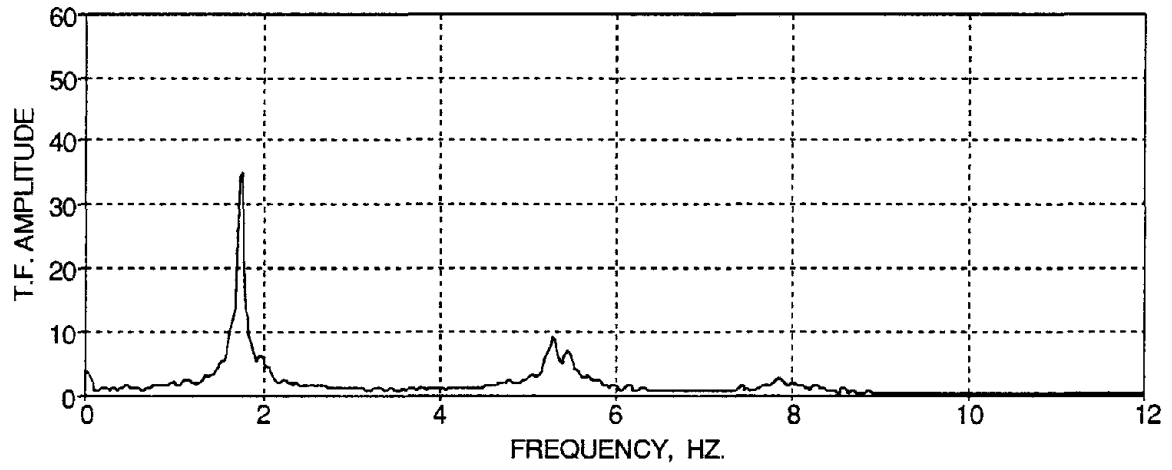


(b) Second Floor

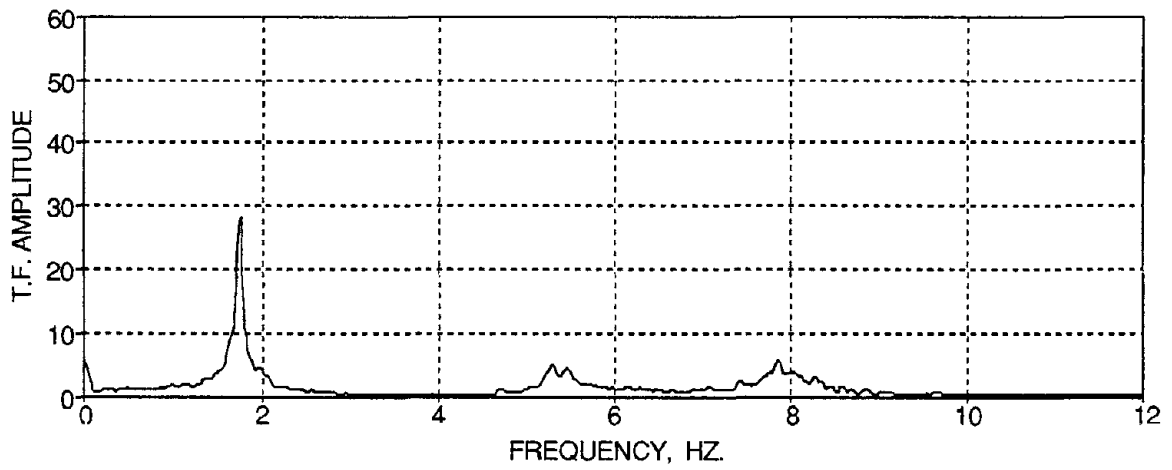


(c) First Floor

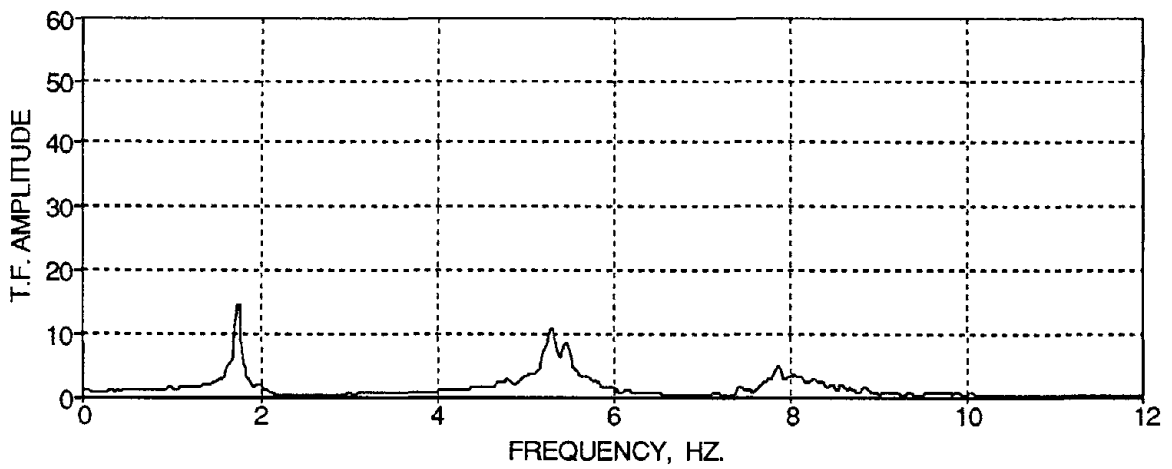
FIG. 4-11 Transfer Functions of the Story Level Accelerations from WHN_B



(a) Third Floor

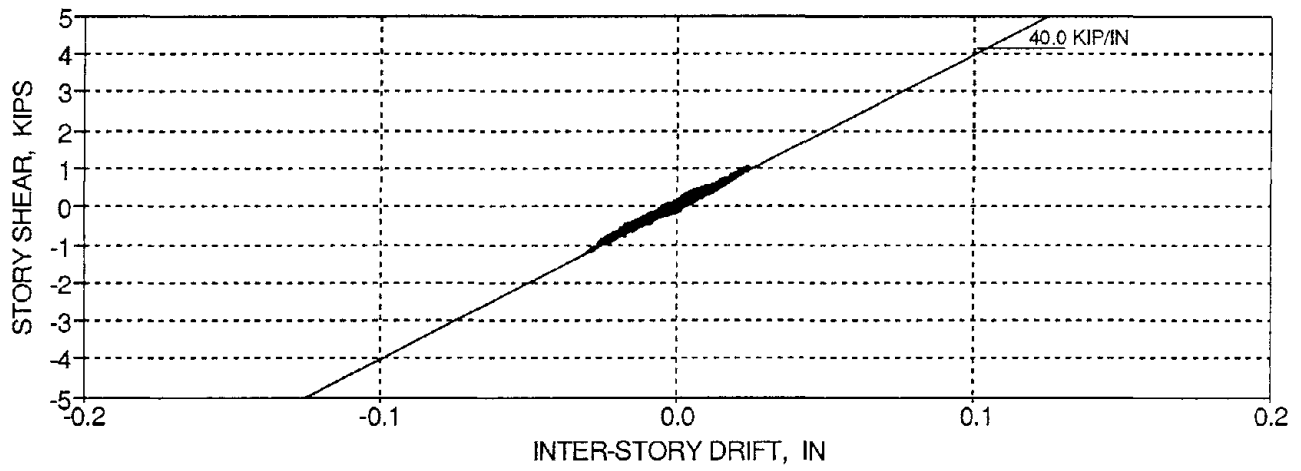


(b) Second Floor

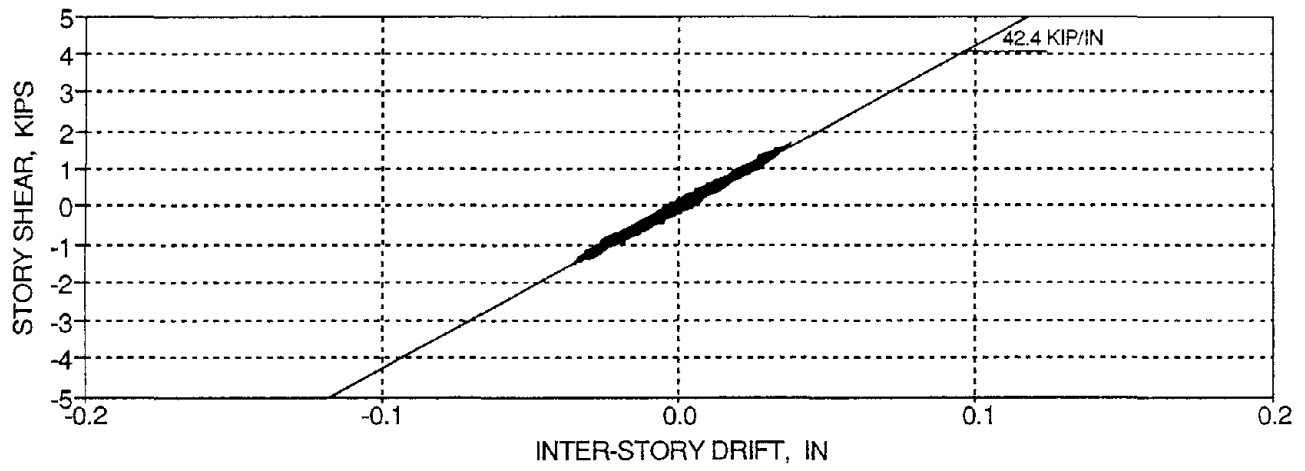


(c) First Floor

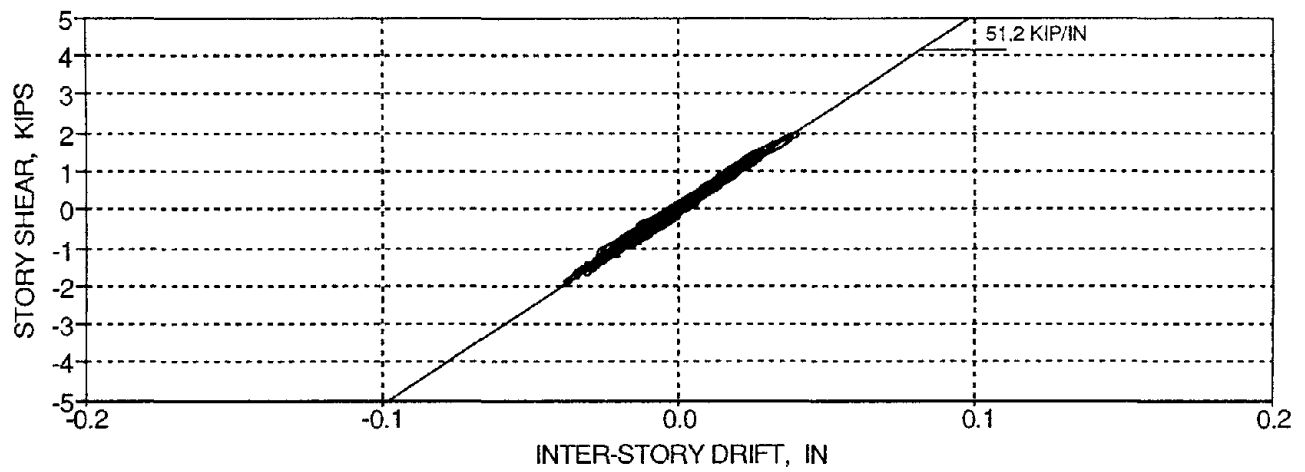
FIG. 4-12 Smoothed Transfer Functions of the Story Level Accelerations from WHN_B



(a) Third Floor



(b) Second Floor



(c) First Floor

FIG 4-13 Story Shear versus Inter-Story Drift Histories for WHN_B

4.5 Analytical Identification of Dynamic Characteristics

The natural frequencies, the modal shapes, and the stiffness matrix were calculated using a dynamic analysis model (STAADTM) based on the structural member properties and their geometry. Using "full" theoretical properties for the members, a mismatch of the first mode of vibration was obtained. Therefore, the moments of inertia are modified in the computational model to fit the first mode frequency as follows:

$$(EI)_{\text{col}} = 0.565 (EI_{\text{col}})_g \quad (4.58a)$$

$$(EI)_{\text{beam}} = 0.565 (EI_{\text{beam}})_g \quad (4.58b)$$

where $(EI_{\text{col}})_g$ is the column stiffness based on the gross column area.
 $(EI_{\text{beam}})_g$ is the beam stiffness based on the gross T-beam area with full slab contribution.

This reduction of elastic stiffness properties is required due to the micro-cracking of the model members, even in their "undamaged" state. Note that the reduction of the gross member stiffness in the beam and column members were chosen to be identical for simplicity. Although in reality, constant member stiffness reductions may not be the case since cracking or damage can be concentrated in either the beam or column members or in only certain locations of a structure.

For comparative purposes, the "fully cracked" stiffnesses of the beams and columns, determined from transformed sections, are: $(EI)_{\text{col}} = 0.23 (EI_{\text{col}})_g$; and $(EI)_{\text{beam}} = 0.13 (EI_{\text{beam}})_g$, respectively. Therefore the initial stiffnesses of the "undamaged" members from Eqs. (4.58a) and (4.58b) lie between the fully cracked and uncracked (gross) section properties. Similar observations were reported by El-Attar et al. (1991b) in the smaller scale test.

The natural frequencies of the unloaded model are thus calculated using the mass matrix from Eq. (4.39) and the input section properties in Eq. (4.58):

$$\mathbf{f}_i'' = \begin{pmatrix} 3.70 \\ 10.81 \\ 16.50 \end{pmatrix} \text{ Hz.} \quad (4.59)$$

The modal shape matrix of the unloaded model is determined as follows:

$$\Phi_{ij}^u = \begin{pmatrix} 1.00 & -0.81 & -0.43 \\ 0.78 & 0.53 & 1.00 \\ 0.40 & 1.00 & -0.88 \end{pmatrix} \quad (4.60)$$

The stiffness matrix of the unloaded model is calculated by using Eq. (4.28) with the calculated modal shapes, Eq. (4.60), and natural frequencies, Eq. (4.59), as:

$$\mathbf{K}_{ij}^u = \begin{pmatrix} 46.7 & -50.9 & 4.4 \\ -50.9 & 102.7 & -56.2 \\ 4.4 & -56.2 & 108.2 \end{pmatrix} \text{ kip/in} \quad (4.61)$$

The story stiffnesses of the unloaded model, defined in Eq. (4.29), are calculated from Eq. (4.61) and shown below:

$$\mathbf{k}_i^u = \begin{pmatrix} 50.9 \\ 56.2 \\ 52.0 \end{pmatrix} \text{ kip/in} \quad (4.62)$$

Likewise the natural frequencies of the loaded model are calculated from the story masses, Eq. (4.46), and the same input section properties as:

$$\mathbf{f}_i = \begin{pmatrix} 1.78 \\ 5.20 \\ 7.94 \end{pmatrix} \text{ Hz.} \quad (4.63)$$

The modal shape matrix of the loaded model is obtained:

$$\Phi_{ij} = \begin{pmatrix} 1.00 & -0.81 & -0.43 \\ 0.78 & 0.53 & 1.00 \\ 0.40 & 1.00 & -0.88 \end{pmatrix} \quad (4.64)$$

The stiffness matrix of the loaded model is obtained from Eq. (4.28) with the calculated modal shapes, Eq. (4.64), and natural frequencies, Eq. (4.63), as:

$$\mathbf{K}_{ij} = \begin{pmatrix} 46.7 & -50.9 & 4.4 \\ -50.9 & 102.8 & -56.3 \\ 4.4 & -56.3 & 108.2 \end{pmatrix} \text{ kip/in} \quad (4.65)$$

The story stiffnesses of the loaded model, defined in Eq. (4.29), are calculated from Eq. (4.65) and shown below:

$$\mathbf{k}_i = \begin{pmatrix} 50.9 \\ 56.3 \\ 51.9 \end{pmatrix} \text{ kip/in} \quad (4.66)$$

For representation of these analytical dynamic characteristics in the comparison, the test label of STAAD is used.

4.5.1 Comparison of Analytical and Experimental Dynamic Characteristics

Tables 4-2 and 4-3 summarize the identified natural frequencies, modal shapes, stiffness matrix, story stiffnesses, equivalent viscous damping ratios, and damping matrix of the unloaded and loaded model, respectively from the experimental identification tests and the analytical evaluation from STAAD.

(a) Unloaded Model Identification Tests

For the unloaded model, it can be observed that the identified natural frequencies from STAAD and the HAMMER test are slightly different, primarily due to the estimated quantities for the story masses, input member stiffnesses, and the small level of excitation of the higher modes from the impact hammer. Large variations in the modal shapes and stiffness matrix can be detected between the identifications of the impact hammer test and STAAD. This is again primarily attributed to the small level excitation in the higher modes with third floor strikes from the impact hammer. Only the characteristics associated with the first mode of vibration are comparable. Therefore it is concluded that the identification of the modal shapes (with exception of the first mode), stiffness matrix, story stiffnesses, and damping matrix from the impact hammer test are not reliable.

(b) Loaded Model Identification Tests

For the loaded model, comparable natural frequencies and modal shape matrices have resulted in all tests, both experimentally and analytically. It can be observed from Tables 4-2 and 4-3 that a 47.6% reduction in the first mode natural frequency (from 3.40 Hz. (HAMMER) to 1.78 Hz. (WHN_B)) occurs due to attaching the additional weights for mass similitude on the model. Similar reductions are also found in the second and third modes of vibration for the model.

Comparable stiffness matrices and story stiffnesses are observed in the PULL, WHN_B, and STAAD tests, in which the story stiffnesses are approximately equivalent for each floor. An important point to note is that the sum of the diagonal terms of the stiffness matrix of the loaded model developed analytically using STAAD corresponded to a 0.5% error compared to the results from the experimental WHN_B test for the undamaged model. Recall that the input member properties in STAAD used a reduced gross member stiffness to match the first mode natural frequency from WHN_B. Since excellent correlation exists between STAADTM and the experimental characteristics, STAADTM is used in the following tests to evaluate the stiffness matrix and story stiffnesses based on the correlation of the experimentally observed first mode natural frequency from the previous white noise excitation.

The identification of the first mode equivalent viscous damping factor is also comparable for each test performed. But variations of the second and third mode damping factors are observed among the various tests. Since a smoothing technique was required for both the SNAP and WHN_B tests, deviations of the higher-order damping factors are expected. Also the damping factor identification from Eq. (4.19) is based on an elastic system, which may be invalid since cracking may have developed in some of the members.

The identified viscous damping matrices of the unloaded and loaded models from the HAMMER and WHN_B tests, respectively are also shown to have large variations. But again since the damping matrix is developed from the modal shapes [see Eq. (4.30)], the determination of the damping matrix from the impact hammer test can be regarded as inaccurate.

Therefore from the above comparisons, it is concluded that the white noise identification test provides an accurate evaluation of the dynamic characteristics of the model. Thus herein only white noise excitations are used to update the dynamic characteristics of the model after an induced base motion. It is also concluded that accurate predictions of the dynamic characteristics

and stiffness matrix of the undamaged model are achieved with STAADTM using a 56.5% reduction in the gross member stiffness properties for correlating the first mode natural frequency.

Table 4-2 Dynamic Characteristics of the Unloaded Model

Test	f_i^u (Hz.)	Φ_{ij}^u	K_{ij}^u (kip/in)	k_i^u (kip/in)	ξ_i^u (%)	C_{ij}^u
HAMMER	$\begin{pmatrix} 3.40 \\ 11.00 \\ 17.60 \end{pmatrix}$	$\begin{pmatrix} 1.00 & -0.67 & -0.62 \\ 0.82 & 0.18 & 1.00 \\ 0.47 & 1.00 & -0.63 \end{pmatrix}$	$\begin{pmatrix} 70.1 & -72.1 & 10.3 \\ -72.1 & 115.5 & -59.2 \\ 10.3 & -59.2 & 97.3 \end{pmatrix}$	$\begin{pmatrix} 72.1 \\ 59.2 \\ 38.1 \end{pmatrix}$	$\begin{pmatrix} 2.7 \\ 1.5 \\ 1.0 \end{pmatrix}$	$\begin{pmatrix} 0.028 & -0.007 & -0.003 \\ -0.007 & 0.028 & -0.005 \\ -0.003 & -0.005 & 0.033 \end{pmatrix}$
STAAD (0.565 EI_p)	$\begin{pmatrix} 3.70 \\ 10.81 \\ 16.50 \end{pmatrix}$	$\begin{pmatrix} 1.00 & -0.81 & -0.43 \\ 0.78 & 0.53 & 1.00 \\ 0.40 & 1.00 & -0.88 \end{pmatrix}$	$\begin{pmatrix} 46.7 & -50.9 & 4.4 \\ -50.9 & 102.7 & -56.2 \\ 4.4 & -56.2 & 108.2 \end{pmatrix}$	$\begin{pmatrix} 50.9 \\ 56.2 \\ 52.0 \end{pmatrix}$	-	-

Table 4-3 Dynamic Characteristics of the Loaded Model

Test	f_i (Hz.)	Φ_{ij}	K_{ij} (kip/in)	k_i (kip/in)	ξ_i (%)	C_{ij}
PULL	$\begin{pmatrix} 1.76 \\ 5.34 \\ 8.15 \end{pmatrix}$	$\begin{pmatrix} 1.00 & -0.82 & -0.41 \\ 0.76 & 0.55 & 1.00 \\ 0.40 & 1.00 & -0.88 \end{pmatrix}$	$\begin{pmatrix} 47.4 & -52.7 & 3.2 \\ -52.7 & 109.3 & -59.8 \\ 3.2 & -59.8 & 113.9 \end{pmatrix}$	$\begin{pmatrix} 52.7 \\ 59.8 \\ 54.1 \end{pmatrix}$	-	-
SNAP	$\begin{pmatrix} 1.86 \\ 5.66 \\ 8.40 \end{pmatrix}$	-	-	-	$\begin{pmatrix} 2.5 \\ 4.8 \\ 4.0 \end{pmatrix}$	-
WHN_B (Eq.(4.20))	$\begin{pmatrix} 1.78 \\ 5.32 \\ 7.89 \end{pmatrix}$	$\begin{pmatrix} 1.00 & -0.82 & -0.46 \\ 0.80 & 0.46 & 1.00 \\ 0.42 & 1.00 & -0.83 \end{pmatrix}$	$\begin{pmatrix} 51.9 & -53.4 & 2.5 \\ -53.4 & 102.4 & -54.4 \\ 2.5 & -54.4 & 104.7 \end{pmatrix}$	$\begin{pmatrix} 53.4 \\ 54.4 \\ 50.3 \end{pmatrix}$	$\begin{pmatrix} 2.0 \\ 2.4 \\ 2.0 \end{pmatrix}$	$\begin{pmatrix} 0.072 & -0.042 & -0.012 \\ -0.042 & 0.097 & -0.029 \\ -0.012 & -0.029 & 0.112 \end{pmatrix}$
WHN_B (Eq.(4.19))	-	-	-	-	$\begin{pmatrix} 1.7 \\ 1.6 \\ 1.4 \end{pmatrix}$	-
STAAD (0.565 EI_p)	$\begin{pmatrix} 1.78 \\ 5.20 \\ 7.94 \end{pmatrix}$	$\begin{pmatrix} 1.00 & -0.81 & -0.43 \\ 0.78 & 0.53 & 1.00 \\ 0.40 & 1.00 & -0.88 \end{pmatrix}$	$\begin{pmatrix} 46.7 & -50.9 & 4.4 \\ -50.9 & 102.8 & -56.3 \\ 4.4 & -56.3 & 108.2 \end{pmatrix}$	$\begin{pmatrix} 50.9 \\ 56.3 \\ 51.9 \end{pmatrix}$	-	-

4.6 Response to Minor Earthquake

After the identifications of the initial dynamic properties for the fully loaded three story model were completed, the Taft N21E accelerogram component, normalized for a peak ground acceleration (PGA) of 0.05 G, was used to excite the model (test label TFT_05). This level of ground acceleration motion is representative of a minor earthquake excitation. Fig. 4-14a and 4-14b show the desired and achieved base acceleration motion of the shaking table. Fig. 4-14c shows a short segment of the desired and achieved base motions, from which a high degree of similarity can be detected.

4.6.1 Global Response

Figs. 4-15 and 4-16 show the story displacement and shear force time histories for the Taft N21E, PGA 0.05 G, base motions. It should be noted that the first and second story shear forces (Figs. 4-16c and 4-16b) were directly recorded through the load cells. Since load cells were not installed in the third story columns, the third story shear forces (Fig. 4-16a) were determined from the third story accelerations (accelerometers AH7 and AH8) multiplied by the inertial story mass. It was observed that the first and second story shear forces recorded from the accelerometers were slightly less than that of the load cells, but the deviation was considered tolerable for the experiment. Figs. 4-17a and 4-17b show a magnified overlaid portion of the story displacements and shear forces, respectively. It can be observed that the story displacements and shears for each floor are moving in phase (peak story response occurring at the same time). Figs. 4-18a and 4-18b show the story displacement, shear forces, and story loads when the maximum first story drift occurred. Again at this point in time, the shape of the story displacements and shear forces resembles the shape of the first mode of vibration. Therefore it is concluded that the response of the model was primarily governed by the first mode of vibration throughout the time history of the minor earthquake.

Table 4-4 summarizes the maximum story displacements, inter-story drifts, shear forces, story loads, and peak accelerations for each floor of the model for TFT_05. It was observed that small levels of story displacements and inter-story drifts (0.28% for the first floor) occur. The induced base shear (5.3 kips) was 6.5% of the total structural weight from TFT_05. The maximum story loads occurred near the peaks of the story drifts, but not at the same time. Also the observed amplifications of the story level accelerations were 86%, 72%, and 148%, respectively for the first, second, and third stories in comparison with the base acceleration.

El-Attar et al. (1991b) observed a maximum first story drift of 0.18% and a base shear demand of 2.3% of the total structural weight during the Taft S69E PGA 0.05 g shaking table motion. However, the prototype structural weight that El-Attar et al. (1991b) used for mass similitude, was slightly greater than what is used in this study due to considerations of non-structural walls and full dead weight contributions (neglected in this study due to weight limitations of the shaking table). Therefore for comparison with this study, the equivalent base shear is determined from the measured demand multiplied by 1.2882 (ratio of prototype weights). Therefore the equivalent base shear is 3.0% of the proportioned weight. It can be observed that differences exist between the tests. Some explanations are due to: (i) the different inertial mass and natural frequencies; (ii) the different Taft component of base motion; and (iii) the different material properties.

TABLE 4-4 Maximum Response for Minor Earthquake TFT_05

Story	Max. Story Displacements (in.)	Max. Inter-Story Drifts (%)	Max. Story Shears (Kips)	Max. Story Loads (Kips)	Peak Story Accelerations (g)
Third	0.30	0.23	3.4	9.1	0.12
Second	0.22	0.24	4.2	8.0	0.09
First	0.14	0.28	5.3 (6.5%W)	5.3	0.09

Fig. 4-19 shows the shear force versus inter-story drift history for each story of the model. As expected, a linear-elastic behavior is observed for all stories. It can be observed that the histories are primarily governed by elastic deformations with loops occurring due to the equivalent viscous damping present in the structure. Fig. 4-20 shows the energy time history for TFT_05. The total input energy to the structural system is 1.7 kip-in. Since the dissipated energies are small and governed by viscous damped energy, the structure is again classified as being governed primarily by elastic deformations.

4.6.2 Local Response

Fig. 4-21 details the qualitative descriptions for the beams and columns of the model for reference in the following and future discussions.

Fig. 4-22 shows the induced shear forces on an interior and exterior first story column (base shear) for ground motion TFT_05 monitored with the load cells. It can be observed that the shears in the interior columns are approximately twice that of the exterior columns. Also note that both the interior and exterior columns have a greater shear force demand for greater axial force. The same observations were made by El-Attar et al. (1991b).

Fig. 4-23 shows the moment versus axial load interaction history for the columns of the first and second stories superimposed on damage state interaction surfaces. The cracking and nominal ultimate surfaces are developed based on the geometric dimensions of the column, a concrete compressive strength of 4.0 ksi, a rebar yield strength of 68.0 ksi, and a concrete crushing strain of 0.003. The projected dynamic ultimate surface, due to strain hardening of the reinforcement and dynamic strain rate effects, is determined based on a concrete crushing strain of 0.010 and a 30% increase in the concrete compressive and rebar yield strengths. It can be observed that the moment versus axial load history in most of the first and second story columns partially extend beyond the cracking surface, but were well within the nominal ultimate bounds. The variations of axial load in the exterior columns can be observed by the slope of the loading on the interaction diagrams. In contrast, little axial load variation can be observed in the interior columns.

Fig. 4-24a and 4-24b show the first story beam bending moment time histories in the south and north sides of the model at the column face along with the ultimate moment surfaces. The development of the ultimate surfaces for the beams considered strength contributions from the slab reinforcement within the flange width from the ACI-318 (18 in.) and also within the full slab width (60 in.). Firstly the positive ultimate moments (plotted on the bottom of the beams) considered tensile contributions of the slab steel and top reinforcement within the ACI-318 and full slab widths since the compression depth is small in the T-beam member. Partially unbonded reinforcement is used to consider the effect of pull-out of the discontinuous bottom longitudinal reinforcement. The rebar area at a section is reduced by the ratio of the provided development length at the section and the required development length of the bar, Hoffmann (1992). Therefore for the moment capacity at the column face, a 50% reduction in beam rebar area is considered based on the prototype section. The negative moments (plotted on the top of the beams) also considers slab steel contributions from the ACI-318 and full slab widths. The projected dynamic ultimate surface assumed a 30% increase in strength from strain hardening of the reinforcement and dynamic strain rate effects. It can be observed that the moment demands in the interior and exterior beams were well below the nominal ultimate bounds in both directions.

The member curvatures of the first story north-east exterior and interior subassemblages were measured using the potentiometers as outlined in Section 3.6.4. Since the measured potentiometer readings of the members include the adjacent member rotations, a first-order correction factor was applied to the potentiometer readings. Fig. 4-25 shows the bending moment versus corrected curvatures for the instrumented members of the first floor north-east exterior and interior joints along with the member moment capacities. Again, an elastic behavior for the members exists. It can also be observed that the moment history for the members were well below their nominal strengths.

The bending moment diagrams for the model when the first story drift was maximum for each direction, along with the corresponding story displacements, are shown in Fig. 4-26. Again it is to be noted that the moment demands were within the nominal ultimate bounds during the minor shaking.

The observed (visual) structural damage to the scaled model due to TFT_05 was primarily located in the lower first story exterior columns as shown in Fig. 4-27. This damage was identified in the form of some slight cracking in the splice zone near the locations of the transverse hoop reinforcement. The remaining structure had no visible signs of damage or cracking of members. Fig. 4-28 shows the damaged state of the model after TFT_05. It can be observed that cracking in some column members has occurred, but yielding has not transpired. The beams remained primarily elastic throughout this low level base motion.

4.6.3 Dynamic Properties after Minor Shaking

After the superimposed minor base motion, the identification of the ensuing dynamic properties of the model are determined from the white noise excitation labeled WHN_C . Figs. 4-29 and 4-30 show the transfer functions and smoothed transfer functions for each floor of the model, respectively. Since small damping and well separated modes can be observed, the averaged natural frequencies are identified as follows and tabulated in Table 4-5:

$$\mathbf{f}_i = \begin{pmatrix} 1.71 \\ 5.08 \\ 7.42 \end{pmatrix} \text{ Hz.} \quad (4.67)$$

Note from Eqs. (4.67) and (4.52) that the first mode natural frequency shifted (softened) from 1.78 Hz. to 1.71 Hz. (3.9% reduction). Therefore there was some deterioration of the model from the TFT_05 base motion. This can be attributed to the cracking in some members of the model. Also cracking is evident in Fig. 4-29 where it can be observed that several excited frequencies occurred near the modes of vibration, including the first mode. Similarly for the same reasoning, reductions of 4.5% and 6.0% can be observed for the second and third modes of vibration, respectively.

The modal shape matrix and participation factors were also identified from the transfer functions and are tabulated in Table 4-5. It can be observed that the modal shapes and participation factors remained relatively the same before and after the TFT_05 base motion.

From the smoothed transfer functions in Fig. 4-30, the equivalent viscous damping factors were determined by the half-power (bandwidth) method as 4.3%, 4.2%, 3.0% and were tabulated in Table 4-5. It can be observed that increases in the modal damping factors of about 100% have occurred due to the wider transfer function magnitude near the natural frequencies. Again note that contributions from hysteretic damping may have taken place.

The updated stiffness matrix of the model was developed from Eq. (4.28) with the dynamic characteristics of WHN_C and shown in Table 4-5 along with the corresponding story stiffnesses. It can be observed that the sum of the diagonal terms of the stiffness matrix after TFT_05 is reduced by 10.6% as compared to WHN_B. Story stiffness reductions of 10.7%, 13.1%, and 12.4%, respectively for the first, second, and third stories have resulted.

Fig. 4-31 shows the story shear versus inter-story drift histories for WHN_C. Again it can be observed that equivalent viscous damping was present in the structural system. The initial stiffnesses after TFT_05 (WHN_C) were tabulated in Table 4-6 along with the results of WHN_B. It can be observed that the stiffnesses from the shear-drift histories were reduced by 4.3%, 7.1%, and 15.5%, respectively for the first, second, and third floors.

To complement the identified first mode natural frequency from WHN_C after the TFT_05 base motion (1.71 Hz.), an analysis is done using STAADTM with the modified stiffness properties:

$$(EI)_{\text{member}} = 0.520 (EI)_g \quad (4.68)$$

where $(EI)_{\text{member}}$ is the beam or column member stiffness based on the respective gross member area reduction.

The analytical prediction of the natural frequencies, modal shapes, and stiffness matrix of the model after TFT_05, based on input member properties in STAAD from Eq. (4.68), are shown in Table 4-7 along with the results from WHN_C. It can be observed that the natural frequencies and modal shape matrices from STAAD are comparable with the identified results from WHN_C. Also note that a 2.7% deviation is observed in the sum of the diagonal terms of the identified stiffness matrix, which is well within the expected experimental variations.

TABLE 4-5 Dynamic Properties and Stiffness Matrix before and after TFT_05

	WHN_B (before)	WHN_C (after)
Natural Frequencies (Hz.)	$\mathbf{f}_i = \begin{pmatrix} 1.78 \\ 5.32 \\ 7.89 \end{pmatrix}$	$\mathbf{f}_i = \begin{pmatrix} 1.71 \\ 5.08 \\ 7.42 \end{pmatrix}$
Modal Shapes	$\Phi_{ij} = \begin{pmatrix} 1.00 & -0.82 & -0.46 \\ 0.80 & 0.46 & 1.00 \\ 0.42 & 1.00 & -0.83 \end{pmatrix}$	$\Phi_{ij} = \begin{pmatrix} 1.00 & -0.84 & -0.42 \\ 0.79 & 0.52 & 1.00 \\ 0.40 & 1.00 & -0.82 \end{pmatrix}$
Modal Participation Factors	$\Gamma_i = \begin{pmatrix} 0.44 \\ 0.12 \\ -0.06 \end{pmatrix}$	$\Gamma_i = \begin{pmatrix} 0.43 \\ 0.13 \\ -0.05 \end{pmatrix}$
Damping Factors (%)	$\xi_i = \begin{pmatrix} 2.0 \\ 2.4 \\ 2.0 \end{pmatrix}$	$\xi_i = \begin{pmatrix} 4.3 \\ 4.2 \\ 3.0 \end{pmatrix}$
Stiffness Matrix (kip/in)	$\mathbf{K}_{ij} = \begin{pmatrix} 51.9 & -53.4 & 2.5 \\ -53.4 & 102.4 & -54.4 \\ 2.5 & -54.4 & 104.7 \end{pmatrix}$	$\mathbf{K}_{ij} = \begin{pmatrix} 44.5 & -46.8 & -0.2 \\ -46.8 & 94.9 & -47.3 \\ -0.2 & -47.3 & 92.2 \end{pmatrix}$
Story Stiffnesses (kip/in)	$\mathbf{k}_i = \begin{pmatrix} 53.4 \\ 54.4 \\ 50.3 \end{pmatrix}$	$\mathbf{k}_i = \begin{pmatrix} 46.8 & (12.4\%) \\ 47.3 & (13.1\%) \\ 44.9 & (10.7\%) \end{pmatrix}$

TABLE 4-6 Low Amplitude Initial Stiffnesses from the Shear versus Inter-Story Drift Histories

Story	WHN_B (kip/in)	WHN_C (kip/in)
Third	40.0	33.8 (15.5%)
Second	42.4	39.4 (7.1%)
First	51.2	49.0 (4.3%)

TABLE 4-7 Analytical and Experimental Comparison of the Dynamic Properties

	Experimental (WHN_C)	Analytical [STAAD (0.520 (EI) _g)]
Natural Frequencies (Hz.)	$\mathbf{f}_i = \begin{pmatrix} 1.71 \\ 5.08 \\ 7.42 \end{pmatrix}$	$\mathbf{f}_i = \begin{pmatrix} 1.71 \\ 4.99 \\ 7.62 \end{pmatrix}$
Modal Shapes	$\Phi_{ij} = \begin{pmatrix} 1.00 & -0.84 & -0.42 \\ 0.79 & 0.52 & 1.00 \\ 0.40 & 1.00 & -0.82 \end{pmatrix}$	$\Phi_{ij} = \begin{pmatrix} 1.00 & -0.81 & -0.43 \\ 0.78 & 0.53 & 1.00 \\ 0.40 & 1.00 & -0.88 \end{pmatrix}$
Stiffness Matrix (kip/in)	$\mathbf{K}_{ij} = \begin{pmatrix} 44.5 & -46.8 & -0.2 \\ -46.8 & 94.9 & -47.3 \\ -0.2 & -47.3 & 92.2 \end{pmatrix}$	$\mathbf{K}_{ij} = \begin{pmatrix} 43.0 & -46.9 & 4.0 \\ -46.9 & 94.7 & -51.8 \\ 4.0 & -51.8 & 99.7 \end{pmatrix}$
Story Stiffnesses (kip/in)	$\mathbf{k}_i = \begin{pmatrix} 46.8 \\ 47.3 \\ 44.9 \end{pmatrix}$	$\mathbf{k}_i = \begin{pmatrix} 46.9 \\ 51.8 \\ 47.9 \end{pmatrix}$

After the conclusion of shaking table test WHN_C, the tests were interrupted and continued the following day. The testing sequence started with another white noise shaking table test, labeled WHN_D. This test was used to verify the current dynamic characteristics of the model and to note any variations from WHN_C due to the lowering and lifting of the shaking table. Figs. 4-32 and 4-33 show the story transfer functions and smoothed transfer functions for the model from base excitation WHN_D, respectively. Since small damping and well separated modes

can be observed, the natural frequencies were tabulated in Table 4-8. It can be observed that the natural frequencies from the white noise excitations WHN_C and WHN_D were identical for the first mode and have small deviations in the second and third modes.

The modal shapes and participation factors were also identified from the story transfer functions of test WHN_D and are shown in Table 4-8. It can be observed that the modal shapes and participation factors were similar for tests WHN_C and WHN_D.

From the smoothed transfer functions, the equivalent viscous damping factors were determined using the half-power (bandwidth) method [Eq. (4.20)] as 4.0%, 2.9%, and 1.3%, for the first, second, and third modes, respectively. Table 4-8 shows comparable damping factors for the first mode of vibration. It can also be observed that deviations occurred in the second and third mode damping factors. This is attributed to the varying amplifications of this mode between the different tests and from the smoothing of the transfer functions. However, this variation is considered satisfactory for such experimental tests.

The stiffness matrix of the model, developed from Eq. (4.28) using the dynamic characteristics determined from white noise excitation WHN_D, is shown in Table 4-8 along with the corresponding story stiffnesses. It can be observed that the stiffness matrices and story stiffnesses determined from tests WHN_C and WHN_D were slightly varied. But the deviations appear to be well within the expected experimental variations, especially since the sum of the diagonal terms are equivalent for both tests.

Fig. 4-34 shows the story shear versus inter-story drift histories for WHN_D. It can be observed that the initial stiffnesses from WHN_D were identical to that from WHN_C.

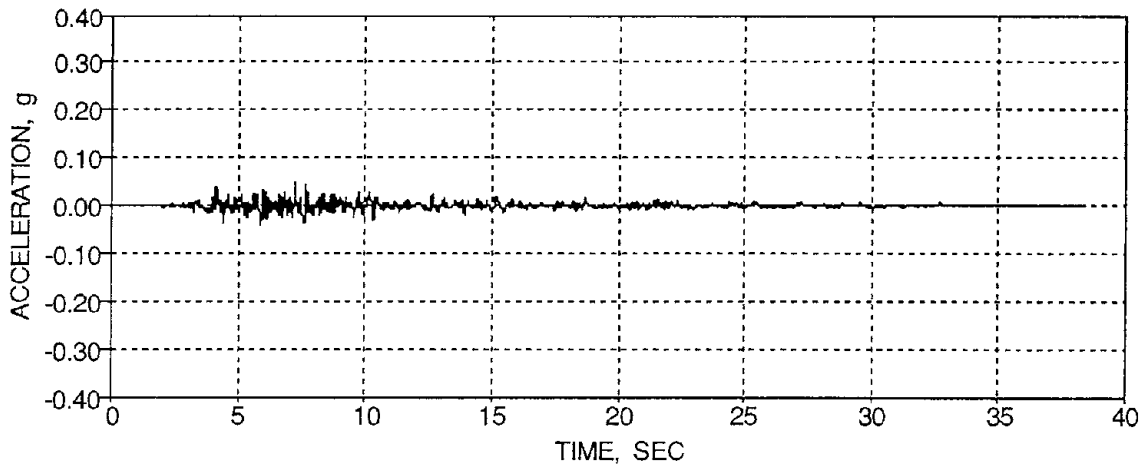
Since the calculated natural frequencies, modal shapes, modal participation factors, damping factors, stiffness matrix, and initial stiffnesses from the shear-drift histories of the model show no appreciable changes in white noise tests WHN_C and WHN_D, it is concluded that no damage occurred due to the vibrations induced during the lowering and lifting process of the shaking table. It is also worth noting that no damage had resulted to the model from the white noise shaking table excitation.

TABLE 4-8 Dynamic Properties and Stiffness Matrix after TFT_05 from WHN_C and WHN_D

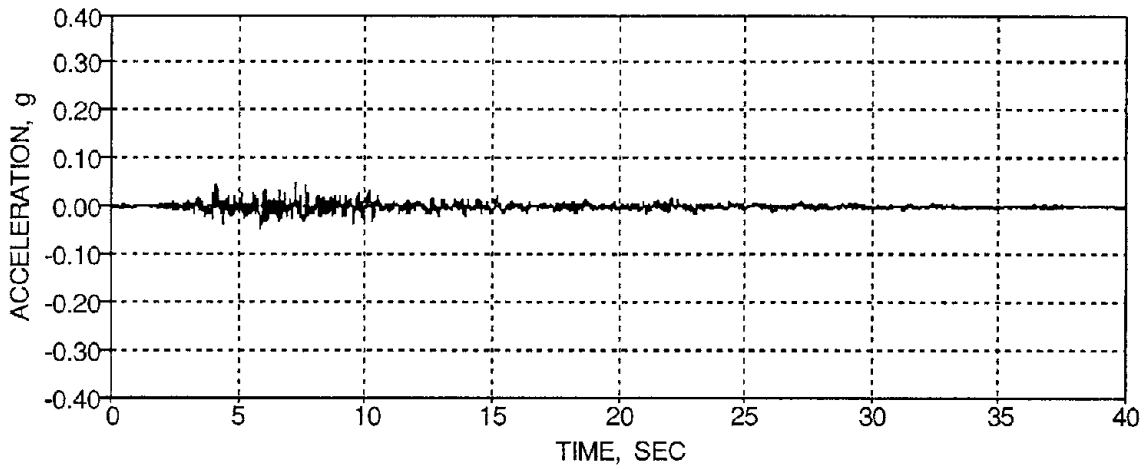
	WHN_C	WHN_D
Natural Frequencies (Hz.)	$\mathbf{f}_i = \begin{pmatrix} 1.71 \\ 5.08 \\ 7.42 \end{pmatrix}$	$\mathbf{f}_i = \begin{pmatrix} 1.71 \\ 5.22 \\ 7.32 \end{pmatrix}$
Modal Shapes	$\Phi_{ij} = \begin{pmatrix} 1.00 & -0.84 & -0.42 \\ 0.79 & 0.52 & 1.00 \\ 0.40 & 1.00 & -0.82 \end{pmatrix}$	$\Phi_{ij} = \begin{pmatrix} 1.00 & -0.88 & -0.40 \\ 0.79 & 0.58 & 1.00 \\ 0.41 & 1.00 & -0.86 \end{pmatrix}$
Modal Participation Factors	$\Gamma_i = \begin{pmatrix} 0.43 \\ 0.13 \\ -0.05 \end{pmatrix}$	$\Gamma_i = \begin{pmatrix} 0.43 \\ 0.13 \\ -0.05 \end{pmatrix}$
Damping Factors (%)	$\xi_i = \begin{pmatrix} 4.3 \\ 4.2 \\ 3.0 \end{pmatrix}$	$\xi_i = \begin{pmatrix} 4.0 \\ 2.9 \\ 1.3 \end{pmatrix}$
Stiffness Matrix (kip/in)	$\mathbf{K}_{ij} = \begin{pmatrix} 44.5 & -46.8 & -0.2 \\ -46.8 & 94.9 & -47.3 \\ -0.2 & -47.3 & 92.2 \end{pmatrix}$	$\mathbf{K}_{ij} = \begin{pmatrix} 44.6 & -45.8 & -2.7 \\ -45.8 & 92.8 & -44.9 \\ -2.7 & -44.9 & 94.1 \end{pmatrix}$
Story Stiffnesses (kip/in)	$\mathbf{k}_i = \begin{pmatrix} 46.8 \\ 47.3 \\ 45.9 \end{pmatrix}$	$\mathbf{k}_i = \begin{pmatrix} 45.8 \\ 44.9 \\ 49.2 \end{pmatrix}$

TABLE 4-9 Low Amplitude Initial Stiffnesses from the Shear versus Inter-Story Drift Histories

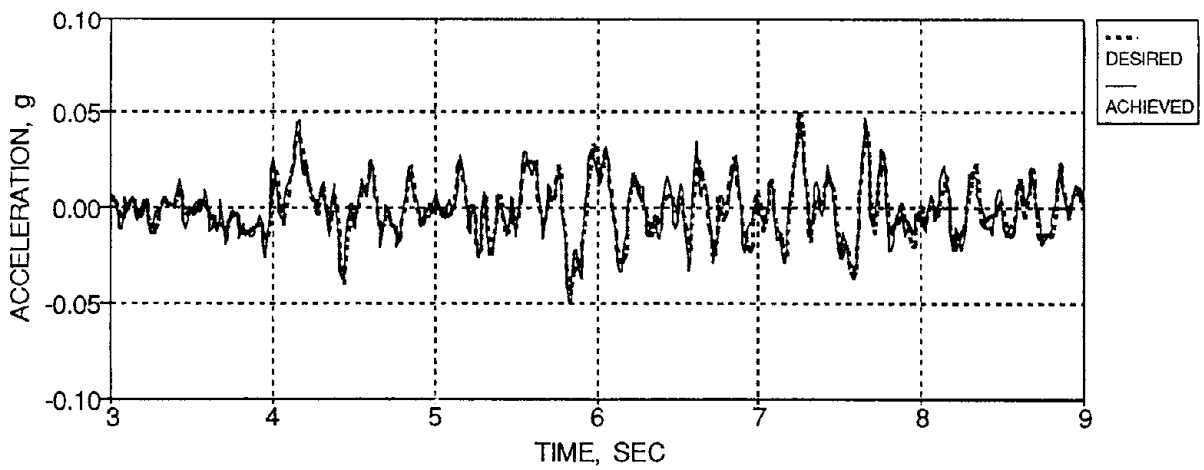
Story	WHN_C (kip/in)	WHN_D (kip/in)
Third	33.8	33.8
Second	39.4	39.4
First	49.0	49.0



(a) Desired Base Motion

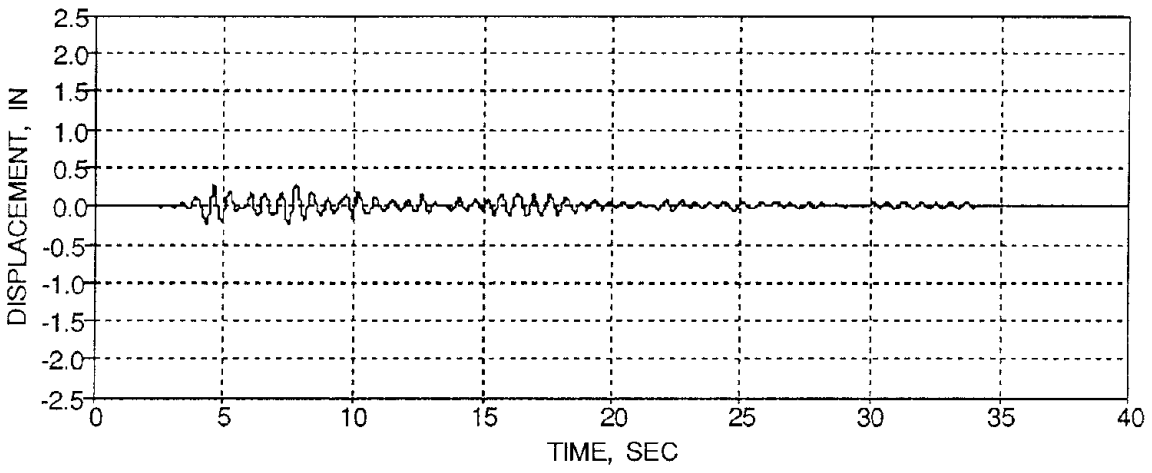


(b) Achieved Base Motion

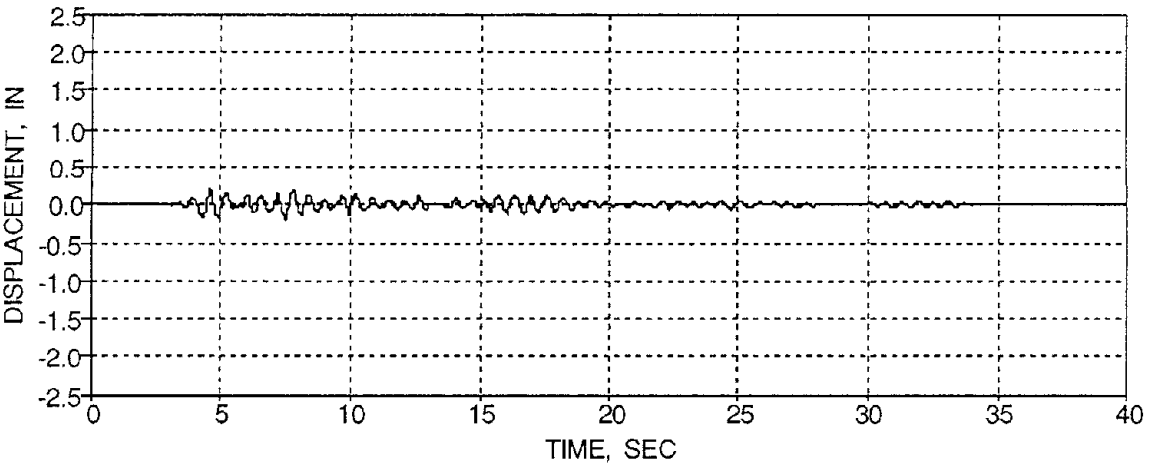


(c) Short Segment Comparison of the Desired and Achieved Base Motions

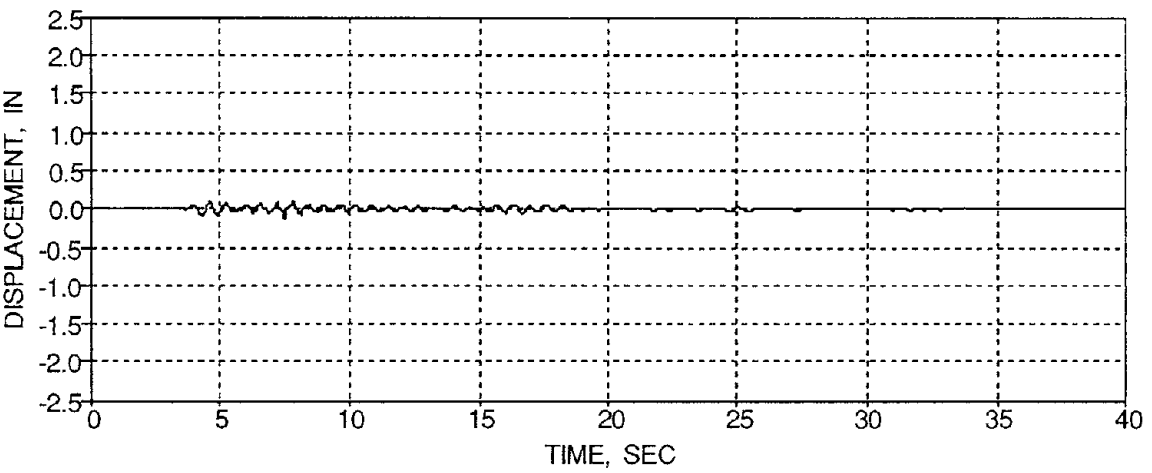
FIG. 4-14 Shaking Table Motion for the Taft N21E Base Motion , PGA 0.05 g



(a) Third Floor

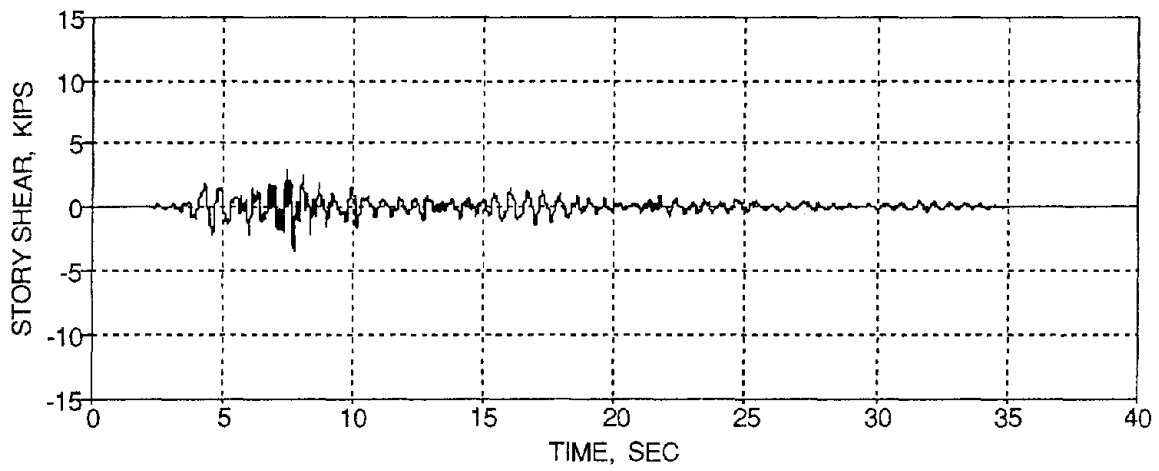


(b) Second Floor

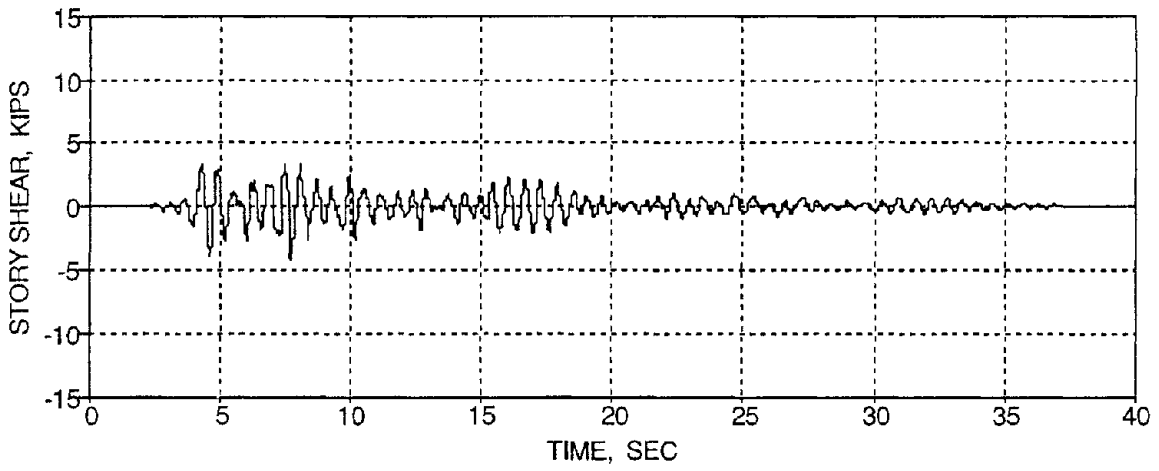


(c) First Floor

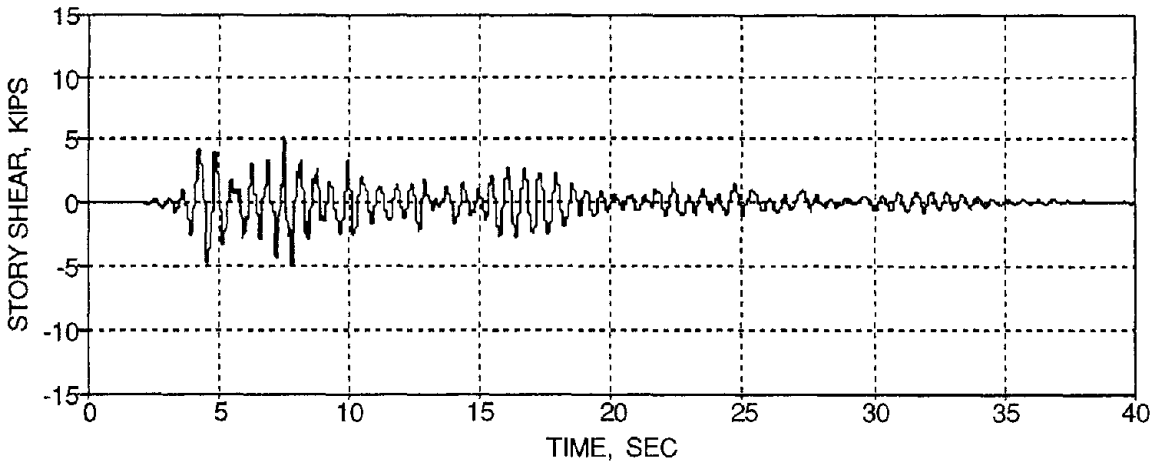
FIG. 4-15 Story Displacement Time Histories for TFT_05



(a) Third Floor

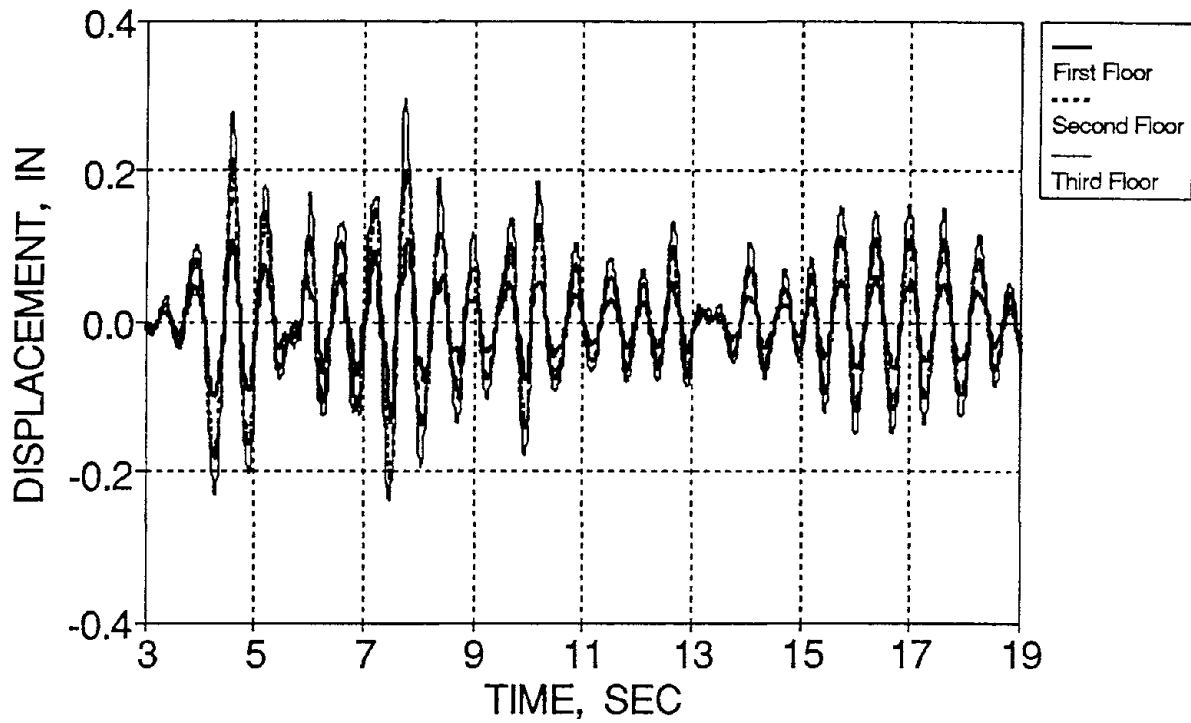


(b) Second Floor

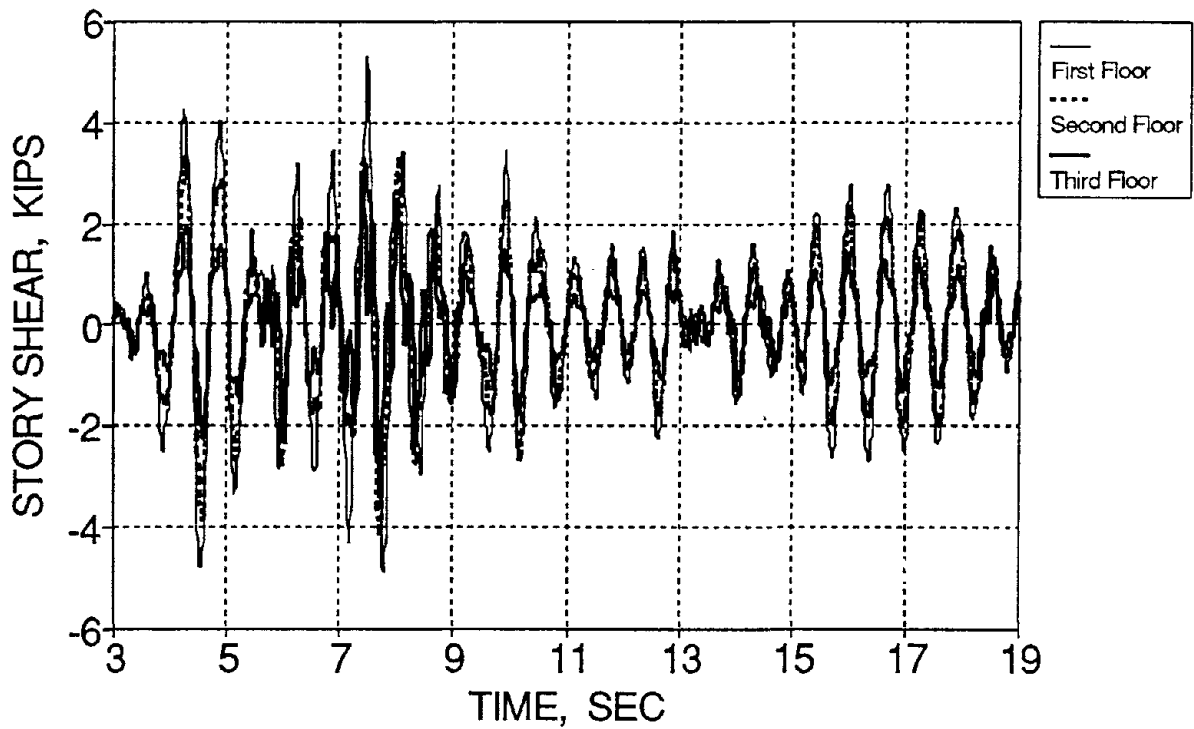


(c) First Floor

FIG. 4-16 Story Shear Force Time Histories for TFT_05

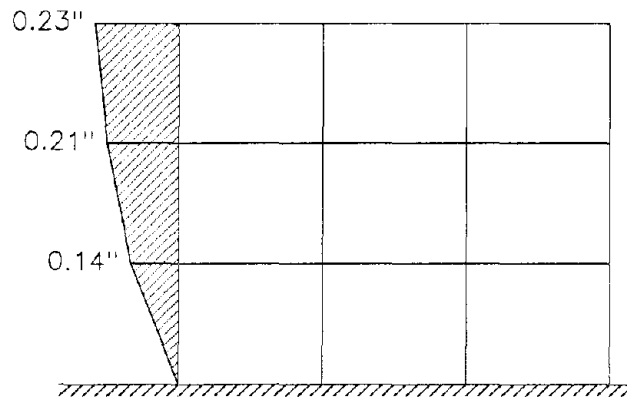


(a) Story Displacements

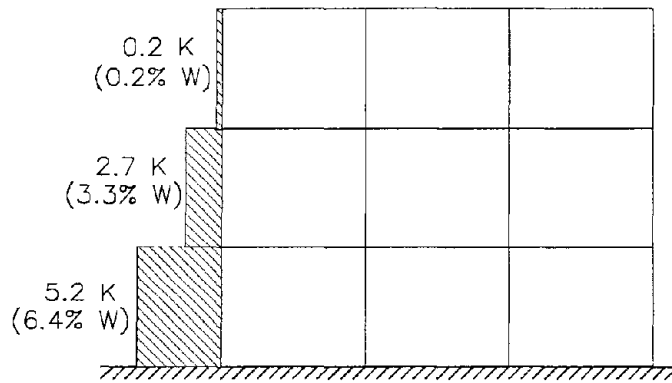


(b) Story Shear Forces

FIG. 4-17 Overlaid Global Response Time History Segments for TFT_05

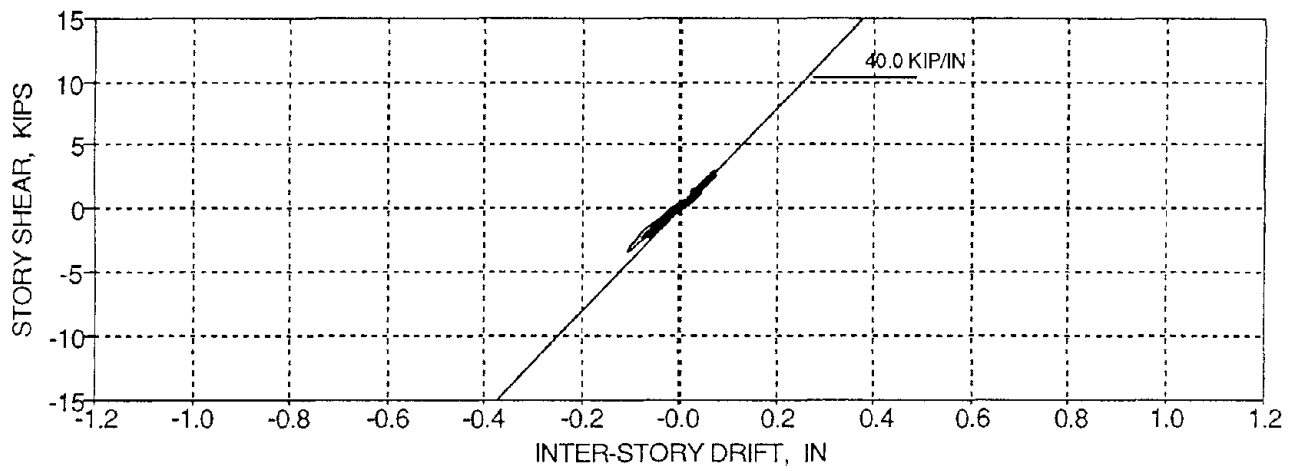


(a) Story Displacements (Time= 7.50 sec)

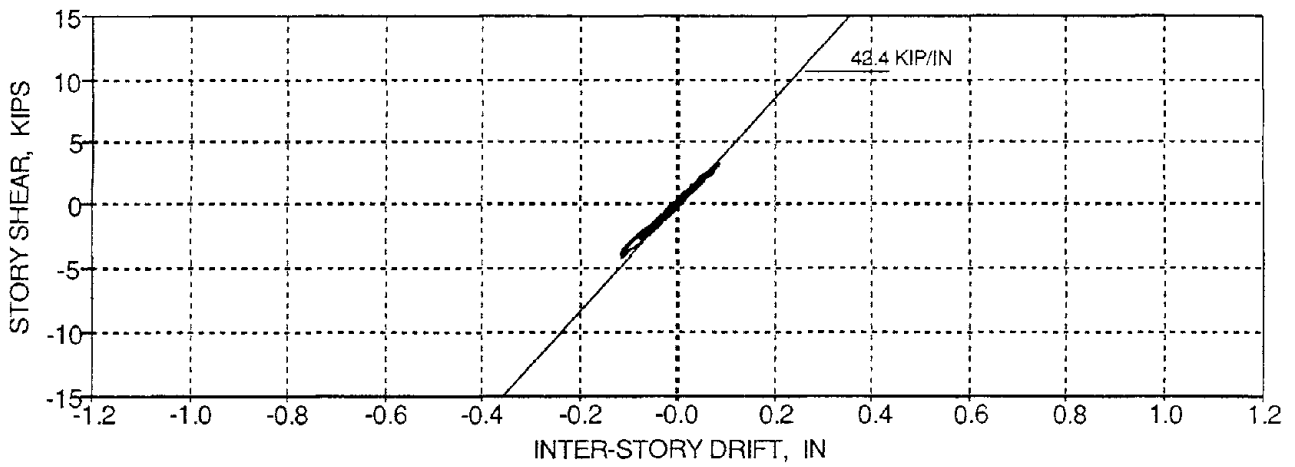


(b) Story Shear Forces (Time = 7.50 sec)

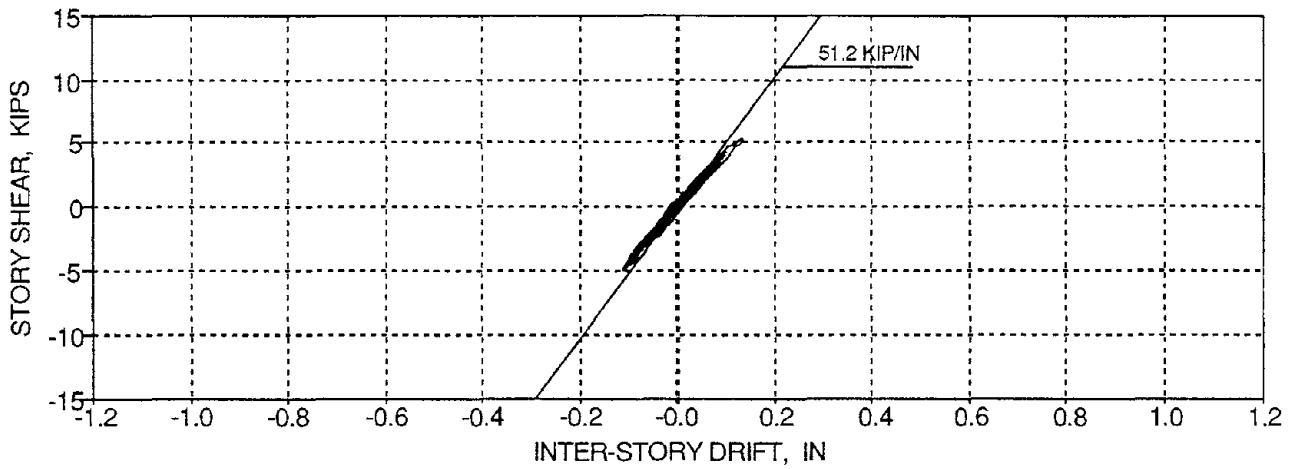
FIG. 4-18 Story Displacements and Shears at Maximum First Story Drift for TFT_05



(a) Third Floor

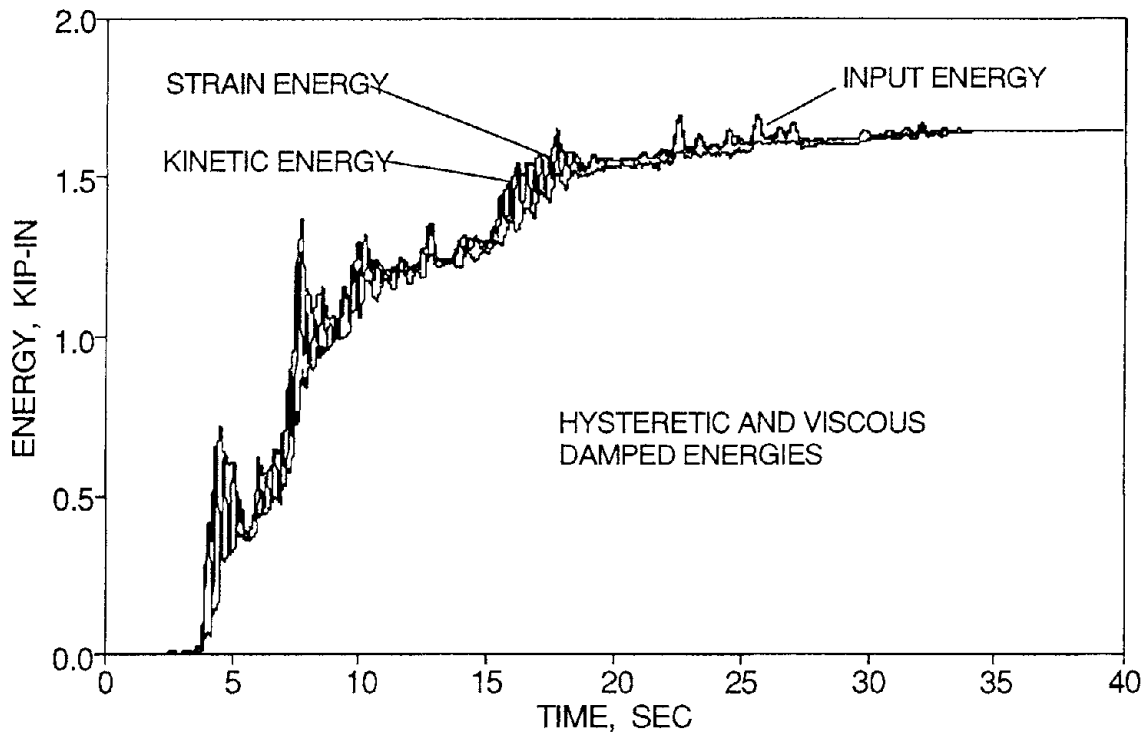


(b) Second Floor

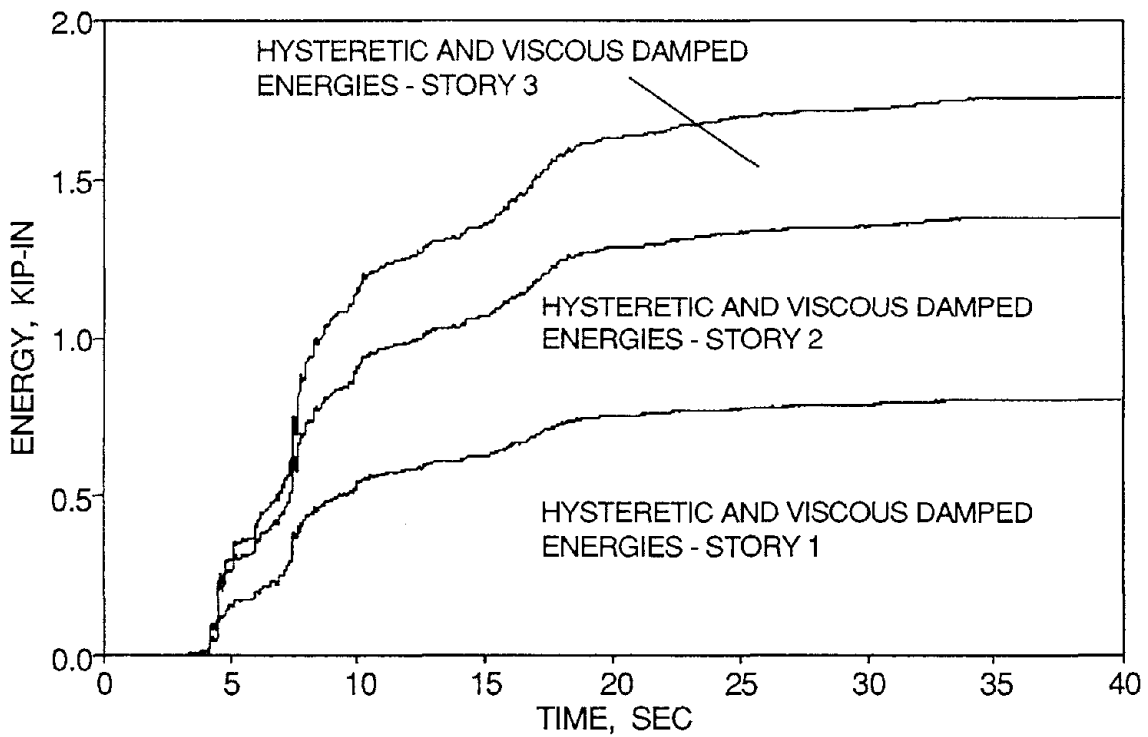


(c) First Floor

FIG 4-19 Story Shear versus Inter-Story Drift Histories for TFT_05



(a) Energy Balance



(b) Story Dissipated Energies

FIG. 4-20 Energy Time History for TFT_05

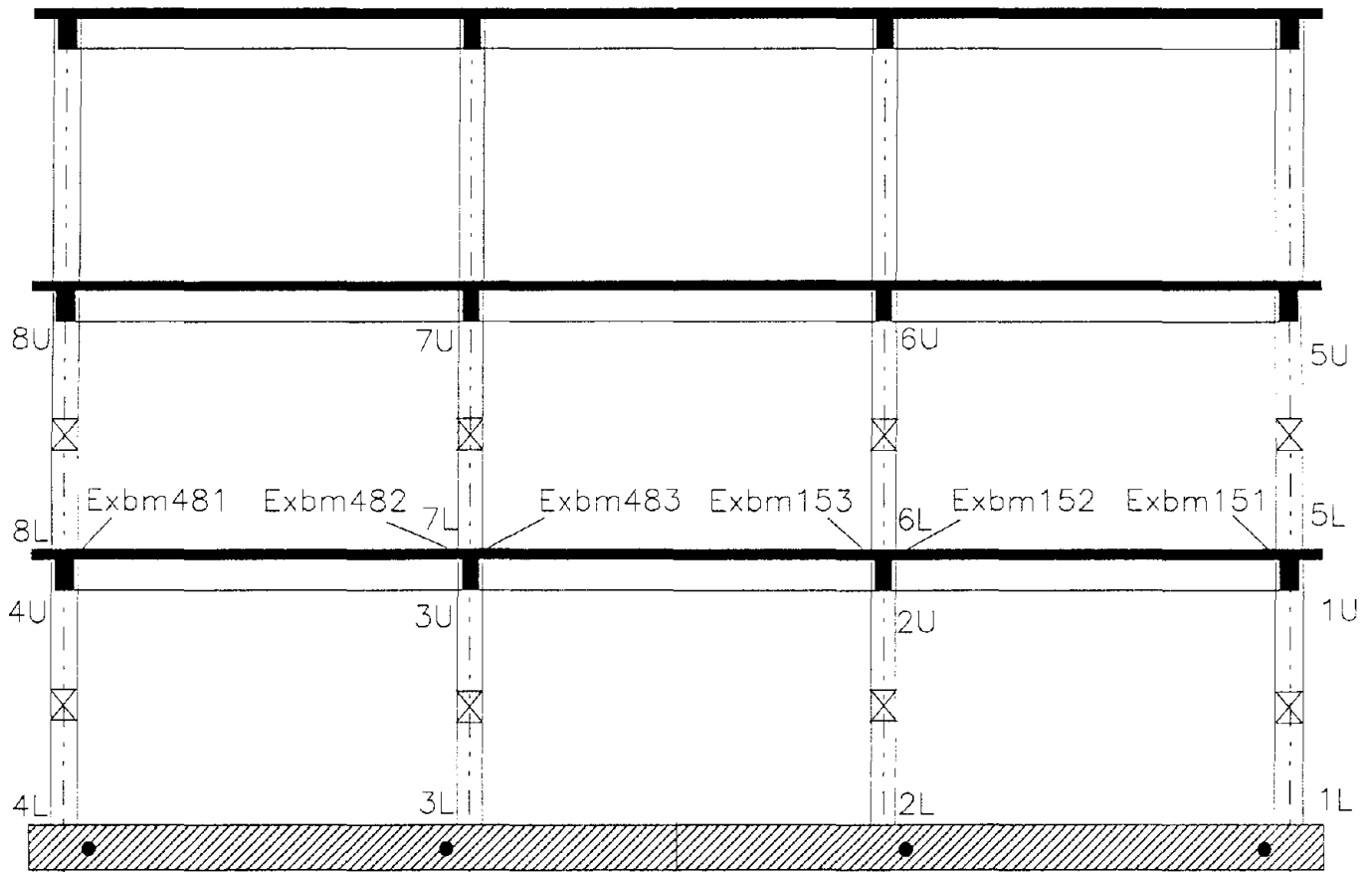
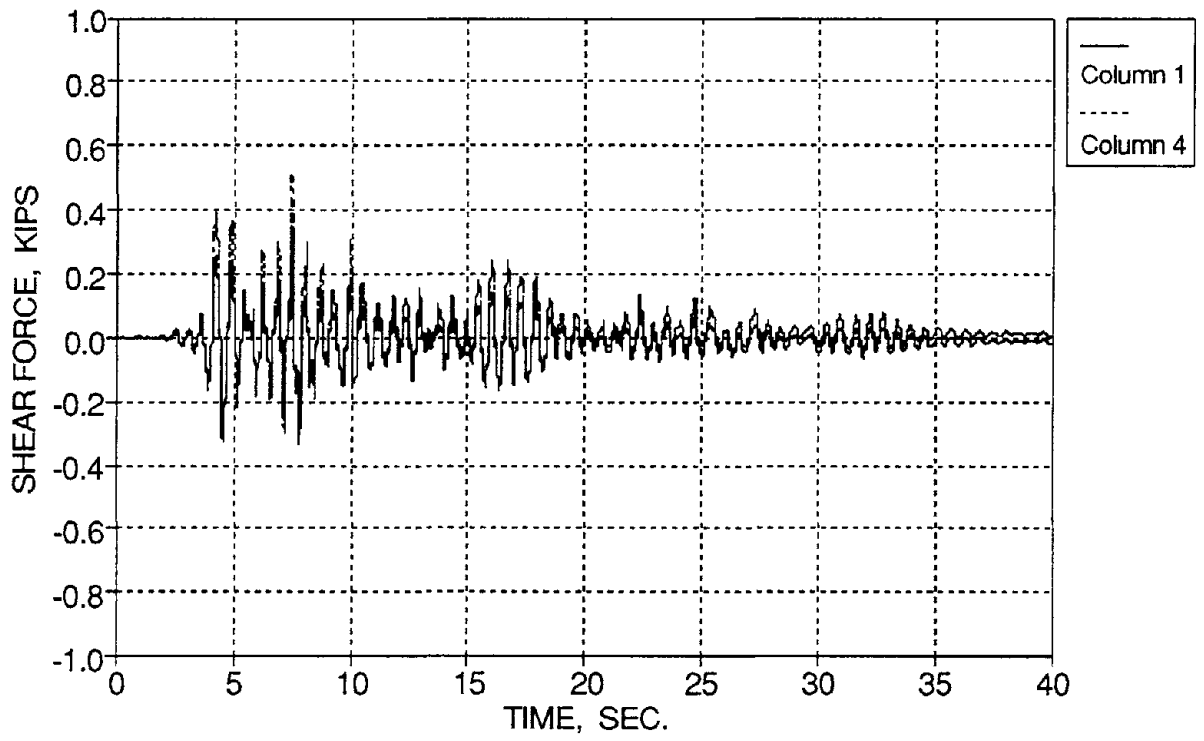
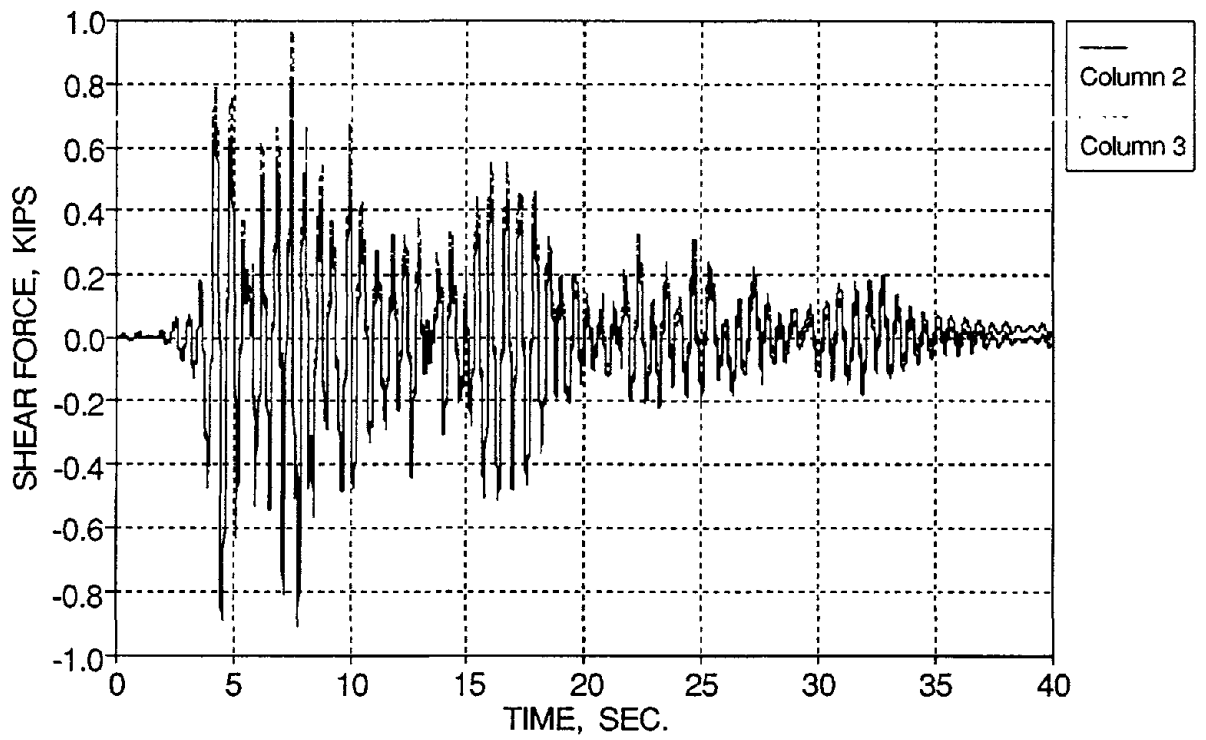


FIG. 4-21 Member Designation

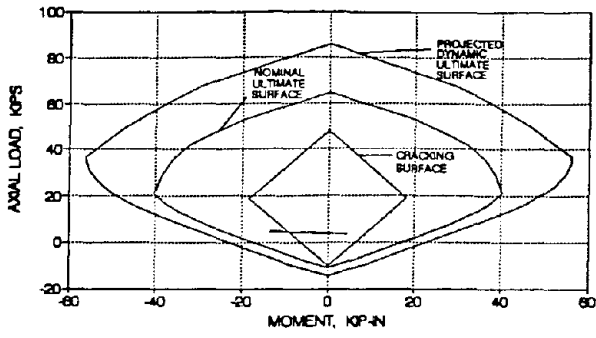


(a) Exterior Columns

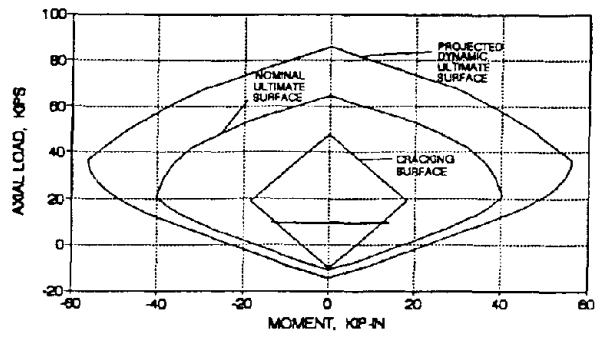


(b) Interior Columns

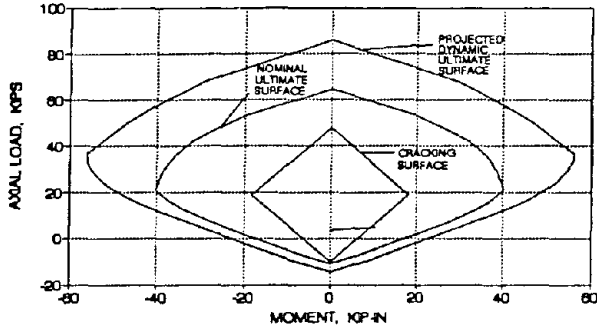
FIG. 4-22 Base Column Shear Forces for TFT_05



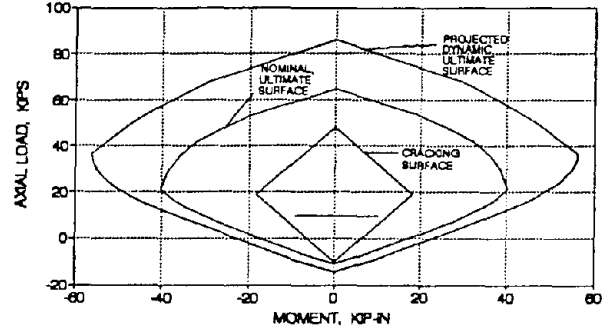
Column 8U



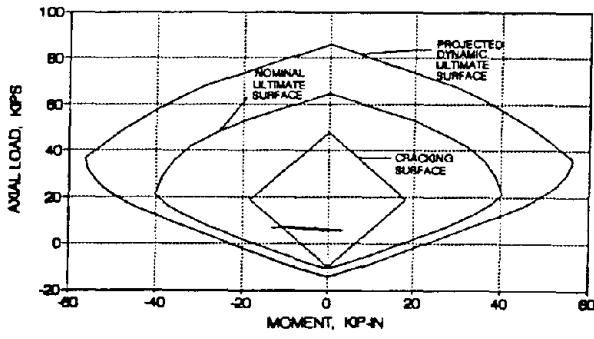
Column 7U



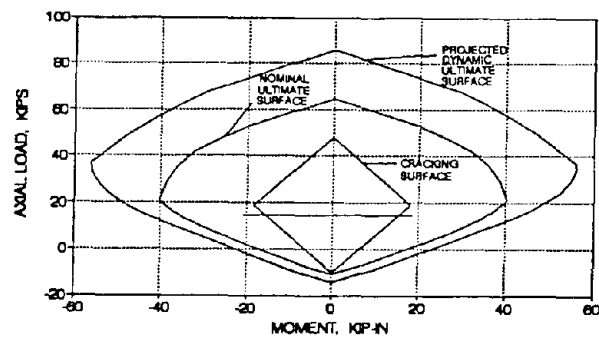
Column 8L



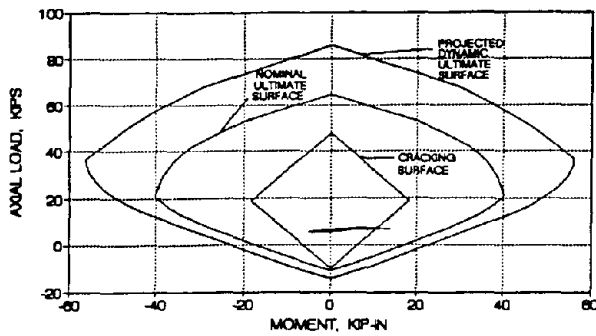
Column 7L



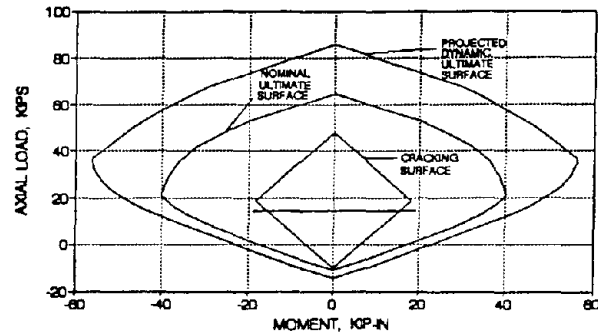
Column 4U



Column 3U

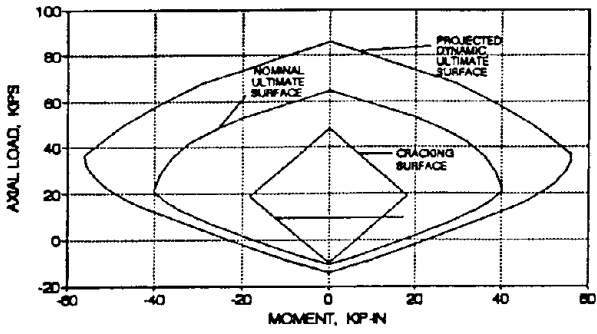


Column 4L

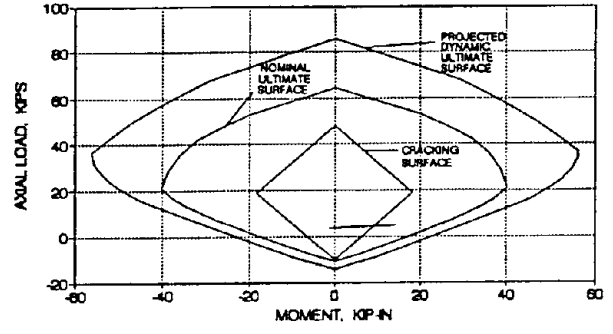


Column 3L

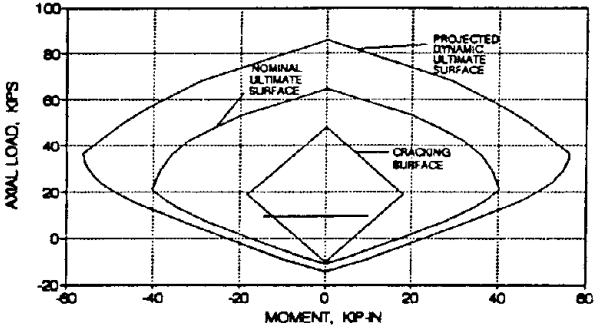
FIG. 4-23a Interaction Histories for the South-East Columns from TFT_05



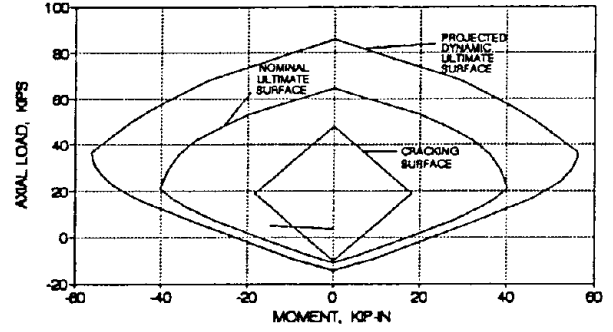
Column 6U



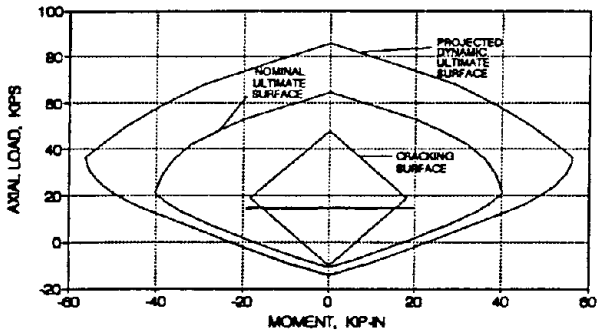
Column 5U



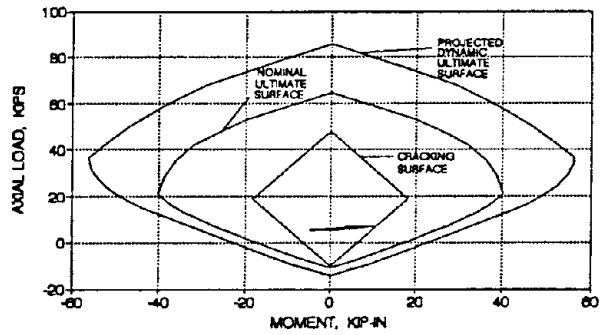
Column 6L



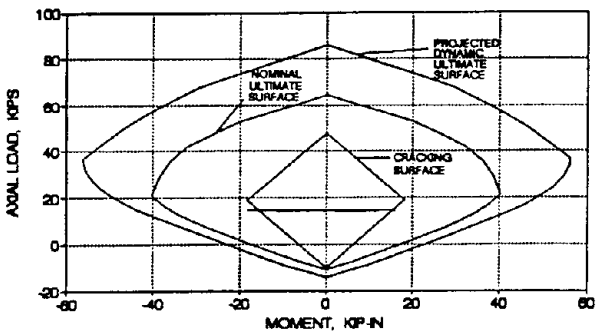
Column 5L



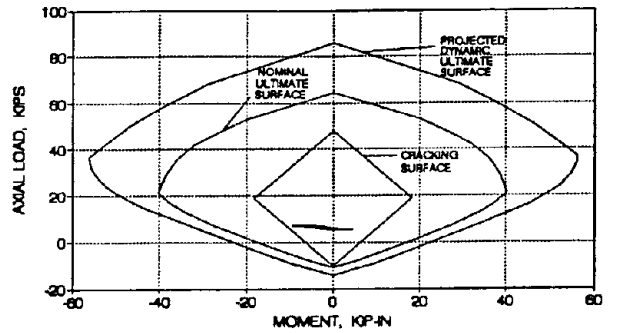
Column 2U



Column 1U

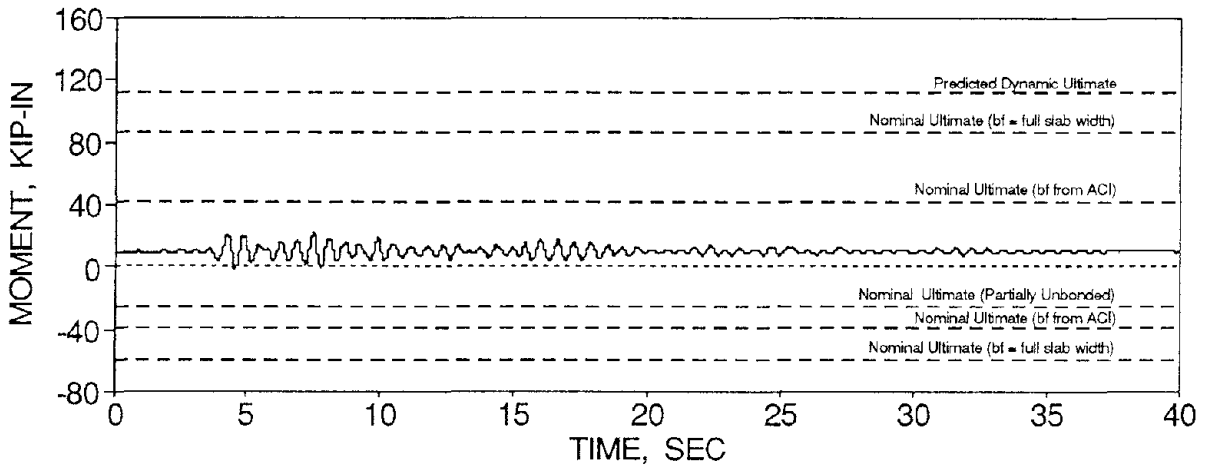


Column 2L

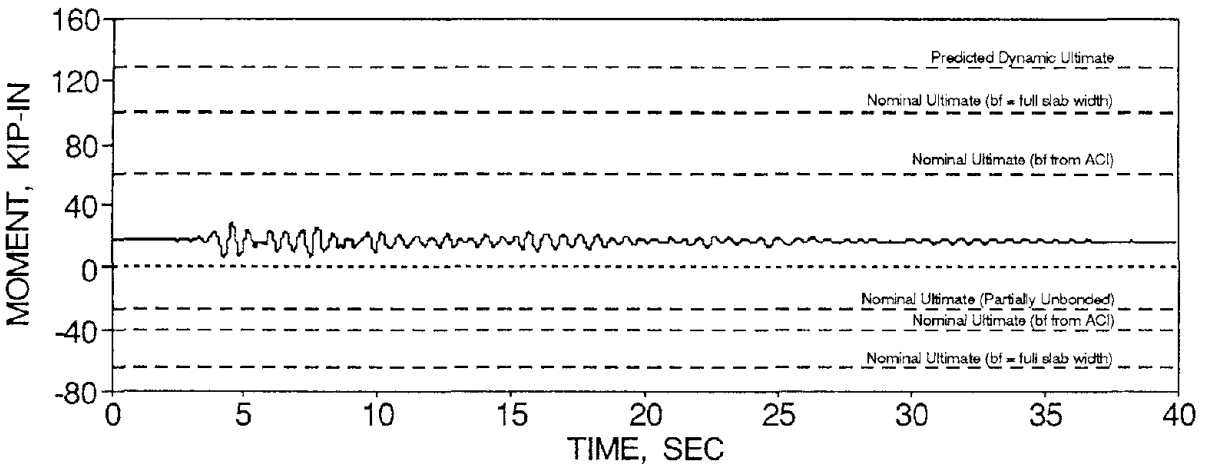


Column 1L

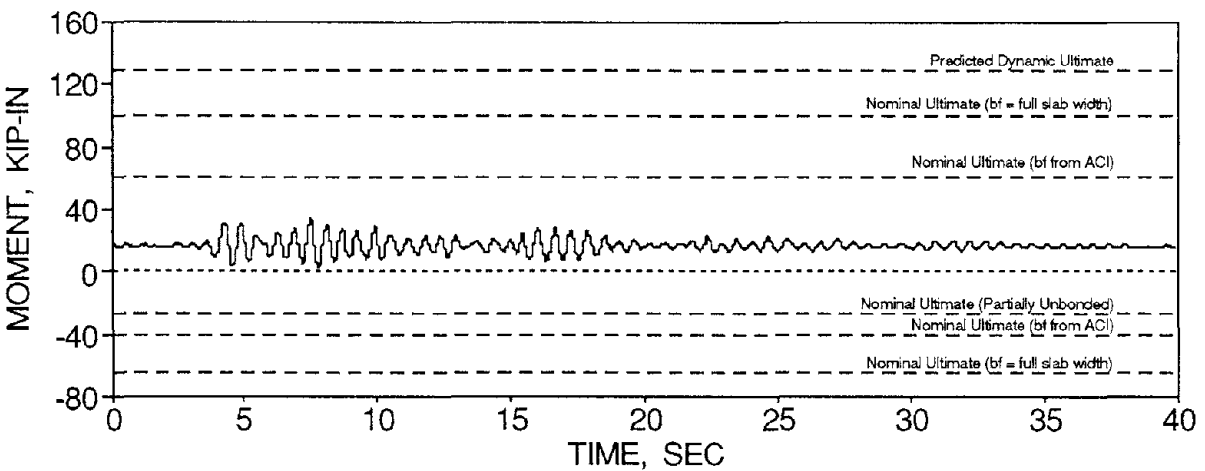
FIG. 4-23b Interaction Histories for the North-East Columns from TFT_05



(a) Exbm481

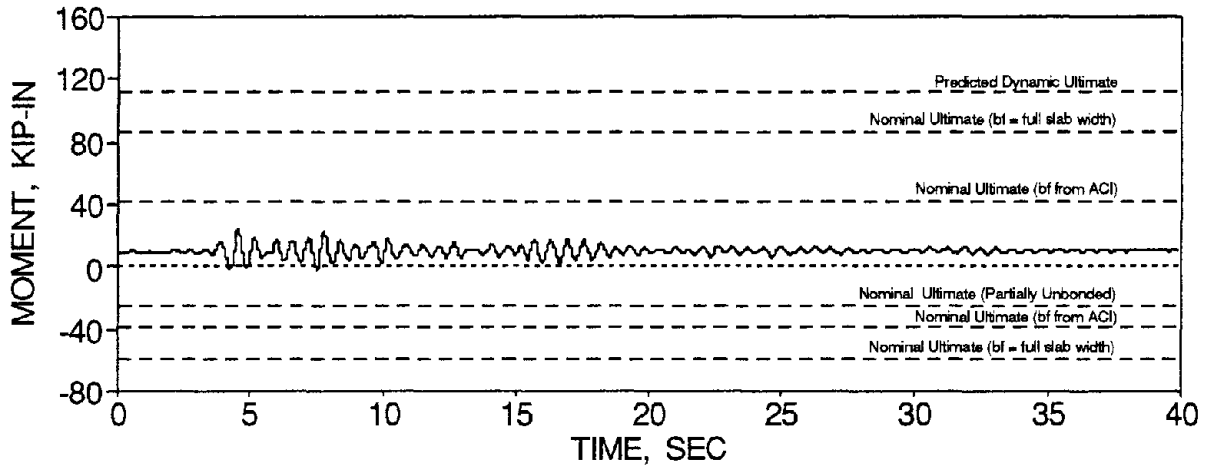


(b) Exbm482

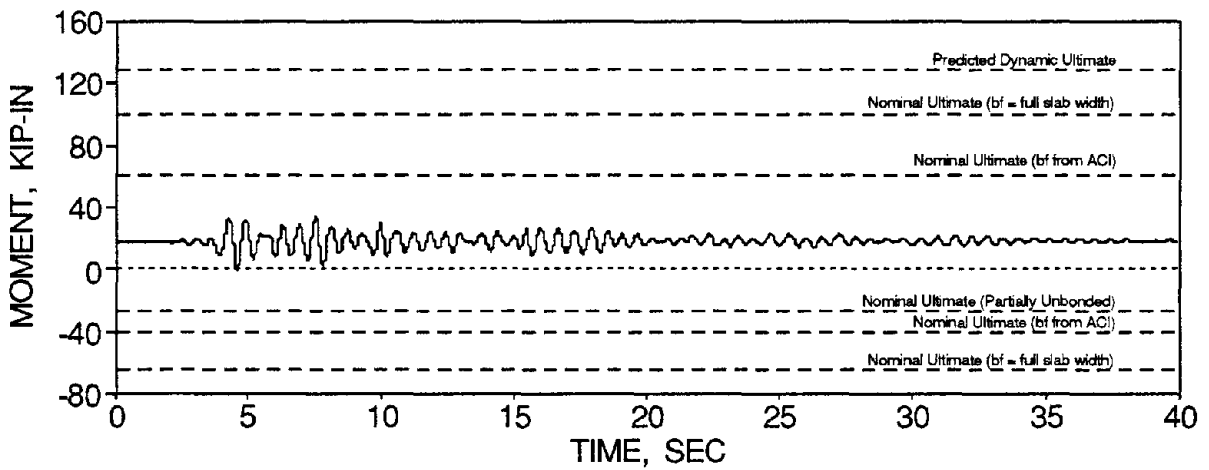


(c) Exbm483

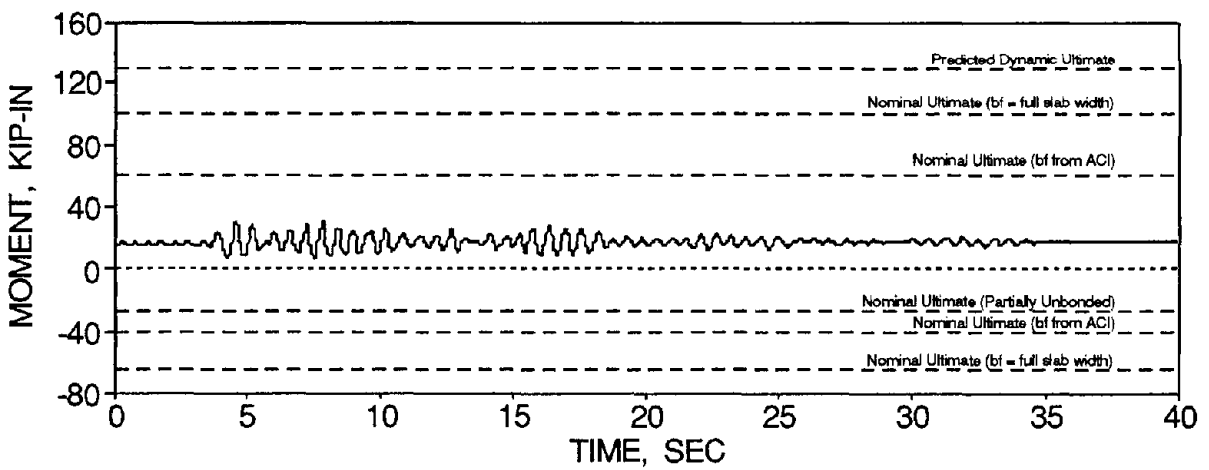
FIG 4-24a First Story Beam Bending Moment Time Histories for TFT_05 - South Side



(a) Exbm151

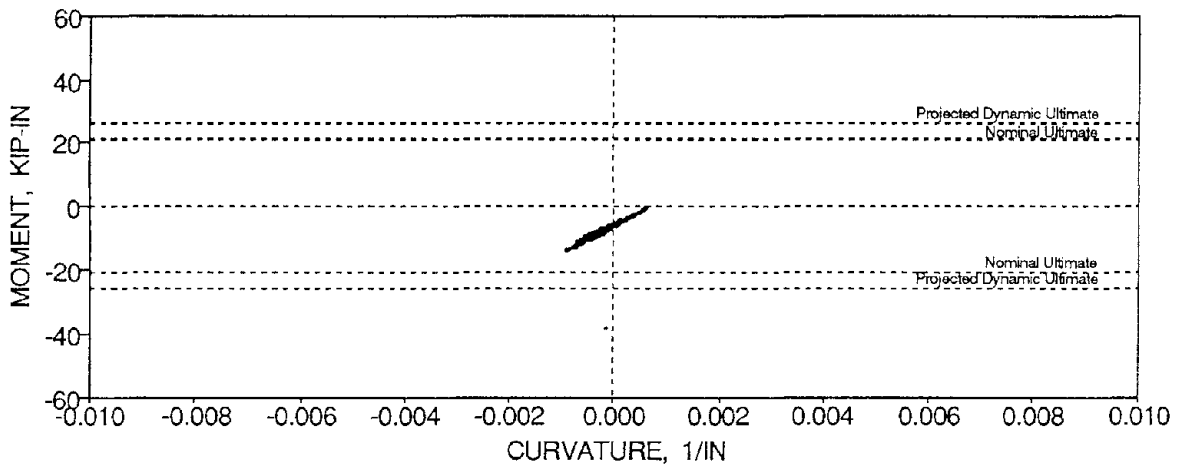


(b) Exbm152

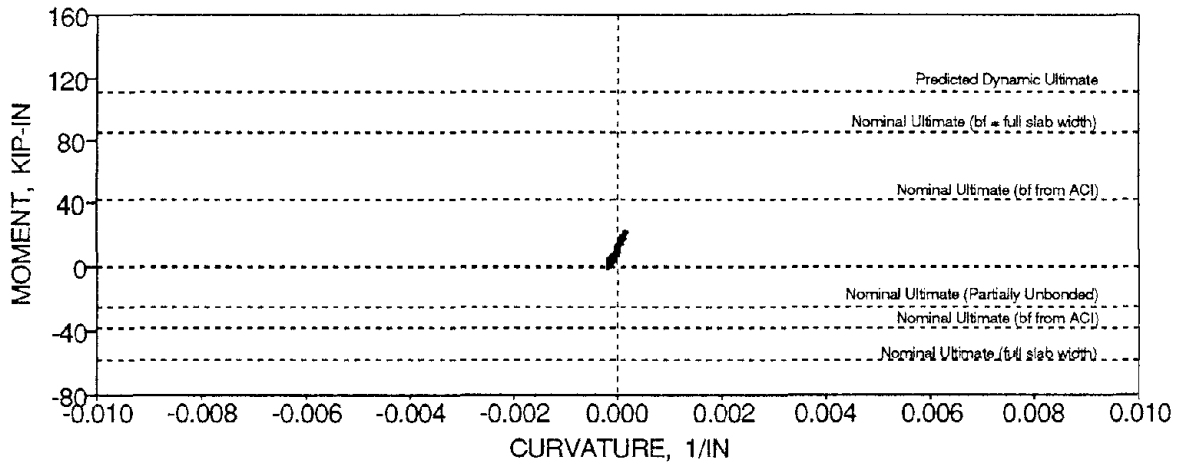


(c) Exbm153

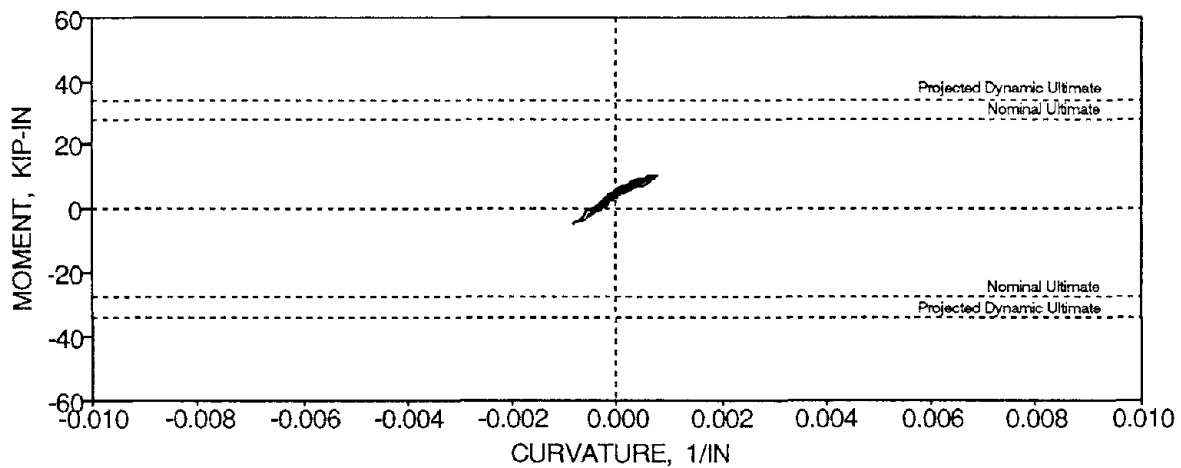
FIG 4-24b First Story Beam Bending Moment Time Histories for TFT_05 - North Side



Column 5L

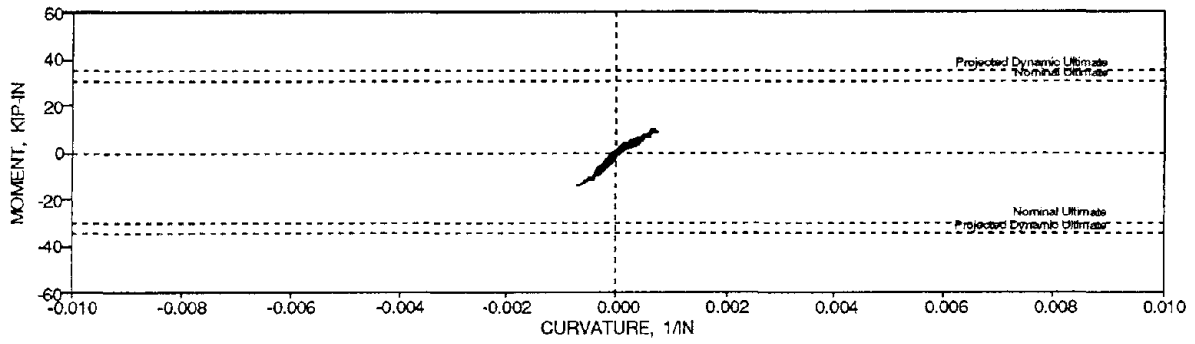


Beam Exbm151

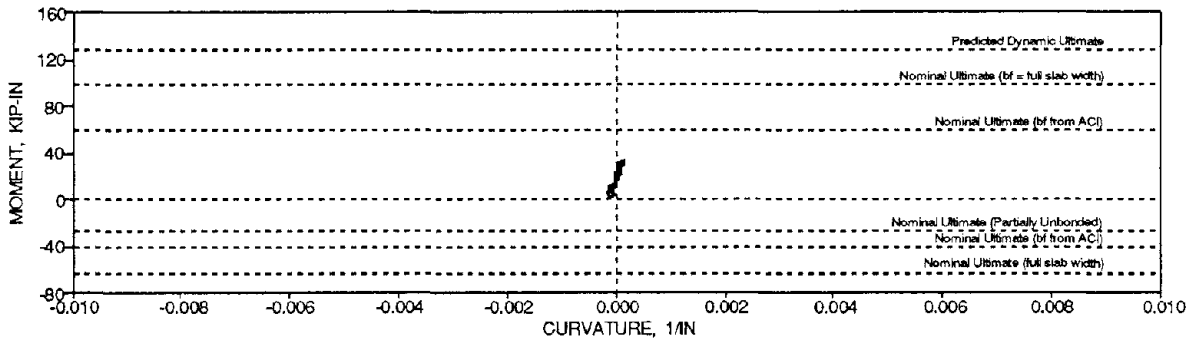


Column 1U

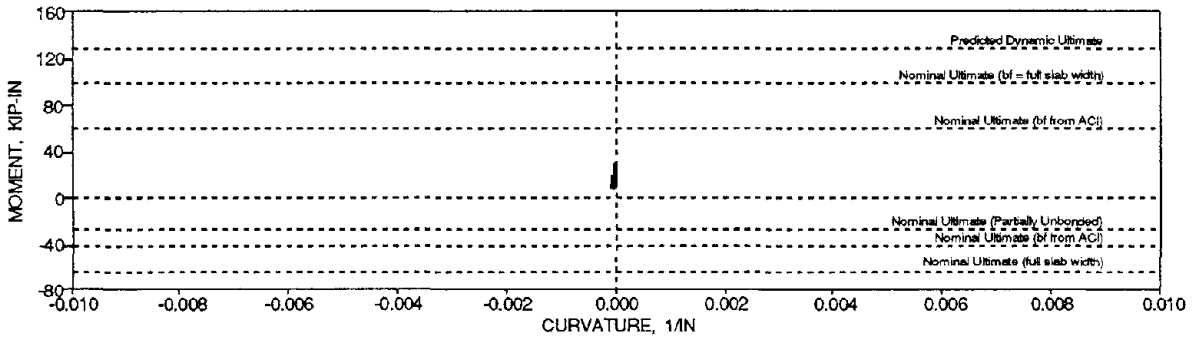
FIG. 4-25a Moment versus Curvature for TFT_05 - Exterior Joint



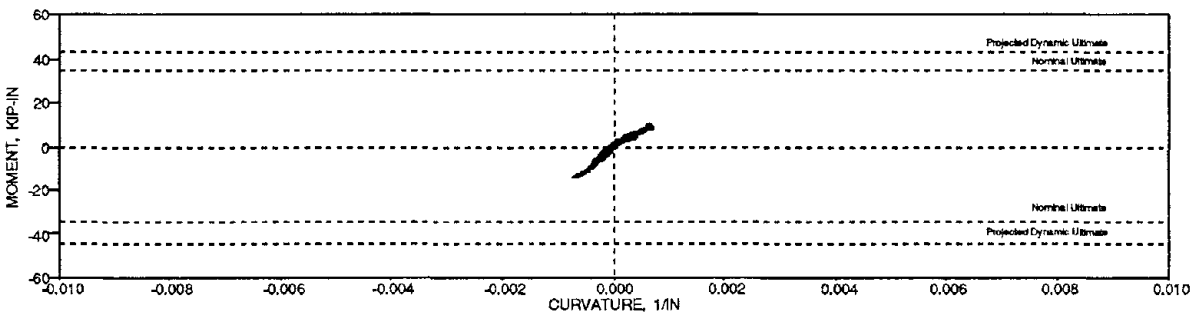
Column 6L



Beam Exbm152

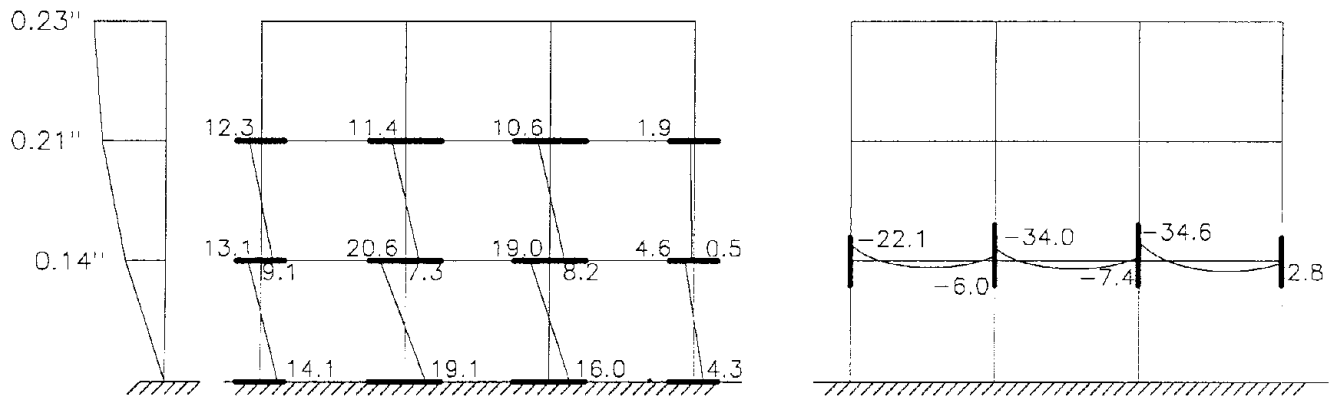


Beam Exbm153



Column 2U

FIG. 4-25b Moment versus Curvature for TFT_05 - Interior Joint

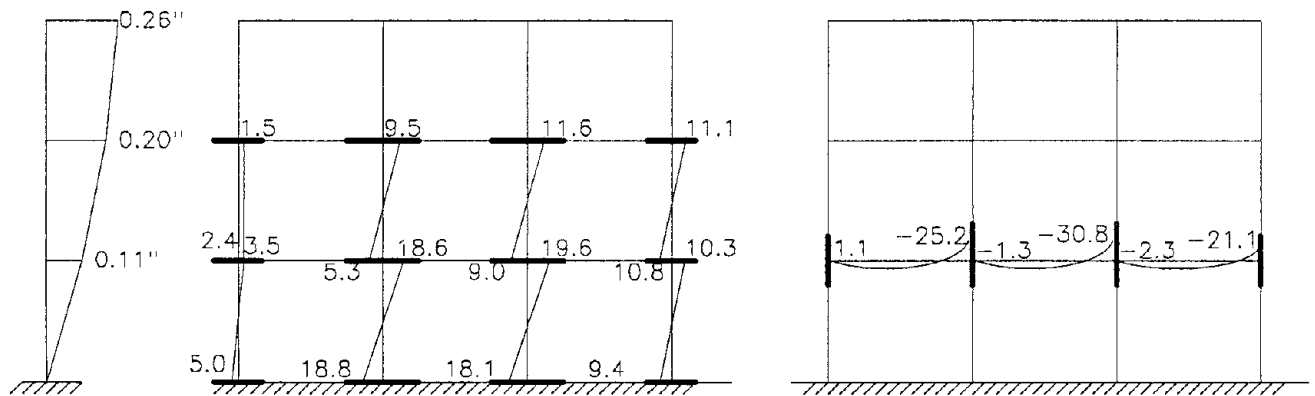
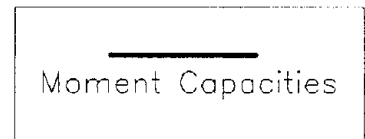


Displacements

Column Moments

Beam Moments

(a) Time = 7.50 sec.



Displacements

Column Moments

Beam Moments

(b) Time = 7.78 sec

FIG. 4-26 Moment Diagram at Maximum First Story Drift from TFT_05

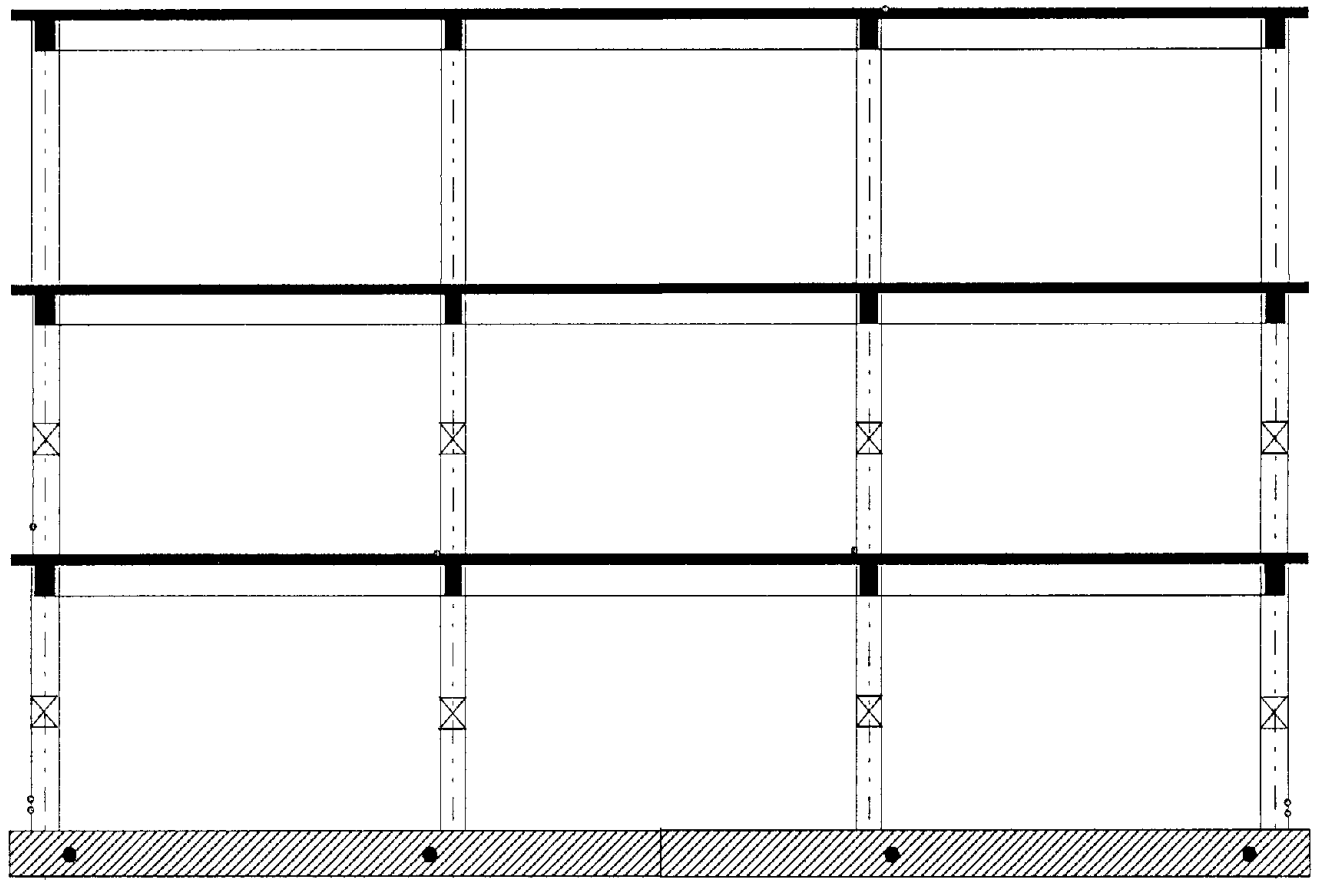
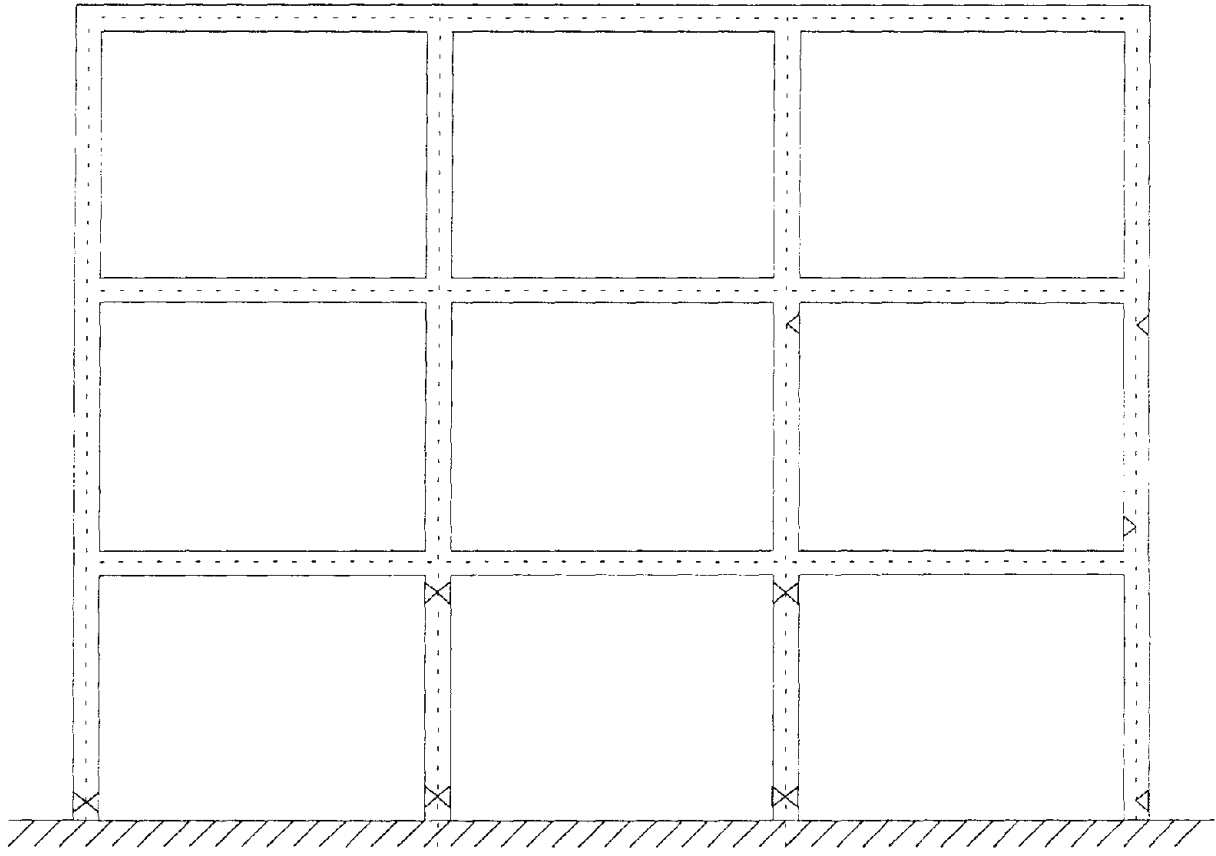


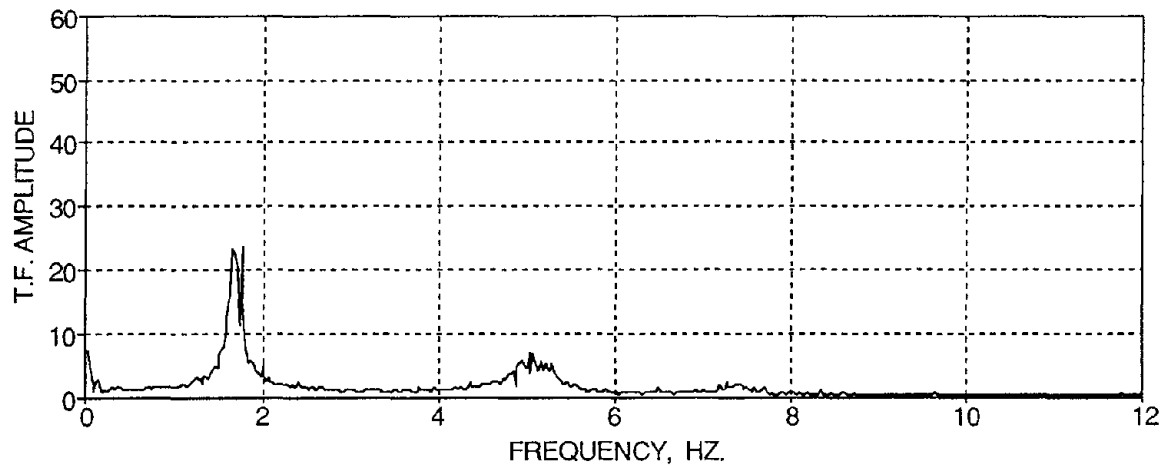
FIG. 4-27 Observed Structural Damage after TFT_05



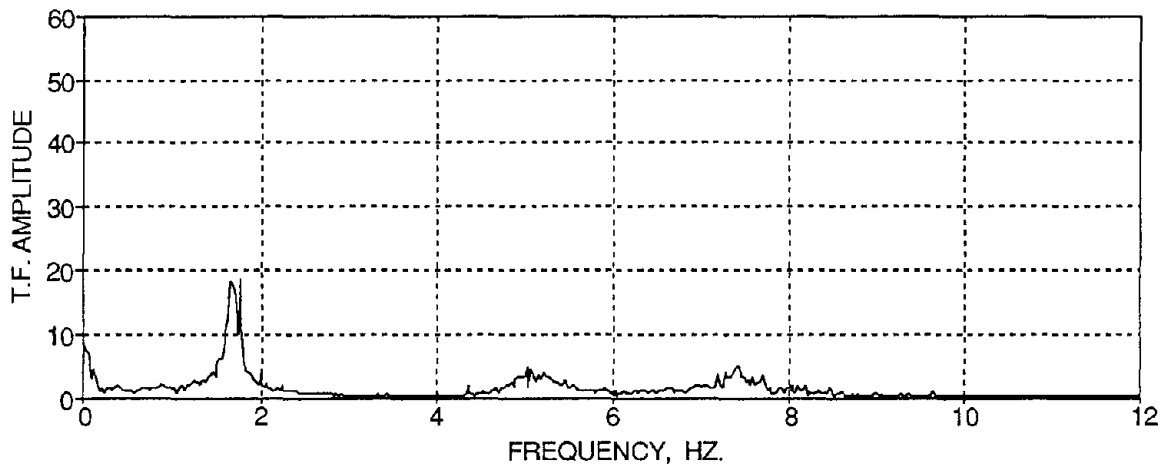
▷ Cracked
▶ Yielded

NOTE: 2nd story beams and above were not quantitatively observed

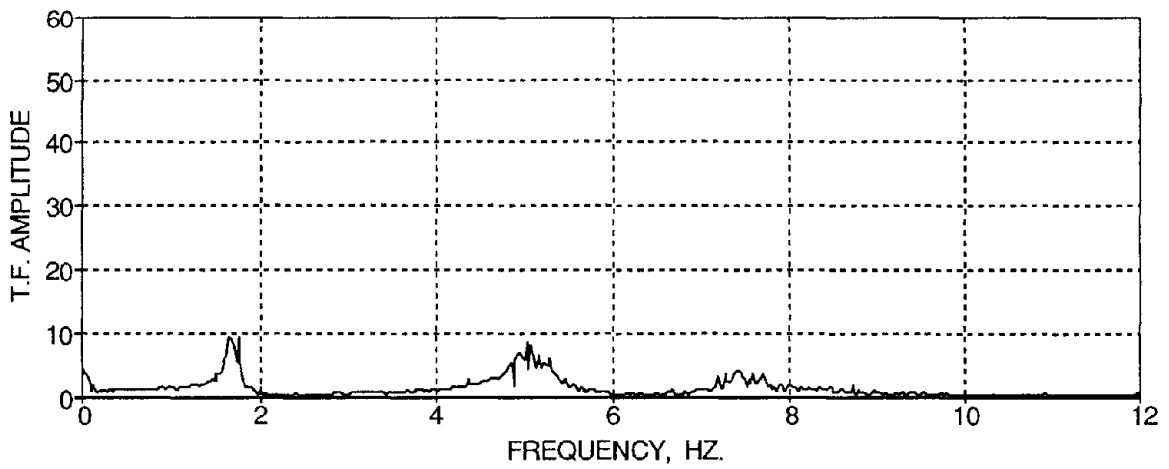
FIG. 4-28 Measured Damage State of the Model after TFT_05



(a) Third Floor

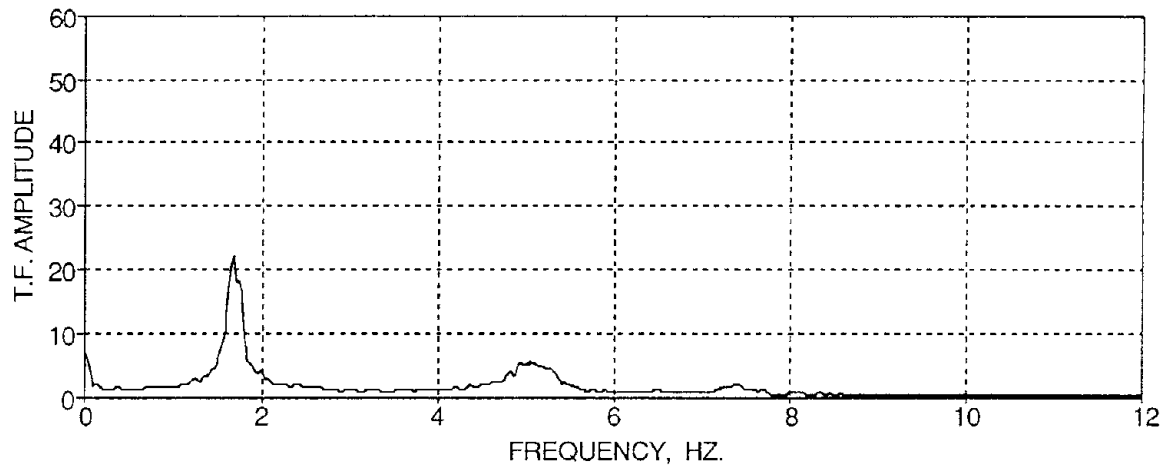


(b) Second Floor

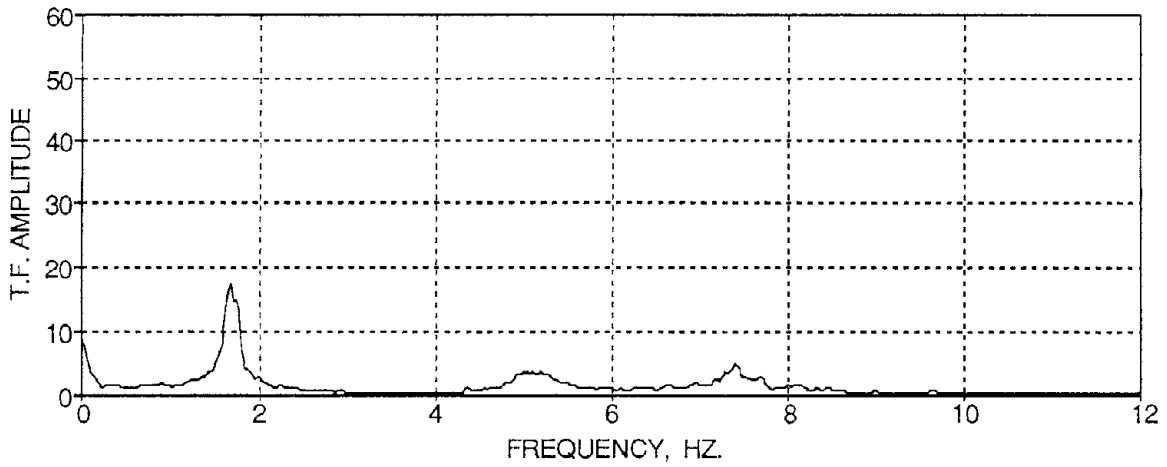


(c) First Floor

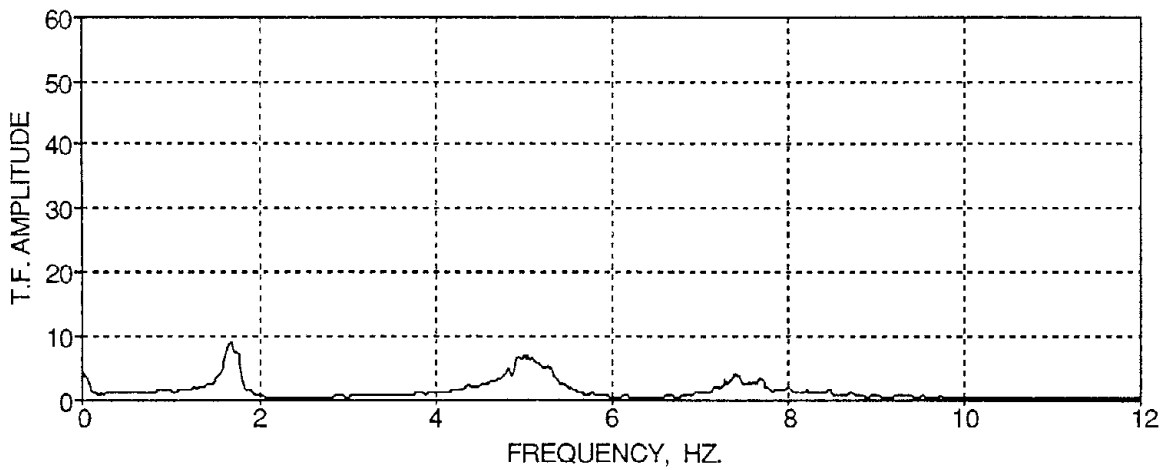
FIG. 4-29 Transfer Functions of the Story Level Accelerations from WHN_C



(a) Third Floor

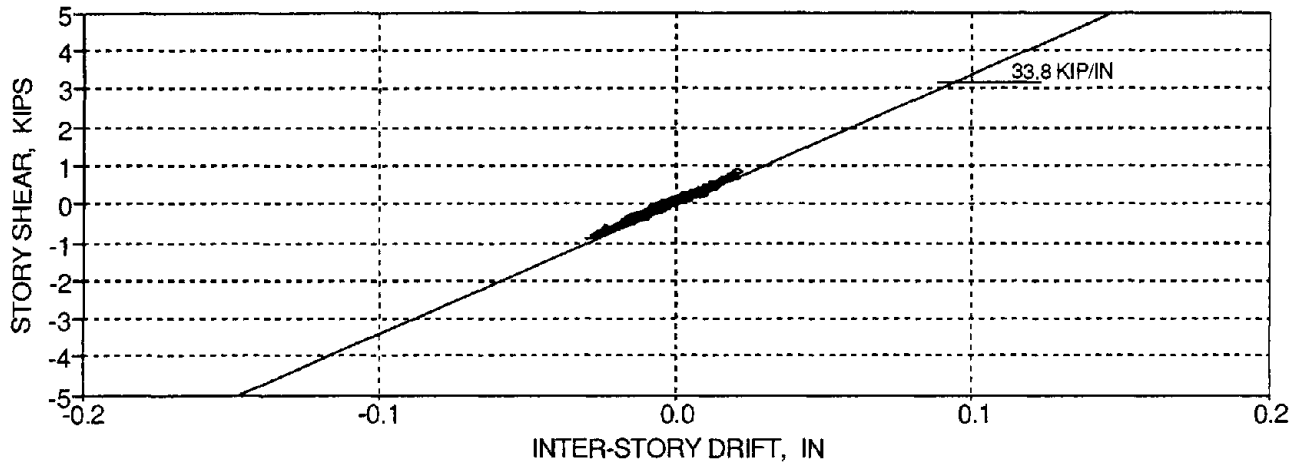


(b) Second Floor

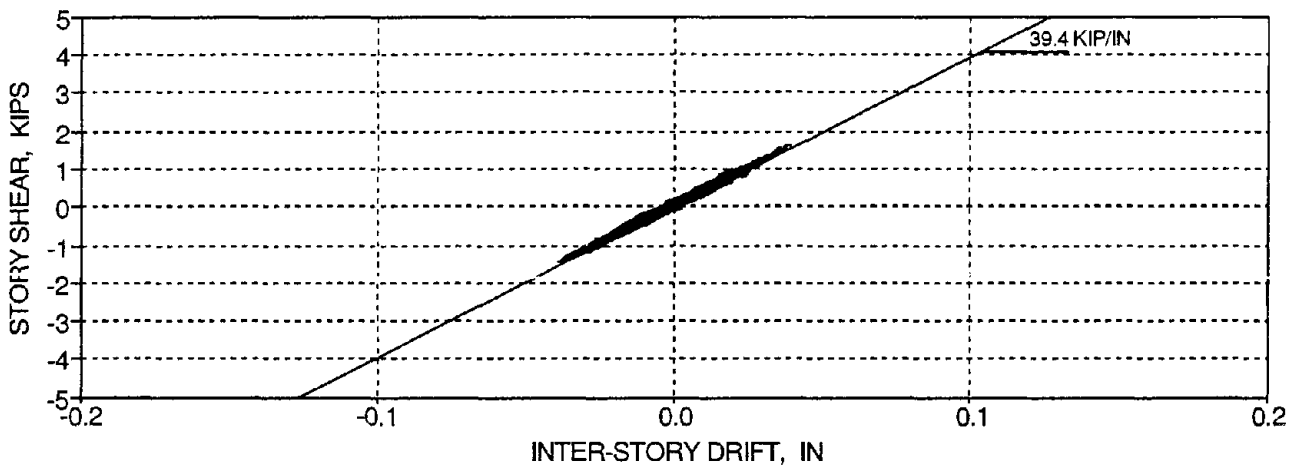


(c) First Floor

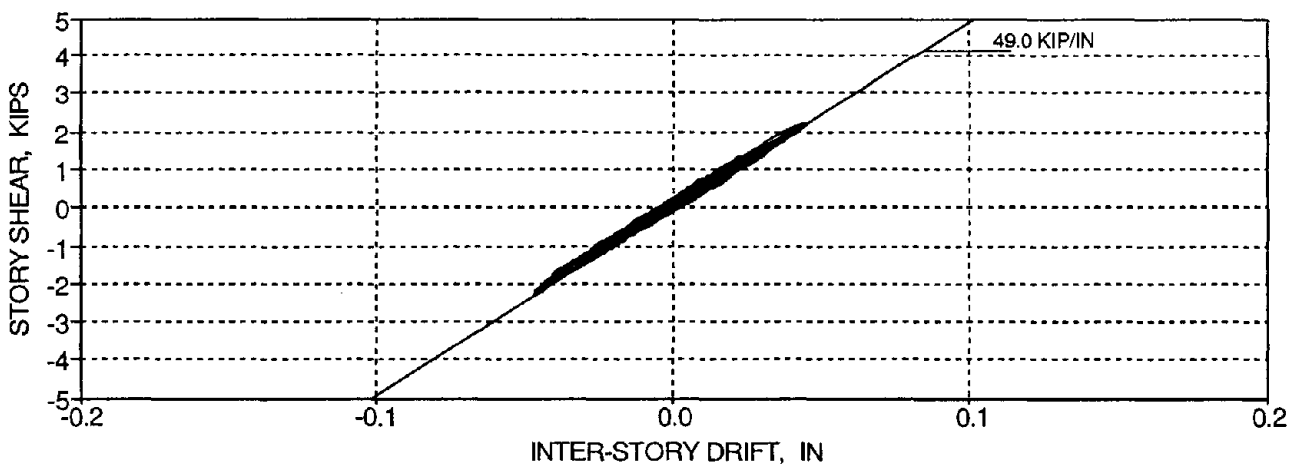
FIG. 4-30 Smoothed Transfer Functions of the Story Level Accelerations from WHN_C



(a) Third Floor

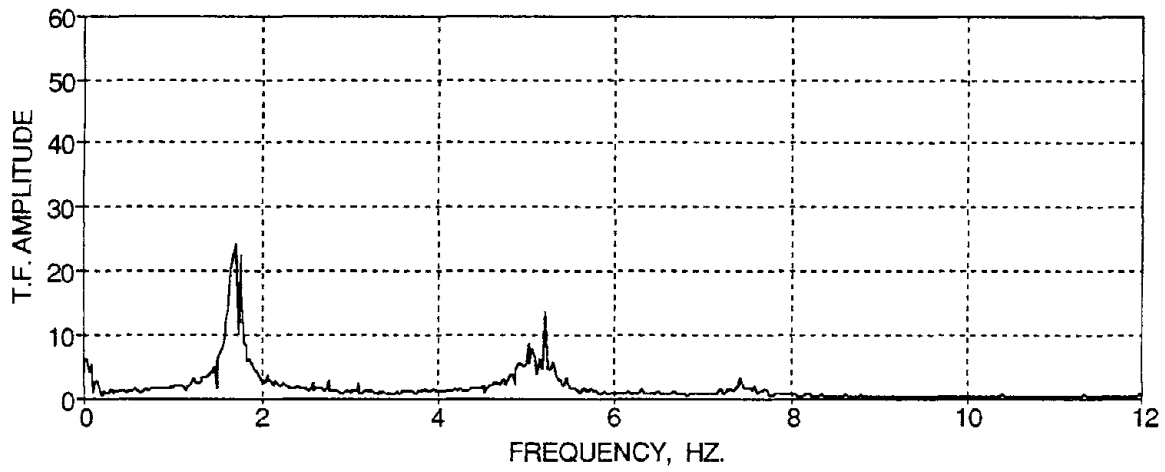


(b) Second Floor

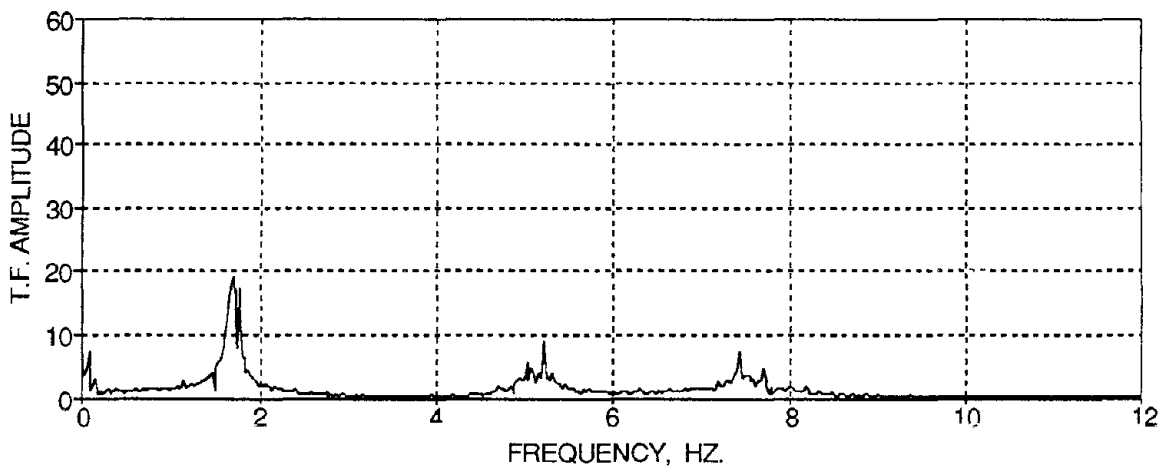


(c) First Floor

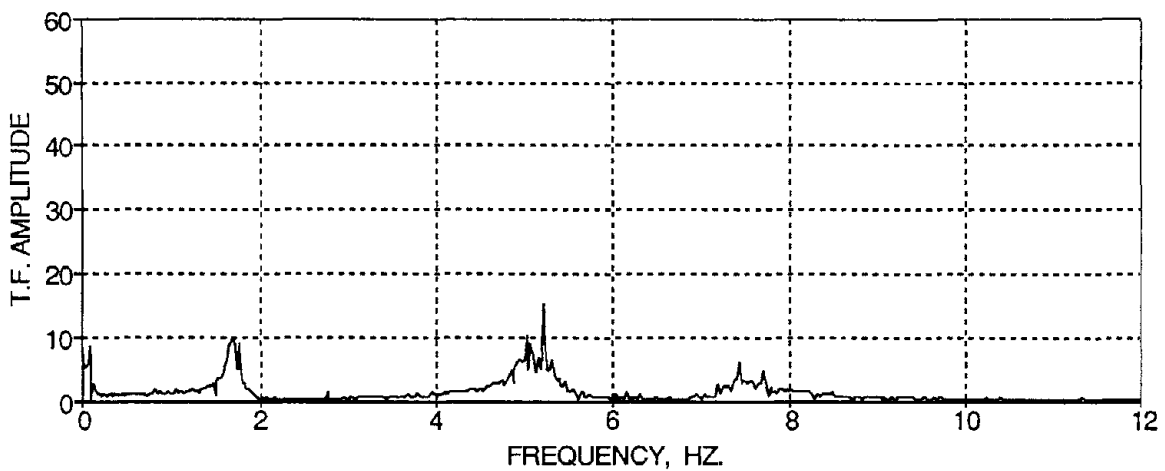
FIG 4-31 Story Shear versus Inter-Story Drift Histories for WHN_C



(a) Third Floor

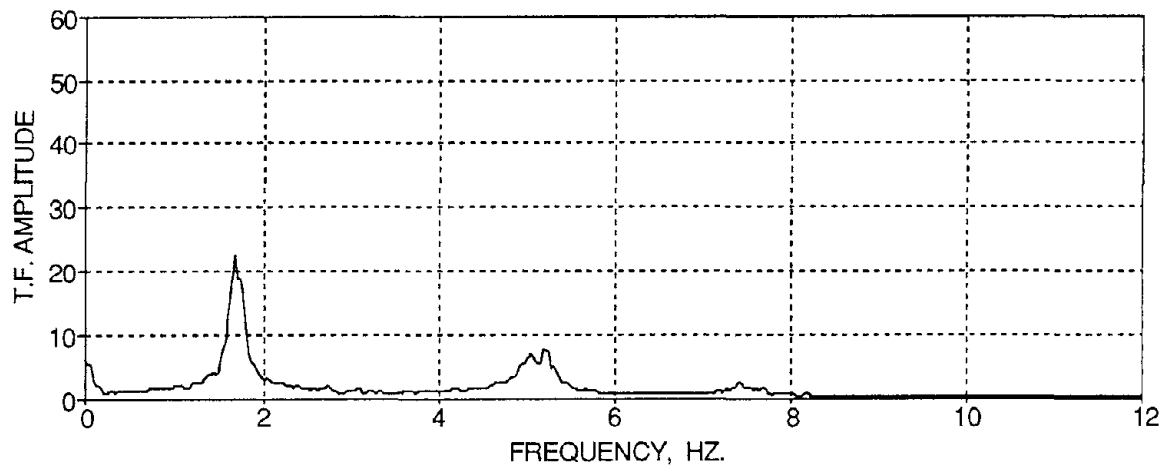


(b) Second Floor

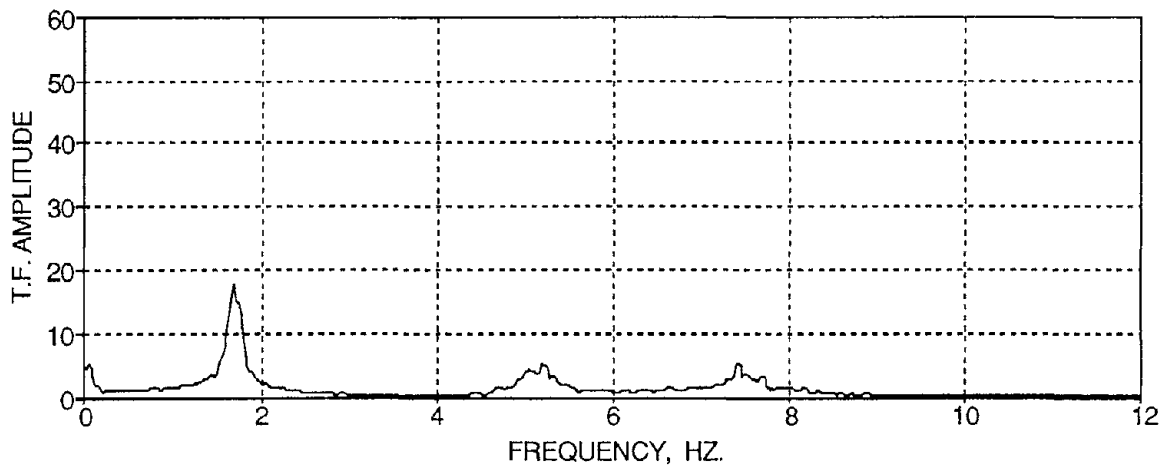


(c) First Floor

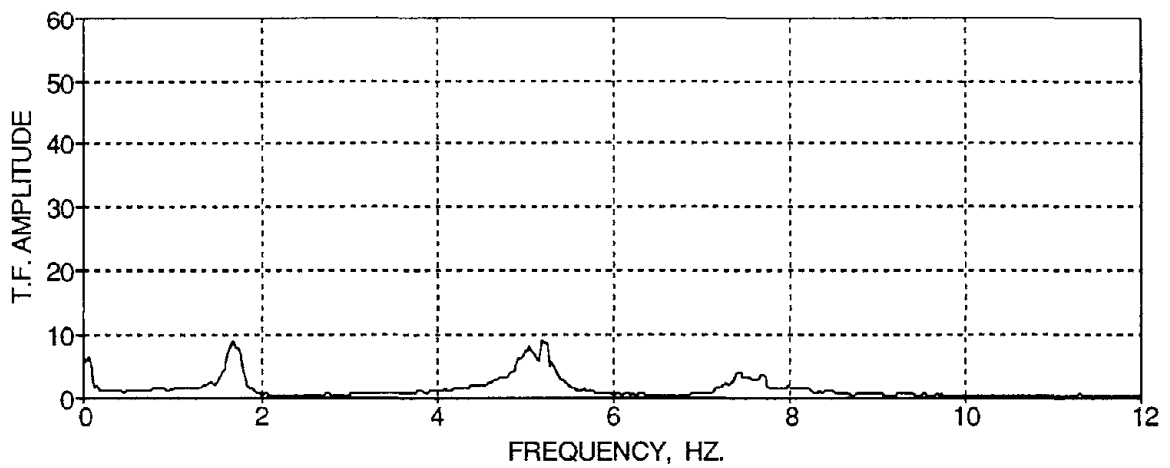
FIG. 4-32 Transfer Functions of the Story Level Accelerations from WHN_D



(a) Third Floor

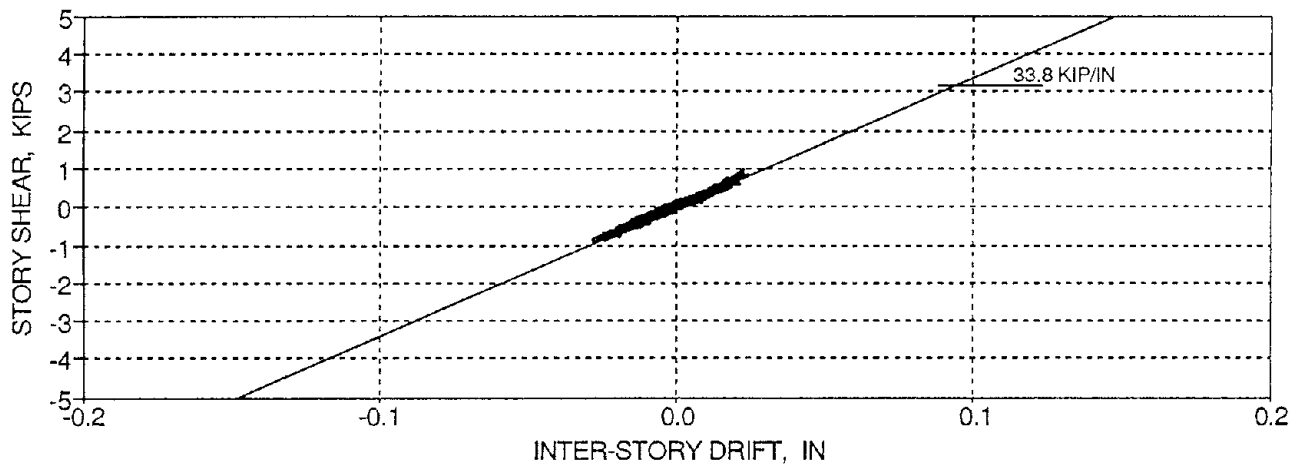


(b) Second Floor

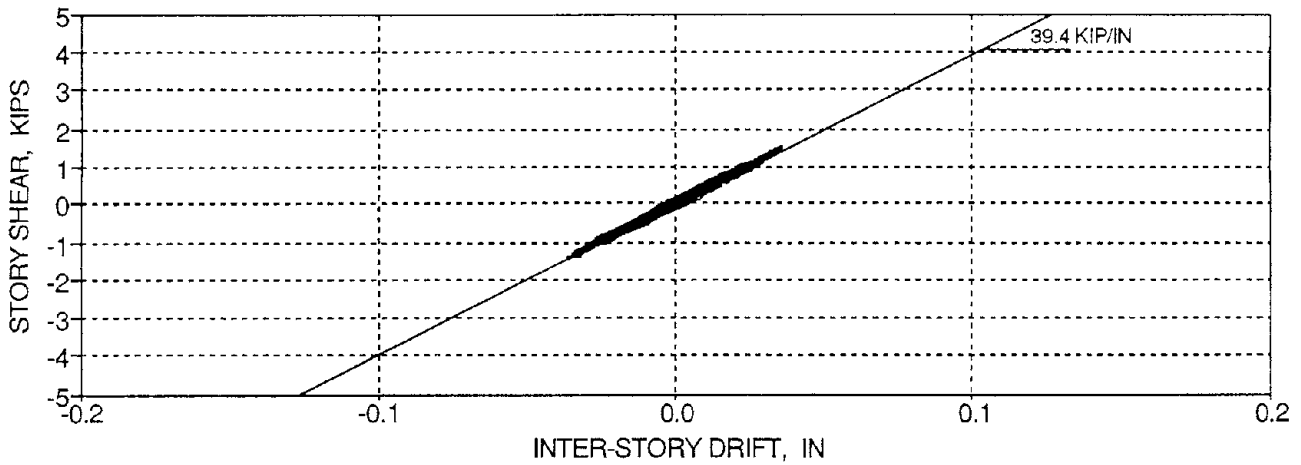


(c) First Floor

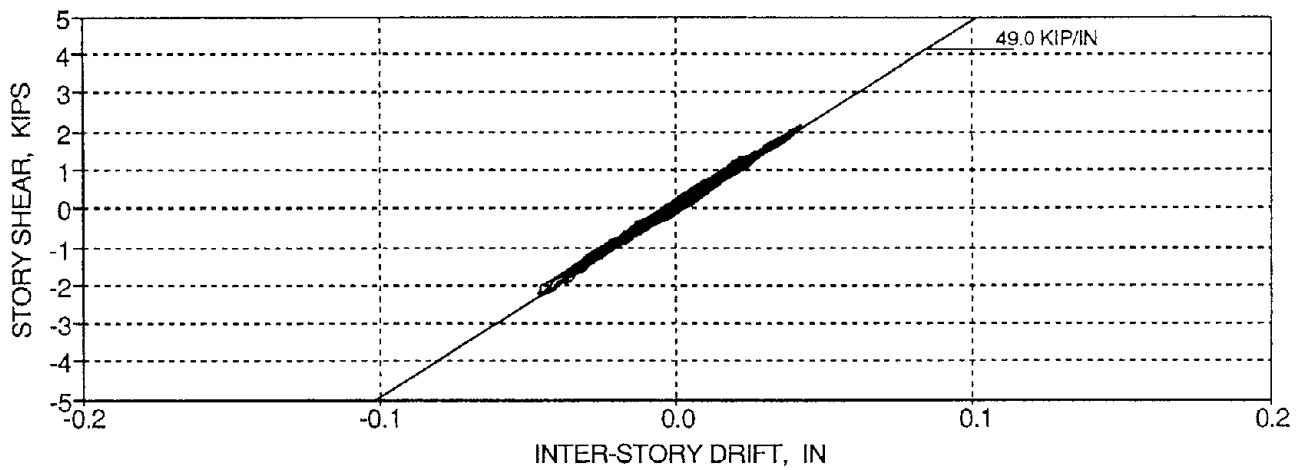
FIG. 4-33 Smoothed Transfer Functions of the Story Level Accelerations from WHN_D



(a) Third Floor



(b) Second Floor



(c) First Floor

FIG 4-34 Story Shear versus Inter-Story Drift Histories for WHN_D

4.7 Summary Discussions

The identification of the initial dynamic characteristics of the undamaged model was presented according to the testing program outlined in Section 3. Tables 4-2 and 4-3 summarize the initial characteristics of the unloaded and loaded model, respectively. It was shown that the white noise excitations provide good correlation with the other tests and will be used throughout the testing for updating the dynamic characteristics.

The global and local response of the model excited by the minor earthquake (Taft N21E, PGA 0.05 g) was presented. It was shown that the behavior of the model was governed by elastic deformations. However cracking was observed in some of the columns. The concluding white noise identification test showed that only slight deterioration in natural frequencies and story stiffnesses resulted from the minor base motion. Therefore it can be concluded that the inherent lateral strength of the LRC model was sufficient to resist the seismic forces of the minor earthquake.

The analytical identifications show that the model has microcracks and that the member stiffnesses are smaller than calculated by assuming uncracked sections. The initial "undamaged" stiffness reduction is almost 45.0% and additional deterioration occurs during minor shaking.

SECTION 5

CONCLUSIONS

The preliminary identifications of dynamic response of a model of a typical lightly reinforced concrete structure was presented.

The design of a prototype three-story moment resisting reinforced concrete frame building typically constructed in low seismicity zones was presented here in and was based on the design load combination of $1.4D + 1.7L$ (gravity load design). Since earthquake loads are neglected in such zones and wind loads on a three-story structure are relatively small after design loading combinations, no lateral loads were considered for the design. The detailing of the structure was in accordance with the general non-seismic provisions of the ACI-318-89 code.

Based on this prototype building, a one-third scale model was designed as shown in this report and constructed at the State University of New York at Buffalo Earthquake Simulation Laboratory. The similitude conditions to model the dynamic behavior of the prototype building were satisfied. The location and purpose of the instrumentation to measure the critical response of the model building during shaking table testing was also identified.

The testing program for identification of the initial dynamic characteristics of the model building was presented. In compliance with this program, a comparison of the achieved dynamic characteristics from different identification tests was also presented. It was shown that the white noise shaking table tests provided a justifiable correlation with the other identification tests and will be used throughout the testing of the model building for updating the dynamic characteristics before and after each simulated earthquake motion.

The analytical identifications showed that the model has microcracks and that the member stiffnesses are smaller than calculated by assuming gross section properties and greater than the fully cracked section properties. The initial "undamaged" stiffnesses were identified to be between 50% and 60% of the uncracked section.

The complete shaking table testing program for the model building was presented along with the ground motions and intensities used for the earthquake simulations. The varying intensities of the ground motions were used to simulate minor, moderate, and severe earthquakes. The global and local response of the model building during the minor earthquake was presented in this report. It was shown that the response of the model was primarily governed by elastic deformations. However some slight cracking was observed in some of the columns. The concluding white noise identification test showed that only slight deteriorations in natural frequencies and story stiffnesses resulted from the minor base motion. Therefore it was concluded that although the gravity load designed buildings are not designed for lateral forces, the inherent lateral strength and flexibility of such buildings are sufficient to resist the forces of minor earthquakes without visible damage. The response of the model building during the moderate and severe earthquakes is presented in Part III of the Evaluation report series (Bracci et al., 1992a).

SECTION 6

REFERENCES

- Abrams, D. (1987). "Influence of Axial Force Variations of Flexural Behavior of Reinforced Concrete Columns", *ACI Structural Journal*, Vol. 84, No. 3, May-June.
- ACI Committee 318 (1989). "Building Code Requirements for Reinforced Concrete (ACI 318-89)", ACI, Detroit.
- Al-Haddad, M.S. and Wight, J.K. (1986). "Feasibility and Consequences of Moving Beam Plastic Hinging Zones for Earthquake Resistant Design of R/C Buildings", University of Michigan/Ann Arbor, Report No. UMCE 86-1.
- Al-Nahlawi, M.K.A. and Wight, J.K. (1989). "An Experimental and Analytical Study of Shear Strength of Lightly Reinforced Concrete Beams", University of Michigan/Ann Arbor, Report No. UMCE 89-7.
- Aycardi, L.E., Mander, J.B., and Reinhorn, A.M. (1992). "Seismic Resistance of Reinforced Concrete Frame Structures Designed only for Gravity Loads in Low Seismicity Zones: Part II - Experimental Performance of Subassemblages", Technical Report NCEER-92-0028, National Center for Earthquake Engineering Research, SUNY/Buffalo.
- Azizinamini, A., Corley, W.G., and Johal, L.S.P. (1992). "Effects of Transverse Reinforcement on Seismic Performance of Columns", *ACI Structural Journal*, Vol. 89, No. 4, July-August, 442-450.
- Bertero, V.V., Aktan, A.E., Charney, F.A., and Sause, R. (1984). "U.S. - Japan Cooperative Earthquake Research Program: Earthquake Simulation Tests and Associated Studies of a 1/5th-Scale Model of a 7-Story Reinforced Concrete Test Structure", Earthquake Engineering Research Center, University of California/Berkeley, California, Report No. UCB/EERC-84/05.
- Blondet, J.M., Clough, R.W., and Mahin, S.A. (1980). "Evaluation of A Shaking Table Test Program on Response Behavior of A Two Story Reinforced Concrete Frame", Earthquake Engineering Research Center, University of California/Berkeley, California, Report No. UCB/EERC-80/42.
- Bracci, J.M., Reinhorn, A.M., and Mander, J.B. (1992a). "Seismic Resistance of Reinforced Concrete Frame Structures Designed only for Gravity Loads in Low Seismicity Zones: Part III - Seismic Performance and Analytical Modeling of Structural Model", Technical Report NCEER-92-0029, National Center for Earthquake Engineering Research, SUNY/Buffalo.
- Bracci, J.M., Reinhorn, A.M., and Mander, J.B. (1992b). "Evaluation of Seismic Retrofit of Reinforced Concrete Frame Structures: Part II - Analytical and Experimental Performance of Retrofitted Model Structure", Technical Report NCEER-92-0031, National Center for Earthquake Engineering Research, SUNY/Buffalo.
- Buchanan, A.H. (1979). "Diagonal Beam Reinforcing for Ductile Frames", *Bulletin of the New Zealand National Society for Earthquake Engineering*, Vol. 12, No. 4, December, 346-356.
- Choudhuri, D., Mander, J.B., and Reinhorn, A.M. (1992). "Evaluation of Seismic Retrofit of Reinforced Concrete Frame Structures: Part I - Experimental Performance of Retrofitted Subassemblages", Technical Report NCEER-92-0030, National Center for Earthquake Engineering Research, SUNY/Buffalo.
- Clough, R.W. and Penzien, J. (1975). *Dynamics of Structures*, McGraw-Hill, Inc., New York.

- Craig, R.R. (1981). *Structural Dynamics*, John Wiley and Sons, Inc., New York.
- Durrani, A. and Wight, J.K. (1987). "Earthquake Resistance of Reinforced Concrete Interior Connections Including a Floor Slab", *ACI Structural Journal*, Vol. 84, No. 4, September-October, 400-406.
- El-Attar, A.G., White, R.N., and Gergely, P. (1991a). "Shaking Table Test of a 1/6 Scale Two-Story Lightly Reinforced Concrete Building", Technical Report NCEER-91-0017, National Center for Earthquake Engineering Research, SUNY/Buffalo.
- El-Attar, A.G., White, R.N., and Gergely, P. (1991b). "Shaking Table Test of a 1/8 Scale Three-Story Lightly Reinforced Concrete Building", Technical Report NCEER-91-0018, National Center for Earthquake Engineering Research, SUNY/Buffalo.
- Hoffmann, G.W. (1992). "Gravity-Load-Designed R/C Buildings", MS Thesis, State University of New York at Buffalo.
- Jacobs, K.H. (1990). "Earthquakes - Not Just California's Problem", Outline of Presentation for Session LC 207 of the RIMS Seminar, April 29, 1990, Boston, MA.
- Kunnath, S.K., Reinhorn, A.M., and Park, Y.J. (1990). "Analytical Modeling of Inelastic Seismic Response of R/C Structures", *Journal of Structural Engineering*, ASCE, Vol. 116, No. 4, April, 996-1017.
- Lao, Larry F. (1990). "The Effect of Detailing on the Seismic Performance of Gravity Load Dominated Reinforced Concrete Frames", MS Thesis, State University of New York at Buffalo.
- Mander, J.B., Priestley, M.J.N., and Park, R. (1988a). "Observed Stress-Strain Behavior of Confined Concrete", *Journal of Structural Engineering*, ASCE, Vol. 114, No. 8, August, 1827-1849.
- Mander, J.B., Priestley, M.J.N., and Park, R. (1988b). "Theoretical Stress-Strain Model for Confined Concrete", *Journal of Structural Engineering*, ASCE, Vol. 114, No. 8, August, 1804-1826.
- Nilson, A.H. (1987). *Design of Prestressed Concrete*, John Wiley and Sons, Inc., New York.
- Nmai, C.K. and Darwin, D. (1984). "Cyclic Behavior of Lightly Reinforced Concrete Beams", The University of Kansas Center for Research, Inc., SM Report No. 12.
- Panahshahi, N., White, R.N., and Gergely, P. (1992). "Reinforced Concrete Compression Lap Splices under Inelastic Cyclic Loading", *ACI Structural Journal*, Vol. 89, No. 2, March-April, 164-175.
- Park, R. and Gamble W.L. (1980). *Reinforced Concrete Slabs*, John Wiley and Sons, Inc, New York.
- Park, R. and Milburn, J.R. (1983). "Comparison of Recent New Zealand and United States Seismic Design Provisions for Reinforced Concrete Beam-Column Joints and Test Results for Four Units Designed According to the New Zealand Code", *Bulletin of the New Zealand National Society of Earthquake Engineering*, Vol. 16, No. 1, March, 21-42.
- Park, R. and Paulay, T. (1975). *Reinforced Concrete Structures*, John Wiley and Sons, Inc.
- Paulay, T. (1989). "Equilibrium Criteria for Reinforced Concrete Beam-Column Joints", *ACI Structural Journal*, Vol. 86, No. 6, November-December, 635-643.
- Paulay, T. and Bull, I.N. (1979). "Shear Effect on Plastic Hinges of Earthquake Resisting Reinforced Concrete Frames", *Bulletin D'Information 132*, Comite Euro-International du Beton, April, 165-172.
- Paulay, T. and Priestley, M.J.N. (1992). *Seismic Design of Reinforced Concrete and Masonry Buildings*, John Wiley and Sons, Inc., New York.

- Paulay, T., Zanza, T.M., and Scarpas, A. (1981). "Lapped Splices in Bridge Piers and Columns of Earthquake Resisting Reinforced Concrete Frames", Report No. 81-6, Department of Civil Engineering, University of Canterbury, Christchurch, August, 116 pp.
- Pessiki, S.P., Conley, C.H., Gergely, P., and White, R.N. (1990). "Seismic Behavior of Lightly-Reinforced Concrete Column and Beam-Column Joint Details", National Center for Earthquake Engineering Research, Report No. NCEER-90-0014, State University of New York at Buffalo.
- Priestley, M.J.N. and Park, R. (1987). "Strength and Ductility of Concrete Bridge Columns Under Seismic Loading", *ACI Structural Journal*, January-February, 61-76.
- Recommended Provisions for the Development of Seismic Regulations for New Buildings, NEHRP 1991 Edition*, FEMA 222/January 1992, Washington D.C.
- Saatcioglu, M. and Ozcebe, B. (1989). "Response of Reinforced Concrete Columns to Simulated Seismic Loading", *ACI Structural Journal*, Vol. 86, No. 1, January-February, 3-12.
- Shahrooz, B.M. and Moehle, J.P. (1987). "Experimental Study of Seismic Response of R.C. Setback Buildings", Earthquake Engineering Research Center, University of California/Berkeley, California, Report No. UCB/EERC-87/16.
- Soroushian, P. and Choi, K.B. (1989). "Local Bond of Deformed Bars with Different Diameters in Confined Concrete", *ACI Structural Journal*, Vol. 86, No. 2, March-April, 217-222.
- STAAD™ (1989). *Integrated Structural Design System*, Research Engineers, Inc., New Jersey.
- Uang, C.-M. and Bertero, V.V. (1990). "Evaluation of Seismic Energy in Structures", *Earthquake Engineering and Structural Dynamics*, Vol. 19, 77-90.
- Wallace, B. and Krawinkler, H. (1984). "Small Scale Model Tests of Structural Components and Assemblies", *ACI special publication SP 84-11*, 305-345.
- Wilby, G.K., Park, R., and Carr, A.J. (1973). "Static and Dynamic Loading Tests on Two Small Three-Dimensional Multistory Reinforced Concrete Frames", *ACI special publication SP 73-3*, 35-63.
- Wolfgram-French, C. and Boroojerdi, A. (1989). "Contribution of R/C Floor Slabs in Resisting Lateral Loads", *Journal of Structural Engineering*, ASCE, Vol. 115, No. 1, January, 1-18.
- Zerbe, H.E. and Durrani, A. (1990). "Seismic Response of Connections in Two-Bay Reinforced Concrete Frame Subassemblies with Floor Slab", *ACI Structural Journal*, Vol. 87, No. 4, July-August, 406-415.

APPENDIX A
SCALING FACTORS FOR MODELING OF DYNAMIC BEHAVIOR

Quantity	General Case	Same Material and Acceleration (Model)	
		Required	Provided
Geometric Length, l	$\lambda_l = ?$	$\lambda_l = 3.00$	$\lambda_l = 3.00$
Elastic Modulus, E	$\lambda_E = ?$	$\lambda_E = 1.00$	$\lambda_E = 1.00$
Acceleration, a	$\lambda_a = ? (= 1/\lambda_l \cdot \lambda_E/\lambda_\rho)$	$\lambda_a = 1.00$	$\lambda_a = 1.00$
Density, ρ	$\lambda_\rho = \lambda_E/(\lambda_l \lambda_a) (= ?)$	$\lambda_\rho = 0.33$	$\lambda_\rho = 1.00$
Velocity, v	$\lambda_v = \sqrt{\lambda_l \cdot \lambda_a}$	$\lambda_v = 1.73$	$\lambda_v = 1.73$
Forces, f	$\lambda_f = \lambda_E \lambda_l^2$	$\lambda_f = 9.00$	$\lambda_f = 9.00$
Stress, σ	$\lambda_\sigma = \lambda_E$	$\lambda_\sigma = 1.00$	$\lambda_\sigma = 1.00$
Strain, ϵ	$\lambda_\epsilon = 1.00$	$\lambda_\epsilon = 1.00$	$\lambda_\epsilon = 1.00$
Area, A	$\lambda_A = \lambda_l^2$	$\lambda_A = 9.00$	$\lambda_A = 9.00$
Volume, V	$\lambda_V = \lambda_l^3$	$\lambda_V = 27.00$	$\lambda_V = 27.00$
Second Moment of Area, I	$\lambda_I = \lambda_l^4$	$\lambda_I = 81.00$	$\lambda_I = 81.00$
Mass, m	$\lambda_m = \lambda_\rho \lambda_l^3$	$\lambda_m = 9.00$	$\lambda_m = 27.00$
Impulse, i	$\lambda_i = \lambda_l^3 \cdot \sqrt{\lambda_\rho \lambda_E}$	$\lambda_i = 15.59$	$\lambda_i = 27.00$
Energy, e	$\lambda_e = \lambda_E \lambda_l^3$	$\lambda_e = 27.00$	$\lambda_e = 27.00$
Frequency, ω	$\lambda_\omega = 1/\lambda_l \cdot \sqrt{\lambda_E/\lambda_\rho}$	$\lambda_\omega = 0.58$	$\lambda_\omega = 0.33$
Time (Period), t	$\lambda_t = \sqrt{\lambda_l/\lambda_a}$	$\lambda_t = 1.73$	$\lambda_t = 1.73$
Gravitational Acceleration, g	$\lambda_g = 1.00$	$\lambda_g = 1.00$	$\lambda_g = 1.00$
Gravitational Force, fg	$\lambda_{fg} = \lambda_\rho \lambda_l^3$	$\lambda_{fg} = 9.00$	$\lambda_{fg} = 27.00$
Critical Damping, ξ	$\lambda_\xi = 1.00$	$\lambda_\xi = 1.00$	$\lambda_\xi = 1.00$

** Note for modeling with constant acceleration, λ_a becomes the independent variable (= 1.00) and λ_ρ becomes the dependent variable (= λ_E/λ_l).

APPENDIX B

GEOMETRIC LAYOUT, STRAIN GAGING, AND CALIBRATION CHARTS OF LOAD CELLS

Special force transducers (load cells) are used to measure the internal force response of the model as specified in section 3. The geometric layout of the a typical load cell is shown in Fig. B-1a. They are fabricated from a thick wall cylindrical steel tube. The turned down wall thickness, height, and radius of the tube are determined based on the expected maximum stresses in the load cells during testing and on the matching the flexural stiffness with that of the column to minimize disturbance in that member. The attachment plates, shown in Fig. B-1b, ensure a uniform stress distribution over the entire load cell and provide anchorage into the columns. Based on the yield strength of the steel tube, the axial, shear, and moment capacity ratings for the load cells are ± 40 kips, ± 5 kips, and ± 40 kip-in, respectively, to ensure linearity and repeatability.

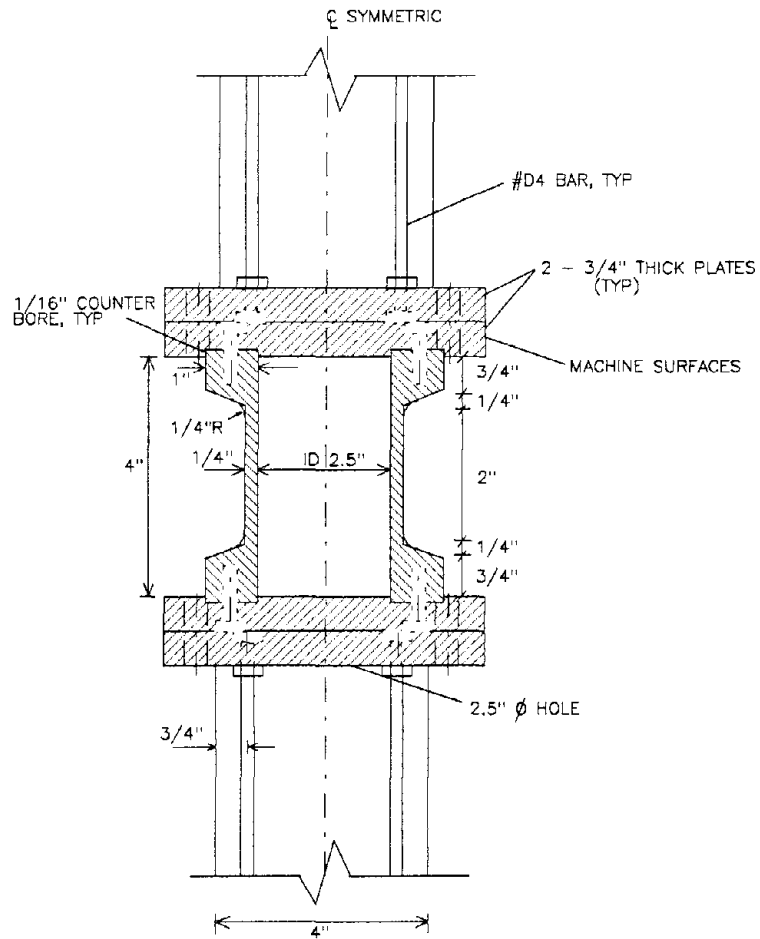
The strain gages used in the load cells are types EA-06-125UR-120 (rosettes) and EA-06-125UW-120 (single gages) from Measurement Group, Inc. The gages have a maximum strain range of ± 0.00375 in. and an overall length and width of 0.30 in. and 0.56 in., respectively. The maximum strain range of the gage is well beyond the elastic range of the cylindrical steel tube, which the load cells are designed. Fig. B-2a shows the strain gage location (A-D) and orientation (1-5) on the steel tube wall. Note that gages 1, 2, and 3 are from a rosette. M-Bond 200 adhesive is used for attaching the gages.

Axial, shear, and moment stresses are measured from Wheatstone bridge circuits wired according to Fig. B-2b. The axial circuits use gages #2 and #6, where gage #6 is a compensating ("dummy") gage used for variations in temperature in the circuit. The shear circuits use gages #1 and #3, which are orientated 45° from the horizontal, and the moment circuits use gages #4 and #5, which are orientated in the vertical direction.

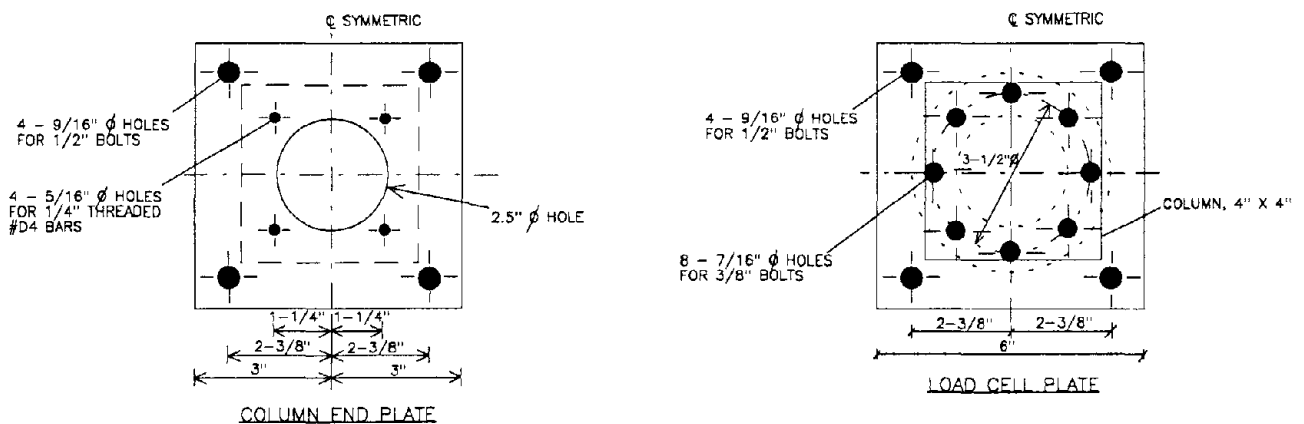
Based on the load capacity ratings of the load cells, calibration factors for the axial, shear, and moment circuits are determined as 4 kips/volt, 0.5 kips/volt, and 4 kip-in./volt, respectively. For calibration, the load cells are bolted together in groups of two and loaded according to Fig. B-3. The pivoting head in Fig. B-3a for axial load calibration helps distribute the axial com-

pressive load evenly across the load cells. The shear setup results in a constant shear force and a linearly varying moment across the load cells. The moments recorded are correlated with a known moment arm to the strain gages for the moment circuits. The moment setup is a two point loading which creates a constant bending moment with no shear force.

The circuits are connected to 2310 Vishay Signal Conditioning Amplifiers from the Measurement Group, Inc. which filters frequencies above 25 Hz. and varies the amplification (gain) of the incoming signal from the wheatstone bridge circuit. Calibration charts are developed, typically shown for a particular load cell in Fig. B-4, based on several series of loading and unloading for each setup and adjustments in amplification from the conditioners to acquire the appropriate calibration factors. Note, that a loop in the unloading states of testing develops in the moment calibrations. However the initial loading is perfectly linear and returns to zero when the load is fully removed, which implies that the load cell behaves elastically. Therefore the loops were created by some errors in the setup, possibly due to some concentrated yielding or friction which develops in the components of the setup.

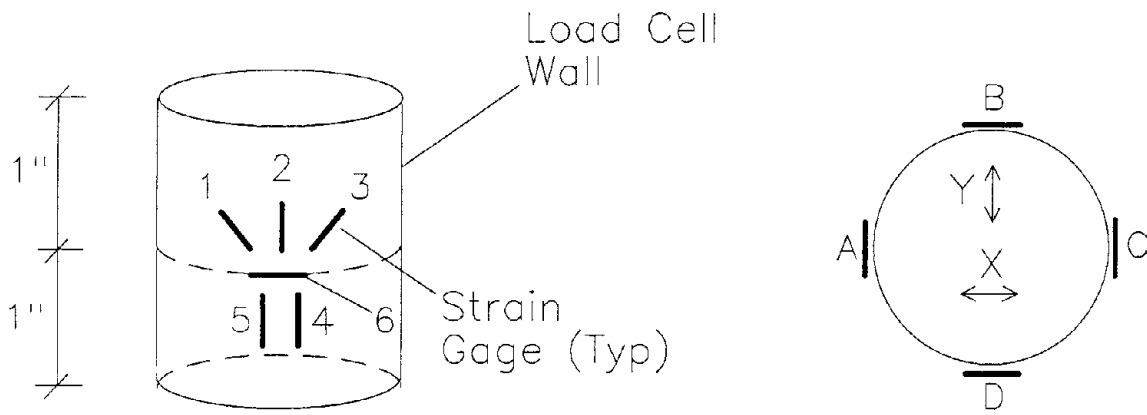


(a) Elevation

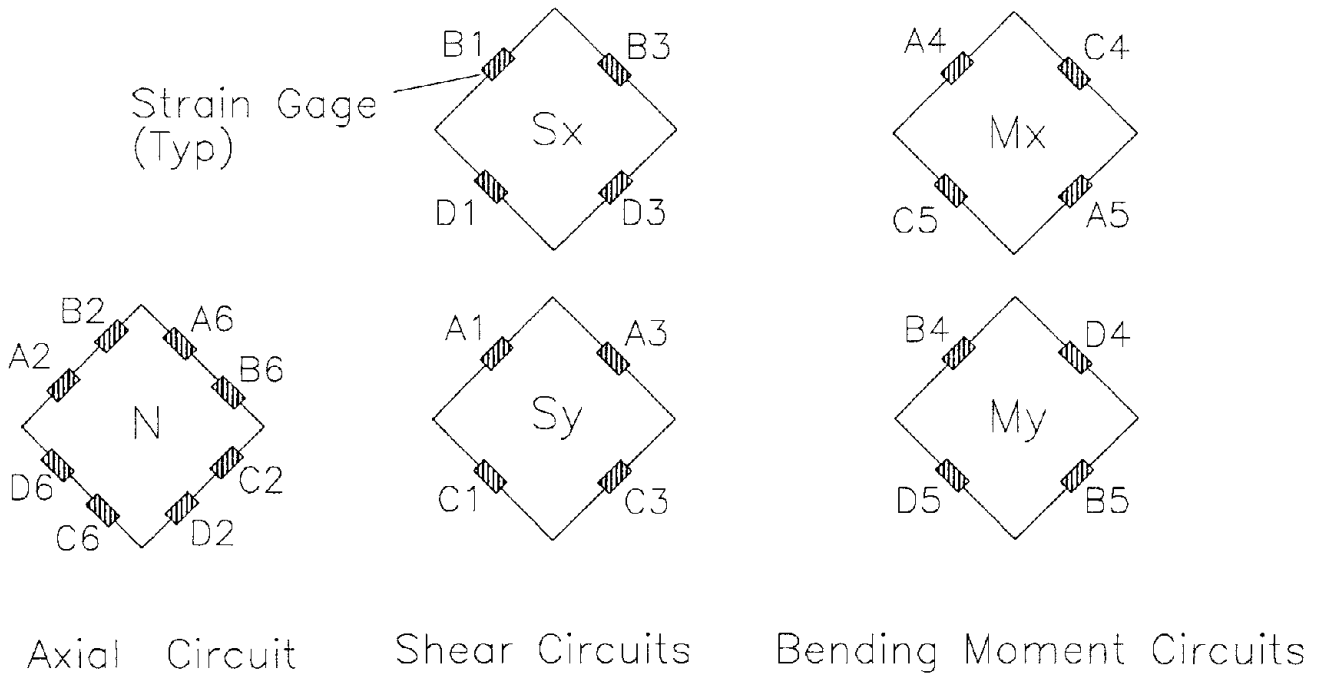


(b) Attachment Plates

FIG. B-1 Load Cell Geometric Layout



(a) Strain Gage Positioning on Load Cell



(b) Wheatstone Bridge Circuits

FIG. B-2 Strain Gage Positioning and Wiring

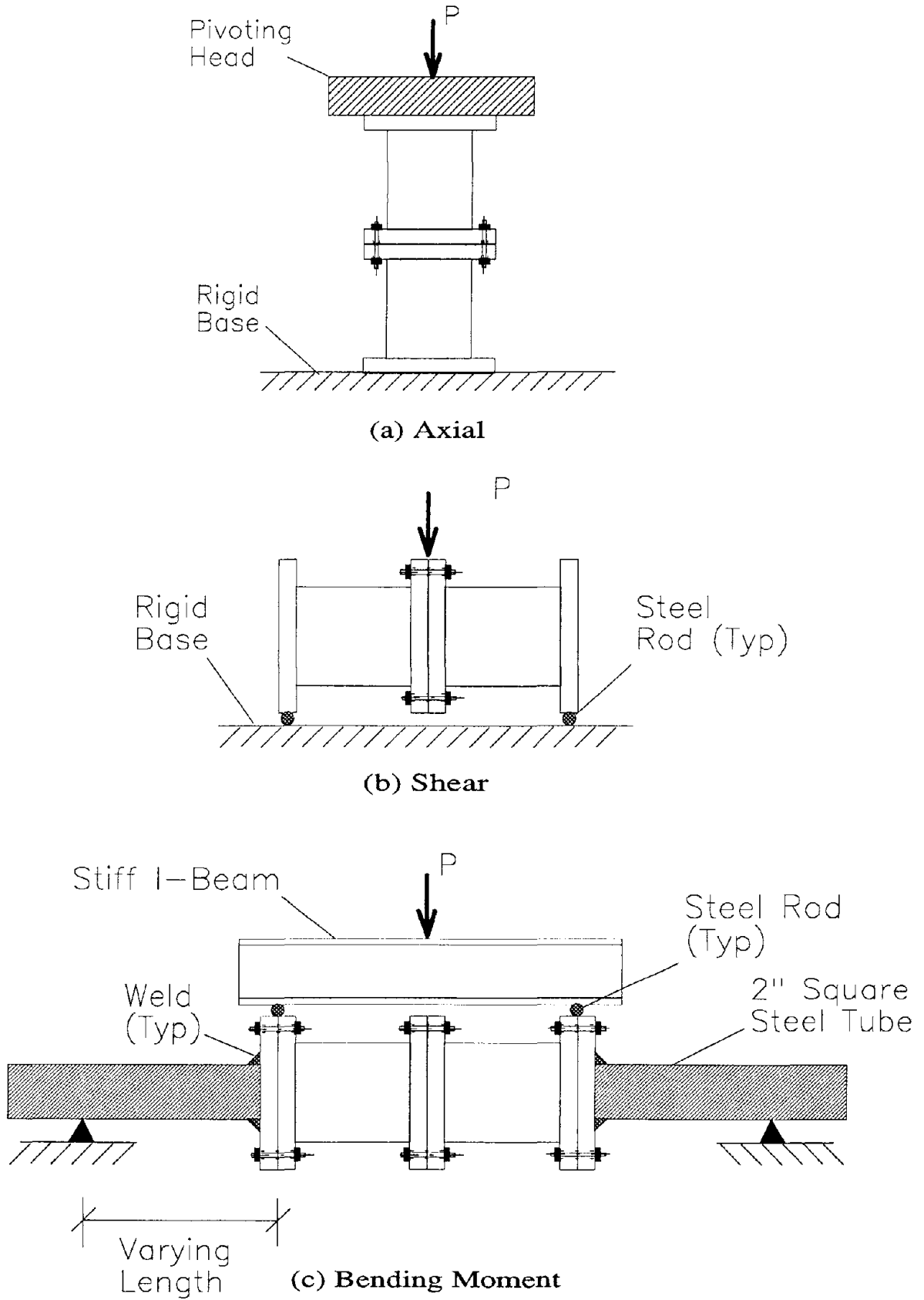


FIG. B-3 Load Cell Calibration Setup

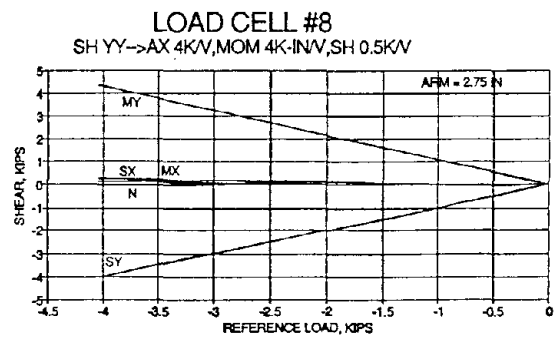
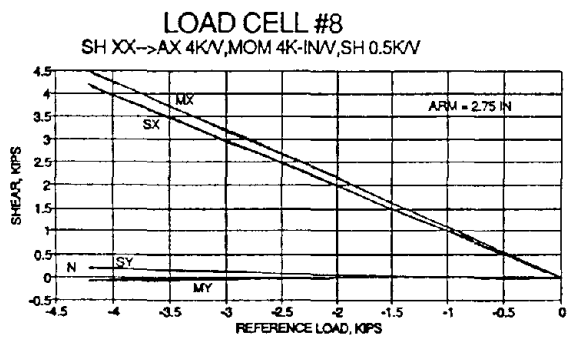
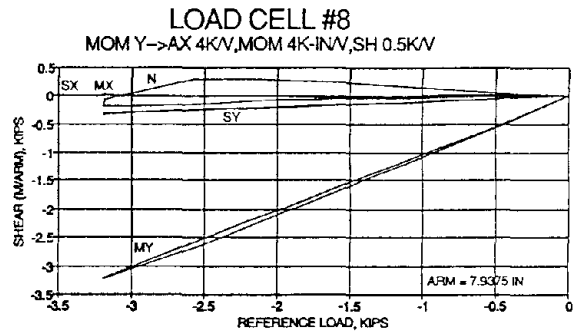
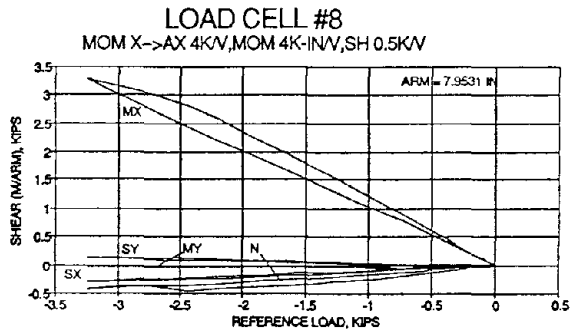
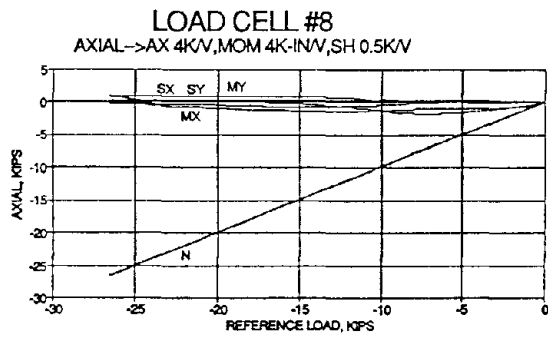


FIG. B-4 Calibration Curves for a Typical Load Cell

**NATIONAL CENTER FOR EARTHQUAKE ENGINEERING RESEARCH
LIST OF TECHNICAL REPORTS**

The National Center for Earthquake Engineering Research (NCEER) publishes technical reports on a variety of subjects related to earthquake engineering written by authors funded through NCEER. These reports are available from both NCEER's Publications Department and the National Technical Information Service (NTIS). Requests for reports should be directed to the Publications Department, National Center for Earthquake Engineering Research, State University of New York at Buffalo, Red Jacket Quadrangle, Buffalo, New York 14261. Reports can also be requested through NTIS, 5285 Port Royal Road, Springfield, Virginia 22161. NTIS accession numbers are shown in parenthesis, if available.

- NCEER-87-0001 "First-Year Program in Research, Education and Technology Transfer," 3/5/87, (PB88-134275/AS).
- NCEER-87-0002 "Experimental Evaluation of Instantaneous Optimal Algorithms for Structural Control," by R.C. Lin, T.T. Soong and A.M. Reinhorn, 4/20/87, (PB88-134341/AS).
- NCEER-87-0003 "Experimentation Using the Earthquake Simulation Facilities at University at Buffalo," by A.M. Reinhorn and R.L. Ketter, to be published.
- NCEER-87-0004 "The System Characteristics and Performance of a Shaking Table," by J.S. Hwang, K.C. Chang and G.C. Lee, 6/1/87, (PB88-134259/AS). This report is available only through NTIS (see address given above).
- NCEER-87-0005 "A Finite Element Formulation for Nonlinear Viscoplastic Material Using a Q Model," by O. Gyebe and G. Dasgupta, 11/2/87, (PB88-213764/AS).
- NCEER-87-0006 "Symbolic Manipulation Program (SMP) - Algebraic Codes for Two and Three Dimensional Finite Element Formulations," by X. Lee and G. Dasgupta, 11/9/87, (PB88-219522/AS).
- NCEER-87-0007 "Instantaneous Optimal Control Laws for Tall Buildings Under Seismic Excitations," by J.N. Yang, A. Akbarpour and P. Ghaemmaghami, 6/10/87, (PB88-134333/AS).
- NCEER-87-0008 "IDARC: Inelastic Damage Analysis of Reinforced Concrete Frame - Shear-Wall Structures," by Y.J. Park, A.M. Reinhorn and S.K. Kunnath, 7/20/87, (PB88-134325/AS).
- NCEER-87-0009 "Liquefaction Potential for New York State: A Preliminary Report on Sites in Manhattan and Buffalo," by M. Budhu, V. Vijayakumar, R.F. Giese and L. Baumgras, 8/31/87, (PB88-163704/AS). This report is available only through NTIS (see address given above).
- NCEER-87-0010 "Vertical and Torsional Vibration of Foundations in Inhomogeneous Media," by A.S. Veletsos and K.W. Dotson, 6/1/87, (PB88-134291/AS).
- NCEER-87-0011 "Seismic Probabilistic Risk Assessment and Seismic Margins Studies for Nuclear Power Plants," by Howard H.M. Hwang, 6/15/87, (PB88-134267/AS).
- NCEER-87-0012 "Parametric Studies of Frequency Response of Secondary Systems Under Ground-Acceleration Excitations," by Y. Yong and Y.K. Lin, 6/10/87, (PB88-134309/AS).
- NCEER-87-0013 "Frequency Response of Secondary Systems Under Seismic Excitation," by J.A. HoLung, J. Cai and Y.K. Lin, 7/31/87, (PB88-134317/AS).
- NCEER-87-0014 "Modelling Earthquake Ground Motions in Seismically Active Regions Using Parametric Time Series Methods," by G.W. Ellis and A.S. Cakmak, 8/25/87, (PB88-134283/AS).
- NCEER-87-0015 "Detection and Assessment of Seismic Structural Damage," by E. DiPasquale and A.S. Cakmak, 8/25/87, (PB88-163712/AS).

- NCEER-87-0016 "Pipeline Experiment at Parkfield, California," by J. Isenberg and E. Richardson, 9/15/87, (PB88-163720/AS). This report is available only through NTIS (see address given above).
- NCEER-87-0017 "Digital Simulation of Seismic Ground Motion," by M. Shinozuka, G. Deodatis and T. Harada, 8/31/87, (PB88-155197/AS). This report is available only through NTIS (see address given above).
- NCEER-87-0018 "Practical Considerations for Structural Control: System Uncertainty, System Time Delay and Truncation of Small Control Forces," J.N. Yang and A. Akbarpour, 8/10/87, (PB88-163738/AS).
- NCEER-87-0019 "Modal Analysis of Nonclassically Damped Structural Systems Using Canonical Transformation," by J.N. Yang, S. Sarkani and F.X. Long, 9/27/87, (PB88-187851/AS).
- NCEER-87-0020 "A Nonstationary Solution in Random Vibration Theory," by J.R. Red-Horse and P.D. Spanos, 11/3/87, (PB88-163746/AS).
- NCEER-87-0021 "Horizontal Impedances for Radially Inhomogeneous Viscoelastic Soil Layers," by A.S. Veletsos and K.W. Dotson, 10/15/87, (PB88-150859/AS).
- NCEER-87-0022 "Seismic Damage Assessment of Reinforced Concrete Members," by Y.S. Chung, C. Meyer and M. Shinozuka, 10/9/87, (PB88-150867/AS). This report is available only through NTIS (see address given above).
- NCEER-87-0023 "Active Structural Control in Civil Engineering," by T.T. Soong, 11/11/87, (PB88-187778/AS).
- NCEER-87-0024 "Vertical and Torsional Impedances for Radially Inhomogeneous Viscoelastic Soil Layers," by K.W. Dotson and A.S. Veletsos, 12/87, (PB88-187786/AS).
- NCEER-87-0025 "Proceedings from the Symposium on Seismic Hazards, Ground Motions, Soil-Liquefaction and Engineering Practice in Eastern North America," October 20-22, 1987, edited by K.H. Jacob, 12/87, (PB88-188115/AS).
- NCEER-87-0026 "Report on the Whittier-Narrows, California, Earthquake of October 1, 1987," by J. Pantelic and A. Reinhorn, 11/87, (PB88-187752/AS). This report is available only through NTIS (see address given above).
- NCEER-87-0027 "Design of a Modular Program for Transient Nonlinear Analysis of Large 3-D Building Structures," by S. Srivastav and J.F. Abel, 12/30/87, (PB88-187950/AS).
- NCEER-87-0028 "Second-Year Program in Research, Education and Technology Transfer," 3/8/88, (PB88-219480/AS).
- NCEER-88-0001 "Workshop on Seismic Computer Analysis and Design of Buildings With Interactive Graphics," by W. McGuire, J.F. Abel and C.H. Conley, 1/18/88, (PB88-187760/AS).
- NCEER-88-0002 "Optimal Control of Nonlinear Flexible Structures," by J.N. Yang, F.X. Long and D. Wong, 1/22/88, (PB88-213772/AS).
- NCEER-88-0003 "Substructuring Techniques in the Time Domain for Primary-Secondary Structural Systems," by G.D. Manolis and G. Juhn, 2/10/88, (PB88-213780/AS).
- NCEER-88-0004 "Iterative Seismic Analysis of Primary-Secondary Systems," by A. Singhal, L.D. Lutes and P.D. Spanos, 2/23/88, (PB88-213798/AS).
- NCEER-88-0005 "Stochastic Finite Element Expansion for Random Media," by P.D. Spanos and R. Ghanem, 3/14/88, (PB88-213806/AS).

- NCEER-88-0006 "Combining Structural Optimization and Structural Control," by F.Y. Cheng and C.P. Pantelides, 1/10/88, (PB88-213814/AS).
- NCEER-88-0007 "Seismic Performance Assessment of Code-Designed Structures," by H.H-M. Hwang, J-W. Jaw and H-J. Shau, 3/20/88, (PB88-219423/AS).
- NCEER-88-0008 "Reliability Analysis of Code-Designed Structures Under Natural Hazards," by H.H-M. Hwang, H. Ushiba and M. Shinozuka, 2/29/88, (PB88-229471/AS).
- NCEER-88-0009 "Seismic Fragility Analysis of Shear Wall Structures," by J-W Jaw and H.H-M. Hwang, 4/30/88, (PB89-102867/AS).
- NCEER-88-0010 "Base Isolation of a Multi-Story Building Under a Harmonic Ground Motion - A Comparison of Performances of Various Systems," by F-G Fan, G. Ahmadi and I.G. Tadjbakhsh, 5/18/88, (PB89-122238/AS).
- NCEER-88-0011 "Seismic Floor Response Spectra for a Combined System by Green's Functions," by F.M. Lavelle, L.A. Bergman and P.D. Spanos, 5/1/88, (PB89-102875/AS).
- NCEER-88-0012 "A New Solution Technique for Randomly Excited Hysteretic Structures," by G.Q. Cai and Y.K. Lin, 5/16/88, (PB89-102883/AS).
- NCEER-88-0013 "A Study of Radiation Damping and Soil-Structure Interaction Effects in the Centrifuge," by K. Weissman, supervised by J.H. Prevost, 5/24/88, (PB89-144703/AS).
- NCEER-88-0014 "Parameter Identification and Implementation of a Kinematic Plasticity Model for Frictional Soils," by J.H. Prevost and D.V. Griffiths, to be published.
- NCEER-88-0015 "Two- and Three- Dimensional Dynamic Finite Element Analyses of the Long Valley Dam," by D.V. Griffiths and J.H. Prevost, 6/17/88, (PB89-144711/AS).
- NCEER-88-0016 "Damage Assessment of Reinforced Concrete Structures in Eastern United States," by A.M. Reinhorn, M.J. Seidel, S.K. Kunnath and Y.J. Park, 6/15/88, (PB89-122220/AS).
- NCEER-88-0017 "Dynamic Compliance of Vertically Loaded Strip Foundations in Multilayered Viscoelastic Soils," by S. Ahmad and A.S.M. Israil, 6/17/88, (PB89-102891/AS).
- NCEER-88-0018 "An Experimental Study of Seismic Structural Response With Added Viscoelastic Dampers," by R.C. Lin, Z. Liang, T.T. Soong and R.H. Zhang, 6/30/88, (PB89-122212/AS). This report is available only through NTIS (see address given above).
- NCEER-88-0019 "Experimental Investigation of Primary - Secondary System Interaction," by G.D. Manolis, G. Juhn and A.M. Reinhorn, 5/27/88, (PB89-122204/AS).
- NCEER-88-0020 "A Response Spectrum Approach For Analysis of Nonclassically Damped Structures," by J.N. Yang, S. Sarkani and F.X. Long, 4/22/88, (PB89-102909/AS).
- NCEER-88-0021 "Seismic Interaction of Structures and Soils: Stochastic Approach," by A.S. Veletsos and A.M. Prasad, 7/21/88, (PB89-122196/AS).
- NCEER-88-0022 "Identification of the Serviceability Limit State and Detection of Seismic Structural Damage," by E. DiPasquale and A.S. Cakmak, 6/15/88, (PB89-122188/AS). This report is available only through NTIS (see address given above).
- NCEER-88-0023 "Multi-Hazard Risk Analysis: Case of a Simple Offshore Structure," by B.K. Bhartia and E.H. Vanmarcke, 7/21/88, (PB89-145213/AS).

- NCEER-88-0024 "Automated Seismic Design of Reinforced Concrete Buildings," by Y.S. Chung, C. Meyer and M. Shinozuka, 7/5/88, (PB89-122170/AS). This report is available only through NTIS (see address given above).
- NCEER-88-0025 "Experimental Study of Active Control of MDOF Structures Under Seismic Excitations," by L.L. Chung, R.C. Lin, T.T. Soong and A.M. Reinhorn, 7/10/88, (PB89-122600/AS).
- NCEER-88-0026 "Earthquake Simulation Tests of a Low-Rise Metal Structure," by J.S. Hwang, K.C. Chang, G.C. Lee and R.L. Ketter, 8/1/88, (PB89-102917/AS).
- NCEER-88-0027 "Systems Study of Urban Response and Reconstruction Due to Catastrophic Earthquakes," by F. Kozin and H.K. Zhou, 9/22/88, (PB90-162348/AS).
- NCEER-88-0028 "Seismic Fragility Analysis of Plane Frame Structures," by H.H.-M. Hwang and Y.K. Low, 7/31/88, (PB89-131445/AS).
- NCEER-88-0029 "Response Analysis of Stochastic Structures," by A. Kardara, C. Bucher and M. Shinozuka, 9/22/88, (PB89-174429/AS).
- NCEER-88-0030 "Nonnormal Accelerations Due to Yielding in a Primary Structure," by D.C.K. Chen and L.D. Lutes, 9/19/88, (PB89-131437/AS).
- NCEER-88-0031 "Design Approaches for Soil-Structure Interaction," by A.S. Veletsos, A.M. Prasad and Y. Tang, 12/30/88, (PB89-174437/AS). This report is available only through NTIS (see address given above).
- NCEER-88-0032 "A Re-evaluation of Design Spectra for Seismic Damage Control," by C.J. Turkstra and A.G. Tallin, 11/7/88, (PB89-145221/AS).
- NCEER-88-0033 "The Behavior and Design of Noncontact Lap Splices Subjected to Repeated Inelastic Tensile Loading," by V.E. Sagan, P. Gergely and R.N. White, 12/8/88, (PB89-163737/AS).
- NCEER-88-0034 "Seismic Response of Pile Foundations," by S.M. Mamoon, P.K. Banerjee and S. Ahmad, 11/1/88, (PB89-145239/AS).
- NCEER-88-0035 "Modeling of R/C Building Structures With Flexible Floor Diaphragms (IDARC2)," by A.M. Reinhorn, S.K. Kunnath and N. Panahshahi, 9/7/88, (PB89-207153/AS).
- NCEER-88-0036 "Solution of the Dam-Reservoir Interaction Problem Using a Combination of FEM, BEM with Particular Integrals, Modal Analysis, and Substructuring," by C-S. Tsai, G.C. Lee and R.L. Ketter, 12/31/88, (PB89-207146/AS).
- NCEER-88-0037 "Optimal Placement of Actuators for Structural Control," by F.Y. Cheng and C.P. Pantelides, 8/15/88, (PB89-162846/AS).
- NCEER-88-0038 "Teflon Bearings in Aseismic Base Isolation: Experimental Studies and Mathematical Modeling," by A. Mokha, M.C. Constantinou and A.M. Reinhorn, 12/5/88, (PB89-218457/AS). This report is available only through NTIS (see address given above).
- NCEER-88-0039 "Seismic Behavior of Flat Slab High-Rise Buildings in the New York City Area," by P. Weidlinger and M. Ettouney, 10/15/88, (PB90-145681/AS).
- NCEER-88-0040 "Evaluation of the Earthquake Resistance of Existing Buildings in New York City," by P. Weidlinger and M. Ettouney, 10/15/88, to be published.
- NCEER-88-0041 "Small-Scale Modeling Techniques for Reinforced Concrete Structures Subjected to Seismic Loads," by W. Kim, A. El-Attar and R.N. White, 11/22/88, (PB89-189625/AS).

- NCEER-88-0042 "Modeling Strong Ground Motion from Multiple Event Earthquakes," by G.W. Ellis and A.S. Cakmak, 10/15/88, (PB89-174445/AS).
- NCEER-88-0043 "Nonstationary Models of Seismic Ground Acceleration," by M. Grigoriu, S.E. Ruiz and E. Rosenblueth, 7/15/88, (PB89-189617/AS).
- NCEER-88-0044 "SARCF User's Guide: Seismic Analysis of Reinforced Concrete Frames," by Y.S. Chung, C. Meyer and M. Shinozuka, 11/9/88, (PB89-174452/AS).
- NCEER-88-0045 "First Expert Panel Meeting on Disaster Research and Planning," edited by J. Pantelic and J. Stoye, 9/15/88, (PB89-174460/AS).
- NCEER-88-0046 "Preliminary Studies of the Effect of Degrading Infill Walls on the Nonlinear Seismic Response of Steel Frames," by C.Z. Chrysostomou, P. Gergely and J.F. Abel, 12/19/88, (PB89-208383/AS).
- NCEER-88-0047 "Reinforced Concrete Frame Component Testing Facility - Design, Construction, Instrumentation and Operation," by S.P. Pessiki, C. Conley, T. Bond, P. Gergely and R.N. White, 12/16/88, (PB89-174478/AS).
- NCEER-89-0001 "Effects of Protective Cushion and Soil Compliancy on the Response of Equipment Within a Seismically Excited Building," by J.A. HoLung, 2/16/89, (PB89-207179/AS).
- NCEER-89-0002 "Statistical Evaluation of Response Modification Factors for Reinforced Concrete Structures," by H.H-M. Hwang and J-W. Jaw, 2/17/89, (PB89-207187/AS).
- NCEER-89-0003 "Hysteretic Columns Under Random Excitation," by G-Q. Cai and Y.K. Lin, 1/9/89, (PB89-196513/AS).
- NCEER-89-0004 "Experimental Study of 'Elephant Foot Bulge' Instability of Thin-Walled Metal Tanks," by Z-H. Jia and R.L. Ketter, 2/22/89, (PB89-207195/AS).
- NCEER-89-0005 "Experiment on Performance of Buried Pipelines Across San Andreas Fault," by J. Isenberg, E. Richardson and T.D. O'Rourke, 3/10/89, (PB89-218440/AS).
- NCEER-89-0006 "A Knowledge-Based Approach to Structural Design of Earthquake-Resistant Buildings," by M. Subramani, P. Gergely, C.H. Conley, J.F. Abel and A.H. Zaghaw, 1/15/89, (PB89-218465/AS).
- NCEER-89-0007 "Liquefaction Hazards and Their Effects on Buried Pipelines," by T.D. O'Rourke and P.A. Lane, 2/1/89, (PB89-218481).
- NCEER-89-0008 "Fundamentals of System Identification in Structural Dynamics," by H. Imai, C-B. Yun, O. Maruyama and M. Shinozuka, 1/26/89, (PB89-207211/AS).
- NCEER-89-0009 "Effects of the 1985 Michoacan Earthquake on Water Systems and Other Buried Lifelines in Mexico," by A.G. Ayala and M.J. O'Rourke, 3/8/89, (PB89-207229/AS).
- NCEER-89-R010 "NCEER Bibliography of Earthquake Education Materials," by K.E.K. Ross, Second Revision, 9/1/89, (PB90-125352/AS).
- NCEER-89-0011 "Inelastic Three-Dimensional Response Analysis of Reinforced Concrete Building Structures (IDARC-3D), Part I - Modeling," by S.K. Kunnath and A.M. Reinhorn, 4/17/89, (PB90-114612/AS).
- NCEER-89-0012 "Recommended Modifications to ATC-14," by C.D. Poland and J.O. Malley, 4/12/89, (PB90-108648/AS).
- NCEER-89-0013 "Repair and Strengthening of Beam-to-Column Connections Subjected to Earthquake Loading," by M. Corazao and A.J. Durrani, 2/28/89, (PB90-109885/AS).

- NCEER-89-0014 "Program EXKAL2 for Identification of Structural Dynamic Systems," by O. Maruyama, C-B. Yun, M. Hoshiya and M. Shinozuka, 5/19/89, (PB90-109877/AS).
- NCEER-89-0015 "Response of Frames With Bolted Semi-Rigid Connections, Part I - Experimental Study and Analytical Predictions," by P.J. DiCorso, A.M. Reinhorn, J.R. Dickerson, J.B. Radzimirski and W.L. Harper, 6/1/89, to be published.
- NCEER-89-0016 "ARMA Monte Carlo Simulation in Probabilistic Structural Analysis," by P.D. Spanos and M.P. Mignolet, 7/10/89, (PB90-109893/AS).
- NCEER-89-P017 "Preliminary Proceedings from the Conference on Disaster Preparedness - The Place of Earthquake Education in Our Schools," Edited by K.E.K. Ross, 6/23/89.
- NCEER-89-0017 "Proceedings from the Conference on Disaster Preparedness - The Place of Earthquake Education in Our Schools," Edited by K.E.K. Ross, 12/31/89, (PB90-207895). This report is available only through NTIS (see address given above).
- NCEER-89-0018 "Multidimensional Models of Hysteretic Material Behavior for Vibration Analysis of Shape Memory Energy Absorbing Devices, by E.J. Graesser and F.A. Cozzarelli, 6/7/89, (PB90-164146/AS).
- NCEER-89-0019 "Nonlinear Dynamic Analysis of Three-Dimensional Base Isolated Structures (3D-BASIS)," by S. Nagarajaiah, A.M. Reinhorn and M.C. Constantinou, 8/3/89, (PB90-161936/AS). This report is available only through NTIS (see address given above).
- NCEER-89-0020 "Structural Control Considering Time-Rate of Control Forces and Control Rate Constraints," by F.Y. Cheng and C.P. Pantelides, 8/3/89, (PB90-120445/AS).
- NCEER-89-0021 "Subsurface Conditions of Memphis and Shelby County," by K.W. Ng, T-S. Chang and H-H.M. Hwang, 7/26/89, (PB90-120437/AS).
- NCEER-89-0022 "Seismic Wave Propagation Effects on Straight Jointed Buried Pipelines," by K. Elhadi and M.J. O'Rourke, 8/24/89, (PB90-162322/AS).
- NCEER-89-0023 "Workshop on Serviceability Analysis of Water Delivery Systems," edited by M. Grigoriu, 3/6/89, (PB90-127424/AS).
- NCEER-89-0024 "Shaking Table Study of a 1/5 Scale Steel Frame Composed of Tapered Members," by K.C. Chang, J.S. Hwang and G.C. Lee, 9/18/89, (PB90-160169/AS).
- NCEER-89-0025 "DYNA1D: A Computer Program for Nonlinear Seismic Site Response Analysis - Technical Documentation," by Jean H. Prevost, 9/14/89, (PB90-161944/AS). This report is available only through NTIS (see address given above).
- NCEER-89-0026 "1:4 Scale Model Studies of Active Tendon Systems and Active Mass Dampers for Aseismic Protection," by A.M. Reinhorn, T.T. Soong, R.C. Lin, Y.P. Yang, Y. Fukao, H. Abe and M. Nakai, 9/15/89, (PB90-173246/AS).
- NCEER-89-0027 "Scattering of Waves by Inclusions in a Nonhomogeneous Elastic Half Space Solved by Boundary Element Methods," by P.K. Hadley, A. Askar and A.S. Cakmak, 6/15/89, (PB90-145699/AS).
- NCEER-89-0028 "Statistical Evaluation of Deflection Amplification Factors for Reinforced Concrete Structures," by H.H.M. Hwang, J-W. Jaw and A.L. Ch'ng, 8/31/89, (PB90-164633/AS).
- NCEER-89-0029 "Bedrock Accelerations in Memphis Area Due to Large New Madrid Earthquakes," by H.H.M. Hwang, C.H.S. Chen and G. Yu, 11/7/89, (PB90-162330/AS).

- NCEER-89-0030 "Seismic Behavior and Response Sensitivity of Secondary Structural Systems," by Y.Q. Chen and T.T. Soong, 10/23/89, (PB90-164658/AS).
- NCEER-89-0031 "Random Vibration and Reliability Analysis of Primary-Secondary Structural Systems," by Y. Ibrahim, M. Grigoriu and T.T. Soong, 11/10/89, (PB90-161951/AS).
- NCEER-89-0032 "Proceedings from the Second U.S. - Japan Workshop on Liquefaction, Large Ground Deformation and Their Effects on Lifelines, September 26-29, 1989," Edited by T.D. O'Rourke and M. Hamada, 12/1/89, (PB90-209388/AS).
- NCEER-89-0033 "Deterministic Model for Seismic Damage Evaluation of Reinforced Concrete Structures," by J.M. Bracci, A.M. Reinhorn, J.B. Mander and S.K. Kunnath, 9/27/89.
- NCEER-89-0034 "On the Relation Between Local and Global Damage Indices," by E. DiPasquale and A.S. Cakmak, 8/15/89, (PB90-173865).
- NCEER-89-0035 "Cyclic Undrained Behavior of Nonplastic and Low Plasticity Silts," by A.J. Walker and H.E. Stewart, 7/26/89, (PB90-183518/AS).
- NCEER-89-0036 "Liquefaction Potential of Surficial Deposits in the City of Buffalo, New York," by M. Budhu, R. Giese and L. Baumgrass, 1/17/89, (PB90-208455/AS).
- NCEER-89-0037 "A Deterministic Assessment of Effects of Ground Motion Incoherence," by A.S. Veletsos and Y. Tang, 7/15/89, (PB90-164294/AS).
- NCEER-89-0038 "Workshop on Ground Motion Parameters for Seismic Hazard Mapping," July 17-18, 1989, edited by R.V. Whitman, 12/1/89, (PB90-173923/AS).
- NCEER-89-0039 "Seismic Effects on Elevated Transit Lines of the New York City Transit Authority," by C.J. Costantino, C.A. Miller and E. Heymsfield, 12/26/89, (PB90-207887/AS).
- NCEER-89-0040 "Centrifugal Modeling of Dynamic Soil-Structure Interaction," by K. Weissman, Supervised by J.H. Prevost, 5/10/89, (PB90-207879/AS).
- NCEER-89-0041 "Linearized Identification of Buildings With Cores for Seismic Vulnerability Assessment," by I-K. Ho and A.E. Aktan, 11/1/89, (PB90-251943/AS).
- NCEER-90-0001 "Geotechnical and Lifeline Aspects of the October 17, 1989 Loma Prieta Earthquake in San Francisco," by T.D. O'Rourke, H.E. Stewart, F.T. Blackburn and T.S. Dickerman, 1/90, (PB90-208596/AS).
- NCEER-90-0002 "Nonnormal Secondary Response Due to Yielding in a Primary Structure," by D.C.K. Chen and L.D. Lutes, 2/28/90, (PB90-251976/AS).
- NCEER-90-0003 "Earthquake Education Materials for Grades K-12," by K.E.K. Ross, 4/16/90, (PB91-113415/AS).
- NCEER-90-0004 "Catalog of Strong Motion Stations in Eastern North America," by R.W. Busby, 4/3/90, (PB90-251984)/AS.
- NCEER-90-0005 "NCEER Strong-Motion Data Base: A User Manual for the GeoBase Release (Version 1.0 for the Sun3)," by P. Friberg and K. Jacob, 3/31/90 (PB90-258062/AS).
- NCEER-90-0006 "Seismic Hazard Along a Crude Oil Pipeline in the Event of an 1811-1812 Type New Madrid Earthquake," by H.H.M. Hwang and C-H.S. Chen, 4/16/90(PB90-258054).
- NCEER-90-0007 "Site-Specific Response Spectra for Memphis Sheahan Pumping Station," by H.H.M. Hwang and C.S. Lee, 5/15/90, (PB91-108811/AS).

- NCEER-90-0008 "Pilot Study on Seismic Vulnerability of Crude Oil Transmission Systems," by T. Ariman, R. Dobry, M. Grigoriu, F. Kozin, M. O'Rourke, T. O'Rourke and M. Shinozuka, 5/25/90, (PB91-108837/AS).
- NCEER-90-0009 "A Program to Generate Site Dependent Time Histories: EQGEN," by G.W. Ellis, M. Srinivasan and A.S. Cakmak, 1/30/90, (PB91-108829/AS).
- NCEER-90-0010 "Active Isolation for Seismic Protection of Operating Rooms," by M.E. Talbott, Supervised by M. Shinozuka, 6/8/9, (PB91-110205/AS).
- NCEER-90-0011 "Program LINEARID for Identification of Linear Structural Dynamic Systems," by C-B. Yun and M. Shinozuka, 6/25/90, (PB91-110312/AS).
- NCEER-90-0012 "Two-Dimensional Two-Phase Elasto-Plastic Seismic Response of Earth Dams," by A.N. Yiagos, Supervised by J.H. Prevost, 6/20/90, (PB91-110197/AS).
- NCEER-90-0013 "Secondary Systems in Base-Isolated Structures: Experimental Investigation, Stochastic Response and Stochastic Sensitivity," by G.D. Manolis, G. Juhn, M.C. Constantinou and A.M. Reinhorn, 7/1/90, (PB91-110320/AS).
- NCEER-90-0014 "Seismic Behavior of Lightly-Reinforced Concrete Column and Beam-Column Joint Details," by S.P. Pessiki, C.H. Conley, P. Gergely and R.N. White, 8/22/90, (PB91-108795/AS).
- NCEER-90-0015 "Two Hybrid Control Systems for Building Structures Under Strong Earthquakes," by J.N. Yang and A. Danielians, 6/29/90, (PB91-125393/AS).
- NCEER-90-0016 "Instantaneous Optimal Control with Acceleration and Velocity Feedback," by J.N. Yang and Z. Li, 6/29/90, (PB91-125401/AS).
- NCEER-90-0017 "Reconnaissance Report on the Northern Iran Earthquake of June 21, 1990," by M. Mehrain, 10/4/90, (PB91-125377/AS).
- NCEER-90-0018 "Evaluation of Liquefaction Potential in Memphis and Shelby County," by T.S. Chang, P.S. Tang, C.S. Lee and H. Hwang, 8/10/90, (PB91-125427/AS).
- NCEER-90-0019 "Experimental and Analytical Study of a Combined Sliding Disc Bearing and Helical Steel Spring Isolation System," by M.C. Constantinou, A.S. Mokha and A.M. Reinhorn, 10/4/90, (PB91-125385/AS).
- NCEER-90-0020 "Experimental Study and Analytical Prediction of Earthquake Response of a Sliding Isolation System with a Spherical Surface," by A.S. Mokha, M.C. Constantinou and A.M. Reinhorn, 10/11/90, (PB91-125419/AS).
- NCEER-90-0021 "Dynamic Interaction Factors for Floating Pile Groups," by G. Gazetas, K. Fan, A. Kaynia and E. Kausel, 9/10/90, (PB91-170381/AS).
- NCEER-90-0022 "Evaluation of Seismic Damage Indices for Reinforced Concrete Structures," by S. Rodriguez-Gomez and A.S. Cakmak, 9/30/90, PB91-171322/AS).
- NCEER-90-0023 "Study of Site Response at a Selected Memphis Site," by H. Desai, S. Ahmad, E.S. Gazetas and M.R. Oh, 10/11/90, (PB91-196857/AS).
- NCEER-90-0024 "A User's Guide to Strongmo: Version 1.0 of NCEER's Strong-Motion Data Access Tool for PCs and Terminals," by P.A. Friberg and C.A.T. Susch, 11/15/90, (PB91-171272/AS).
- NCEER-90-0025 "A Three-Dimensional Analytical Study of Spatial Variability of Seismic Ground Motions," by L-L. Hong and A.H.-S. Ang, 10/30/90, (PB91-170399/AS).

- NCEER-90-0026 "MUMOID User's Guide - A Program for the Identification of Modal Parameters," by S. Rodriguez-Gomez and E. DiPasquale, 9/30/90, (PB91-171298/AS).
- NCEER-90-0027 "SARCF-II User's Guide - Seismic Analysis of Reinforced Concrete Frames," by S. Rodriguez-Gomez, Y.S. Chung and C. Meyer, 9/30/90, (PB91-171280/AS).
- NCEER-90-0028 "Viscous Dampers: Testing, Modeling and Application in Vibration and Seismic Isolation," by N. Makris and M.C. Constantinou, 12/20/90 (PB91-190561/AS).
- NCEER-90-0029 "Soil Effects on Earthquake Ground Motions in the Memphis Area," by H. Hwang, C.S. Lee, K.W. Ng and T.S. Chang, 8/2/90, (PB91-190751/AS).
- NCEER-91-0001 "Proceedings from the Third Japan-U.S. Workshop on Earthquake Resistant Design of Lifeline Facilities and Countermeasures for Soil Liquefaction, December 17-19, 1990," edited by T.D. O'Rourke and M. Hamada, 2/1/91, (PB91-179259/AS).
- NCEER-91-0002 "Physical Space Solutions of Non-Proportionally Damped Systems," by M. Tong, Z. Liang and G.C. Lee, 1/15/91, (PB91-179242/AS).
- NCEER-91-0003 "Seismic Response of Single Piles and Pile Groups," by K. Fan and G. Gazetas, 1/10/91, (PB92-174994/AS).
- NCEER-91-0004 "Damping of Structures: Part 1 - Theory of Complex Damping," by Z. Liang and G. Lee, 10/10/91, (PB92-197235/AS).
- NCEER-91-0005 "3D-BASIS - Nonlinear Dynamic Analysis of Three Dimensional Base Isolated Structures: Part II," by S. Nagarajaiah, A.M. Reinhorn and M.C. Constantinou, 2/28/91, (PB91-190553/AS).
- NCEER-91-0006 "A Multidimensional Hysteretic Model for Plasticity Deforming Metals in Energy Absorbing Devices," by E.J. Graesser and F.A. Cozzarelli, 4/9/91, (PB92-108364/AS).
- NCEER-91-0007 "A Framework for Customizable Knowledge-Based Expert Systems with an Application to a KBES for Evaluating the Seismic Resistance of Existing Buildings," by E.G. Ibarra-Anaya and S.J. Fenves, 4/9/91, (PB91-210930/AS).
- NCEER-91-0008 "Nonlinear Analysis of Steel Frames with Semi-Rigid Connections Using the Capacity Spectrum Method," by G.G. Deierlein, S-H. Hsieh, Y-J. Shen and J.F. Abel, 7/2/91, (PB92-113828/AS).
- NCEER-91-0009 "Earthquake Education Materials for Grades K-12," by K.E.K. Ross, 4/30/91, (PB91-212142/AS).
- NCEER-91-0010 "Phase Wave Velocities and Displacement Phase Differences in a Harmonically Oscillating Pile," by N. Makris and G. Gazetas, 7/8/91, (PB92-108356/AS).
- NCEER-91-0011 "Dynamic Characteristics of a Full-Size Five-Story Steel Structure and a 2/5 Scale Model," by K.C. Chang, G.C. Yao, G.C. Lee, D.S. Hao and Y.C. Yeh," 7/2/91.
- NCEER-91-0012 "Seismic Response of a 2/5 Scale Steel Structure with Added Viscoelastic Dampers," by K.C. Chang, T.T. Soong, S-T. Oh and M.L. Lai, 5/17/91 (PB92-110816/AS).
- NCEER-91-0013 "Earthquake Response of Retaining Walls; Full-Scale Testing and Computational Modeling," by S. Alampalli and A-W.M. Elgamal, 6/20/91, to be published.
- NCEER-91-0014 "3D-BASIS-M: Nonlinear Dynamic Analysis of Multiple Building Base Isolated Structures," by P.C. Tsopelas, S. Nagarajaiah, M.C. Constantinou and A.M. Reinhorn, 5/28/91, (PB92-113885/AS).

- NCEER-91-0015 "Evaluation of SEAOC Design Requirements for Sliding Isolated Structures," by D. Theodossiou and M.C. Constantinou, 6/10/91, (PB92-114602/AS).
- NCEER-91-0016 "Closed-Loop Modal Testing of a 27-Story Reinforced Concrete Flat Plate-Core Building," by H.R. Somaprasad, T. Toksoy, H. Yoshiyuki and A.E. Aktan, 7/15/91, (PB92-129980/AS).
- NCEER-91-0017 "Shake Table Test of a 1/6 Scale Two-Story Lightly Reinforced Concrete Building," by A.G. El-Attar, R.N. White and P. Gergely, 2/28/91, (PB92-222447/AS).
- NCEER-91-0018 "Shake Table Test of a 1/8 Scale Three-Story Lightly Reinforced Concrete Building," by A.G. El-Attar, R.N. White and P. Gergely, 2/28/91.
- NCEER-91-0019 "Transfer Functions for Rigid Rectangular Foundations," by A.S. Veletsos, A.M. Prasad and W.H. Wu, 7/31/91.
- NCEER-91-0020 "Hybrid Control of Seismic-Excited Nonlinear and Inelastic Structural Systems," by J.N. Yang, Z. Li and A. Danielians, 8/1/91, (PB92-143171/AS).
- NCEER-91-0021 "The NCEER-91 Earthquake Catalog: Improved Intensity-Based Magnitudes and Recurrence Relations for U.S. Earthquakes East of New Madrid," by L. Sceber and J.G. Armbruster, 8/28/91, (PB92-176742/AS).
- NCEER-91-0022 "Proceedings from the Implementation of Earthquake Planning and Education in Schools: The Need for Change - The Roles of the Changemakers," by K.E.K. Ross and F. Winslow, 7/23/91, (PB92-129998/AS).
- NCEER-91-0023 "A Study of Reliability-Based Criteria for Seismic Design of Reinforced Concrete Frame Buildings," by H.H.M. Hwang and H-M. Hsu, 8/10/91, (PB92-140235/AS).
- NCEER-91-0024 "Experimental Verification of a Number of Structural System Identification Algorithms," by R.G. Ghanem, H. Gavin and M. Shinozuka, 9/18/91, (PB92-176577/AS).
- NCEER-91-0025 "Probabilistic Evaluation of Liquefaction Potential," by H.H.M. Hwang and C.S. Lee, 11/25/91, (PB92-143429/AS).
- NCEER-91-0026 "Instantaneous Optimal Control for Linear, Nonlinear and Hysteretic Structures - Stable Controllers," by J.N. Yang and Z. Li, 11/15/91, (PB92-163807/AS).
- NCEER-91-0027 "Experimental and Theoretical Study of a Sliding Isolation System for Bridges," by M.C. Constantinou, A. Kartoum, A.M. Reinhorn and P. Bradford, 11/15/91, (PB92-176973/AS).
- NCEER-92-0001 "Case Studies of Liquefaction and Lifeline Performance During Past Earthquakes, Volume 1: Japanese Case Studies," Edited by M. Hamada and T. O'Rourke, 2/17/92, (PB92-197243/AS).
- NCEER-92-0002 "Case Studies of Liquefaction and Lifeline Performance During Past Earthquakes, Volume 2: United States Case Studies," Edited by T. O'Rourke and M. Hamada, 2/17/92, (PB92-197250/AS).
- NCEER-92-0003 "Issues in Earthquake Education," Edited by K. Ross, 2/3/92, (PB92-222389/AS).
- NCEER-92-0004 "Proceedings from the First U.S. - Japan Workshop on Earthquake Protective Systems for Bridges," 2/4/92, to be published.
- NCEER-92-0005 "Seismic Ground Motion from a Haskell-Type Source in a Multiple-Layered Half-Space," A.P. Theoharis, G. Deodatis and M. Shinozuka, 1/2/92, to be published.
- NCEER-92-0006 "Proceedings from the Site Effects Workshop," Edited by R. Whitman, 2/29/92, (PB92-197201/AS).

- NCEER-92-0007 "Engineering Evaluation of Permanent Ground Deformations Due to Seismically-Induced Liquefaction," by M.H. Baziar, R. Dobry and A-W.M. Elgamal, 3/24/92, (PB92-222421/AS).
- NCEER-92-0008 "A Procedure for the Seismic Evaluation of Buildings in the Central and Eastern United States," by C.D. Poland and J.O. Malley, 4/2/92, (PB92-222439/AS).
- NCEER-92-0009 "Experimental and Analytical Study of a Hybrid Isolation System Using Friction Controllable Sliding Bearings," by M.Q. Feng, S. Fujii and M. Shinozuka, 5/15/92, (PB93-150282/AS).
- NCEER-92-0010 "Seismic Resistance of Slab-Column Connections in Existing Non-Ductile Flat-Plate Buildings," by A.J. Durrani and Y. Du, 5/18/92.
- NCEER-92-0011 "The Hysteretic and Dynamic Behavior of Brick Masonry Walls Upgraded by Ferrocement Coatings Under Cyclic Loading and Strong Simulated Ground Motion," by H. Lee and S.P. Pravel, 5/11/92, to be published.
- NCEER-92-0012 "Study of Wire Rope Systems for Seismic Protection of Equipment in Buildings," by G.F. Demetriades, M.C. Constantinou and A.M. Reinhorn, 5/20/92.
- NCEER-92-0013 "Shape Memory Structural Dampers: Material Properties, Design and Seismic Testing," by P.R. Witting and F.A. Cozzarelli, 5/26/92.
- NCEER-92-0014 "Longitudinal Permanent Ground Deformation Effects on Buried Continuous Pipelines," by M.J. O'Rourke, and C. Nordberg, 6/15/92.
- NCEER-92-0015 "A Simulation Method for Stationary Gaussian Random Functions Based on the Sampling Theorem," by M. Grigoriu and S. Balopoulou, 6/11/92, (PB93-127496/AS).
- NCEER-92-0016 "Gravity-Load-Designed Reinforced Concrete Buildings: Seismic Evaluation of Existing Construction and Detailing Strategies for Improved Seismic Resistance," by G.W. Hoffmann, S.K. Kunnath, J.B. Mander and A.M. Reinhorn, 7/15/92, to be published.
- NCEER-92-0017 "Observations on Water System and Pipeline Performance in the Limón Area of Costa Rica Due to the April 22, 1991 Earthquake," by M. O'Rourke and D. Ballantyne, 6/30/92, (PB93-126811/AS).
- NCEER-92-0018 "Fourth Edition of Earthquake Education Materials for Grades K-12," Edited by K.E.K. Ross, 8/10/92.
- NCEER-92-0019 "Proceedings from the Fourth Japan-U.S. Workshop on Earthquake Resistant Design of Lifeline Facilities and Countermeasures for Soil Liquefaction," Edited by M. Hamada and T.D. O'Rourke, 8/12/92, (PB93-163939/AS).
- NCEER-92-0020 "Active Bracing System: A Full Scale Implementation of Active Control," by A.M. Reinhorn, T.T. Soong, R.C. Lin, M.A. Riley, Y.P. Wang, S. Aizawa and M. Higashino, 8/14/92, (PB93-127512/AS).
- NCEER-92-0021 "Empirical Analysis of Horizontal Ground Displacement Generated by Liquefaction-Induced Lateral Spreads," by S.F. Bartlett and T.L. Youd, 8/17/92.
- NCEER-92-0022 "IDARC Version 3.0: Inelastic Damage Analysis of Reinforced Concrete Structures," by S.K. Kunnath, A.M. Reinhorn and R.F. Lobo, 8/31/92, to be published.
- NCEER-92-0023 "A Semi-Empirical Analysis of Strong-Motion Peaks in Terms of Seismic Source, Propagation Path and Local Site Conditions, by M. Kamiyama, M.J. O'Rourke and R. Flores-Berrones, 9/9/92, (PB93-150266/AS).
- NCEER-92-0024 "Seismic Behavior of Reinforced Concrete Frame Structures with Nonductile Details, Part I: Summary of Experimental Findings of Full Scale Beam-Column Joint Tests," by A. Beres, R.N. White and P. Gergely, 9/30/92, to be published.
- NCEER-92-0025 "Experimental Results of Repaired and Retrofitted Beam-Column Joint Tests in Lightly Reinforced Concrete Frame Buildings," by A. Beres, S. El-Borgi, R.N. White and P. Gergely, 10/29/92, to be published.

- NCEER-92-0026 "A Generalization of Optimal Control Theory: Linear and Nonlinear Structures," by J.N. Yang, Z. Li and S. Vongchavalitkul, 11/2/92.
- NCEER-92-0027 "Seismic Resistance of Reinforced Concrete Frame Structures Designed Only for Gravity Loads: Part I - Design and Properties of a One-Third Scale Model Structure," by J.M. Bracci, A.M. Reinhorn and J.B. Mander, 12/1/92.